ANL-6723

ANL-6723

ARGONNE RECORD COPY
DO NOT DESTROY

Argonne National Laboratory

BIOLOGICAL AND MEDICAL RESEARCH DIVISION

SEMIANNUAL REPORT

January through June 1962

LEGAL NOTICE

This report was prepared as an account of Government sponsored work. Neither the United States, nor the Commission, nor any person acting on behalf of the Commission:

A. Makes any warranty or representation, expressed or implied, with respect to the accuracy, completeness, or usefulness of the information contained in this report, or that the use of any information, apparatus, method, or process disclosed in this report may not infringe privately owned rights; or

B. Assumes any liabilities with respect to the use of, or for damages resulting from the use of any information, apparatus, method, or process disclosed in this report.

As used in the above, "person acting on behalf of the Commission" includes any employee or contractor of the Commission, or employee of such contractor, to the extent that such employee or contractor of the Commission, or employee of such contractor prepares, disseminates, or provides access to, any information pursuant to his employment or contract with the Commission, or his employment with such contractor.

ERRATUM

ANL-6535

p. 57 Line 8: Change "Yakovlev and Ivanov. . ." to read "The results. . ."

ANL-6723
Biology & Medicine
(TID-4500, 20th Ed.)
AEC Research and
Development Report

ARGONNE NATIONAL LABORATORY
9700 South Cass Avenue
Argonne, Illinois

BIOLOGICAL AND MEDICAL RESEARCH DIVISION SEMIANNUAL REPORT

January through June 1962

May 1963

Preceding Report:
ANL-6535 July through December 1961

Operated by The University of Chicago
under
Contract W-31-109-eng-38
with the
U. S. Atomic Energy Commission

TABLE OF CONTENTS

Page

Early alterations in plasma proteins in the gamma-irradiated chick
Emily J. B. Christian and S. Phyllis Stearner 5

Progress report: Survival of guinea pigs given low daily gamma-ray exposure - Fourth year
George A. Sacher, Douglas Grahn and Robert J. Robertson . . 10

Progress report: A note on self-absorption and reciprocity law in radiation dosimetry
Ernesto Trucco 16

Fast and epithermal fluxes in neutron radiobiological facilities
Norman A. Frigerio and Donn L. Jordan. 28

Incidence of mammary neoplasms in neutron- and gamma-irradiated female Sprague-Dawley rats
Howard H. Vogel, Jr. and Donn L. Jordan 33

Progress report: Lethality of fractionated doses of fission neutrons and Co^{60} gamma rays in mice
Donn L. Jordan and Howard H. Vogel, Jr. 41

Thymic tumor incidence and longevity in female mice irradiated with fission neutrons or Co^{60} gamma rays
Howard H. Vogel, Jr. and Donn L. Jordan 44

Progress report: Diseases of laboratory animals
Lack of susceptibility of the Syrian hamster to ectromelia virus
Robert J. Flynn and Isabel L. Greco 50
A disease of mice characterized by lung congestion
Robert J. Flynn, Isabel L. Greco, and Patricia B. Jinkins . . 53

A comparison of radiation-induced granulocytopenia in several mammalian species
Harvey M. Patt and Mary A. Maloney. 56

Comparative analysis of neutrophil kinetics in X-irradiated dog and monkey
Mary A. Maloney, Harvey M. Patt and Charlotte L. Weber. . 61

TABLE OF CONTENTS

Page

Effect of age and radiation on the lens of the eye in the mouse
Robert L. Straube 63

Monte Carlo calculations for the stochastic theory of mortality
George A. Sacher and Ernesto Trucco 65

Comparative kinetics of acute radiation lethality
S. Phyllis Stearner, Sylvanus A. Tyler and
Margaret H. Sanderson 67

A model of the kinetics of injury processes associated with acute lethality in the gamma-irradiated mouse
Sylvanus A. Tyler and S. Phyllis Stearner 73

Toxicity of plutonium in mice
Miriam P. Finkel and Birute O. Biskis 82

Progress report: Toxicity and metabolism of radionuclides.
III. Semiannual report for period ending May 31, 1962
William P. Norris, Louise S. Lombard, Carl E. Rehfeld,
Thomas W. Speckman and Herman M. Slatis 100

Absence of repair of mutational damage in continuous cultures
Herbert E. Kubitschek and Harold E. Bendigkeit 138

The study of normal variation
II. Observations on the inheritance of hair on the pinna of the ear
Herman M. Slatis 140

Strophanthin and isonicotinic acid hydrazide as possible radiation protectors
Robert N. Feinstein and Marilyn Coulon 142

Progress report: Plutonium removal, Tumor incidence studies. III
Marcia W. Rosenthal, Joan Fried Markley, and
Arthur Lindenbaum 144

TABLE OF CONTENTS

Page

Progress report: Plutonium removal
V. Ultrafilterability and disappearance of plutonium from plasma as a function of DTPA treatment and of the physical state of the plutonium
Arthur Lindenbaum, Joan Fried Markley, Marcia W. Rosenthal, William M. Westfall and Elizabeth S. Moretti 146

Metabolism of methionine and S-adenosylmethionine in Neurospora
Lila Abrahamson 149

Beta-scintillation counting of radioactive tracers on filter paper
Walter E. Kisieleski and Donald Logsdon 153

Differential migration of sterol acetates on silica gels and its application to the fractionation of sterol mixtures
Peter D. Klein and Patricia A. Szczepanik 155

Progress report: Biosynthesis of methionine from homocysteine and sulfonium derivatives in Escherichia coli
Morris Pfeffer and Stanley K. Shapiro 165

Phosphate metabolism and effect of thiophosphate in Chlorella
Takuya R. Sato 174

Alkaline hydrolysis of S-adenosylmethionine in tritiated water
F. Schlenk and Julia L. Dainko 178

Use of mixtures of DPND isomers in establishing reaction mechanisms of dehydrogenases
John F. Thomson and Jacqueline J. Darling 181

Electron microscopy of centrifuged Amoeba proteus
Edward W. Daniels 185

Development as the means of multiplication of organelles and organelle systems in Paramecium
Charles F. Ehret and Gérard de Haller 186

An electron microscope study of the spore of the microsporidian Thelohania californica
R. R. Kudo and Edward W. Daniels 190

TABLE OF CONTENTS

Page

An autoradiographic technique for light and electron microscopy
O. T. Minick 198

Examination of stimulatory effects of ionizing radiations in plants
John Skok and William Chorney. 202

Autoradiographic investigation of the mitotic cycle of Ehrlich ascites tumor cells in vivo
Renato Baserga and Walter E. Kisieleski 203

Biochemistry of glucose oxidase
I. Methemoglobin formation after glucose oxidase injection in mice
Robert N. Feinstein and Marilyn Coulon 205

Catalase activity in various inbred mouse strains
Robert N. Feinstein and Marilyn Coulon 208

Attempts at reduction of erythrocyte catalase level
Robert N. Feinstein, Marilyn Coulon and Elizabeth Thompson 211

Effect of nicotinamide on growth of mouse Ehrlich ascites tumor
Robert N. Feinstein, Marilyn Coulon and Elizabeth Thompson 215

Dynamics of tumor growth
Anna Kane Laird 216

Radiation-induced chromosomal aberrations and variant clones in mammalian cells cultivated in vitro
Agnes N. Stroud, Austin M. Brues and Beverly M. Svoboda . . 223

Utilization of DNA and RNA precursors as indicators of drug effect on cancer cells
Agnes N. Stroud, Gerald O. McDonald, Beverly R. Svoboda and Austin M. Brues. 237

Chromosome studies of various strains of human tumors H.Ad.1 and H.Ep.3 maintained in rodents
Agnes N. Stroud, Beverly R. Svoboda and Harold B. Haley . . 243

Publications 252

EARLY ALTERATIONS IN PLASMA PROTEINS IN THE GAMMA-IRRADIATED CHICK

Emily J. B. Christian and S. Phyllis Stearner

Changes in membrane permeability have been described as an early effect of radiation in various biological systems. Decrease in intradermal pressure in rat skin and the cock's comb immediately after X-irradiation has been recorded;[1] increased vascular permeability to dyes that bind protein has been observed in the irradiated rabbit[2] and rat;[3] and instances of radiation-induced cell swelling have been described.[4] In the chick, permeability changes leading to critical circulatory insufficiency have been identified in connection with the initial radiation mortality response (within 2 days after exposure); decrease in circulating blood volume and severe hypotension have been reported.[5,6] The present investigations are concerned with early postirradiation changes in concentration of the principal plasma proteins (within 6 hr after exposure) and their possible significance in the early lethality.

Methods

Three-day-old chicks were exposed to total body γ-irradiation from a 5000-curie Co^{60} source. A single dose of 400 r, 700 r, or 1200 r was used, and the total exposure time in each case was 10 min. After irradiation chicks were kept in brooders maintained at about 35°C, with free access to food and water. Blood samples for plasma protein determinations were taken from both control and irradiated chicks by a standard procedure. After the animal had been weighed and lightly anesthetized with ether, the heart was exposed and at least 0.5 cc blood was withdrawn into a slightly heparinized syringe. The animal was then killed and necropsied, with grossly visible lesions recorded. The blood sample was transferred to a hematocrit tube and centrifuged for 30 min at 4500 rpm. After the hematocrit value had been read, the plasma was stored at -8°C. At least 6 chicks were used for each sampling time in each dose group. A total of 122 irradiated and 23 control chicks was sampled.

Plasma samples were brought to room temperature and 0.01-ml aliquots were taken for determination of total protein concentration and for electrophoretic separation of major protein components. Total plasma protein was measured by the method of Lowry et al.,[7] employing Folin-Ciocalteau phenol reagent. One-half hour after the reagent was added the samples were read in a Coleman Jr. spectrophotometer at 700 mμ and compared with a bovine serum albumin standard curve. Standard solutions were prepared fresh each day. The protein components of the plasma were

separated by the Spinco paper-strip electrophoresis method, using the standard procedure B as described in the Spinco Model R Instruction Manual.[8] The relative concentrations of the protein components were evaluated on the Analytrol (Model RB). From the integrated areas under the curve and total plasma protein concentration, absolute concentrations of the protein fractions were calculated.

Results

In the 3-day chick the total plasma protein concentration is 3.62 g%, of which 1.53 g% is albumin and the remainder globulin. Total globulin can be separated into α, β, and γ fractions, but the concentrations of the α and β fractions are relatively small and variable. Therefore, only total globulin values will be considered.

The effect of irradiation on total protein, albumin, and globulin concentrations is shown in Table 1. After exposure to 400 r, the total protein concentration shows little change, while after 700 r the concentration falls gradually, reaching a low of 1.87 g% at 6 hr. After exposure to 1200 r, however, the protein concentration falls more rapidly, and is approximately 50% of normal (1.80 g%) at 3 hr. The albumin fraction shows little change after 400 r. After 700 r the concentration slowly falls to about half the control level (0.71 g%) at the end of the 6-hr period, but after 1200 r it decreases to 0.45 g% within 3 hr. Changes in concentration of globulins are less marked. After 400 r there is little change, while in the other two dose groups there is a slow decrease in concentration.

TABLE 1

Effect of total-body γ-irradiation on plasma protein concentration of the chick

Time after exposure, hr	Total protein, g%			Albumin, g%			Globulins, g%		
	400 r	700 r	1200 r	400 r	700 r	1200 r	400 r	700 r	1200 r
Control	3.62	3.62	3.62	1.53	1.53	1.53	2.09	2.09	2.09
Immed.	-	-	3.94	-	-	1.80	-	-	2.14
0.5	3.30	2.90	3.45	1.57	1.23	1.41	1.73	1.67	2.04
1	3.38	3.09	3.37	1.37	1.29	1.29	2.01	1.80	2.08
2	3.30	2.42	2.25	1.41	1.05	0.74	1.89	1.37	1.51
3	3.11	2.61	1.80	1.43	1.08	0.45	1.68	1.53	1.35
4	3.18	2.23	1.97	1.53	0.87	0.49	1.65	1.36	1.48
6	3.08	1.87	2.25	1.40	0.71	0.60	1.68	1.16	1.65

Postirradiation increases in red cell hematocrit values can be correlated with the decreased plasma protein concentration (Table 2). Although determinations of plasma volume were not made on these animals, the

increase in hematocrit values after 3-6 hr indicates that plasma volume has decreased. Plasma volumes have been calculated (Table 3), assuming a constant red cell mass and a total blood volume 6.5% of the body weight.* The estimated decrease after 1200 r is especially marked, but probably represents an underestimate of the true decrease in plasma volume. Evidence of hemorrhage, frequently seen after 3 hr, indicates that there is also a decrease in the circulating red cell mass and, therefore, an even greater decrease in circulating plasma volume.

TABLE 2

Effect of γ-irradiation on hematocrit of the chick
(control value = 25.9%)

Dose, r	% Red cell mass						
	Time after irradiation, hr						
	0	0.5	1	2	3	4	6
400		23.5	23.0	23.4	24.0	24.9	25.5
700		25.6	25.6	27.2	27.4	32.7	31.1
1200	26.0	28.0	30.6	39.1	37.1	37.3	32.2

TABLE 3

Effect of γ-irradiation on plasma volume of the chick
(control = 2.03 cc)

Dose, r	Estimated volume, cc						
	Time after irradiation, hr						
	0	0.5	1	2	3	4	6
400		2.21	2.28	2.23	2.22	2.14	2.01
700		2.09	1.98	1.79	1.85	1.38	1.53
1200	2.13	1.83	1.61	1.18	1.15	1.18	1.52

From observed mean protein concentrations and calculated plasma volumes in each group we have calculated the total albumin and globulin in the circulating plasma. Changes in these components in each of the

*In connection with earlier work, we have estimated the total blood volume of the 3- to 4-day white Leghorn chick to be 6.5% of body weight. I^{131}-labeled serum albumin was used for determination of plasma volume and erythrocytes labeled with Cr^{51} in vitro for red cell mass.

three irradiated groups during the 6-hr period of observation are shown in Figures 1 and 2. The response resembles that based on concentration but the changes are more profound. For example, within 3 hr after 1200 r, the quantity of circulating albumin falls to less than 20% of the control value (Figure 1), while globulins fall to less than 40% (Figure 2). The apparent increase in plasma proteins at 6 hr after exposure to 1200 r probably reflects selection within the irradiated group, due to deaths that occurred before 6 hr, rather than an actual increase in concentration.

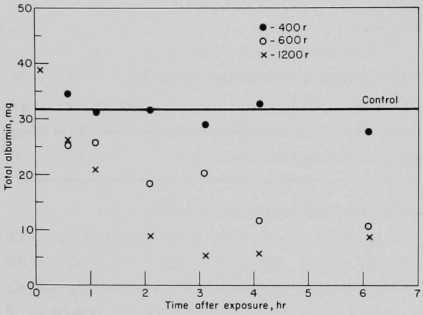

Figure 1. Effect of Co^{60} γ-irradiation on the total albumin content of the circulating plasma of the 3-day chick.

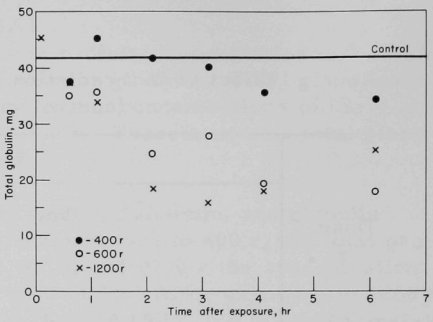

Figure 2. Effect of Co^{60} γ-irradiation on the total globulin content of the circulating plasma.

Discussion

The relation of the observed change in plasma protein concentration to the initial lethal response is suggested by the dose-time relation for this mode of radiation death. The lethal range (1-99% mortality) for Co^{60} γ-irradiation delivered over short exposure times is approximately 700-1200 r. Survival within 8 hr after irradiation is shown in Figure 3. It is only after 1200 r that mortality is high and deaths begin to occur before 3 hr. A marked decrease in albumin occurs at 2 hr in this exposure group. Although the albumin concentration at 6 hr after 700 r is comparable to that in the group exposed to 1200 r, the rate of decrease is

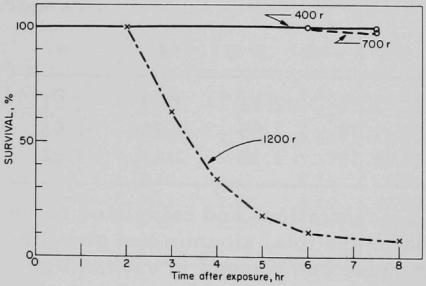

Figure 3. Survival within 8 hr after Co^{60} γ-irradiation (exposure time = 10 min).

much slower (Figure 1). The effect on the quantity of circulating globulins is similar but somewhat less drastic. No change in the quantity of circulating protein was noted after the "sublethal" exposure of 400 r.

After irradiation over short exposure periods with doses in the lethal range for the initial response, it appears that there are severe early changes in permeability of the capillary endothelium, leading to decreased plasma protein concentration and plasma volume. Preliminary results with doses protracted over longer exposure times indicate that the permeability change is dependent on exposure time. A dose of 1000 r delivered in 8 hr or 2300 r delivered in 17.6 hr is followed by little or no change in plasma proteins.[9]

References

1. Brinkman, R. and H. B. Lamberts. Direct registration of an instantaneous X-ray effect in rats and man. Nature 181, 774-775 (1958).
2. Rigdon, R. H. and H. Curl. Effect of roentgen irradiation on capillary permeability and inflammation in the skin of the rabbit. Am. J. Roentgenol. 49, 250-257 (1943).
3. Willoughby, D. A. Pharmacological aspects of the vascular permeability changes in the rat's intestine following abdominal radiation. Brit. J. Radiol. 33, 515-519 (1960).
4. Failla, G. Some aspects of the biological action of ionizing radiations. Am. J. Roentgenol. 44, 649-664 (1940).
5. Stearner, S. P., M. H. Sanderson, E. J. Christian and A. M. Brues. Evidence of circulatory failure in the early radiation response of the chicken. Am. J. Physiol. 192, 620-624 (1958).
6. Stearner, S. P., A. M. Brues, M. Sanderson and E. J. Christian. Role of hypotension in the initial response of X-irradiated chicks. Am. J. Physiol. 182, 407-410 (1955).
7. Lowry, O. J., N. J. Rosebrough, A. L. Farr and R. J. Randall. Protein measurements with the Folin phenol reagent. J. Biol. Chem. 193, 265-275 (1951).
8. Spinco Model R Paper Electrophoresis System Instruction Manual. Beckman/Spinco Division, Palo Alto, California.
9. Christian, E. J. B and S. P. Stearner. Unpublished results.

PROGRESS REPORT: SURVIVAL OF GUINEA PIGS GIVEN LOW DAILY GAMMA-RAY EXPOSURE - FOURTH YEAR

George A. Sacher, Douglas Grahn, and Robert J. Robertson

A little more than four years ago, the first replication of guinea pigs was entered into a program of periodic duration-of-life γ-ray exposure at levels ranging from 1.3 to 36 r per week. Since the last progress report[1] enough data have accumulated to permit a preliminary analysis of the effects on the mortality curve.

The exposure and control conditions and other features of the experiment are given in Table 4. Animals in exposed groups received their exposures on 1 to 6 nights each week, depending on the exposure pattern. Exposures were delivered to the guinea pigs in their living cages, and were given over a 12- to 15-hr period beginning at 6 P.M. The remaining days of the week were spent in the animal quarters, side by side on the same racks with the control pigs. Half of the control pigs were stationary, i.e., remained in the animal quarters, while the other half were mobile, i.e., were moved to a position in the gamma room corridor and returned to the home room each week. Subgroups of the mobile group matched the various fractionation patterns of the exposed groups. Analysis of the control data revealed that the stationary and mobile controls had almost identical mortality experience, so the control data are given here for the pooled group of 120 animals.

TABLE 4

Schedule of entries and numbers entered

	Replication No.					Total
	1	2	3	4	5	
Days to June 6, 1962	1394	1310	1233	1149	1051	
Control, stationary	12	12	12	12	12	60
Control, moving	12	12	12	12	12	60
1.35 r/week (1.35 x 1)	30	30	18	8	8	96
5.4 r/week (1.35 x 4)	16	16	8	-	8	48
13 r/week (2.6 x 5)	16	14	-	10	-	40
24 r/week (6 x 4)	-	4	4	-	4	12
24 r/week (24 x 1)	-	4	4	-	4	12
36 r/week (6 x 6)	8	-	-	8	-	16
						344

The survival of controls is comparable to that for Lorenz's inbred pigs and inferior to the survival of his hybrid group.[2]

The survival of the treatment groups at 350, 700, and 1050 days after onset of exposure is tabulated in Table 5. Mean after-survival times are recorded for groups in which dying-out was complete. Age-specific mortality rates are recorded for 350-day intervals up to 1400 days.

TABLE 5

Survival, mortality rates, and mean after-survival times

Total dose, r/week	No. of exposures		1-350 days	351-700 days	701-1050 days	1051-1594 days	Percent at 1050 days	Mean after-survival, days
Control		Survival*	120	111	93	63	52.5	-
		Mortality rate	0.08	0.18	0.39	0.73		
1.35	1	Survival	96	87	76	53	55.5	-
		Mortality rate	0.10	0.14	0.36	0.93		
5.4	4	Survival	48	47	45	34	71.0	-
		Mortality rate	0.02	0.07	0.28	0.53		
13	5	Survival	40	38	30	17	42.5	-
		Mortality rate	0.05	0.24	0.57	1.02		
24	4	Survival	12	10	5	0	0	600
		Mortality rate	0.18	0.69	-	-		
36	6	Survival	16	11	4	20	12.5	588
		Mortality rate	0.37	1.01	0.69	-		
24	1	Survival	12	8	3	0	0	477
		Mortality rate	0.41	0.98	-	-		

*Number living at beginning of interval.

Mortality rates were computed by the formula:

$$\Omega(t) = \ln N(t - h/2) - \ln N(t + h/2) = \Delta \ln N$$

The quantity Ω is the mean death rate in the interval $(t - h/2, t + h/2)$, and should not be confused with the actuary's death rate, $q_x = \Delta N/N$, which is not an estimate of the mean rate and which is seriously biased when percent mortality in an interval becomes appreciable, as it must in small samples.

The Ω values are plotted in Figure 4 on a logarithmic scale versus age, to yield the Gompertz transforms for the 7 experimental groups. The following features may be noted.

1. The Gompertz transform (G. T.) for controls is slightly convex upward, but does not depart significantly from linearity, and has a doubling time very near to 300 days.

2. The G. T. for 1.35 r/week is not significantly different from control.

3. The G. T. for 5.4 r/week lies below the control G. T. in all 4 time intervals; the reduction of mortality in the 5.4 r/week group is highly significant.

4. The set of G. T.'s for the 5.4, 13, 24, and 36 r/week groups are steeper than the control G. T., and essentially parallel one to another; the doubling time for these groups is roughly 200 days.

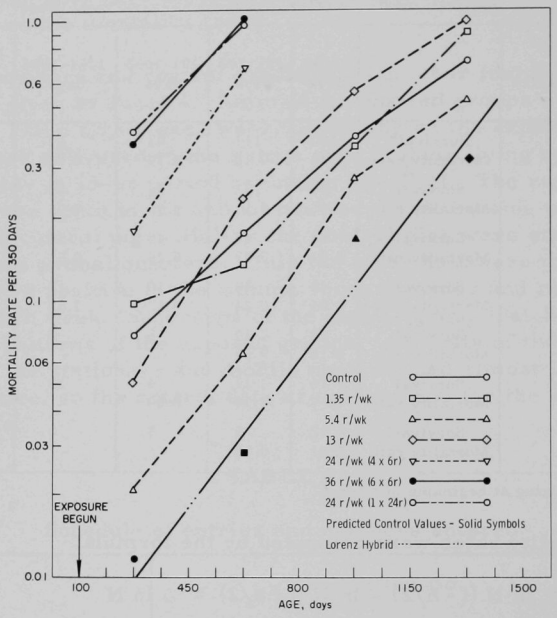

Figure 4. Mortality rates (on a logarithmic-scale) versus age. Rates are plotted at midpoint of interval for which they were computed. The predicted control points are an extrapolation, to zero dose rate, of the mortality rates observed in the exposed groups. The "Lorenz hybrid" line is an independent visual estimate of the mortality rate trend observed in a group of hybrid guinea pigs maintained by Lorenz.

In Figure 5, the Ω values are plotted on a log scale versus exposure dose per week. One notes that in the range from 5.4 through 36 r/week the curves are approximately parallel one to another, and from 5.4 through 24 r/week they are approximately linear. The dashed lines indicate approximately how the log mortality rate versus daily dose functions would

continue below 5.4 r/week if the relation of injury to daily dose were linear down to zero, and the solid symbols on the ordinate are then the expected control mortality rates on the linear hypothesis. These symbols are reproduced in Figure 4. The straight line passing through them is an independent visual estimate of the straight line fitting the G. T. for Lorenz' hybrid guinea pig control group, with a doubling time of 210 days.

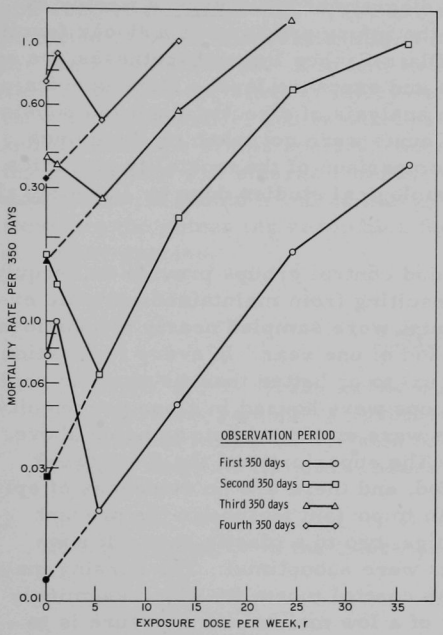

Figure 5

Mortality rates versus mean exposure dose per week for groups given 4, 5, or 6 fractions weekly for the first through fourth 350-day intervals. Solid symbols with dashed lines represent predicted control values obtained by extrapolation to zero dose.

Discussion

These data give evidence for the following propositions about the effects of periodic duration-of-life exposure on guinea pigs.

1. The parallelism of the G. T.'s for the levels 5.4 through 36 r/week bears out the hypothesis that the mortality of periodically exposed guinea pigs arises from an injury process in a physiological system which is extremely sensitive to radiation damage, but which equilibrates recovery with injury within a comparatively few months after the beginning of exposure. This is one of the hypotheses that the experiment was set up to test.

1A. As a corollary to 1., the parallelism also signifies that there is as yet no evidence for a nonrecovering component of radiation injury in the guinea pig. This is not entirely surprising, for if a nonrecovering

component existed, and had a dosage sensitivity about that of this nonrecovering component in the mouse, it would be difficult to detect in the presence of the large steady-state component of injury demonstrated here. Estimation of the irreparable component will require special procedures, such as carefully chosen terminated exposures. The terminated exposures employed by Lorenz were too large (or too intense) for this purpose.

2. The near-linearity of the diagram of log Ω versus weekly exposure dose (Figure 5) suggests that the injury produced is a linear function of weekly dose. In other words, the Blair-Sacher linear hypotheses are apparently valid for this injury process and exposure level. More convincing information would have to come from analysis of directly observed physiological damage, e.g., blood counts. Counts were not taken on the guinea pigs in the present experiment, but comparison of the mortality statistics reported here with the thorough hematological studies done by Lorenz et al. should be revealing.

3. The data for 5.4-r/week and control groups provide an unequivocal instance of improved survival resulting from maintained periodic exposure. The exposed and control groups were sampled nearly proportionally from 5 replications set up over a period of one year. In every replication, the 5.4-r/week group had survival equal to or better than its specific replication control. The two exposure groups were housed in close propinquity 3 days of each week. Mobile controls were employed but, as noted above, movement had no effect on survival. The superiority of the 5.4-r/week group is manifest over a 4-year period, and there are no evidences of epidemic death in the control groups. An important feature in the present experiment is the housing of guinea pigs, two to a plastic cage. It soon became apparent that these conditions were suboptimal. The housing may have created the conditions for excess control mortality which seemingly must be present if a beneficial effect of a low maintained exposure is to appear. However, the same pattern of control mortality in excess of that in low-level exposed groups was presented by Lorenz' inbred guinea pigs. In his hybrid guinea pigs, on the other hand, the controls had an excellent survival record with virtually no early death, and here there was a linear decrement of survival with daily dose which held down to zero dose.

4. The control survival "predicted" by linear extrapolation of the data from exposed groups (Figures 4 and 5) agrees quite well with the survival observed in Lorenz hybrid controls. These predicted values are the behavior expected in a hypothetical control population free of the excess mortality which by hypothesis is greatly reduced or abolished by optimal maintained exposures. It is indeed fortunate that the predicted G. T. can be matched with an observed one, for without such confirmation, the extrapolation would be much less credible. The data from the present experiment and the data obtained by Lorenz are consistent to an astonishing degree. This encourages the belief that we will eventually attain a correct understanding of the mechanisms underlying the high radiosensitivity of the guinea pig.

5. The effect of fractionation pattern on mortality can be read directly from a comparison of the 3 G. T. curves in the upper left of Figure 4. It can be seen that 24 r given in one session per week is almost exactly equal in effect to 36 r given in 6 fractions of 6 r each, that is, a 4-fold increase in dose per fraction leads to a 1.5-fold increase in effectiveness.

The analysis and interpretations presented here are preliminary and subject to correction. They are discussed at length because of the importance of these observations for the design of the experimental program for the reactor JANUS. It is now evident that the guinea pig provides favorable conditions for study of injury-lethality relations, dose-rate and fractionation dependence, and paradoxical improved survival. In the light of the known reactions of this species, there is reason to anticipate that interesting phenomena will emerge from the comparison of fast neutron and γ-ray exposures. It should be noted that in its response to maintained low-level exposure the guinea pig resembles the rhesus monkey more closely than any other species.

References

1. Sacher, G. A., D. Grahn and R. J. Robertson. Survival of guinea pigs given periodic gamma-ray exposure for the duration of life. Biological and Medical Research Division Semiannual Report, July through December, Argonne National Laboratory, ANL-6535. pp. 13-14 (1961).

2. Lorenz, E., W. E. Heston, A. B. Eschenbrenner and M. K. Deringer. Biological studies in the tolerance range. Radiology 49, 274-285 (1947).

PROGRESS REPORT: A NOTE ON SELF-ABSORPTION AND RECIPROCITY LAW IN RADIATION DOSIMETRY

Ernesto Trucco

I. The reciprocity law in radiation dosimetry was originally formulated by King;[1] much of his work is also given in Meyer and von Schweidler's book on radioactivity.[2] Later Mayneord[3] extended the reciprocity theorem as follows:

> "the integral dose throughout any volume whatever due to a finite source uniformly filled with radioactive material is equal to the integral dose throughout the original source if the 'receiver' be filled with radiating material of the same uniform density."

In particular, if the absorbing medium has arbitrary volume but the radiation is emitted by a point source, the true absorbed integral dose can be determined from the reciprocal situation: replace the absorber by a homogeneous* source of the same shape, and measure the radiation intensity at one point only, i.e. the location of the original source.

It is an interesting theoretical problem to calculate the results expected from either procedure. This requires evaluating the integrals given by King and Mayneord for the particular volume under consideration. Thus, for example, Kovalev[4] computed the intensity of radiation at a point, Q, due to a homogeneous cylindrical source, for the special case when Q is located on the cylinder surface at equal distance from both ends of the cylinder (Figure 6). In his calculations Kovalev assumes that the radioactive

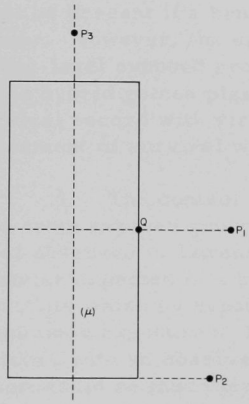

Figure 6

Illustrating Kovalev's calculation. Cylindrical source filled with a radioactive substance of uniform density and absorption coefficient μ. Intensity of radiation computed for point Q if $\mu \neq 0$, and also for points like P_1, P_2, P_3 if $\mu = 0$.

*This means having the radiating material distributed with uniform density throughout the volume.

material inside the cylinder absorbs the radiation according to the simple exponential law; the absorption coefficient is denoted by μ. If $\mu = 0$, Kovalev's results also apply to points P_1, P_2, and P_3 located as shown in Figure 6.

For a spherical source similar calculations were performed more than 30 years ago by Souttar;[5] however, he neglected all absorption effects. We have generalized Souttar's work to include these effects. If μ_1 and μ_0 denote, respectively, the absorption coefficients inside and outside the sphere, the radiation intensity at a point P, $I_P(\mu_1, \mu_0)$, is given by

$$I_P(\mu_1, \mu_0) = C \iiint \frac{e^{-(\mu_0 \xi_0 + \mu_1 \xi_1)}}{(\xi_0 + \xi_1)^2} dV \quad , \tag{1}$$

where C is a constant,* the integration is extended to the volume of the whole sphere, and the meaning of ξ_0, ξ_1 is indicated in Figure 7.

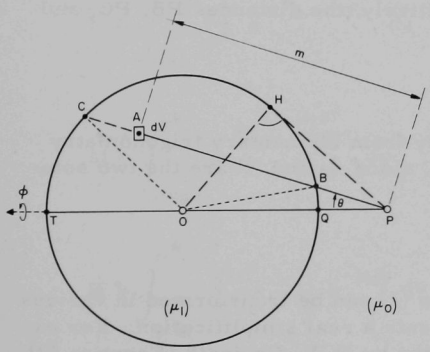

Figure 7

Spherical source; μ_1 = absorption coefficient of uniformly distributed radioactive material inside sphere; μ_0 = absorption coefficient of external medium (usually air). The following quantities are introduced in the equations:

$\overline{OQ} = \overline{OB} = \overline{OH} = \overline{OC} = \overline{OT} = R$	$\overline{AB} = \xi_1$
$\overline{OP} = g$	$\overline{BP} = \xi_0$
$\overline{PQ} = a$	$\overline{CP} = \xi'$
$\overline{PT} = b$	$\overline{PA} = m$
$\overline{PH} = s$	

The triple integral appearing in Equation (1) cannot be expressed in closed form by means of elementary functions. However, introducing a system of polar coordinates (m, θ, ϕ) with origin at P (Figure 7), replacing ξ_1 by $m - \xi_0$ and dV by $m^2 dm \sin\theta \, d\theta \, d\phi$, the integrations over ϕ and m can be performed at once. We then obtain

$$I_P(\mu_1, \mu_0) = \frac{2\pi C}{\mu_1} \int_{\theta=0}^{\theta_0} e^{-\mu_0 \xi_0} \left[1 - e^{-\mu_1(\xi' - \xi_0)} \right] \sin\theta \, d\theta \quad , \tag{2}$$

*Let d be the density of the radioactive material inside the sphere. Then, if a small mass, Δm, of that material were concentrated in a volume element Δv, the intensity at unit distance from this fictitious point source in the absence of absorption would be equal to $C\Delta v = C/d \cdot \Delta m$.

where

$$\theta_0 = \text{arc tg } \frac{R}{s} \qquad \left(0 < \theta_0 < \frac{\pi}{2}\right) \quad , \tag{3}$$

$$\xi_0(\theta) = g \cos\theta - \sqrt{g^2 \cos^2\theta - s^2} \tag{4}$$

$$\xi'(\theta) = \frac{s^2}{\xi_0(\theta)} = g \cos\theta + \sqrt{g^2 \cos^2\theta - s^2} \quad . \tag{5}$$

The symbols in these equations have the following meaning (see Figure 7):

a) g is the distance from the center of the sphere, O, to the point P;

b) R denotes the radius of the sphere, and

$$s \equiv \sqrt{g^2 - R^2} \quad ;$$

c) ξ_0, ξ', and ξ_1 are, respectively, the distances $\overline{PB}$, $\overline{PC}$, and $\overline{BA}$, so that

$$\xi_0 + \xi_1 = m \quad .$$

Equations (4) and (5) follow very easily from elementary trigonometry applied to the triangles COP and BOP, since ξ_0 and ξ' are the two solutions of the quadratic equation

$$R^2 = x^2 + g^2 - 2\,gx \cos\theta \quad .$$

The right hand side of Equation (2) can be transformed in various ways, none of which, however, represents a real simplification. For example, if we put $\cos\theta = u$, as was done by D. V. Gopinath, Equation (2) takes the form

$$I_P(\mu_1, \mu_0) = \frac{2\pi C}{\mu_1} \int_{u=\sqrt{1-z^2}}^{1} e^{-\mu_0(gu - w)} \left[1 - e^{-2\mu_1 w}\right] du \tag{6}$$

with

$$z \equiv \frac{R}{g} \qquad (0 < z < 1) \tag{7}$$

and

$$w(u) = [R^2 - g^2 (1 - u^2)]^{1/2} \quad .$$

On the other hand, introducing ξ_0 as a new independent variable instead of θ, so that

$$2\,g\cos\theta = \xi_0 + \frac{s^2}{\xi_0}$$

and

$$\sin\theta\,d\theta = \frac{1}{2g}\left(\frac{s^2}{\xi_0^2} - 1\right) d\,\xi_0 \quad ,$$

we find

$$\frac{g\mu_1}{\pi C}\,I_P(\mu_1, \mu_0) = -L + M + K \quad , \tag{8}$$

where L, M, and K represent the following quantities:

$$L \equiv \int_{y=a}^{s} \frac{s^2}{y^2}\, e^{\nu y - \frac{\mu_1 s^2}{y}}\, dy \quad ,$$

$$M \equiv \int_{y=a}^{s} e^{\nu y - \frac{\mu_1 s^2}{y}}\, dy \quad ,$$

$$K \equiv \int_{y=a}^{s} \left(\frac{s^2}{y^2} - 1\right) e^{-\mu_0 y}\, dy \quad .$$

In these equations we have put

$$\nu \equiv \mu_1 - \mu_0$$

and

$$a \equiv g - R$$

($a > 0$ if the point P lies outside the sphere). Integrating by parts we see that

$$L = \frac{1}{\mu_1}\left[e^{-\mu_0 s} - e^{-\mu_0 a - 2\mu_1 R}\right] - \frac{\nu}{\mu_1}\,M \quad .$$

Furthermore, the integral K can be written in closed form as follows:

$$K = \frac{1}{\mu_0}\left[e^{-\mu_0 s} - e^{-\mu_0 a}\right] + be^{-\mu_0 a} - se^{-\mu_0 s} + \mu_0 s^2\left[Ei(-\mu_0 a) - Ei(-\mu_0 s)\right] , \tag{9}$$

where

$$b \equiv g + R \quad ,$$

and the remaining symbols have the same meaning as before. Also, in Equation (9)

$$Ei(-x) \equiv -\int_{t=x}^{\infty} \frac{e^{-t}}{t}\, dt \qquad (x > 0)$$

is the exponential integral. It can be considered as a known function for all practical purposes, since extensive tables, as well as approximate formulae to compute it for very small and very large values of x, are available.[6,7]

However, there seems to be no simple expression for M, although it is interesting to note that the integrand in M is essentially equal to the generating function of Bessel coefficients. We have putting

$$\zeta \equiv 2\, s \sqrt{\nu\mu_1} \quad ,$$

$$t_1 \equiv \sqrt{\frac{a\nu}{b\mu_1}} \quad ,$$

and

$$t_2 \equiv \sqrt{\frac{\nu}{\mu_1}} \quad ,$$

$$M = s \cdot \sqrt{\frac{\mu_1}{\nu}} \int_{t=t_1}^{t_2} e^{\frac{\zeta}{2}\left(t - \frac{1}{t}\right)}\, dt \quad . \tag{10}$$

It is well known (pp. 14-15 of Reference 8) that

$$e^{\frac{\zeta}{2}\left(t - \frac{1}{t}\right)} = J_0(\zeta) + \sum_{n=1}^{\infty}\left[t^n + (-1)^n t^{-n}\right] J_n(\zeta) \quad ,$$

so that, inserting this expression into Equation (10) and performing the integration over t, the quantity M can be represented as a Neumann series (p. 522 of Reference 8) in the variable ζ.* But this fact does not seem to have important consequences for practical applications.

The following are interesting special cases of Equation (2).

1. In practice we may often set $\mu_0 = 0$, $\mu_1 \neq 0$. Then Equation (8) becomes

$$I_P(\mu_1, 0) = \frac{2\pi C}{g\mu_1}\left\{g - s - \frac{\left(1 - e^{-2\mu_1 R}\right)}{2\mu_1} + \int_{y=a}^{s} e^{\mu_1\left(y - \frac{s^2}{y}\right)} dy\right\} , \quad (11)$$

and Equation (6) simplifies to

$$I_P(\mu_1, 0) = \frac{2\pi C}{\mu_1}\int_{u=\sqrt{1-z^2}}^{1}\left[1 - e^{-2\mu_1 w}\right] du , \quad (12)$$

or, introducing the new independent variable

$$t(u) = \frac{w(u)}{R} = \left[1 - \frac{(1-u^2)}{z^2}\right]^{1/2} ,$$

$$I_P(\mu_1, 0) = \frac{2\pi C}{\mu_1}\int_{t=0}^{1}\left(1 - e^{-2\mu_1 R t}\right)\frac{z^2 t}{\sqrt{1 + z^2(t^2 - 1)}} dt .$$

Integrating by parts this is transformed into

$$I_P(\mu_1, 0) = \frac{2\pi C}{\mu_1}\left\{1 - e^{-2\mu_1 R} - 2\mu_1 R\int_{t=0}^{1}\left[1 + z^2(t^2-1)\right]^{1/2} e^{-2\mu_1 R t} dt\right\}$$

$$= 4\pi C R\int_{t=0}^{1}\left[1 - \sqrt{1 + z^2(t^2-1)}\right] e^{-2\mu_1 R t} dt . \quad (13)$$

---

*Slight modifications are appropriate if $\mu_1 < \mu_0$. Then ζ, t_1, and t_2 become purely imaginary; hence the Bessel functions $J_n(\zeta)$ are conveniently replaced by $i^n I_n(-i\zeta)$.

2. If both media have the same absorption coefficient ($\mu_0 = \mu_1 = \mu \neq 0,\ \nu = 0$) we obtain

$$I_P(\mu, \mu) = \frac{\pi C}{g\mu} \left\{ \mu s^2 \left[Ei(-\mu a) - Ei(-\mu b) \right] + be^{-\mu a} - ae^{-\mu b} + \frac{1}{\mu} \left[e^{-\mu b} - e^{-\mu a} \right] \right\} \quad . \tag{14}$$

This case, however, is less likely to be met with in actual experimental situations.

3. Letting μ_0 and μ_1 tend to zero we find

$$I_P(0, 0) = \frac{\pi C}{g} \left\{ 2gR + (g^2 - R^2) \ln \left(\frac{g - R}{g + R} \right) \right\} \quad , \tag{15}$$

which coincides with Souttar's result provided we equate our constant C to his quantity $\rho/4$. (Souttar's a corresponds to our R and his x to our g.)

Remembering that $z = R/g$, Equation (15) can also be written in the form

$$I_P(0, 0) = 4\pi CR \left\{ \frac{1}{2} - \frac{(1 - z^2)}{4z} \ln \left(\frac{1 + z}{1 - z} \right) \right\} \quad . \tag{16}$$

Thus, if we put

$$\rho \equiv 2\mu_1 R \quad , \tag{17}$$

the quantity

$$k \equiv \frac{I_P(\mu_1, 0)}{I_P(0, 0)} \tag{18}$$

i.e., the ratio of intensities at P with and without absorption inside the sphere (if $\mu_0 = 0$), may be represented as a function of the two parameters z, ρ as follows:

$$\left.\begin{aligned} k &= F(z, \rho) \\ \text{with} \quad F(z, \rho) &= \frac{2 \displaystyle\int_{t=0}^{1} \left[1 - \sqrt{1 + z^2(t^2 - 1)} \right] e^{-\rho t}\, dt}{\left[1 - \dfrac{(1 - z^2)}{2z} \ln \left(\dfrac{1 + z}{1 - z} \right) \right]} \quad . \end{aligned}\right\} \tag{19}$$

4. If the point P moves to Q, on the surface of the sphere, the intensity at Q becomes

$$I_Q(\mu_1) = \frac{\pi C}{R\mu_1^2}\left[-1 + 2\mu_1 R + e^{-2\mu_1 R}\right] \tag{20}$$

and is, of course, independent of μ_0.

5. For the sake of completeness we also mention the case $g < R$ (i.e. P inside the sphere). Then a simple calculation gives

$$I_P(\mu_1) = \frac{4\pi C}{\mu_1} + \frac{\pi C(R^2 - g^2)}{g}\left[Ei(-\beta) - Ei(-\alpha)\right]$$

$$+ \frac{\pi C}{g\mu_1^2}\left[(1+\alpha)\, e^{-\beta} - (1+\beta)\, e^{-\alpha}\right] , \tag{21}$$

where

$$\alpha \equiv \mu_1 (R - g) > 0 ,$$

and

$$\beta \equiv \mu_1 (R + g) .$$

If

$$\mu_1 \to 0$$

this becomes

$$I_P(0) = \frac{\pi C}{g}\left[2gR - (R^2 - g^2)\ln\left(\frac{R-g}{R+g}\right)\right] \qquad (g \le R) . \tag{22}$$

II. In this Division, Sinclair has performed several experiments to determine the average absorbed dose of spherical (and cylindrical) specimens exposed to Co^{60} γ-radiation.[9] He suggests that, theoretically, the effect of absorption can be taken into account as follows: the ratio k, Equation (18) above, should be equal to the self-absorption coefficient for the sphere, say v, as given in Thirring's and von Schweidler's papers.[10,11] While this procedure constitutes a useful approximation when R/g is small, as in Sinclair's experiments, it is not rigorously correct. In fact, the intensity I_P [Equation (1)], which is the appropriate quantity to use in applying the reciprocity law, refers to the amount of radiant energy absorbed by a small volume element at P, whereas the self-absorption coefficient, v, may

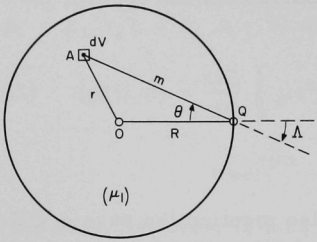

Figure 8. Spherical source, as in Figure 7, showing details for the calculation of the self-absorption coefficient v.

be interpreted as the ratio of two currents. More precisely, let Q be a point on the sphere and define

$$j_Q(\mu_1) = C \iiint \frac{(m^2 + R^2 - r^2)}{2m^3 R} e^{-\mu_1 m} \, dV \quad , \tag{23}$$

where C is a constant, $m = \overline{QA}$, $r = \overline{OA}$ (Figure 8), and the integration is extended to the whole sphere. We see that $j_Q(\mu_1)$ differs from $I_Q(\mu_1)$, Equation (1) with $P \to Q$, in that the integrand of Equation (23) contains the factor $\frac{(m^2 + R^2 - r^2)}{2mR} = \cos \Lambda$. Thus, $j_Q(\mu_1)$ is the normal component of the energy flux through an infinitesimal surface dS at Q, due to all volume elements inside the sphere. The ratio v is defined as $j_Q(\mu_1)$ divided by the same quantity for $\mu_1 = 0$:*

$$v = \frac{j_Q(\mu_1)}{j_Q(0)} \quad . \tag{24}$$

Now, $j_Q(\mu_1)$ can easily be calculated:

$$j_Q(\mu_1) = 2\pi C \int_{\theta=0}^{\pi/2} \int_{m=0}^{2R\cos\theta} \cos\theta \; e^{-\mu_1 m} \, dm \sin\theta \, d\theta$$

$$= \frac{2\pi C}{\mu_1} \int_{u=0}^{1} u \left[1 - e^{-\rho u}\right] du$$

$$= \frac{4\pi CR}{\rho^3} \left[\frac{\rho^2}{2} - 1 + (\rho + 1) e^{-\rho}\right] \quad .$$

On the other hand,

$$j_Q(0) = \frac{4\pi CR}{3} \quad ,$$

and so:

$$v(\rho) = \frac{3}{\rho^3} \left[-1 + \frac{\rho^2}{2} + (\rho + 1) e^{-\rho}\right] \tag{25}$$

---

*Actually $v = \frac{J_Q(\mu_1)}{J_Q(0)}$, where J_Q is the integral of j_Q over the surface of the whole sphere. However, for for this particular geometry the surface integration merely adds a factor $4\pi R^2$ to both the numerator and the denominator of Equation (24).

or, expanding the exponential function in powers of ρ

$$v(\rho) = 3 \sum_{\lambda=0}^{\infty} (-1)^{\lambda} \frac{1}{(\lambda+1)(\lambda+3)} \frac{\rho^{\lambda}}{\lambda!}$$

$$= 1 - \frac{3}{8}\rho + \frac{1}{10}\rho^2 - \frac{1}{48}\rho^3 + - \ldots \quad , \tag{26}$$

which is von Schweidler's result.

Let us compare this with the corresponding ratio of intensities for a point Q on the surface of the sphere. From Equation (19) or (20) we obtain

$$\frac{I_Q(\mu_1)}{I_Q(0)} = F(1, \rho) = 2 \int_{t=0}^{1} (1-t)\, e^{-\rho t}\, dt$$

$$= \frac{2}{\rho^2}\left[-1 + \rho + e^{-\rho}\right] = 2 \sum_{\lambda=0}^{\infty} \frac{(-1)^{\lambda}}{(\lambda+2)!} \rho^{\lambda}$$

$$= 1 - \frac{\rho}{3} + \frac{\rho^2}{12} - \frac{\rho^3}{60} + - \ldots$$

$$= 2e^{-\rho} \sum_{\lambda=0}^{\infty} \frac{1}{(\lambda+2)} \frac{\rho^{\lambda}}{\lambda!} \quad . \tag{27}$$

Since we also have

$$v(\rho) = \frac{3}{2} e^{-\rho} \sum_{\lambda=0}^{\infty} \frac{(\lambda+4)}{(\lambda+2)(\lambda+3)} \frac{\rho^{\lambda}}{\lambda!} \quad ,$$

it is clear that, for any fixed positive value of ρ, the right hand side of Equation (27) will be larger than $v(\rho)$.

Strictly speaking, therefore, Equations (18) and (19) should be used in applying the reciprocity theorem when $\mu_0 = 0$. Even so, of course, the results will be only approximately true. In particular, the three restrictive assumptions mentioned by Kovalev (Reference 4, page 116) must always be kept in mind.

Von Schweidler's ratio, $v(\rho)$, a quantity which depends only on the geometry of the source and on the absorption coefficient within the source,

is merely a number which may conveniently be used to characterize the effects of self-absorption for the source as a whole. But, at least in the simple case of the sphere, a ratio such as $F(1, \rho)$, Equation (27), could equally well serve the same purpose.

Returning now to Equation (19), we may expand the denominator on the right hand side in powers of z:

$$1 - \frac{(1 - z^2)}{2z} \ln \left(\frac{1+z}{1-z}\right) = 2 \cdot \sum_{n=1}^{\infty} \frac{z^{2n}}{(2n-1)(2n+1)} ,$$

which shows that $F(z, \rho)$ depends on z^2 rather than on z itself. Then, using de l'Hôpital's rule, we let z^2 tend to zero and find:

$$\lim_{z \to 0} k = -\frac{3}{2} \int_{t=0}^{1} (t^2 - 1)\, e^{-\rho t}\, dt$$

$$= \frac{3}{\rho^3} \left[-1 + \frac{\rho^2}{2} + (\rho + 1)\, e^{-\rho}\right] = v(\rho) .$$

From this last equation it follows that, as we have already mentioned, Sinclair's procedure will be applicable within the limits of experimental error if R/g is kept sufficiently small.

References

1. King, L. V. Absorption problems in radioactivity. Phil. Mag. 23, 242-250 (1912).

2. Meyer, S., and E. von Schweidler. Radioaktivität. Teubner, Berlin, 1927. pp. 82-87.

3. Mayneord, M. V. Energy absorption. IV. The mathematical theory of integral dose in radium therapy. Brit. J. Radiol. 18, 12-19 (1945).

4. Kovalev, E. E. The intensity of gamma radiation emitted by a cylindrical source. Intern. J. Appl. Radiation and Isotopes 3, 113-118 (1958).

5. Souttar, H. S. On fields of radiation from radon seeds. Brit. J. Radiol. 4, 681-689 (1931).

6. Tables of sine, cosine, and exponential integrals, vol. I. Federal Works Agency, Work Projects Administration for the City of New York, 1940.

7. Bromwich, T. J. I'A. An Introduction to the Theory of Infinite Series, 2nd ed. Macmillan, London, 1947. pp. 334 ff.

8. Watson, G. N. Theory of Bessel Functions, 2nd ed. University Press, Cambridge; Macmillan Co., New York, 1945. pp. 14-15.

9. Sinclair, W. K. Absorbed dose in externally irradiated biological specimens I. Co^{60} gamma radiation. Biological and Medical Research Division Semiannual Report, January through June 1961. Argonne National Laboratory, ANL-6464. pp. 133-142.

10. Thirring, H. Über den Einfluss der Absorption im Inneren eines radioaktiven Präparates auf die ausgesendete Strahlung. Physik. Zeitschr. 13, 266-268 (1912).

11. von Schweidler, E. Über die Strahlung, einer mit radioaktivem Material erfüllten Kugel. Physik Zeitschr. 13, 453-454 (1912).

FAST AND EPITHERMAL FLUXES IN NEUTRON RADIOBIOLOGICAL FACILITIES

Norman A. Frigerio and Donn L. Jordan

It has been shown that a high degree of contamination of fast neutron fluxes by thermal and epithermal neutrons is an inevitable consequence of the shielding used in fast neutron radiobiological facilities.(1) The presence of such moderated neutrons is evident from the foil measurements which have been made in these facilities(2-7) and is significant even in such relatively "bare" facilities as Godiva.(8) Recent studies (9,10) have indicated that neutrons in the epithermal region (0.1 to 500,000 ev) are of considerable biological importance and probably have RBE values higher than those characteristic of either fast or purely thermal neutrons. Further, the radiobiology of neutrons in this energy region is but poorly understood. Thus, in fast neutron studies, it would be well to eliminate, or at least minimize, contamination of fast neutron fluxes by such epithermal neutrons.

Elimination of purely thermal neutrons from fast fluxes is a relatively simple process since thermal absorbers of high cross section are readily available. Such absorbers, placed over the neutron source and around the significant moderating shields, effectively remove all of the direct and reflected thermal neutrons from the fast flux. Li^6 is to be preferred since it alone, of the practical thermal absorbers, produces no gamma contamination of the fast neutron flux.

Absorbers with useful removal cross sections for epithermal neutrons are not at present available and, consequently, the absorption method is not feasible. However, at least in fission neutron facilities, the ratio of fast flux to epithermal flux delivered to a given point in the facility is primarily a function of the distance of the point from the fission source. Thus, it is possible to minimize the epithermal contribution to the dose received by an organism in a fission neutron facility by locating the organism close to the fission source. The effects of shielding on neutron spectra are illustrated, using CP-5(11) and the JANUS reactor as examples.

To a good approximation the animal positions can be considered to lie at the center of a rectangular space with the converter at one end of the longest dimension, x, and with the center of the converter taken as the coordinate origin.

Each thermal neutron yields 2.5 fission neutrons (pp. 1-26 of Reference 12). Thus, the converter represents a source, to the animal space, of fission neutrons of strength S_0, given by

$$S_0 = 2.5\pi a^2 \phi_{Th} [1 - \exp(-\Sigma_f h)] \quad . \qquad (1)$$

Here a is the effective radius of the converter plate, ϕ_{Th} the thermal flux at the plate, Σ_f the macroscopic fission cross section of the plate, and h its thickness.

The fission neutron flux, ϕ_f, at the animal position at distance d from the converter plate is then given by[13]

$$\phi_f = \frac{S_0}{4\pi a^2} \ln \frac{d^2 + a^2}{d^2} \tag{2}$$

At the shield walls the fission flux rapidly suffers random moderation and reflection so that $\overline{\phi}_m$, the mean moderated flux at the animal space after n reflections from the wall, is given by

$$\overline{\phi}_m = \frac{S_0}{4\pi \overline{b}^2} (\beta + \beta^2 + \beta^3 \ldots . \beta^n) \quad . \tag{3}$$

Here β is the fraction reflected from the shield walls, usually called the albedo (pp. 6-41 of Reference 12) and $\overline{b}$ the mean distance from the walls to the animal position. In the real case n is very large and $\beta < 1$ so that Equation (3) reduces to

$$\overline{\phi}_m = \frac{S_0}{4\pi \overline{b}^2} \left(\frac{1}{1-\beta} - 1\right) \tag{4}$$

for large values of n.

This moderated flux will add to the fission flux by causing new fissions at the converter plate. The mean flux of new fission neutrons from this source, $\overline{\phi}_{f'}$, is given by

$$\overline{\phi}_{f'} = \frac{2.5\, \overline{\phi}_m [1 - \exp(-\Sigma_f' h)]}{4} \ln \frac{d^2 + a^2}{d^2} \quad . \tag{5}$$

Here Σ_f' is the macroscopic fission cross section for moderated fission neutrons.

For a small converter plate located close to the animal position, the thermal entry port simply represents a thermal source of strength $\phi_{Th}\pi c^2$, where c is the effective radius of the port since no fission multiplication occurs at the port. Although no further moderation can occur in the completely moderated thermal neutrons, reflection results in a thermal flux at the small converter plate close to the animal position which is given by an equation of the form of Equation (3). Hence, the small plate is a source of strength S_0', given by

$$S_0' = \frac{\pi c^2}{4(\bar{b})^2} \phi_{Th} a^2 (\beta + \beta^2 + \beta^3 \ldots . \beta^n) (1 - \exp(-\Sigma_f h)) \quad . \qquad (6)$$

For large values of n this reduces to

$$S_0' = \frac{\pi c^2 \phi_{Th} a^2}{4(\bar{b})^2} \left[\frac{1}{1-\beta} - 1 \right] \left[1 - \exp(-\Sigma_f h) \right] \qquad (7)$$

as before, and S_0' may be substituted for S_0 in Equations (2) through (5).

The results of calculations for the two conditions (a) large plate-large distance and (b) small plate-small distance are presented in Table 6 for JANUS and for CP-5. It can be seen that condition (b) results in a much higher ratio of fission flux to moderated flux at the animal position than does condition (a). Thus condition (b) is much to be preferred for investigations of the effects of undegraded fission spectra.

TABLE 6

Calculated and observed fission neutron fluxes and moderated neutron fluxes at CP-5 and JANUS under condition (a) (large converter plate - large distance to exposure position) and under condition (b) (small plate - small distance).

Facility	CP-5		JANUS	
Condition	a	b	a	b
Converter plate area, cm^2	1650	80	10,000	80
Distance,* cm	150	1	390	1
Calculated $(\phi_f + \phi_{f'})/\bar{\phi}_m$	1.04	710	1.15	4150
Observed ϕ fast/ϕ epithermal	1.00	287	-	-

* Distance from exposure position to converter plate.

It proved possible to check this conclusion experimentally at the CP-5 facility. Known masses of gold and sulfur, with and without cadmium casings, were exposed in the facility under the normal operating conditions of a 1650-cm^2 converter plate 150 cm from the animal position. The boral shutter and plate were removed, and the pile was operated at 4.6 megawatts.

Then the large converter plate was replaced by an 81-cm^2 plate 1 cm from the animal position, and a new set of gold and sulfur foils was exposed as before. Thermal, epithermal and fast fluxes were computed as in previous studies,[1] and the results are also presented in Table 6. Despite the simplifying assumptions necessary in the derivations and the crudity of foil measurements for spectral studies, the agreement is surprisingly good.

From the form of the various equations it can be seen that the critical parameters are a and d. Thus, for a given facility, some optimum combination of these must exist which will yield the highest fission flux and lowest moderated flux. This can be estimated from the equations given, and checked, where appropriate, by foil measurements.

References

1. Frigerio, N. A. Moderated neutron flux. Biological and Medical Research Division Semiannual Report, July through December 1957, Argonne National Laboratory, ANL-5841. pp. 123-127.
2. Handloser, J. S. and N. Delihas. Neutron flux within the Brookhaven biological facility. Brookhaven National Laboratory Report, BNL-386 (1955).
3. Hughes, D. J. Pile Neutron Research. Addison-Wesley, Cambridge, 1953. pp. 58-64.
4. Sheppard, C. W., M. Slater and G. J. Atta. A theory for heterogeneous ion chambers and neutron response of Victoreen dosimeters. Radiation Research 7, 342-356 (1957).
5. Walton, H., Jr. Thermal contribution to a fast neutron exposure. Quarterly Report of Biological and Medical Research Division, Argonne National Laboratory. ANL-5378 (1955), pp. 121-122.
6. Delihas, N., and H. J. Curtis. The relative biological effectiveness of fission neutrons for the production of acute mortality in mice. Radiation Research 8, 166-180 (1958).
7. Curtis, H. J., personal communication.
8. Rosen, L. Energy spectra. Proc. Intern. Conf. Peaceful Uses of Atomic Energy, United Nations, Geneva, 1956. Vol. 4, p. 100.
9. Bateman, J. L. and H. H. Rossi. The dependence of RBE on energy of fast neutrons. Radiation Research 15, 694-706 (1961).
10. Storer, J. B., P. S. Harris, J. E. Furchner and W. H. Langham. The relative biological effectivenss of various ionizing radiations in mammalian systems. Radiation Research 6, 188-288 (1957).

11. Vogel, H. H., Jr., J. W. Clark and D. L. Jordan. Modification of the gamma-neutron radiation chamber for use at the Argonne Research Reactor. Quarterly Report of Biological and Medical Research Division, Argonne National Laboratory. ANL-5288 (1954), pp. 35-36.

12. Etherington, H. Nuclear Engineering Handbook. McGraw-Hill, New York, 1958. pp. 1-26.

13. Hine, G. J. and G. L. Brownell. Radiation Dosimetry. Academic Press, New York, 1956. pp. 762-763.

INCIDENCE OF MAMMARY NEOPLASMS IN NEUTRON- AND GAMMA-IRRADIATED FEMALE SPRAGUE-DAWLEY RATS

Howard H. Vogel, Jr., and Donn L. Jordan

Over the past several years a series of reports has appeared showing that total-body irradiation of young female Sprague-Dawley rats with single sublethal doses of X- or gamma radiation resulted in the production of numerous mammary gland neoplasms.[1,2] The response to total-body irradiation appeared to be dose-dependent in the range studied (25-400 r).[2] The present experiments were designed (a) to compare the relative effects of two external radiations, fission neutrons and Co^{60} gamma rays, on the induction of mammary neoplasms in this rat, (b) to study the effects of different dose-rates of these radiations on this end-point, and (c) to extend observations on the incidence and frequency of these neoplasms, as well as to obtain longevity data in irradiated and control rats.[3]

Materials and Methods

Animals

The animals used were young female Sprague-Dawley rats bred at Argonne National Laboratory; the original breeding colony ("specific-pathogen-free") was started with Sprague-Dawley rats taken by cesarean section and fostered by Lobund "germ-free" mothers.[4] All rats used in this experiment were taken from litters born during the same week (1/10/60 - 1/16/60). After weaning, the female rats were isolated in an animal room for a period of several weeks before being randomly assigned to experimental and control groups. The first irradiation was carried out when the animals were approximately 60 days old.

Irradiation

Fission neutrons. Fifty-seven rats in four dose-rate groups were irradiated with 100 rads of fission neutrons once a week for four weeks. The intensities used were 1, 3, 6, and 35 rads/min. Thus the rats received a total of 400 rads of neutrons, but each weekly fraction was a brief exposure lasting only from 3 to 85 minutes, depending on the dose rate. Rats were exposed in special rotation cages, 8 or 9 together, as previously described.[5]

The four neutron dose rates were obtained by varying the size of the opening in a boral shutter within the thermal column of the CP-5 reactor (25%, 50% or 100% open) and by removing the shutter completely. This controlled the number of thermal neutrons allowed to reach a uranium converter plate, the source of the fission neutrons, thus changing the flux and intensity.

Co^{60} gamma irradiation. Gamma-irradiated rats were also divided into four dose-rate groups (1, 3, 6 and 35 rads/min). They were exposed to 200 rads of Co^{60} gamma rays once a week for four weeks.

Exposures to both neutrons and gamma rays were made in the gamma-neutron radiation chamber[6] at CP-5, with the exception of the highest gamma-ray dose rate, for which the High-Level Gamma Room[7] was used, since this intensity could not be attained in the CP-5 gamma chamber. The other three gamma-ray dose rates were achieved by varying the distance between the animal exposure position and 18 Co^{60} sources.[6] The weekly exposures to gamma rays took from 6 minutes to more than 3 hours.

All animals were maintained in temperature-controlled rooms (74 ± 3°F) and were given food and water ad libitum. Mortality checks were made twice a day. Every two weeks, the rats were examined carefully for palpable mammary tumors, and growth of tumors was measured with calipers. Animals were weighed once a month.

Each rat was necropsied, but no histological work was carried out in this experiment, since the pathology and relative frequency of mammary neoplasms in this rat strain has been studied intensively by other investigators.[2, 8, 9]

Results

The regime of fractionated radiation exposures used in this experiment produced a large number of mammary tumors. Of 112 irradiated rats, 92% had palpable mammary neoplasms. The incidence of these tumors, for all dose-rate groups and both radiations, is listed in Table 7. It is clear from these data that the incidence of neoplasms is very high, that the latent period is not long, and that the process is a continuing one. Mammary tumors began to appear in each of the irradiated groups within 70 days after the first exposure, and new tumors continued to appear in the irradiated rats throughout their lives. The longest time from first irradiation to palpable mammary tumor in this series of rats was 569 days. Only 2 rats exposed to gamma rays and 7 exposed to neutrons died without palpable mammary tumors.

TABLE 7

Incidence of palpable mammary neoplasms in female Sprague-Dawley rats given neutron- or gamma-irradiation at four different dose rates

Periods, days from first irradiation	Fission neutrons						$Co^{60}\gamma$-rays					
	Dose-rate, rads/min				Total incidence	Cumulative %	Dose-rate, rads/min				Total incidence	Cumulative %
	1	3	6	35			1	3	6	35		
1-100	5	3	5	4	17	30	3	5	2	2	12	22
101-200	3	3	2	2	10	47	1	2	1	3	7	34
201-300	3	1	3	2	9	63	4	1	2	2	9	51
301-400	0	4	1	2	7	75	3	3	5	1	12	72
401-500	1	0	2	2	5	84	2	1	3	3	9	90
501-600	0	2	0	0	2	88	1	1	1	1	4	96
Totals	12	13	13	12	50		14	13	14	12	53	
No definite mammary tumors observed	2	1	1	3	7	12	0	0	0	2	2	4

In Figure 9 the cumulative incidence (%) of rats with mammary tumors is plotted against time in months after first irradiation. It is clear from this graph that the neutron-irradiated rats had a shorter latent period and an increased tumor rate over most of their life span. This is interesting since the neutron dose in rads was only half that given the gamma-irradiated animals. Clearly, the RBE (n/gamma) for this endpoint is greater than 2.

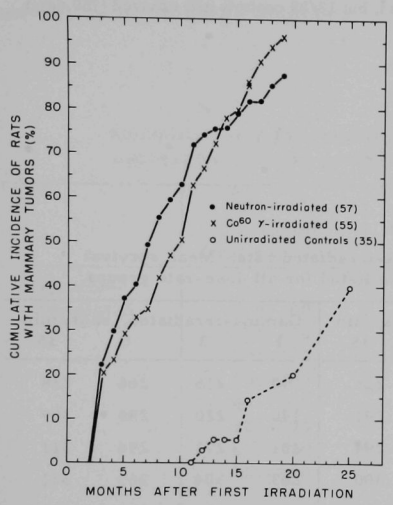

Figure 9

Cumulative incidence of female Sprague-Dawley rats with mammary neoplasms. Rats irradiated with either fission neutrons (100 rads a week, for four weeks) or Co^{60} γ-rays (200 rads a week, for four weeks) compared with unirradiated controls. Numbers in parentheses are number of rats.

In Figure 10 the cumulative mortality is plotted against time, for the 26-month period after first exposure, with the dose-rate groups combined. These mortality data indicate that the neutrons are more effective than the gamma rays, even though the total neutron dose was less by a factor of two. The RBE for this second endpoint must also exceed 2. It is interesting to note that the RBE (n/gamma) for acute 30-day mortality in the female mouse (CF No. 1) under these experimental conditions was reported to be 2.7.[5] Of the control unirradiated rats, 65% were alive after 2 years. When this graph was constructed, 800 days after first exposure, 13 of the 35 control rats were still alive. During the course of this experiment we had no difficulties with epizootic infections or the respiratory infections common in many rat colonies.[9] In Table 8 are listed the survivorship data for the 8 dose-rate groups of irradiated animals. The numbers in each dose-rate group are small, but there is no evidence that a change in intensity causes any significant difference in life span in either the neutron- or the gamma-irradiated rats. Therefore the groups were combined for analysis in Figure 10.

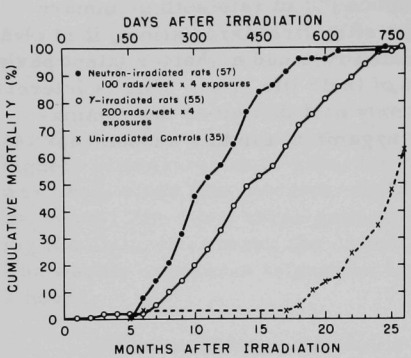

Figure 10

Cumulative mortality plotted for neutron- and γ-irradiated rats, and their unirradiated controls. After 26 months all of the irradiated rats were dead, but 13/35 controls still survived (780 days).

TABLE 8

Longevity data for the neutron- and gamma-irradiated rats. Mean survival times and standard errors of the means are listed for all dose-rate groups.

	Neutron-irradiated, rads/min				Gamma-irradiated, rads/min			
	1	3	6	35	1	3	6	35
Longevity, days	165	160	155	215	90	215	266	238
	189	175	158	291	190	220	288	309
	228	246	189	294	201	273	294	311
	232	252	191	300	263	304	365	331
	239	265	264	309	358	332	394	341
	258	273	290	312	416	343	410	382
	267	299	317	356	492	368	428	411
	276	299	343	361	528	380	463	509
	311	400	372	367	561	427	466	532
	385	425	382	397	573	506	510	551
	391	435	411	398	618	508	512	610
	401	500	484	415	635	660	533	661
	431	618	511	441	679	683	584	683
	485	732	528	473 518	697		588	773
Number of animals	14	14	14	15	14	13	14	14
Mean survival times, days	304.1	362.8	328.2	363.1	450.1	401.5	435.8	474.4
Standard error of the mean, days	±26.2	±44.4	±34.2	±20.6	±53.2	±41.8	±28.3	±44.3

The mortality rates over an 800-day period, for both irradiated and control rats, are listed in Table 9. All dose rates have been combined for the irradiated populations. The mortality rate was calculated as the ratio between the number of rats dying within periods of 100 days, and the number of rats alive at the beginning of each 100-day period. This table demonstrates that the neutron-irradiated rats died early (only 5 rats in this group survived past the fifth 100-day period). It is apparent that by 500-600 days, when mortality rates are very high among irradiated rats, the controls are not yet dying in large numbers.

TABLE 9

Mortality rates for irradiated and unirradiated rats calculated for successive 100-day periods. All dose-rate groups are combined.

	Interval, days from first exposure	Number of deaths within interval	Number of rats alive at start of interval	Probability of death
Gamma-irradiated	0-100	1	55	0.02
	101-200	1	54	0.02
	201-300	9	53	0.17
	301-400	13	44	0.30
	401-500	8	31	0.26
	501-600	13	23	0.56
	601-700	9	10	0.90
	701-800	1	1	1.00
			0	
Neutron-irradiated	0-100	0	57	0.00
	101-200	8	57	0.14
	201-300	18	49	0.37
	301-400	15	31	0.48
	401-500	11	16	0.70
	501-600	3	5	0.60
	601-700	1	2	0.50
	701-800	1	1	1.00
			0	
Unirradiated controls	0-100	0	35	0.00
	101-200	1	35	0.03
	201-300	0	34	0.00
	301-400	0	34	0.00
	401-500	0	34	0.00
	501-600	4	34	0.12
	601-700	5	30	0.16
	701-800	12	25	0.48
			13	

The data on probability of tumor formation per period are given in Table 10 for both irradiated and control animals. It appears that an irradiated rat has 2 to 3 chances in 10 to develop a mammary tumor during each 100-day period from 100-500 days after first exposure. During this same time the probability that mammary tumors will appear in the control rats is extremely low.

TABLE 10

Probability of mammary neoplasms in neutron-irradiated, γ-irradiated, and unirradiated control rats. Rates were calculated for successive 100-day periods for the irradiated animals. All dose-rate groups are combined.

	Interval, days from first exposure	Number alive at start of interval	Number of rats showing first mammary tumors	Probability of tumor formation
Neutron-irradiated	1-100	57	17	0.30
	101-200	57	10	0.18
	201-300	49	9	0.18
	301-400	31	7	0.23
	401-500	16	5	0.31
	501-600	5	2	0.40
Gamma-irradiated	1-100	55	12	0.22
	101-200	54	7	0.13
	201-300	53	9	0.17
	301-400	44	12	0.27
	401-500	31	9	0.29
	501-600	23	4	0.17
Unirradiated	1-100	35	0	0.00
	101-200	35	0	0.00
	201-300	34	0	0.00
	301-400	34	2	0.06
	401-500	34	2	0.06
	501-600	34	3	0.09
	601-700	30	5	0.17

There was some variation in the time from appearance of the first palpable mammary tumor to the death of the irradiated rats (Table 11). In a few cases, mortality followed rapidly (within a few weeks) after the tumor was first seen. However, in most cases there was a definite steady growth of the tumor, often with new tumors appearing in different sites. Of the neutron-irradiated rats, 76% died between 51 and 200 days after the tumor first appeared. Similarly, 70% of the gamma-irradiated rats died between 51 and 250 days after first observed tumor. Thus, in these Sprague-Dawley female rats, in most cases 2 to 7 or 8 months were required for the mammary tumor to grow large enough to cause the death of the rat.

TABLE 11

Time from first palpable neoplasm to death in the irradiated rats

Time, days	Neutron-irradiated	γ-irradiated
1-50	6	6
51-100	15	7
101-150	10	13
151-200	13	9
201-250	4	7
251-300	0	4
301-350	2	4
>350	0	2
Total	50	52

Many of the rats developed more than one mammary tumor. The data for multiple tumors are listed in Table 12. It is evident that between one-third and one-half of the irradiated rats developed 2 or more mammary tumors during their lifetimes. In both the neutron- and gamma-irradiated animals, an over-all average of 1.5 tumors per rat was observed.

TABLE 12

Distribution of mammary neoplasms observed in neutron- and gamma-irradiated rats

Number of tumors	Neutron-irradiated rats		γ-irradiated rats	
	No.	%	No.	%
0	7	12	2	4
1	25	44	32	58
2	20	35	16	29
3	5	9	4	7
4	-	-	1	2
Total	57	100	55	100

80 mammary neoplasms observed in 50 neutron-irradiated rats = average of 1.5 tumors/rat.

80 mammary neoplasms observed in 53 gamma-irradiated rats = average of 1.5 tumors/rat.

References

1. Bond, V. P., E. P. Cronkite, C. J. Shellabarger, S. W. Lippincott, J. Furth, and R. A. Conard. Mechanisms of induction of mammary neoplasms in rats by radiation: Relation to dose and ovarian status. Progress in Nuclear Energy, Series VI, Biological Sciences. Pergamon Press, London, 1959 Vol. 2, pp. 131-145.

2. Shellabarger, C. J., V. P. Bond, and E. P. Cronkite. Studies on radiation induced mammary gland neoplasia in the rat. IV. The response of females to a single dose of sublethal total-body gamma radiation as studied until the first appearance of breast neoplasia or death of the animals. Radiation Research 13, 242-249 (1960).

3. Vogel, H. H., Jr. and D. L. Jordan. Mammary tumor incidence in female Sprague-Dawley rats irradiated with either fission neutrons or Co^{60} γ-rays. Progress Report (13-month period after first irradiation). Biological and Medical Research Division, Summary Report January through December 1960, Argonne National Laboratory. ANL-6368. pp. 30-32.

4. Flynn, R. J. Personal communication.

5. Rambach, W. A., J. A. D. Cooper, H. L. Alt, H. H. Vogel, Jr., J. W. Clark, and D. L. Jordan. The effect of single and multiple doses of Co^{60} gamma-radiation and fission neutron radiation on the incorporation of Fe^{59} into the rat erythropoietic system. Radiation Research 10, 148-166 (1959).

6. Vogel, H. H., Jr., R. A. Blomgren, and N. J. G. Bohlin. Gamma-neutron radiation chamber for radiobiological studies. Nucleonics 11 (3), 28-31 (1953).

7. Sacher, G. A., D. Grahn, S. Lesher, and K. F. Hamilton. The gamma-ray toxicity program: Calibration and equipment. Quarterly Report of Biological and Medical Research Division, Argonne National Laboratory. ANL-5378 (1955). pp. 91-94.

8. Davis, R. K., T. T. Stevenson, and K. A. Busch. Tumor incidence in normal Sprague-Dawley rats. Cancer Research 16, 194-197 (1956).

9. Finerty, J. C., R. T. Binhammer, M. Schneider, and A. W. B. Cunningham. Neoplasms in rats exposed to single-dose total-body X-radiation. J. Natl. Cancer Inst. 14, 149-153 (1953).

PROGRESS REPORT. LETHALITY OF FRACTIONATED DOSES OF FISSION NEUTRONS AND CO^{60} GAMMA RAYS IN MICE

Donn L. Jordan and Howard H. Vogel, Jr.

The low-level face of the JANUS reactor was designed to permit exposure of animals to extremely low dose rates of fission neutrons; intensities of less than one rad per week should be possible. To obtain some preliminary information to aid in the experimental design for animal irradiation at JANUS, a series of exposures has been carried out at the CP-5 reactor.

The fission neutron facility at CP-5 was designed primarily for single acute exposures.(1) At present, neutron dose rates from 1 to 100 rads/minute are utilized, with the reactor operating at the standard 4.6 megawatts; although continuous exposures at low dose rates over extended periods are not possible, a dose rate of 1 rad/min can be obtained by closing completely a boral shutter in the thermal column of this reactor.(2) This reduces to a minimum the number of thermal neutrons reaching the uranium converter plate and decreases the resultant flux of fission neutrons.

In the present experiment CF No. 1 female mice were exposed to 300 rads of Co^{60} γ-rays or to 60 rads of fission neutrons each week for 13 weeks. The total weekly dose was delivered in 1, 3, or 6 equal fractions for each radiation (Table 13). For these exposures the relative biological effectiveness (RBE) between neutrons and γ-rays was assumed to be 5 (300 rads:60 rads). The RBE for single acute exposures for this mouse at this facility has been reported to be 2.8,(3) but there is considerable evidence that it is higher when animals are irradiated at low rates over long periods.(4) The exposure times were brief (10 min to 5 hr) since the dose rate was approximately 1 rad per min of either fission neutrons or γ-rays.

TABLE 13

Exposure conditions

Irradiation	Number of mice	Exposures/week	Dose/exposure, rads	Dose/week, rads	Total dose, rads
Co^{60} γ-rays	24	6	50	300	3900
	24	3	100	300	3900
	24	1	300	300	3900
	24	0	0	0	0
Fission neutrons	32	6	10	60	780
	32	3	20	60	780
	32	1	60	60	780
	16	0	0	0	0

Mortality figures for the first 100 days following the initial exposure are given in Table 14. It is apparent that the total γ-ray dose was much more lethal than the corresponding neutron dose. The RBE appears to be considerably less than 5 and may be about the same as that found after single acute exposures of the two radiations.

TABLE 14

Mortality 100 days after initial irradiation

Irradiation	Fractionation group	Number dead / number irradiated	Mortality, %
Gamma-rays	6x	13/24	54
	3x	22/24*	92
	1x	23/24**	96
Fisson neutrons	6x	4/32	13
	3x	3/32	9
	1x	1/32	3
Unirradiated controls		1/40 (accidental death)	2

* The mean survival time of the 22 animals that had died was 76.2 days.

** The mean survival time of the 23 animals that had died was 76.3 days.

It is possible that a lower thermal flux may be obtained at CP-5 by increasing the amount of moderating graphite in the thermal column in front of the boral shutter. Experiments are now being planned, utilizing this condition for achieving lower dose rates, to compare the effects of fractionation and protraction of these radiations.

References

1. Vogel, H. H., Jr., R. A. Blomgren, and N. J. G. Bohlin. Gamma-neutron radiation chamber for radiobiological studies. Nucleonics 11 (3), 28-31 (1953).

2. Rambach, W. A., J. A. D. Cooper, H. L. Alt, H. H. Vogel, Jr., J. W. Clark, and D. L. Jordan. The effect of single and multiple doses of Co^{60} gamma-radiation and fission neutron radiation on the incorporation of Fe^{59} into the rat erythropoietic system. Radiation Research 10, 148-166 (1959).

3. H. H. Vogel, Jr., N. A. Frigerio, and D. L. Jordan. Life shortening in mice irradiated with either fission neutrons or cobalt-60 gamma rays. Radiology 77, 600-612 (1961).

4. Neary, G. J., E. V. Hulse, and R. H. Mole. The relative biological efficiency of fast neutrons and gamma-rays for life shortening in chronically irradiated CBA mice. Intern. J. Radiation Biol. 4, 239-248 (1962).

THYMIC TUMOR INCIDENCE AND LONGEVITY IN FEMALE MICE IRRADIATED WITH FISSION NEUTRONS OR CO^{60} γ-RAYS

Howard H. Vogel, Jr., and Donn L. Jordan

When mice are exposed to single acute doses of ionizing radiations, one of the most obvious pathological syndromes resulting is the lymphoid neoplasm. These tumors in mice, often termed lympoid leukemias, have many of the characteristics of lymphosarcomas. Leukemic cells may or may not be present in the peripheral blood. The thymus gland often has a central role in the development of murine leukemia,[1,2] and when it is enlarged, the pathology has been described as thymic lymphoma[3] although most workers attempt to follow Dunn's classification[4] of reticular tumors in the mouse.

Materials and Methods

Young adult female mice of strain CF No. 1 (Carworth Farms, N.Y.) were isolated in one animal room when 5-6 weeks of age and used when approximately 100 days old. Since there is evidence that fractionation or intermittent delivery of a given radiation dose is more leukemogenic than the same total dose given at one time,[5,6] the exposures were carried out over a 21-day period (Table 15). Mice were irradiated at weekly intervals with either 100 rads fission neutrons or 200 rads γ-rays at 4 different dose rates.

TABLE 15

Longevity data in mice exposed once a week for four weeks to fission neutrons or gamma rays

Number of mice	Exposure/week, rads	Number of exposures	Dose rate, rads/min	Mean after-survival* ± standard error, days
Fission neutrons				
32	100	4	1	206.2 ± 18.7
31	100	4	3	145.0 ± 18.7**
32	100	4	6	171.9 ± 15.6
31	100	4	35	148.4 ± 18.8
Co^{60} γ-rays				
22	200	4	1	248.3 ± 21.4
24	200	4	3	247.9 ± 26.6
24	200	4	6	219.5 ± 26.5
22	200	4	35	172.5 ± 21.8
Unirradiated controls				
32	-	-	-	455.8 ± 26.2

* Mean survival times calculated from time of last irradiation. (Pre-irradiation period approximately 121 days)

** One cage in this group of irradiated mice showed very early deaths, 6 mice dying within 90 days after exposure. If this presumably infected cage is omitted from the data, the mean after-survival time of the remaining 24 mice in Group B is approximately 170 days.

Results

Longevity

Figure 11 shows the cumulative mortality of the irradiated mice and the unirradiated controls. For each radiation, the four dose-rate groups are pooled: 126 mice received a total of 400 rads of fission neutrons, and 92 mice were exposed to 800 rads of Co^{60} γ-rays. Reduction in life span in the irradiated mice is obvious. Of the control unirradiated mice, 50% survived 500 days, but only 5% of the neutron-irradiated animals and 15% of the γ-irradiated mice lived more than one year. Based on either the mean survival time (Table 15) or median survival time (Figure 11), lifetimes were reduced by approximately 65% in the neutron-irradiated mice and by approximately 50% in the γ-exposed animals. It is also clear that although the total γ-ray dose in rads was twice the neutron dose, the latter radiation was more effective in reducing longevity. It can, therefore, be stated that, in the CF No. 1 female mouse under this radiation schedule, the relative biological effectiveness (RBE) of fission neutrons/Co^{60} γ-rays was clearly greater than 2 for life-span reduction. (The RBE for this mouse under the experimental conditions at Argonne's CP-5 reactor was 2.8; $LD_{50/30}$ was 323 rads for neutrons and 883 for Co^{60} γ-rays.)

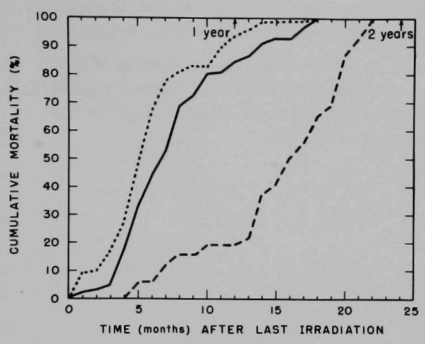

Figure 11. Cumulative mortality for neutron and γ-irradiated mice and unirradiated controls for 2-year period following last fractionated exposure. Dotted line, fission neutrons (126 mice); solid line, Co^{60} γ-rays (92 mice); dashed line, unirradiated controls (32 mice).

Figure 12 shows the mortality vs. time curves for each of the dose-rate groups separately. The mean after-survival times with their standard errors are given in Table 15 for each group. These data strongly suggest a relationship between dose-rate and life span for both radiations. The numbers in each group are small (between 22 and 32), but the lower the instantaneous dose rate, the longer the life span under the conditions of this experiment. The mean survival times of both neutron- and γ-irradiated mice were significantly shorter ($P = 0.02$) when the dose rate was 35 rads/min than when it was 1 rad/min.

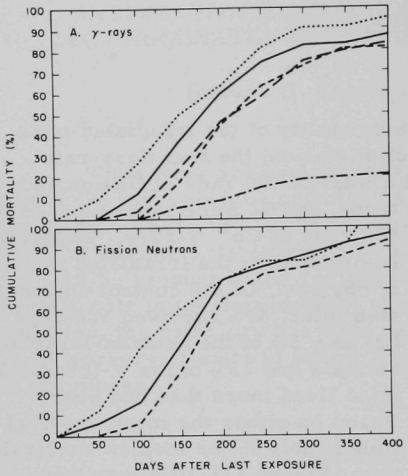

Figure 12

Cumulative mortality for four dose-rate groups of Co^{60} γ-irradiated (upper) and neutron-exposed (lower) mice. Dotted line, 35 rads/min; solid line, 6 rads/min; long dashes, 3 rads/min; short dashes, 1 rad/min; dash-dot-dash, unirradiated controls.

Because the 3 rad/min dose-rate group of the neutron-irradiated mice was presumably infected, it was not included in the data for this graph (see footnote, Table 15).

Incidence of Thymic Tumors

Unirradiated control mice. Thymic tumors were observed at autopsy mainly toward the end of the life span: of 10 controls examined between 572 and 637 days, 7 showed thymic enlargement. Of the other 3, one died with a rectal neoplasm, one with lung tumors, and one was undiagnosed. Thymic tumors are relatively rarer in young CF No. 1 female mice, but they appear to be common as the mice approach 3 years of age.

Irradiated mice. Table 16 gives thymic tumor incidence in the irradiated animals: of 82 mice, exposed to one or the other radiation and necropsied between 90 and 221 days after the last exposure, 80% showed

TABLE 16

Thymic tumor incidence observed in female CF No. 1 mice at autopsy*
(90-221 days after last irradiation)

Dose rate, rads/min	Number of thymic tumors/number of mice autopsied	
	Neutrons	γ-rays
1	14/16	4/5
3	11/13	6/7
6	11/18	6/6
35	6/9	7/8
Total	42/56 (75%)	23/26 (90%)

* Mice were autopsied whenever possible.

grossly enlarged thymus glands. Thus thymic tumors, with or without involvement of other reticular tissues, comprise the chief cause of death in this period in all dose-rate groups for both radiations (Figure 13).

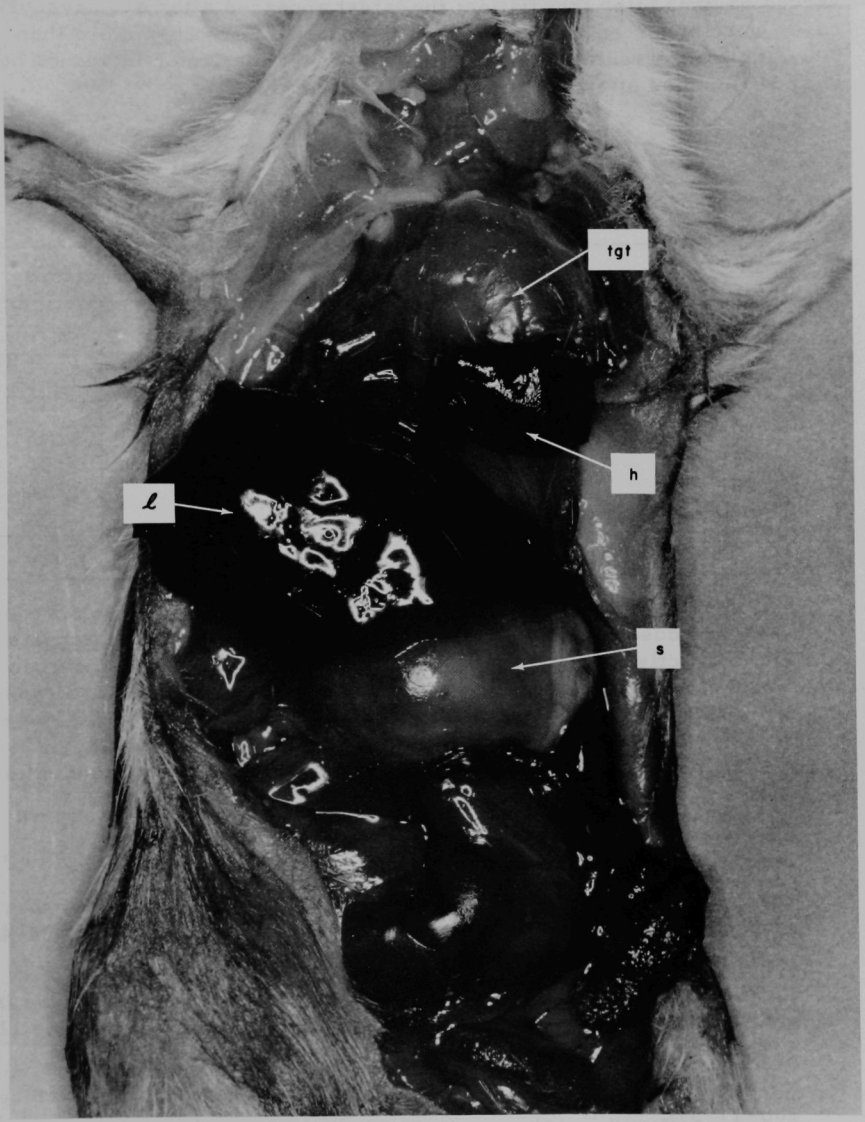

Figure 13. Enlarged thymic gland of neutron-irradiated mouse. Note that tumor has grown around the heart and is gradually constricting its action - tgt, thymus gland tumor; h, heart; l, liver; s, stomach.

Of 80 irradiated mice with thymic tumors observed at autopsy, more than 2 out of 3 died between 106 and 191 days after the last irradiation (γ-rays: 22/30 = 73%; neutrons 32/50 = 64%). The earliest case was observed 53 days after irradiation; the latest appeared after 415 days. Four cases were observed before 90 days, but only 10 were seen more than 200 days after irradiation. Thus the peak of thymic tumor incidence here is at 3-7 months after the last exposure (Table 17).

Table 17

Thymic tumor cases observed at autopsy
for all dose-rate groups combined

Time after last irradiation, days	Co^{60} γ-rays		Fission neutrons	
	Number	%	Number	%
0-50	0	0	0	0
51-100	1	3	8	16
101-150	13	43	19	38
151-200	9	30	16	32
201-250	5	17	3	6
>250	2	7	4	8
Total	30	100	50	100

Previous reports[7,8] have suggested a relationship between leukemia incidence and dose rate of radiation. The present experiment supports this concept indirectly; there appears to be a significant difference between mean survival times of the extreme dose-rate groups (1 rad/min and 35 rads/min), and thymic tumor is the chief cause of death in all groups tested. However, further work must be undertaken with larger numbers of animals and a wider range of radiation intensities before a definitive answer can be given to this problem.

References

1. Duhig, J. T. and S. Warren. Leukemia and reticular neoplasms in the mouse after intermittent irradiation. Radiation Research 14, 404-420 (1961).

2. Kaplan, H. S. and M. B. Brown. Development of lymphoid tumors in non-irradiated thymic grafts in thymic irradiated mice. Science 119, 439-440 (1959).

3. Miller, J. F. A. P. Role of the thymus in murine leukemia. Nature 183, 1069 (1959).

4. Dunn, T. B. Normal and pathologic anatomy of the reticular tissue in laboratory mice, with a classification and discussion of neoplasms. J. Natl. Cancer Inst. 14, 1281-1433 (1954).

5. Sacher, G. A. and A. M. Brues. Analysis of lymphoma induction by X-ray in mice. Cancer Research 9, 620 (1949). Abstract

6. Kaplan, H. S. Radiation-induced leukemia in mice: A progress report. Radiation Biology and Cancer. University of Texas Press, Austin, 1959. pp. 289-302.

7. Mole, R. H. Effects of dose-rate and protraction: A symposium. I. Patterns of response to whole-body irradiation; the effect of dose intensity and exposure time on duration of life and tumor production. Brit. J. Radiol. 32, 497-501 (1959).

8. Mole, R. H. The development of leukemia in irradiated animals. Brit. Med. Bull. 14, 174-177 (1958).

PROGRESS REPORT: DISEASES OF LABORATORY ANIMALS

During the period covered by this report, our efforts were confined principally to three projects: 1) the organizing and editing of a text on laboratory animal diseases, 2) a study to determine whether hamsters are susceptible to or can act as passive carriers of ectromelia virus, and 3) studies of a disease of mice that was first recognized in our animal quarters in February 1962. The progress of the first of these three projects continues satisfactorily. Details concerning the other two are given below.

Lack of Susceptibility of the Syrian Hamster to Ectromelia Virus

Robert J. Flynn and Isabel L. Greco

The Syrian hamster (*Mesocricetus auratus*) has proved to be extremely useful in cancer research as an experimental host for heterologous transplantations both of animal and human neoplasms. Tumors from colonies of laboratory mice in which ectromelia is enzootic may be infected with this virus.[1] For this reason, and also because the two species are frequently maintained in close proximity, it became important to know whether hamsters are susceptible to ectromelia virus. A group of hamsters, some vaccinated and some unvaccinated, were, therefore, challenged with the virus. For comparative purposes, some vaccinated and unvaccinated mice were also challenged.

Materials and Methods

The hamsters used were females, 3 to 4 weeks old, obtained from Pied Piper Farms, Inc., Newark, Delaware. The mice were 5- to 6-week-old CF#1/Anl females.

The hamsters were housed individually in plastic cages. The mice were housed in stainless steel cages, usually 5 vaccinated and 5 unvaccinated mice per cage, but occasionally 7 or 8 unvaccinated mice per cage. All were given water and Wayne Lab Blox ad libitum.

The mice and hamsters to be vaccinated were inoculated with the IHD-T strain of vaccinia virus by intradermal scarification near the base of the tail, 3 weeks prior to challenge with ectromelia virus.

The ectromelia virus used was a strain recovered from a natural outbreak that occurred at Argonne National Laboratory in 1959. It was maintained in a frozen state for some of the elapsed time and by serial animal passage for the remainder. To insure maximum virulence, it was

serially passed through mice 3 or 4 times at 3- to 4-day intervals immediately prior to its use in this study. On the day the mice and hamsters were to be challenged, 2 moribund mice that had been inoculated with the ectromelia virus 4 days earlier were killed. The livers were each homogenized in 25 ml of sterile isotonic saline solution, pooled, centrifuged at 2780 x g for 15 min, and filtered through a Millipore HA filter (pore size 0.45 μ ± 0.02 μ). To the original filtrate (referred to here as 10^0) was added sterile isotonic saline solution to produce 10^{-2}, 10^{-4}, 10^{-6}, 10^{-8}, and 10^{-10} dilutions.

Mice were given 0.1-ml inoculations intraperitoneally or 0.02 ml intradermally in the footpads. Hamsters were given 0.1 ml of the higher concentrations only, intraperitoneally or intradermally in the footpads. All animals were observed daily for three weeks. On the 21st day all survivors were anesthetized with ether and exsanguinated by cutting the brachial artery, and serum samples were examined individually for evidence of ectromelia-produced antibodies.

Hemagglutinin inhibition (HAI) titrations were made using a 1% suspension of chicken red blood cells and a dilution of vaccinia hemagglutinin (HA) prepared from the Levaditi strain grown on the chorioallantoic membrane of embryonated hens' eggs.[1] If HAI "antibodies" were found, a 1:10 dilution of the serum was heated in a waterbath to 56°C for 30 min and retested; the heating inactivates a nonspecific inhibitor of vaccinia HA that may be present in serum.[1,2]

Results

For unvaccinated mice the median lethal dose of ectromelia virus was about 0.02 - 0.1 ml of the 10^{-8} dilution (Table 18). Seven mice survived

TABLE 18

Survival and HAI antibody production in unvaccinated and vaccinated mice challenged with ectromelia virus

Inoculation route	Inoculum dilution	Number inoculated	Deaths	Survivors	HAI-positive survivors
		Unvaccinated			
Intradermal	10^0	5	5	0	
	10^{-2}	5	3	2	1
	10^{-4}	8	6	2	2
	10^{-6}	8	5	3	2
	10^{-8}	8	4	4	1
	10^{-10}	7	0	7	0
Intraperitoneal	10^0	5	5	0	
	10^{-2}	5	5	0	
	10^{-4}	5	5	0	
	10^{-6}	5	4	1	0
	10^{-8}	5	2	3	0
	10^{-10}	5	0	5	0
		Vaccinated			
Intradermal	10^0	5	0	5	5
	10^{-2}	5	0	5	3
	10^{-4}	5	0	5	3
	10^{-6}	5	0	5	5
	10^{-8}	5	0	5	0
	10^{-10}	5	0	5	0
Intraperitoneal	10^0	5	2	3	2
	10^{-2}	5	0	5	2
	10^{-4}	5	0	5	2
	10^{-6}	5	0	5	0
	10^{-8}	5	0	5	0
	10^{-10}	5	0	5	0

the 10^{-2}, 10^{-4}, and 10^{-6} dilutions, and of these 5 had developed HAI antibody indicating that they had experienced infection with ectromelia virus. There were no deaths among the vaccinated mice challenged intradermally, but 16 of the 20 mice given the four highest concentrations exhibited HAI antibodies.* All vaccinated mice survived intraperitoneal challenge except 2 that received undiluted filtrates; of 18 that survived the 4 highest doses, 6 developed HAI antibody.

There were no deaths among the hamsters, vaccinated or unvaccinated (Table 19); none appeared sick at any time, nor did any exhibit skin lesions. Refractoriness to intradermal vaccination was indicated by a complete absence of lesions at the site of inoculation. Only 2 hamsters developed HAI antibody: 1 unvaccinated and 1 vaccinated animal challenged intraperitoneally with undiluted filtrate.

TABLE 19

Survival and HAI antibody production in unvaccinated and vaccinated hamsters challenged with ectromelia virus

Inoculation route	Inoculum dilution	Number inoculated	Deaths	Survivors	HAI-positive survivors
		Unvaccinated			
Intradermal	10^0	4	0	4	0
	10^{-2}	4	0	4	0
	10^{-4}	3	0	3	0
Intraperitoneal	10^0	2	0	2	1
		Vaccinated			
Intradermal	10^0	4	0	4	0
	10^{-2}	4	0	4	0
	10^{-4}	4	0	4	0
Intraperitoneal	10^0	3	0	3	1

It is concluded that Syrian hamsters are almost completely refractory to ectromelia virus. It appears hardly conceivable that they could function either as natural hosts or reservoirs for this virus. It was shown also that mice vaccinated with IHD-T strain vaccinia virus can withstand challenge with many lethal doses of the virus.

* Since vaccination of mice with IHD-T strain vaccinia does not produce HAI antibodies, it does not preclude use of the HAI test for diagnosis of ectromelia infection in such mice.[1]

A Disease of Mice Characterized by Lung Congestion

Robert J. Flynn, Isabel L. Greco,
and Patricia B. Jinkins

In February, 1962, a group of about 100 CF#1/Anl female mice, 6-7 months of age, developed an illness clinically characterized by sudden decrease in the consumption of food and water, listlessness, and loss of weight. The condition lasted for about 2 weeks during which time a total of 7 animals died. Necropsy disclosed congested lungs and a completely empty gastrointestinal tract. No other gross abnormalities were noted.

A similar illness appeared about 2 weeks later in another mouse room housing about 1200 CF#1/Anl female mice about 600 days of age. Within 4 days, 4 animals in a cage of 15 died. Three had congested lungs; the condition of the lungs of the fourth could not be determined because of extensive postmortem autolysis. By the next day all the animals in the room appeared to be ill. Food and water consumption were greatly decreased. Many animals grew very thin and cyanotic, their fur became ruffled and they tended to sit hunched and isolated in corners. A few were seen leaning to one side in a manner suggesting a disturbance of the central nervous system.

Within 21 days, 292 of the approximately 1200 mice died. In 206 of these, the lungs were affected. Usually all lobes were completely congested, but occasionally only part of one or more lobes, usually the dorsal part, was involved. In those dying early in the epizootic, the gastrointestinal tract was completely empty. Toward the end of the third week, a complication resembling paralysis of the ileum was frequently observed: the small intestine was greatly distended and filled with fluid; the colon was empty and contracted.

Microscopically, the lungs of mice that died early were markedly congested and somewhat edematous. In those that died later, polymorphonuclear cells and macrophages were observed in great numbers in the bronchial exudate, and small necrotic areas were frequently observed in the bronchial epithelium. In some cases, slight degeneration was observed in the liver parenchyma, in the tubular epithelium of the kidneys, and in the neurons of the cerebrum.

In 134 of the 292 mice, the only lesion noted was congested lungs. In 43, congested lungs and extensive other pathology were observed; these probably would have died within the succeeding 30 days. In 29, congested lungs were observed, along with other pathology likely to have led to death during the next 60-90 days. The remaining 86 had no lung lesions, and their deaths were apparently unrelated to the disease. An extension of the mortality curve covering the previous 600 days indicates an expected mortality rate of about 4/day, or 84 deaths for 21 days - a figure in excellent agreement with the number of deaths apparently unrelated to the disease.

Repeated bacteriological tests were made of the lungs, livers, spleens, brains, and other tissues of the affected mice. No bacteria were recovered other than those usually considered secondary invaders.

Repeated virological tests were also made. Many groups of animals of various ages were inoculated subcutaneously, intraperitoneally, and intracerebrally with both filtered and nonfiltered homogenates of tissues from affected mice. The chorioallantoic membranes of fertile hen eggs were also inoculated with filtrates of affected tissues. All such tests were negative. We were never able to reproduce the disease and no growth occurred on the egg membranes.

Frozen samples of affected tissues were sent to Dr. Wallace P. Rowe of the National Institutes of Health, who inoculated 20- to 21-day-old mice with filtrates of homogenates of these tissues and 3 weeks later tested their serums for antibodies of known mouse viruses. The filtrates were nonpathogenic for the weanling mice and negative for the viruses for which he tested (K virus, mouse adenovirus, mouse hepatitis virus, and the REO viruses).

An attempt at therapy was inconclusive. Because a few animals given trial injections of oxytetracycline hydrochloride (2.5 mg/mouse/day) seemed to show improvement, all the animals in the room were treated similarly, each day, for 4 days. A few days later the mice began to eat and drink, but it is possible that the disease had run its course by the time therapy was initiated.

The disease was observed shortly thereafter in 3 other animal rooms that housed younger animals, about one year of age. Food and water consumption decreased sharply; the animals became thin and cyanotic, but very few deaths occurred. In these rooms, the disease ran its course in about 2-4 weeks. A few animals were treated with oxytetracycline.

Although the clinical signs of the disease seemed to cease after about 2-4 weeks, congested lungs were still frequently observed many weeks later. The condition now appears to be enzootic throughout the entire mouse colony. All attempts to pass this disease by animal inoculation were discontinued when it became impossible to find groups of animals free of the disease. The incidence in apparently healthy CF#1 female mice raised at this Laboratory ranged from 6% to 22%. In mice of the same age, sex, and strain, received from a commercial vendor,* the incidence was zero on arrival, but ranged from 6% to 12% in groups sampled 2 weeks later.

The authors wish to thank Dr. Birute O. Biskis for her assistance in describing the pathology observed.

---

* Carworth, Inc., New City, Rockland County, New York.

References

1. Briody, B. A. Response of mice to ectromelia and vaccinia viruses. Bacteriol. Rev. 23, 61-95 (1959).

2. Cassel, W. A. and B. Fater. Nonspecific inhibition of vaccinia hemagglutinin. Science 126, 301-302 (1957).

A COMPARISON OF RADIATION-INDUCED GRANULOCYTOPENIA IN SEVERAL MAMMALIAN SPECIES

Harvey M. Patt and Mary A. Maloney

In studies with dog and monkey,[1-3] we observed that the granulocyte blood level could be buffered for several days by cells in the differentiating marrow pool, even if new cell formation was inhibited by X-irradiation. This followed from the findings that 1) the maturation of metamyelocyte to segmented cell proceeded in a normal fashion; 2) the release of mature cells from marrow to blood was not affected; and 3) the turnover of granulocytes in blood was also unchanged during the first few days after exposure. Thus, the delay in onset of definite granulocytopenia after irradiation is understandable, even though the normal blood turnover is only a matter of a few hours.[4,5]

In the light of these observations, we have compared the initial granulocyte (neutrophil, heterophil) decline in several species after comparable irradiation, using available data. Definite granulocytopenia after exposure to 500 to 600 r begins after the first day in mouse, rat, and hamster,[6-9] after the second day in rabbit,[10] and after the third day in dog and monkey.[1,11,12] Although this dosage covers the acute lethal range for the several species (i.e., 30-day LD_{0-10} for rabbits - LD_{100} for dogs), the granulocyte decline is strikingly similar after the variable latent period. This is shown in Figure 14, where the latent period has been subtracted from the time after irradiation to provide a common time axis.

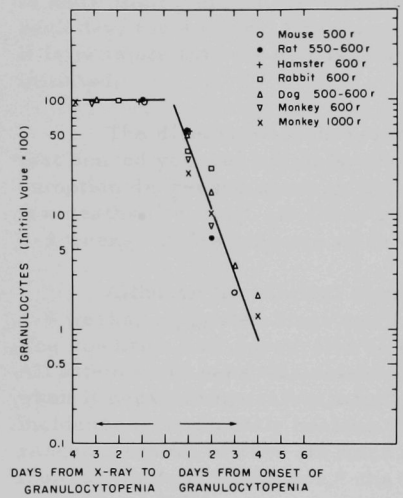

Figure 14. Comparison of primary granulocytopenia in several irradiated species

If the survival curve for mouse bone marrow cells[13] is applicable, fewer than 5% of cells capable of clonal growth will survive a dose of 500 to 600 rad. While the absorbed dose (rad) will be less than the air dose (r) used as a basis of comparison here, it is probably sufficient in all instances to bring production to a near standstill for a time, because of cell death and the associated mitotic block. This receives support from the fact that the rate of granulocyte decline in the monkey is the same

after exposure to 600 r and 1000 r (Figure 14).[14] Under such circumstances, the similar initial blood depopulation rate would suggest a similar normal disappearance in these species. As may be noted in Figure 14, the early blood granulocyte disappearance appears to be exponential with a half-time of 10 to 15 hr. Independent studies in normal dog, monkey and man[3-5] point to a random disappearance of granulocytes from circulation with a half-time of 5 to 10 hr. A similar pattern was described earlier in cross-circulation studies of normal and irradiated cats.[15]

We wish to suggest that the duration of the latent period before the onset of definite granulocytopenia is a reflection of the size of the nonmitotic differentiating pool in the several species. Although there is some evidence for this, the possibility of a quantitative relationship between marrow pool size and the sequence of events in blood in the various species requires further study. Other factors might, of course, be contributory; for example, differences in degree of early marrow bleeding could influence cell release. It is obviously desirable to include other species in the analysis, but we have been unable thus far to find such data on the early granulocytopenia after comparable radiation exposure.

We have been concerned here only with the rate of development of granulocytopenia as a measure of initial injury. The subsequent pattern, namely the time to reach minimal levels and the time for recovery to preirradiation values, may differ considerably in the various species.[11] Even with large doses of radiation there will be some production of cells, albeit at a low level, when mitosis is resumed. Moreover, as granulocytopenia becomes profound, the time spent by the newly-formed segmented cells in marrow may decrease,[2] and this will tend to prolong the time to reach a minimal blood level. However, the opposite situation may also result; for example, as infectious processes develop, granulocyte removal from circulation may be accelerated. For reasons of this sort, the clearest relationship between the initial injury and the blood level in the various species is given by the early granulocyte decay after dosages sufficient to block production, such that the influence of possible differences in marrow pool size will be minimized. Granulocyte recovery is more rapid in mouse, rat and rabbit than in monkey and dog after comparable exposure. The reasons for this are not known but should become evident with further understanding of the comparative dynamics of granulocyte renewal. The blood granulocyte mass differs in these species and if the normal blood turnover is the same as suggested in the present analysis, the effective or net production rates will vary accordingly. It is of interest to note that the net production estimated in this way increases by a factor of three from rat to rabbit, monkey and dog. This, as well as the size of the stem cell compartment relative to production requirements and the degree of normally occurring ineffective granulopoiesis, could provide a basis for some of the differences in recovery among species.

The granulocyte response described here may be contrasted with the prompt lymphopenia of irradiation. While the former is a consequence of the disturbed granulopoiesis, the latter is brought about to a considerable extent by direct killing of small lymphocytes in blood, lymph and lymphoid tissues.(16-18) However, with exception of species differences in the latent period, the primary granulocytopenia appears to be species independent, which is also the case for the prompt lymphopenia. The foregoing is not necessarily inconsistent with the suggested exponential relationship between the basal metabolic rate of the various species and the time at which all leucocytes as a group attain minimal levels after an $LD_{50/30}$ exposure to X-rays.(19) Minimal leucocyte levels (which are difficult to establish with precision) are reached earlier in species with higher rates of metabolism. However, the rabbit, which was not included in the analysis, would represent a serious departure from the proposed linearity.(19) Although acute lethality is intimately associated with leucocyte depression, this pertains mainly to the granulocytes, and it will be recalled that the granulocyte-lymphocyte ratio differs considerably in the various species. Since other physiologic derangements also contribute to acute lethal action, it would seem more appropriate to examine possible species differences in injury and recovery after a similar dosage of radiation rather than after a similar degree of lethality.

Summary

Comparison of the early granulocytopenia in several mammalian species after comparable irradiation reveals a similar rate of decline, which approximates the normal rate of disappearance from circulation. The time between irradiation and onset of granulocytopenia varies and may perhaps be related to species differences in the nonmitotic differentiating marrow pool.

References

1. Patt, H. M. and M. A. Maloney. Kinetics of neutrophil balance in normal and irradiated states. In Proceedings of IX International Congress of Radiology, ed. B. Rajewsky. Georg Thieme, Stuttgart, 1961. pp. 1027-1035.

2. Maloney, M. A. and H. M. Patt. Radiation effects on neutrophil balance. In Ciba Foundation Symposium on Haemopoiesis, ed. G. E. W. Wolstenholme and M. O'Connor. Churchill, London, 1960. pp. 262-270.

3. Maloney, M. A., H. M. Patt and C. L. Weber. Comparative analysis of neutrophil kinetics in x-irradiated dog and monkey. In Proceedings of II International Congress of Radiation Research, in press.

4. Mauer, A. M., J. W. Athens, H. R. Warner, H. Ashenbrucker, G. E. Cartwright and M. M. Wintrobe. An analysis of leukocyte radioactivity curves obtained with radioactive diisopropylfluorophosphate (DFP^{32}). The Kinetics of Cellular Proliferation, ed. F. Stohlman. Grune and Stratton, New York, 1959. pp. 231-238.

5. Patt, H. M. and M. A. Maloney. Kinetics of neutrophil balance. The Kinetics of Cellular Proliferation. ed. F. Stohlman. Grune and Stratton, New York, 1959. pp. 201-207.

6. Patt, H. M., R. L. Straube, E. B. Tyree, M. N. Swift and D. E. Smith. Influence of estrogens on the acute x-irradiation syndrome. Am. J. Physiol. 159 269-280 (1949).

7. Stearner, S. P., E. L. Simmons and L. O. Jacobson. Effects of total-body x-irradiation on rats. III. Effect on peripheral blood and blood-forming tissues. Biological Effects of External X and Gamma Radiation, Pt. 2, ed. R. E. Zirkel. USAEC TID-5220 (1956). pp. 315-345.

8. Ingram, M. and W. B. Mason. Effects of acute exposure to x-radiation on the peripheral blood of experimental animals. Biological Effects of External Radiation, ed. H. A. Blair. McGraw-Hill, New York, 1954. pp. 58-83.

9. Fulton, G. P., D. L. Joftes, R. Kagan and B. R. Lutz. Hematologic findings in the total body x-irradiated hamster. Blood 9, 622-631(1954).

10. Jacobson, L. O. The hematologic effects of ionizing radiation. Radiation Biology, Vol. 1, ed. A. Hollaender. McGraw-Hill, New York, 1954. pp. 1029-1090.

11. Cronkite, E. P. and G. Brecher. The protective effect of granulocytes in radiation injury. Ann. N. Y. Acad. Sci. 59, 815-833 (1955).

12. Eldred, E. and B. Eldred. Effects of total body x-irradiation on the peripheral blood of the monkey. Blood 8, 262-269 (1953).

13. Till, J. E. and E. A. McCulloch. A direct measurement of the radiation sensitivity of normal mouse bone marrow cells. Radiation Research 14, 213-222 (1961).

14. Patt, H. M. and M. A. Maloney. Unpublished observations.

15. Lawrence, J. S., D. M. Ervin and R. M. Wetrich. Life cycle of white blood cells. Am. J. Physiol. 144, 284-296 (1945).

16. Trowell, O. A. The sensitivity of lymphocytes to ionizing radiation. J. Path. Bacteriol. 64, 687-704 (1952).

17. Hulse, E. V. Lymphocyte depletion of the blood and bone marrow of the irradiated rat: A quantitative study. Brit. J. Haematol. 5, 278-283 (1959).

18. Schrek, R. Qualitative and quantitative reactions of lymphocytes to x-rays. Ann. N. Y. Acad. Sci 95, 839-848 (1961).

19. Michaelson, S. M. and L. T. Odland. Relationship between metabolic rate and recovery from radiation injury. Radiation Research 16, 281-285 (1962).

COMPARATIVE ANALYSIS OF NEUTROPHIL KINETICS IN X-IRRADIATED DOG AND MONKEY

Mary A. Maloney, Harvey M. Patt
and Charlotte L. Weber

While radiation effects are generally similar in mammals, important differences are known which can be related to specific biological properties. There is a strong species component in blood neutrophil changes after irradiation. This might be related to differences in kinetics of neutrophil balance. In earlier work with dogs,[1,2] we determined that the decline in blood neutrophils after whole-body X-irradiation with 500 r was consistent with their normal rate of disappearance and occurred upon exhaustion of cells in the nonmitotic differentiating marrow pool. Initial studies with monkeys, also based on autoradiographic analyses with tritiated thymidine (H^3T), indicate a similar picture.*

There seems to be no difference between monkey and dog in the initial labeling of proliferating cells after H^3T injection. Although the subsequent sequence in the monkey has not been studied at closely-spaced intervals, as in the dog, the chronology of development is approximately the same. Thus about 10 percent of labeled metamyelocytes are evident in monkey marrow by 12 hours after H^3T administration (200 μc/kg body weight; specific activity 360 mc/millimole); labeled band cells are seen after the first day and segmented cells after the second day. The blood pattern is shown in Figure 15, where it will be seen that labeled neutrophils appear about a day later in monkey than in dog. We believe that this may be due to the larger reservoir of mature neutrophils in monkey marrow. With this exception, the curves describing the percentage of labeled cells in blood of monkey and dog are quite similar.

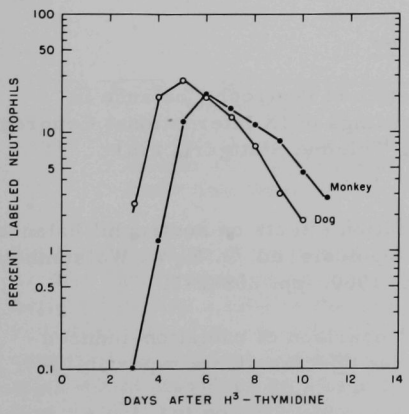

Figure 15. Appearance of labeled neutrophils in peripheral blood of dog and monkey (mean values are derived from studies in 4 dogs and 2 monkeys).

Whole body X-radiation (1000 r) was given to two monkeys 24 hours after H^3T injection. Autoradiographic analysis of aspirated marrow samples indicates that differentiation and release of cells from marrow to blood proceeded in a normal fashion. This is apparent from the blood pattern shown in Figure 16, where we may note also the similarity in disappearance of labeled cells and

*Part of this study was carried out at the United States Public Health Service Wisconsin Primate Center.

in development of radiation-induced neutropenia. As in the dog, there is a delay in onset of the primary neutropenia after irradiation. Definite neutropenia begins about a day later in the monkey. This is perhaps a reflection of the larger pool of segmented cells in marrow.

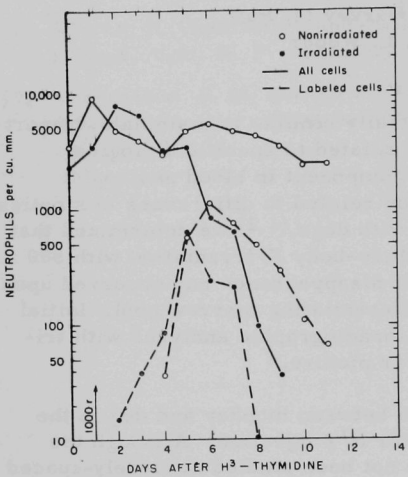

Figure 16. Appearance of labeled neutrophils in peripheral blood of an unirradiated monkey and a monkey irradiated one day after injection of tritiated thymidine.

In the light of these observations in monkey and dog, we have compared the initial granulocyte (neutrophil, heterophil) decline in several species after comparable irradiation, using available data.(3) The rate of decline after exposure to 500-600 r is similar in mouse, rat, hamster, rabbit, dog and monkey, and approximates the normal rate of disappearance from circulation. The time between irradiation and onset of granulocytopenia varies and may perhaps be related to species differences in the nonmitotic differentiating marrow pool. We conclude from these studies that the initial injury as regards granulocytopoiesis is essentially similar among species, the major differences being in the kinetics of recovery.

References

1. Patt, H. M. and M. A. Maloney. Kinetics of neutrophil balance in normal and irradiated states. Proceedings of IX International Congress of Radiology, ed. B. Rajewsky, Georg Thieme, Stuttgart, 1961. pp. 1027-1035.

2. Maloney, M. A. and H. M. Patt. Radiation effects on neutrophil balance. Ciba Foundation Symposium on Haemopoiesis, ed. G. E. W. Wolstenholme and M. O'Connor. Churchill, London, 1960. pp. 262-270.

3. Patt, H. M. and M. A. Maloney. A comparison of radiation-induced granulocytopenia in several mammalian species. This report, p. 56.

EFFECT OF AGE AND RADIATION ON THE LENS OF THE EYE IN THE MOUSE

Robert L. Straube

To increase our understanding of the physiological process of aging and the chronic somatic effects of ionizing radiation, we have characterized several physiological parameters in the CF No. 1 female mouse as a function of age and radiation injury. One such cellular system studied was the lens of the eye.

In most mammals the lens grows continually throughout life, new lenticular fibrils being added by the mitotic activity of relatively undifferentiated cells of the equator. The lens is encased in an avascular capsule that prevents exchange, at the cellular level, with the rest of the body. The lenticular fibrils that form the outer layers of the cortex are the most recent; those in the nucleus were laid down early in life and gradually become more dense, eventually being compressed into a hyaline mass in which individual fibers can scarcely be recognized. We found that the dried lens weight varies with the age of the mouse (Figure 17), confirming the findings in other species.[1,2] The lens weight increases from less than 1 mg at birth to about 10 mg at 100 weeks of age, the increase being most rapid during the first 40 weeks and somewhat slower thereafter. Variation is minimal, and an accurate estimation of age to ±2 weeks can be made in the early period. Radiation affects the lens by inhibiting lenticular mitosis. Degeneration and cell death may occur in this early phase. The mechanism of radiation cataract formation is not completely known, but the formation of abnormal, swollen lens fibers, which become opaque as they differentiate and are slowly pushed toward the posterior pole, is believed to play a role in the development of the eventual opacity. Since radiation "ages" the lens by decreasing the induction period for and increasing the incidence of cataracts, one might assume a priori that irradiation would also have an effect upon the normal physiological increase in lens weight, but no such effect was apparent. This is true for both the chronic and acute lens weight response. Mice irradiated (whole-body) with 500 r at the age of 2 months and sacrificed at the age of 41 weeks showed no deviation from the normal (8.29 ± 0.11 mg for the 20 irradiated animals, versus 8.34 ± 0.14 mg for the unirradiated controls). Twenty-three of these

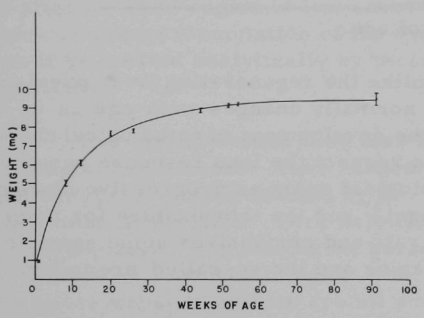

Figure 17. The effect of age on the weight of the dried lens of the eye in CF No. 1 female mice. Mean ± S.E.

irradiated mice survived for 52 weeks after irradiation; 13% of the exposed lenses developed cataracts. In addition, 13-week-old mice subjected to 800 r whole-body x-irradiation 10 days before sacrifice showed no radiation effect on lens weight (4.93 ± 0.06 mg for irradiated mice versus 4.98 ± 0.09 mg for controls). Animals irradiated at 2 months of age with 400 r and sacrificed at monthly intervals thereafter, although still in the active growth phase, showed no significant deviation from the pattern in the unirradiated animals (Table 20).

TABLE 20

Effect of 400 r total-body X-irradiation on the dried lens weight (mg) in CF No. 1 female mice

Radiation dose, r	Age, weeks		
	15	20	25
400*	6.48 ± 0.10	7.00 ± 0.18	7.81 ± 0.12
0	6.43 ± 0.15	6.91 ± 0.16	7.86 ± 0.11

*Irradiated at 9.5 weeks of age.

It is of interest to note that, unlike the regenerating liver previously studied, the rate at which lens weight normally changes with age is unaltered by ionizing radiation despite the development of pathological changes incident to cataract formation. In this respect the lens response resembles such radioresistant criteria of physiological aging as progressive change in mucopolysaccharides of rib cartilage(3) and the temperature for maximum contractility of tail tendon(4) in rats and emphasizes some specific similarities and differences between aging and the so-called premature aging of irradiation.

References

1. Lord, R., Jr. The lens as an indicator of age in cottontail rabbits. J. Wildlife Management 23, 358-360 (1959).

2. Lord, R., Jr. The lens as an indicator of age in the grey fox. J. Mammal. 42, 109-111 (1961).

3. Anderson, B., and Odell, T. T., Jr. Changes in rat cartilage mucopolysaccharide with age and radiation. J. Gerontol. 15, 249-252 (1960).

4. Verzár, F. Influence of ionizing radiation on the age reaction of collagen fibers. Gerontologia 3, 163-170 (1959).

MONTE CARLO CALCULATIONS FOR THE STOCHASTIC THEORY OF MORTALITY

George A. Sacher and Ernesto Trucco

The basic ideas underlying the stochastic theory of mortality are set forth in a previous report[1] and we shall not repeat them here; further details have also been reported.[2] The current model system we are studying consists of a cubic potential (giving a quadratic force or "restoration function") from which particles escape under the influence of Brownian motion. In all but the simplest cases the probability of escape cannot be calculated explicitly and must be found by means of machine computation. Hence, a Monte Carlo program was set up, and some preliminary results of these studies have been presented (Reference (1), Figures 23 and 24).

Further curves of a similar nature were obtained subsequently. However, one essential difficulty still remains: the method is inadequate for the case of very small escape probabilities. Even the procedure of "forcing escapes,"[1] was not sufficient to improve this undesirable state of affairs. (The region of low escape rates is of special interest for a more complete formulation of the theory, and only in very few instances can it be treated analytically by means of the Chandrasekhar-Kramers equations.)

For these reasons, and also because the Monte Carlo program was unsatisfactory in some other respects, a new and different approach to the problem is now being studied by Dr. David A. Woodward of the Applied Mathematics Division. Very briefly, it can be summarized as follows. The desired quantity (e.g., expected percentage of escapes in a given situation) is written as a Wiener integral, i.e., the integral of a certain functional in the space whose elements are all possible trajectories of particles in free Brownian motion. The problem then consists in finding the value of this integral, say I. To that end, it is replaced by a related integral, I', according to a method known as "Simpson's rule for Wiener integrals."[3] I' can now be evaluated by performing a sequence of Monte Carlo trials. The actual runs are carried out with a simplified force function from which all linear terms have been eliminated. It is expected that an estimation for I' better than the one previously obtained will result from these techniques. Since, however, the new program has not yet been written, further details will be given in subsequent reports. Meanwhile the work of Dr. Woodward is gratefully acknowledged.

References

1. Sacher, G. A., and E. Trucco. Preliminary results from the Monte Carlo study in the stochastic theory of mortality. Biological and Medical Research Division, Summary Report, January through December 1960, Argonne National Laboratory. ANL-6368. pp. 56-60.

2. Sacher, G. A., and E. Trucco. The stochastic theory of mortality. Ann. N. Y. Acad. Sci. 96, 985-1007 (1962).

3. Cameron, R. H. A "Simpson's Rule" for the numerical evaluation of Wiener's integrals in function space. Duke Mathematical J. 18, 111-130 (1951).

COMPARATIVE KINETICS OF ACUTE RADIATION LETHALITY

S. Phyllis Stearner, Sylvanus A. Tyler
and Margaret H. Sanderson

Acute mortality (death within 30 days after exposure) is a convenient indicator by which the extent of radiation injury is commonly measured. Yet, different mechanisms of lethal injury are expressed within this time period, indicated by different symptoms or time of death. For the most part, modes of acute death in the mouse and the bird appear to be comparable. A notable exception is an early mortality, associated with circulatory failure, that has been described in some birds. This mortality occurs within the first 2 days after irradiation in the chick and duck,(1) but not in the parakeet,(2,3) pigeon(4,5) or canary.(6) Available evidence, however, suggests that injury processes that terminate as early mortality in the chick and duck are also active in other birds and in mammals as well, although they do not produce lethal consequences. Such effects as intra- and extracellular swelling and capillary dilatation have been described. For a general description of the kinetics of acute radiation lethality, it is of interest to compare the dose - exposure-time relations for later acute mortality (3-30 days) in the mouse and in birds that do and do not exhibit 0-2 day deaths.

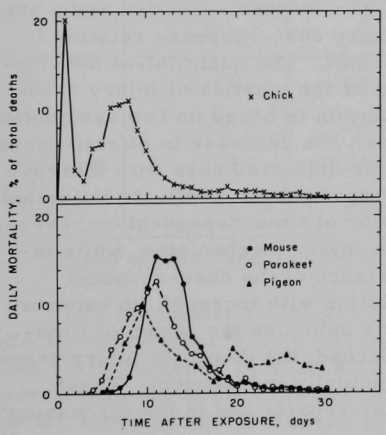

Figure 18. Daily distribution of deaths within 30 days after Co^{60} γ-irradiation for doses over the 30-day lethal range (all treatment groups combined).

All exposures are to Co^{60} γ-rays, protracted over single continuous periods ranging from 5 min to 1440 min (24 hours). Details of the response for doses in the 30-day lethal range only (1-99% mortality) receive major emphasis in this analysis.

Comparison of the daily frequency of mortality for the 3 avian forms (chick, parakeet, pigeon) and for the mouse (Figure 18) shows a striking similarity. In the chick, in which there is an early mortality, a second peak occurs between days 6 and 8. In the pigeon, parakeet and mouse, on the other hand, there is no comparable early mortality, and the major portion of the fatalities occurs between about 6 and 15 days, with peak frequency between 10 and 13 days. In birds in

which an early mortality does not occur, hematopoietic failure appears to be the dominant lesion with exposures over the 30-day lethal range. There is bone marrow and lymphoid aplasia, and reduction of mortality by bone marrow transplants has been reported.[7] Thus the situation is comparable to that found in the mouse. In the chick, a mode of death expressed within 5-6 days has been described.[8] In the mortality frequency shown here, it overlaps the 7- to 30-day response; it is distinguishable, however, with exposures over a higher dose range. In other birds, the dose-exposure time relations for the earlier modes of death are such that there is less overlapping with hematopoietic death. Over the dose range with which we are concerned here hematopoietic death predominates; therefore, in the chick only the 7- to 30-day response is included in the analysis.

Description of the time-dose relation for acute mortality in the chick,[8,9] the chick embryo,[10,11] and the parakeet and pigeon[3] have been previously reported; details for the mouse are described in the accompanying report.[12] A summary comparison of the time-dose relations for LD_{50} values for the 4 species may be made from Figure 19. With increase in exposure time through 400-500 min there is a decrease in effectiveness of the delivered dose. With exposure periods of 960 and 1440 min, however, there is little further reduction, and a stationary dose-response relation is attained. The quantitative description of the kinetics of injury accumulation is based on two assumptions. First, the decrease in effectiveness of the delivered dose with increase in exposure time reflects the lethal action of time-dependent or reversible injury mechanisms, while invariance of the dose-response relation with increase in exposure time indicates the action of time-independent or irreversible processes. Second, the dominant injury processes expressed in the acute period are mutually independent. These assumptions are explicitly stated in earlier reports and in the discussion on the mouse.

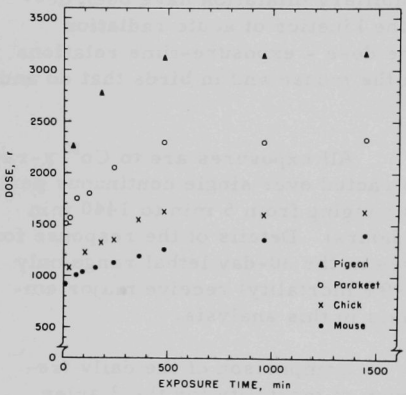

Figure 19. Relation of LD_{50} to exposure time for 3 avian species and the mouse.

On the basis of this model, the stable dose-response relation approximated by the longest exposure groups represents the time-independent effect. The LD_{50} values and estimates of σ for this effect are given in Table 21. The increased effectiveness of the delivered dose with shorter

exposure periods represents the action of time-dependent processes. Statistical partition of the mortality due to each of the two processes is accomplished according to the following expression

$$R_{d,t} = P_{d,t} + Q_d - P_{d,t}Q_d; \; P_{d,t} = \frac{R_{d,t} - Q_d}{1 - Q_d}$$

where $R_{d,t}$ is the total proportion dying from a dose d delivered in time t, $P_{d,t}$ is the proportion dying of time-dependent effects, and Q_d is the proportion that succumbs to time-independent effects. The instantaneous dose-mortality distribution, estimated from the shortest exposure time groups, reflects the sensitivity of the species to the time-dependent effects lethally expressed in this period. The LD_{50} values and estimates of σ for this effect are also given in Table 21.

TABLE 21

Comparison of acute radiosensitivity to Co^{60} gamma rays

Species	Irreversible effect (Protracted exposures),* r		Reversible effect (D_0) (Instantaneously delivered exposures), r		Reference
	LD_{50}	$\hat{\sigma}$	LD_{50}	$\hat{\sigma}$	
Mouse	1381	133	985	84	12
Chick	1630	313	1110	340	8
Parakeet	2297	680	1500	450	3
Pigeon	3159	846	2050	550	3

*Based on 960- and 1440-min exposures.

To normalize the kinetics of the dose sensitivity of the time-dependent effect, with respect to species and quality of radiation, we use the ratio D/D_0. This ratio gives the relation between the dose, D, required when exposure is protracted over some time period, and the instantaneous dose, D_0, required for the same effect. A linear relationship for all species is evident (Figure 20); for the 3 avian forms the slopes are not significantly different, but for the mouse the slope is less, indicating a less rapid rate of reversal. The reciprocal of the slope is an estimate of the time constant (τ) of the linear reversal process. The relationship shown in Figure 20 is represented by the expression

$$\frac{D}{D_0} = 1 + \frac{t}{\tau}$$

where t is exposure time. For the birds τ is equal to about 300 min, while for the mouse it is equal to 1547 min. On the basis of the constant (linear) reversal, the reversal rates are independent of accumulated dose. The reversal rate is normally distributed and has been postulated to be an inherent characteristic of the individual animal. For the mouse, 50 percent of the animals can reverse at a rate equal to at least 0.75 r/min. In the 3 species of birds, the reversal rate per unit of injury is equivalent, but in terms of roentgens the reversal rates vary depending on dose sensitivity. Thus the mean rates are: chick - 3.7 r/min; parakeet - 5.0 r/min; and pigeon - 6.8 r/min.

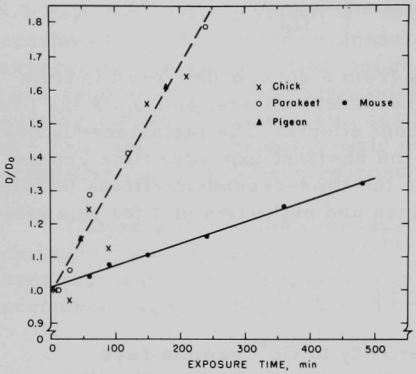

Figure 20. Relation between average D/D_0 and exposure time for the time-dependent effect; a comparison of 3 avian species and the mouse. Curves were drawn by the method of least squares.

In the chick and the mouse, linearly reversible processes have also been recognized for modes of acute death preceding that due to hematopoietic failure. In the chick, lethal mechanisms expressed within 3-6 days show a time-independent effect and a time-dependent effect with kinetics similar to that described for the later acute mortality. The estimate of the time constant for the reversible effect is 290 min and the reversal rate is about 4 r/min. In the mouse, the 3-6 day "intestinal syndrome" also shows time-dependent and time-independent components, but the reversal rate associated with time-dependent effects is more rapid than that described for the later acute lethality. The value for τ is approximately equal to 725 min, compared to 1547 min for the later mortality, and the mean reversal rate is about 2 r/min.

The model, as proposed, ascribes the lack of a time effect for the longer exposures to an irreversible process that is independently expressed. Alternatively, a single time-dependent mechanism that either reverses for a limited time only, or reverses a limited amount of dose only, could be postulated as descriptive of lethal effects expressed within this mortality period. From results of different types of protracted exposures, we know that the reversal cannot be limited solely by a time period (e.g., about 500 min for the bird or 1000 min for the mouse). For example, the static dose-response relation for 480- to 1440-min exposures in the chick indicates that reversal may continue for longer periods. Nevertheless, from available data we cannot exclude the possibility that the reversal is limited both by total dose and by reversal rate; that is, reversal occurs either at a rate that is a characteristic constant of the individual animal or at the

rate of delivery (whichever is less) but there is a limitation on the total dose that can be reversed. On the basis of this model, the D/D_0 ratios with respect to exposure time for the unpartitioned mortality take the form shown in Figure 21. In all species, the stationary dose-response relation for the longer exposures is approximately 1.5 that of instantaneously delivered doses. However, the time constant associated with this amount of reduction in dose effectiveness is about twice as large in the mouse as in the birds. In the 3 species of birds, the reversal rate per unit of injury is again equivalent, although the actual rate in roentgens differs by a factor of 2.

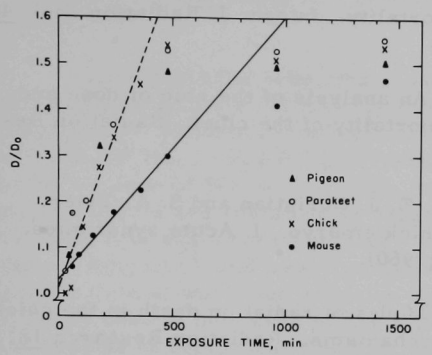

Figure 21. Relation between D/D_0 and exposure time for total unpartitioned mortality. Curves were drawn by the method of least squares.

Further investigations with various types of split-dose exposures will be helpful in indicating which model is more probable. In neither case, however, is the type of kinetics descriptive of the reversal processes altered by the nature of the limiting factor; that is, the attainment of the lethal bound for an independent irreversible component, or some saturation effect.

References

1. Stearner, S. P. The effect of variation in dosage rate of roentgen rays on survival in young birds. Am. J. Roentgenol. 65, 265-271 (1951).

2. Schlumberger, H. G. and U. K. Henschke. The effect of total-body X-irradiation on the parakeet. Proc. Soc. Exptl. Biol. Med. 92, 261-266 (1956).

3. Stearner, S. P. and S. A. Tyler. Comparative aspects of acute radiation mortality in birds. Intern. J. Radiation Biol. 5, 205-215 (1962).

4. Stearner, S. P., M. H. Sanderson, and E. J. Christian. The initial postirradiation period in the pigeon. Biological and Medical Research Division Semiannual Report, January through June 1957, Argonne National Laboratory. ANL-5732. pp. 65-67.

5. Skalka, M. and M. Hill. The effect of X-irradiation on pigeons. Folia Biol. 5, 60-70 (1959).

6. Stearner, S. P. Unpublished results.

7. Shaw, D. H. and H. Vermund. Modification of radiation effects in the pigeon, Columba livia. II. Effects of delayed bone marrow implantation. Proc. Soc. Exptl. Biol. Med. 107, 414-420 (1961).

8. Tyler, S. A. and S. P. Stearner. Discrimination among injury processes reflected in acute radiation mortality. Intern. J. Radiation Biol. 4, 495-509 (1962).

9. Stearner, S. P. and Tyler, S. A. An analysis of the role of dose and dose rate in the early radiation mortality of the chick. Radiation Research 7, 253-266 (1957).

10. Stearner, S. P., M. H. Sanderson, E. J. Christian and S. A. Tyler. Modes of radiation death in the chick embryo. I. Acute syndromes. Radiation Research 12, 286-300 (1960).

11. Tyler, S. A. and S. P. Stearner. Modes of radiation death in the chick embryo. II. A model of lethal mechanisms. Radiation Research 12, 301-316 (1960).

12. Tyler, S. A. and S. P. Stearner. A model of the kinetics of injury processes associated with acute lethality in the mouse following Co^{60} gamma radiation. This report, p. 73

A MODEL OF THE KINETICS OF INJURY PROCESSES ASSOCIATED WITH ACUTE LETHALITY IN THE GAMMA-IRRADIATED MOUSE

Sylvanus A. Tyler and S. Phyllis Stearner

To explain the reduction in effectiveness of ionizing radiations in producing an acute lethal damage to mammals, several models have been proposed.(1) Meredith(2) showed that the kinetics of acute radiation mortality in CF No. 1 mice for protracted exposures up to 6 hr could be viewed as an instance of Schwartzschild's law. This law states that equivalent radiation effects are sustained by irradiated groups for which the product of the dose rate and a constant power of the exposure time is numerically the same. Kingery(3) and Lea(4) proposed a model based on the assumption that the rate at which the effective dose accumulates is equal to the rate at which dose is delivered minus a term consisting of a constant (with dimensions of reciprocal time) multiplied by the effective dose already obtained (the exponential reversal hypothesis). Blair(5) augmented this model by assuming that the effective dose represents the direct sum of two injury accumulation processes: 1) a residual effect that accumulates according to the exponential reversal hypothesis (also called the reversible portion of the effect) and 2) the direct effect of a portion of the delivered dose for which reversal is absent (also called the irreversible portion). Brown, et al.(6) showed that the postulation that the rate of accumulation of the effective dose is lower than the rate of delivery by a constant amount (linear reversal hypothesis*) is tenable for exposure periods up to 6 hr; male "R" mice were subjected to 250 kv X-irradiation in their experiments. Tyler and Stearner(8) proposed that acute irradiation initiates in the organism several lethal effects that accumulate independently and that individually can cause the death of an organism. Death occurs when any single effect passes the critical level (or lethal bound) associated with that effect. As in Blair's model, both reversible and irreversible injury processes are postulated; but contrary to his assumptions, reversible effects are assumed subject to a linear reversal during exposure and the delivered dose is not partitioned between these two effects.

We shall demonstrate that the last kinetic model of injury accumulation will describe the course of mortality observed for the 30-day lethal range after a single, protracted exposure of mice to Co^{60} γ-rays.

---

*The linear reversal hypothesis was previously proposed as a description of the kinetics of radiation injury that attains lethal proportions within 2 days after an irradiation with Co^{60} γ-rays in the young chick.(7)

Experiment

Male and female LAF_1 mice were exposed at approximately 120 days of age to a single, continuous dose of Co^{60} γ-rays. The exposure period was varied from 10 to 1440 min. The delivered dose ranged from 850 to 4000 r, as measured in air. Under these radiation conditions, mortality ranges from a few percent within 30 days to 100 percent within 5 days. Animals were irradiated in groups of 3 in Lucite containers. Food and water were available at all times. Observations from both male and female mice are combined since no pronounced sex differences were evident in time or pattern of acute deaths or pathology at death.

The 30-day Lethal Range

The range of doses within which the percentage of deaths occurring within 30 days after irradiation is greater than zero and less than 100 is referred to as the 30-day lethal range. It can be seen from Table 22 and Figure 22 that the lethal range is dependent on length of protraction. Also, over this range, very few deaths are observed before the ninth day. Thus, deaths occurring between 9 and 30 days constitute the mortality usually summarized in acute experiments. The plot of LD_{50} versus exposure time (Figure 23) clearly demonstrates the increase in dose required to produce death in 50 percent of the exposed animals as the protraction is lengthened. We shall ignore the 10-min exposure groups since the observed mortality in these groups is incompatible with the over-all trend established by groups of other exposures (Figure 22). The dependence of LD_{50} on exposure time (Figure 23) cannot be explained completely by either a linear or exponential reversal model since both models require a continuing increase in LD_{50} as the exposure time is increased. Two general models that are consistent with the observed empirical pattern have been considered:

1. At least 2 types of injury processes are operative; one accounts for the loss of dose effectiveness with increase in exposure time and the other produces an irreversible injury (within the range tested);

2. The observed kinetics reflect a single underlying process that reduces the effectiveness of the radiation for a limited time only, or until some dose has been delivered.

We have chosen to adopt the first of these general models to characterize the injury kinetics reflected by the observed dependence of 9-30 day mortality in the mouse on dose and exposure period (see Reference 9 for more detail).

TABLE 22

Daily frequency of deaths among LAF_1 mice after acute exposure to Co^{60} gamma rays

Dose, r	Post-irradiation day 1	2	3	4	5	6	7	8	9	10	11	12	13	14	15	16	17	18	19	20	21	22	23	24	25	26	27	28	29	30	Survivors	Number of Animals
Exposure time 60 min																																
0800																															36	36
0850																					1										71	72
0900							1						2	2	1		1			1	1										63	72
0950									1		1	5	2	2	1	1			1						1						56	71
1000									1	6	4	4	7	3	2	3	1	1	3		1										35	71
1050									2	5	6	9	8	4	3	6	1		1		1										26	72
1200							1	3	12	18	12	11	8	3	1	1	1														1	72
1400					2	2	7	2	18	23	9	3																				66
1500					1	3	8	16	18	12	2																					60
1600				4	6	5	12	16	10	7																						60
1700				4	8	17	16	13	11	3																						72
1800				3	12	18	17	12	4																							66
1900				10	33	12	11	5	1																							72
2000				8	37	16	9	2																								72
2100				10	24	6	7	1																								48
																															288	982
Exposure time 240 min																																
0900																															72	72
1000					1								4	1	2																64	72
1100								3		3		6	1	4	1	3	1	1		2	1										45	71
1200							2		4	10	9	8	7	9	3	1	1	1	1		2		1								13	72
1300								3	8	17	20	11	3	3	2	1	1	1													2	72
1400							1	2	12	23	17	12	2	3																		72
1500							1	6	15	33	12	4	1																			72
1600						1	4	10	11	28	14	3	1																			72
1800					1	2	6	20	28	8	3	3	1																			72
1900					1	4	9	21	26	8	2	1																				72
2000					1	10	15	22	16	6	1	1																				72
2200				12	18	13	18	7	3	1																						72
2300				10	31	11	10	7	3																							72
2400				5	13	6	17	13	11	6	1																					72
2500				14	25	7	5	10	9	2																						72
																															196	1079

Dose, r	1	2	3	4	5	6	7	8	9	10	11	12	13	14	15	16	17	18	19	20	21	22	23	24	25	26	27	28	29	30	Survivors	Number of Animals
Exposure time 480 min																																
1000																															60	60
1100											1		1			1	1					1					1				60	66
1200									1		1	5	7	1	2	1	1	1				1					1				44	66
1300						1	1		2	2	6	3	12	6	6		2	3			2										26	72
1400						1		2	2	13	17	11	6	6	4	2	3	1				1									3	72
1500								6	9	20	14	12	6	3						1											1	72
1600							4	3	23	24	12	5	1																			72
1800						1	2	10	16	16	18	6	3																			72
2000							5	9	32	19	7																					72
2100					1	4	14	15	25	6	6	1																				72
2200				3	5	4	16	17	20	2	4	1																				72
2300				2	2	1	17	19	21	7	3																					72
2400				6	9	12	18	13	13	1																						72
2600				18	17	7	19	5	3	2	1																					72
2700				2	2	10	11	9	7		1																					42
2800				13	23	9	8	7	5	1																						66
3000				19	20	7	10	6	4																							66
																															194	1158
Exposure time 960 min																																
1100										1		1		1																	69	72
1150														1	2	1															68	72
1200										1		1		1	1	2	1						1					1			63	72
1300									1		1	4	1	1	6	4	1	1													52	72
1400								1		1	2	4	7	5	6	6	2	2	1	1					1		1				32	72
1500								1	2	5	5	14	9	9	6	6	2	4	2	1		1			1			1			3	72
1600					2		2	2	5	6	15	13	15	8	3	1																72
1700								1	6	15	19	16	5	6	2	1			1													72
2000					1	1		3	10	24	20	6	7																			72
2200						1	2	6	20	25	14	2	2																			72
2300						1	3	18	18	19	11	1	1																			72
2400					1	4	9	13	20	21	4																					72
2600					1	10	2	26	18	6																						72
2700				1	11	17	14	9	17	3																						72
2800				4	30	12	14	8	3	1																						72
3000				1	30	20	9	9	2	1																						72
3200				3	20	14	8	2	1																							48
3500					11		1																									12
																															287	1212

Dose, r	1	2	3	4	5	6	7	8	9	10	11	12	13	14	15	16	17	18	19	20	21	22	23	24	25	26	27	28	29	30	Survivors	Number of Animals
Exposure time 1440 min																																
1200							1							3																	68	72
1300										1	1	2	3	1	3	2					1	1									57	72
1400									1		2	2	9	3	4	7	2		2												40	72
1500									3	1	2	14	6	14	6	3	3		2		1	1			1	2					13	72
1600					1	1	2	2	3	8	16	10	10	10	1	2	1														5	72
1700							2		4	10	12	22	9	9	3		1															72
2000							3	3	7	23	22	7	5	2																		72
2200				1		3	4	7	20	24	8	3	2																			72
2300					2	6	9	13	19	16	6	1																				72
2400					2	8	12	19	17	12	1	1																				72
2500				1	7	15	13	19	12	5																						72
2600				4	6	9	10	17	11	10	5																					72
2800				6	13	10	15	11	13	4																						72
3000				2	23	17	11	4	3																							60
3200				8	15	18	1	4	2																							48
3500				2	14	7		1																								24
3800				5	15	4																										24
4000					24																											24
																															183	1116

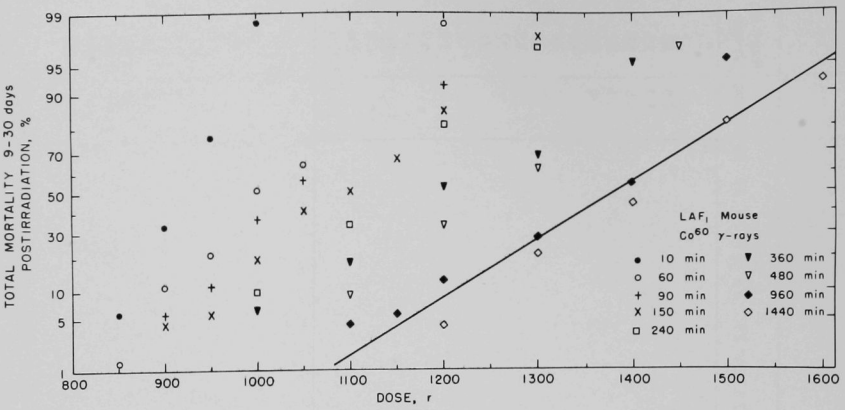

Figure 22. Probit transform of percent mortality between 9 and 30 days post-irradiation in LAF_1 mice versus dose, by exposure-time groups.

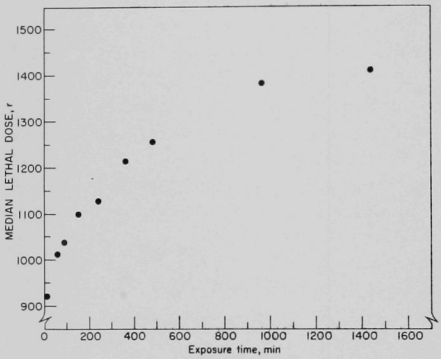

Figure 23. LD_{50} versus exposure time for the proportion of LAF_1 mice dying between 9 and 30 days after Co^{60} γ-irradiation.

We assume that these two processes are independent and that the lethality due to the time-dependent process is described without contamination by the dose-mortality curve of the combined 960- and 1440-min exposure groups (Figure 22). The contribution of this mortality is then removed from the total mortality observed in all groups* exposed less than 960 min. The corrected mortalities are exhibited with respect to exposure time and dose in Figure 24, and represent the mortality due solely to the time-independent process (reversible effects). For each group we determined the ratio between the dose (D) received over some exposure time and the dose (D_{60}) required, if delivered in 60 min, to produce the same group mortality. The mean ratio D/D_{60} for each exposure time was computed; the linearity of the relationship between these ratios and exposure time is shown in Figure 25. Using the least squares constants obtained for the relationship above, the linear function representing the D/D_0 versus exposure time relation was approximated (Figure 25) and the instantaneous dose-mortality

*Group refers to the collection of irradiated animals that receive the same dose at the same rate.

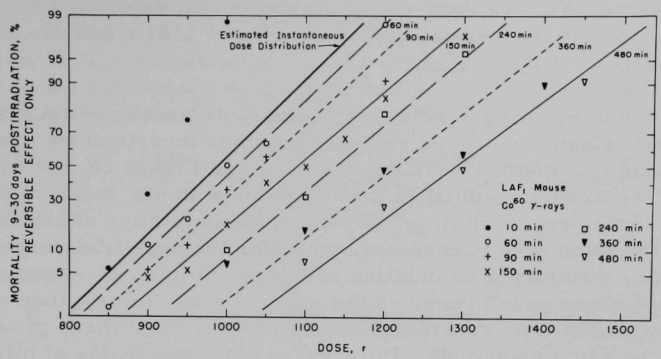

Figure 24. Probit transform of percent mortality between 9 and 30 days post-irradiation attributed to reversible effects versus dose, by exposure-time groups.

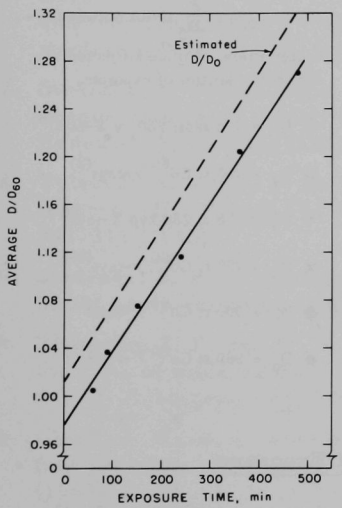

Figure 25. Average $\frac{D}{D_{60}}$ ratio versus exposure time.

distribution was determined (Figure 24). The symbol D_0 represents the dose that if given instantaneously, would produce the observed group mortality. Since a reduction in reversible effects is assumed to take place during an exposure, the full effect of the dose will be registered only if delivery is instantaneous. Thus the mortality distribution of instantaneous doses measures the tolerance of the organisms to the non-reversed effects. Using the estimated D_0 line in Figure 24 and the linear model

$$\frac{D}{D_0} = 1 + \frac{t}{\tau} \quad ,$$

the theoretical curves at exposures from 90 to 480 min in Figure 24 were constructed. The time constant τ = 1547 min and the instantaneous dose distribution (LD_{50} = 985 r, $\hat{\sigma}$ = 84 r) together represent all the information displayed in Figure 24 (except for the 10 min groups) and are the essential parameters associated with the reversible effect. Thus, acute mortality occurring between 9 and 30 days after exposure (the 30-day lethal range) can be explained by postulating two injury processes that independently contribute to the observed mortality - a linear reversal process that is the dominant lethal process at short exposures and an irreversible process that governs the lethality with exposures of

very low rate. For the dose-mortality curve that expresses the population sensitivity to the irreversible process, LD_{50} = 1381 r and $\hat{\sigma}$ = 133 r (Figure 22).

It is interesting to note that comparable experimental results with continuous, single exposures reported by other investigators can be compared using this method of standardization. In Figure 26, the computed D/D_0 ratios based on published data together with our results are plotted with respect to exposure time. Several strains of mice and different qualities of radiation are represented, but under the dose transformation used, the kinetics of injury accumulation are very similar. If we assume that the groups represented received the same average injury, then we could surmise that the time constants associated with all of these groups have roughly the same magnitude. Differences between strains of mice and qualities of radiation may simply alter proportionately the amount of radiation required for a unit of injury.

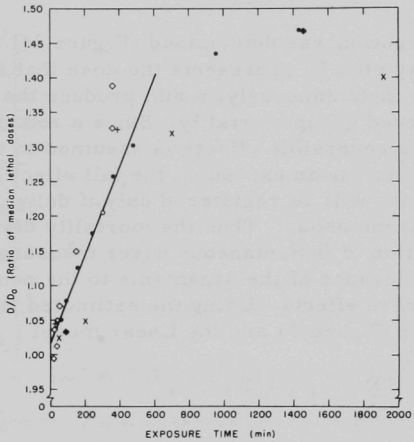

Figure 26. Comparison of $\frac{D}{D_0}$ ratios between selected strains of mice subjected to different qualities of exposure.

◇ D_0 = 775 rads; 250 kv X-rays[6]

○ D_0 = 753 r; Co^{60} γ-rays[2]

+ D_0 = 475 r; 250 kvp X-rays[2]

× D_0 = 772 r; Co^{60} γ-rays[10]

◆ D_0 = 900 r; Co^{60} γ-rays[11]

● D_0 = 960 r; Co^{60} γ-rays[12]

Mortality within 9 Days of Exposure

With increase in dose in the supralethal range, radiation deaths occur in increasing proportion before the ninth day after exposure (Table 22). For the highest dose used in these experiments (400 r delivered in 1440 min), 100% mortality was achieved by the fifth postirradiation day. Two periods of peak mortality can be discerned in the daily mortality patterns - 3 to 6 days and 6 to 9 days. These periods correspond roughly to the postirradiation time of appearance of the intestinal syndrome and of bacteremia, respectively. Different processes of injury accumulation are lethally expressed within these periods. However, the kinetics of these processes can be shown to fall into one of the two types that characterize radiation effects of the 9-30 day period.

References

1. Quastler, H. Time-dose relations in radiation effects. Proceedings of Conference on Research on the Radiotherapy of Cancer. American Cancer Society, New York, 1961. pp. 100-112.

2. Meredith, O. M. Models for Acute Radiation Mortality Response in Mice Exposed to 250 kvp X-rays or Co^{60} Gamma Rays. University of California, Los Angeles, 1961. Report UCLA-488.

3. Kingery, L. B. Saturation in roentgen therapy; its estimation and maintenance. Preliminary report. Arch. Dermatol. 1, 423-433 (1920).

4. Lea, D. E. Actions of Radiations on Living Cells. Macmillan Co., New York, 1947.

5. Blair, H. A. A quantitative description of latent injury from ionizing radiation. Symposium on Information Theory in Biology, ed. H. P. Yockey. Pergamon Press, New York, 1958. pp. 331-340.

6. Brown, J. A. H., M. J. Corp and D. R. Westgarth. Effect of dose-rate and fractionation of X-ray dose on acute lethality in mice. Intern J. Radiation Biol. 2, 371-381 (1960).

7. Stearner, S. P. and S. A. Tyler. An analysis of the role of dose and dosage rate in the early radiation mortality of the chick. Radiation Research 7, 253-266 (1957).

8. Tyler, S. A. and S. P. Stearner. Modes of radiation death in the chick embryo. II. A model of lethal mechanisms. Radiation Research 12, 301-316 (1960).

9. Stearner, S. P., S. A. Tyler and M. H. Sanderson. Comparative kinetics of acute radiation lethality. This report, pp. 67.

10. Thomson, J. F. and W. W. Tourtellotte. The effect of dose rate on the LD_{50} of mice exposed to gamma radiation from Co^{60} sources. Am. J. Roentgenol. 69, 826-829 (1953).

11. Clark, J. W., D. L. Jordan and H. H. Vogel, Jr., Biological effects of fast neutrons and gamma rays. Am. J. Roentgenol. 77, 524-530 (1957).

12. Stearner, S. P. Unpublished observations.

TOXICITY OF PLUTONIUM IN MICE

Miriam P. Finkel and Birute O. Biskis

The major consequences of exposure of experimental animals to plutonium were known within the first few years after this new element became available for biological experimentation.[1,2] In order to compare plutonium toxicity with that of other radioelements under a set of standard conditions, we designed an experiment in 1951 with 900 mice. Although these studies have contributed to several communications published between 1953 and 1959,[3-7] they have not been reported in detail. One reason is that the animals were plagued with an intestinal infection, which seriously reduced both the population and our interest in analyzing the data. Since it is not unusual for mouse colonies to carry endemic infections, it is important that the situation be recognized when it does occur and that it be taken into account during the processing of the data. This experiment now has been examined with a view to differentiating between those pathological lesions induced by infectious and other diseases and those specifically caused by plutonium. Care has been taken to present the results in such a way that recognition of changes due to plutonium is least influenced by extraneous diseases.

Materials and Methods

The CF No. 1 female mice scheduled for the experiment arrived in the Laboratory when they were 5-6 weeks old. Many died during the next three weeks, their major symptom being diarrhea. The best-appearing animals were selected when they were 9-10 weeks old, the hope being that the disease had run its course and would cause little further difficulty. They were assigned 15 to a cage by a system of random numbers. One week later Pu^{239} citrate in acid, isotonic solution was injected into one of the lateral tail veins. The control mice were injected with a comparable solution without plutonium. The amounts administered in $\mu c/kg$, based upon the 24-g average body weight of the entire population before injection, are listed in Table 23 for each group.

Experimental routine included daily observation of the animals and the selection of moribund individuals for sacrifice. We felt that the error introduced into the survival data by killing animals *in extremis* was more than offset by getting fresh material for histologic study. In addition, this procedure made it possible to obtain a peripheral blood sample from a tail vein just before autopsy. Hemoglobin determinations and white blood cell and differential counts were made routinely.

TABLE 23

Experimental plan

Group	Amount injected μc/kg	Number of cages	Number of mice
1	40.6	1	15
2	26.5	1	15
3	15.6	2	30
4	6.1	3	45
5	3.1	3	45
6	1.7	4	60
7	0.69	5	75
8	0.34	6	90
9	0.16	6	90
10	0.08	7	105
11	0.04	8	120
12	0	14	210
	Total	60	900

Tissues taken for histologic study at the time of autopsy included lung, thymus, liver, spleen, kidney, ovary, and mesenteric node. Any other tissues that appeared abnormal were also preserved. After the viscera had been removed, an X-ray picture of the skeleton was taken. The thoracic and lumbar vertebrae and a femur, as well as any other areas that appeared abnormal on the roentgenogram, were then taken for histologic study. Animals that died a natural death were inspected grossly, and their tissues were examined histologically if autolysis was not advanced. The amount and kind of material available for study is summarized in Table 24.

TABLE 24

Extent of material

Number of mice	Contribution	Number of mice	Contribution
900	Total	850	Histopathology of soft tissues and/or bone and/or hematology
2	Missing		
12	Accidental death	834	Soft tissue histopathology
886	Death date and roentgenogram	815	Skeletal histopathology
12	Too autolyzed for autopsy	749	Terminal hematology
874	Some autopsy record		
24	Gross autopsy only		

Results

Survival

The average survival time of the mice within each dosage group and within each cage of each group is illustrated in Figure 27. The values for some cage units within a given group were so different that they seemed not to belong to the same population. Analysis of variance indicated that the probability of seeing chance variations as great or greater than those observed within Groups 4, 5, 6, 7, 9, 11, and 12 was less than 0.01. The probability for Group 10 was between 0.01 and 0.05, and only for Groups 3 and 8 was it greater than 0.05. Obviously, something besides plutonium had had a profound effect upon survival, and comparison of dosage groups on the basis of average survival time alone has little meaning in this experiment. It should be noted that even in Groups 5, 6, and 7, which had received 3.1, 1.7, and 0.69 μc Pu/kg, respectively, the average survival time of one cage unit was the same as, or exceeded, the average of the control group.

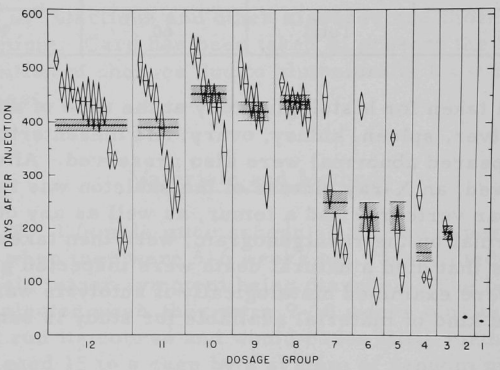

Figure 27

Average survival time. The broad horizontal bar and shaded area mark the mean and standard error of the mean for each dosage group. The diamonds represent the mean and standard error for each cage unit.

The number of mice dying within successive 25-day periods is plotted for each dosage group in Figure 28. When all the mice are considered, there seems to be very little difference in the frequency distributions among Groups 8 through 12. When only those animals that belong to cage units with relatively good survival are considered, Groups 6 and 7 also seem to fall in line with the control and lower dosage groups. One might be tempted at this point to eliminate from further study all members of those cages that displayed poor survival relative to others in the same group. Such a procedure, however, would remove many mice that lived as long as "the average mouse," or even longer.

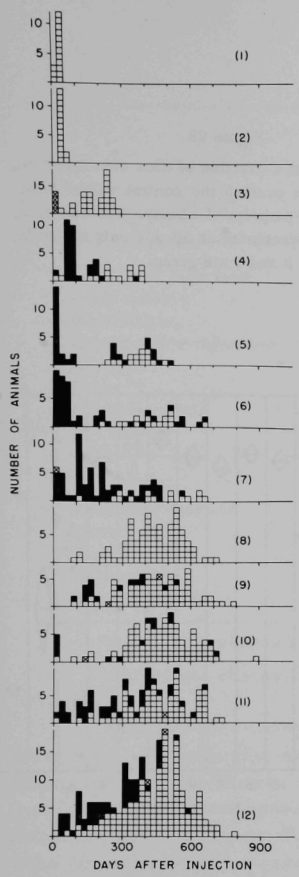

Figure 28

Frequency distribution of death with time after injection. X indicates animals killed accidentally or missing. Black squares mark animals belonging to cage units with poor survival relative to others in the same dosage group.

Life expectancy is plotted in Figure 29. This method of presenting survival data has an advantage over cumulative mortality because it emphasizes the living population rather than the dead. Such a change of emphasis is particularly useful when death from infection occurs early in an experiment. The data show a rather sharp distinction between dosage Groups 5 and 6, and it is clear that life expectancy was reduced by the administration of 3.1 μc Pu/kg or more. Life expectancy of Groups 6 and 7 (1.7 and 0.69 μc/kg, respectively) was very similar to that of the control group between 300 and 600 days; consequently the reduction observed before and after this period may not have been due to plutonium. Smaller amounts of plutonium (0.34-0.04 μc/kg) did not decrease life expectancy.

Terminal Hematology

The hemoglobin values of the moribund animals are presented in Figure 30. The administration of 15.6 μc Pu/kg or more markedly reduced the amount of hemoglobin; 6.1 μc/kg or less seemed to have no effect.

The concentration of white blood cells is given in Figure 31. A large portion of the observed variation was due to values from animals with tumors of the reticular tissues, a disease that is frequently associated with an elevated white count. When cases of reticular tumors were excluded from the calculations, most mean cell counts were lower, and there was less variation. A change in leucocyte concentration occurred between Groups 6 and 7, those mice that received 0.69 μc/kg or less having an average count about the same as that of the control mice.

Terminal Pathology

It is not always possible, and often not appropriate, to designate a single specific reason for death. In fact, in this experiment the immediate cause of death usually was the intravenous administration of sodium pentobarbital. In spite of unavoidable errors, however, an attempt has been made to assign a primary cause of death to each mouse. The listing in Table 25 gives an over-all view of the disease situation.

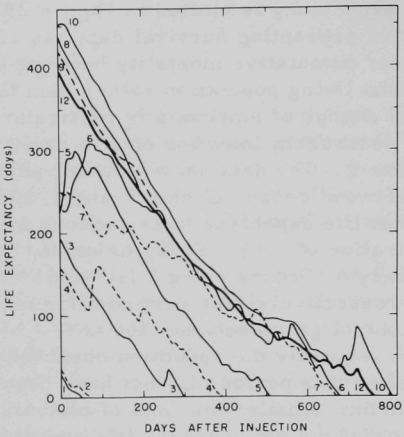

Figure 29

Life expectancy as a function of time after injection. Some values that overlap the control values have been omitted for purposes of clarity. For example, Group 11 is not represented at all, and only the early values for Groups 8 and 9 are given.

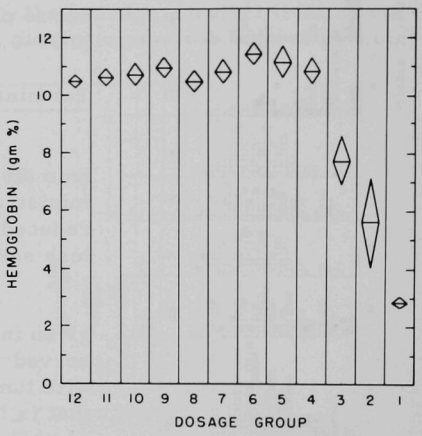

Figure 30

Terminal hemoglobin values in g/100 ml. The diamonds represent the mean and standard error of the mean for each group.

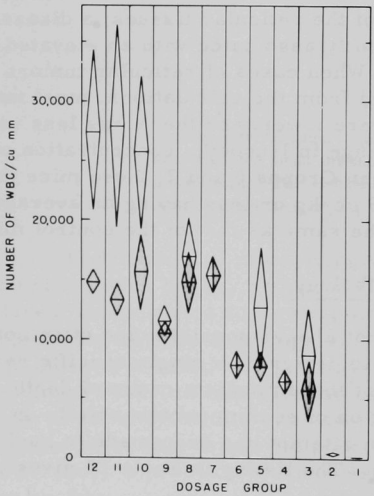

Figure 31

Terminal number of white blood cells/mm^3. The mean and standard error of the mean for all samples in each group are represented by the open diamonds. The shaded diamonds exclude cases of reticular tissue tumors; in Group 3 one very abnormal count also was excluded.

TABLE 25

Terminal pathology

Disease	Major cause of death		Present at death	
	Number of cases	%	Number of cases	%
Non-neoplastic	540	61.0		
Intestinal infection	219	24.7	334	37.7
Amyloidosis	156	17.6	214	24.2
Dermatitis	19	2.2	99	11.2
Respiratory infection	17	1.9	36	4.1
Kidney*	16	1.8	49	5.5
Liver**	13	1.5	246	27.8
Miscellaneous	46	5.2		
Not known	54	6.1		
Neoplastic	346	39.0	(927)	(104.8)
Reticular tissues	132	14.9	175	19.8
Lung	86	9.7	433	48.9
Mammary	63	7.1	90	10.2
Osteogenic	47	5.3	66	7.4
Miscellaneous	18	2.0	163	18.4

*Amyloid degeneration of kidney and liver is not included.

**Pathologic change associated with intestinal infection is not included.

The greatest single cause of death was intestinal infection. The next was amyloidosis, and tumors of the reticular tissues were third. Respiratory infections, which had been a major problem in previous experiments, were responsible for only 17 deaths. Other points of particular interest are: 1) liver disease was responsible for only 13 deaths, but it was present in 246 cases; 2) almost 50% of the mice had lung tumors; 3) the "average mouse" had 1.05 tumors.

Since the main subject of this report is plutonium toxicity, not mouse pathology, only those conditions that might be important in assessing toxicity will be considered further.

Intestinal infection. Salmonella infection, which had caused many deaths before the experiment began, continued to be a problem throughout the first year. Even after 500 days a few animals showed the gross and microscopic lesions typical of this disease. Other intestinal infections included seven cases of Pseudomonas and some that remained unidentified.

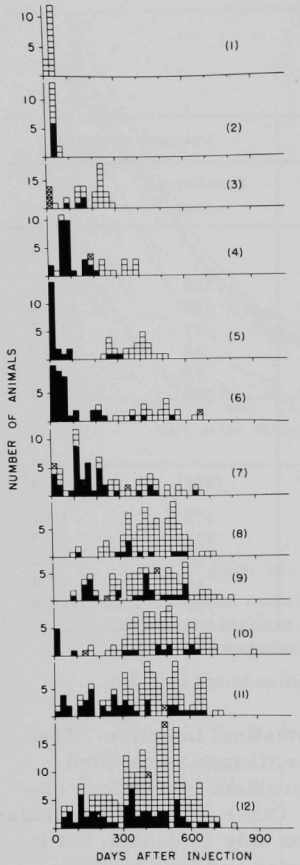

Figure 32

Frequency distribution of death with time after injection. X indicates animals missing or killed accidentally. Black squares indicate mice dying with intestinal infection.

The frequency distribution of death with intestinal infection is given in Figure 32. Except for a very high incidence soon after injection in Groups 4, 5, and 6 and the absence of early cases in Group 8, there was no pattern associated with dosage group.

Amyloidosis. Amyloid disease was almost as serious a factor in depleting the population as was intestinal infection. Deposits occurred most frequently in the liver, kidney, spleen, and ovary. Amyloidosis was usually present in mice that had dermatitis. The Chi-square test (with Yates' correction) gives a value of 96.1 which is a probability of much less than 0.001 that there is no association between these two conditions. Chronic skin infection seemed to be due in large part to an infestation with mites. Mites are no longer a problem in our mouse colony, and in recent experiments amyloidosis has been very rare. The frequency distribution in Figure 33 shows that the disease was not influenced by plutonium administration.

Liver pathology. Both fatty and parenchymatous degeneration of the liver occurred. However, it is very difficult to evaluate these changes in terms of plutonium toxicity because both Salmonella and Pseudomonas infections often were associated with liver lesions, and amyloid deposits were common. The frequency distribution of death with fatty or parenchymatous degeneration of the liver is plotted in Figure 34. Although no cases of fatty degeneration were seen among the control mice, it has been seen in the controls of other experiments. There is a suggestion that cases appeared sooner among animals that received 0.69 μc Pu/kg or more.

Inclusion bodies were found within the nuclei of some hepatic cells in a few animals (Figure 35). They seemed to occur most frequently in mice belonging to the higher dosage groups. In general, both the number of cells involved and the number of inclusions per nucleus were greater after larger amounts of plutonium had been given. In this experiment

nuclear inclusions were not seen in any livers of control mice, but they have been seen occasionally in other old control animals. The proportion of livers studied histologically that showed nuclear inclusions, fatty degeneration, or parenchymatous degeneration is given in Table 26.

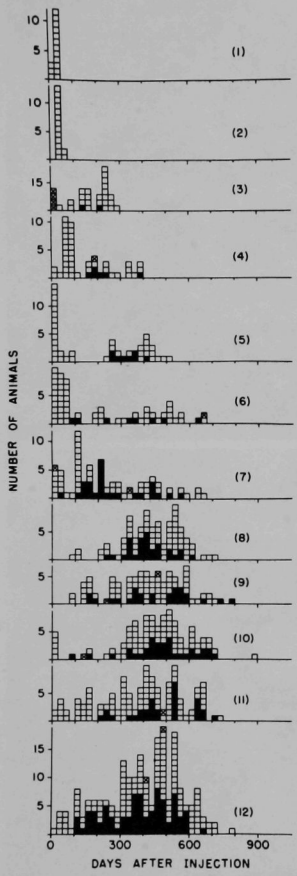

Figure 33

Frequency distribution of death with time after injection. X indicates animals missing or killed accidentally. Black squares indicate animals dying with amyloidosis.

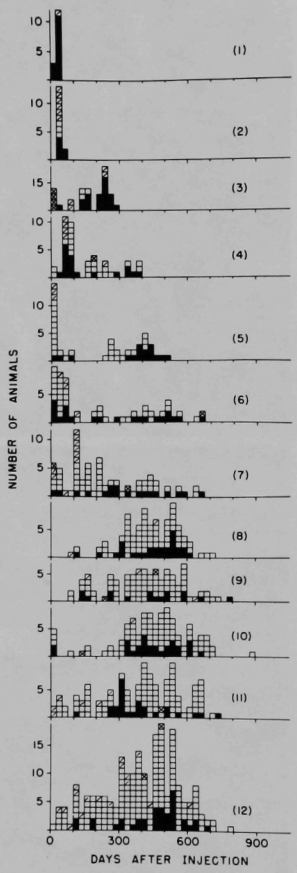

Figure 34

Frequency distribution of death with time after injection. X indicates animals missing or killed accidentally. / indicates animals whose livers were not examined histologically. Black squares indicate mice dying with fatty or parenchymatous degeneration of the liver.

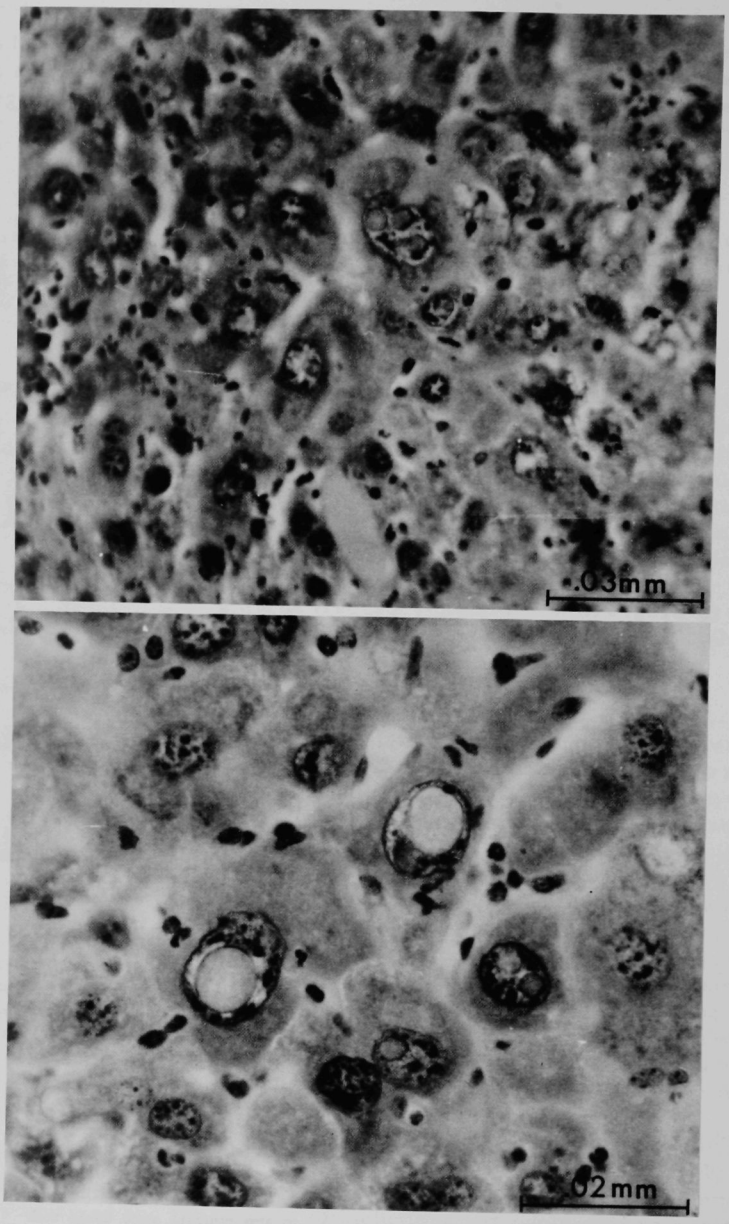

Figure 35. Microphotographs of liver of mouse 233 days after the administration of 15.6 μc Pu/kg. Several of the hepatic cell nuclei are larger than normal, and they contain one or more inclusion bodies.

TABLE 26

Incidence of liver changes

Dose, μc/kg	Number of mice studied histologically	Histologic alteration		
		Parenchymatous degeneration, %	Fatty degeneration, %	Nuclear inclusions, %
40.6	14	78.6	21.4	7.1
26.5	9	22.2	44.4	0
15.6	22	86.4	0	36.4
6.1	39	20.5	25.6	5.1
3.1	43	32.6	4.7	11.6
1.7	56	21.4	17.9	1.8
0.69	66	21.2	6.1	0
0.34	88	28.4	2.3	1.1
0.16	86	15.1	3.5	1.1
0.08	104	24.0	2.9	4.8
0.04	114	19.3	3.5	1.8
0	192	18.8	0	0

No mice in this experiment had malignant tumors of the liver, but there were 35 hepatomas. Hepatoma incidence, which is given in Table 27, seems not to be associated with the amount of plutonium that had been administered.

Mammary tumors. There were 101 mammary adenocarcinomas and five mammary adenoacanthomas within the total population. Since most of the deaths with mammary tumors occurred more than 300 days after the start of the experiment, the proportion of mice with tumors tended to be greater among those dosage groups that lived longer (Table 27).

Lung tumors. Lung tumors appeared as early as 50 days after injection, and the incidence of these tumors continued to increase with age (Figure 36). As a consequence, the lower dosage groups had larger proportions of mice with lung tumors than the higher dosage groups (Table 27). Seventy-nine percent of the neoplasms that were examined histologically were adenocarcinomas; the rest were adenomas.

Tumors of the reticular tissues. The proportion of animals that died with any one of the tumors of the blood-forming tissues is given in Table 28. The increase in incidence with decrease in amount of plutonium over part of the dosage range was due to the fact that all but the lymphocytic tumors occur primarily in middle or advanced age. The time factor is included in Figure 37, where there is no evidence that plutonium changed the normal incidence of reticular tissue tumors.

Osteogenic sarcomas. Sixty-six of the 886 mice had malignant tumors of bone when they died. Most of these belonged to dosage Groups 3 through 8, but there were three in Group 9 and two in the control group (Figure 38). The earliest death with a bone tumor took place 223 days after injection and the last 671 days after.

These 66 mice had 138 malignant bone tumors, all of which were osteogenic sarcomas. Most of the cases of multiple neoplasms appeared in dosage Groups 4, 5, and 6, and within these groups the tumors seemed to be distributed at random among the animals. Consequently, calculation of incidence on the basis of number of tumors rather than number of animals with tumors is preferable. The results of both calculations are given in Table 29, as well as alternative calculations based on total initial population or population alive at 200 days. The latter is a better measure of the carcinogenic response since it eliminates those mice that died early of intestinal infection and other extraneous diseases.

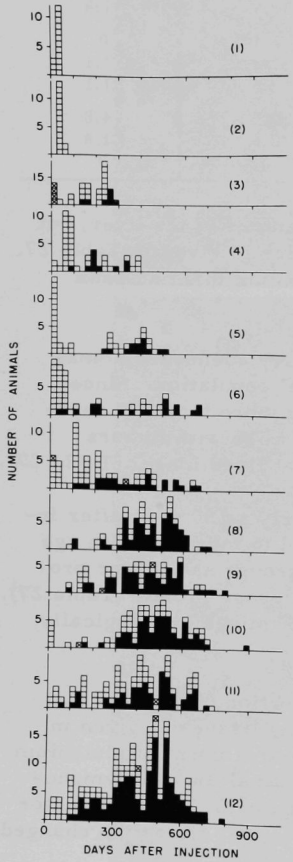

Figure 36

Frequency distribution of death with time after injection. X indicates animals missing or killed accidently. Black squares indicate mice dying with lung tumors.

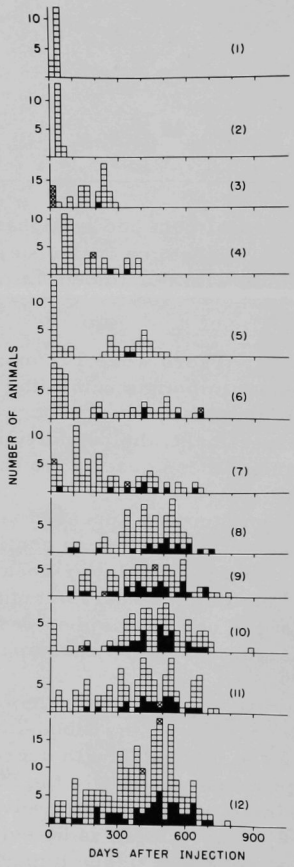

Figure 37

Frequency distribution of death with time after injection. X indicates animals missing or killed accidently. Black squares indicate mice dying with tumors of the reticular tissues.

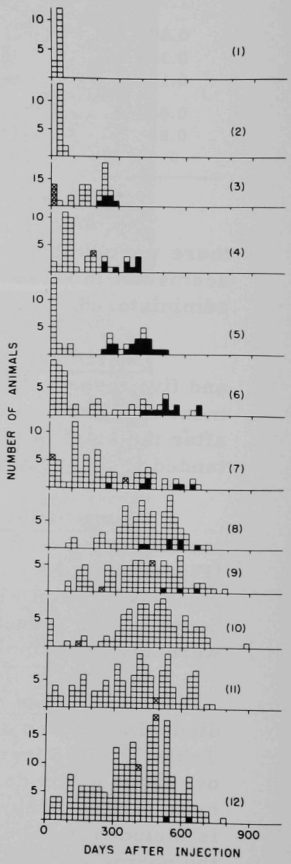

Figure 38

Frequency distribution of death with time after injection. X indicates animals missing or killed accidently. Black squares indicate mice dying with osteogenic sarcomas.

TABLE 27

Incidence of liver, mammary, and lung tumors

Group	Dose, μc/kg	Number of mice	Tumor		
			Hepatoma, %	Mammary, %	Lung, %
1	40.6	15	0	0	0
2	26.5	15	0	0	0
3	15.6	26	0	7.7	26.9
4	6.1	44	0	6.8	22.7
5	3.1	45	4.4	6.7	28.9
6	1.7	59	0	5.1	32.2
7	0.69	73	1.4	4.1	37.0
8	0.34	90	2.2	13.3	67.8
9	0.16	88	3.4	9.1	65.9
10	0.08	104	5.8	16.3	59.6
11	0.04	119	7.6	24.4	47.1
12	0	208	5.8	12.5	60.1

TABLE 28

Tumors of the reticular tissues

Group	Percent with reticular tumor	Tumor type					
		Lymphocytic, %	Granulocytic, %	Plasma cell, %	Reticulum cell sarcoma		Unclassified, %
					Type A, %	Type B, %	
1	0	0	0	0	0	0	0
2	0	0	0	0	0	0	0
3	3.8	3.8	0	0	0	0	0
4	4.5	4.5	0	0	0	0	0
5	4.4	4.4	0	0	0	0	0
6	8.5	5.1	1.7	0	1.7	0	0
7	12.4	6.8	1.4	1.4	1.4	0	1.4
8	23.4	6.7	5.6	8.9	1.1	1.1	0
9	31.7	12.5	4.5	12.5	1.1	0	1.1
10	28.6	8.6	1.9	13.3	1.0	3.8	0
11	21.7	7.5	4.2	7.5	2.5	0	0
12	24.3	9.5	1.4	9.5	1.0	2.4	0.5
Total pop.	19.7	7.7	2.4	7.1	1.1	1.1	0.3

TABLE 29

Osteogenic sarcomas

Group	Mice with tumors	Total tumors	Ratios				Average tumor expectancy
			No. T-mice* / Total no. mice	No. T-mice / No. alive 200 days	No. tumors / Total no. mice	No. tumors / No. alive 200 days	
1	0	0	0	-	0	-	-
2	0	0	0	-	0	-	-
3	6	9	0.23	0.40	0.35	0.60	0.71
4	9	41	0.20	0.69	0.91	3.2	4.3
5	20	42	0.44	0.77	0.93	1.6	1.9
6	12	26	0.20	0.43	0.43	0.93	1.6
7	7	7	0.093	0.18	0.093	0.18	0.28
8	7	8	0.078	0.091	0.089	0.10	0.16
9	3	3	0.033	0.039	0.033	0.039	0.06
10	0	0	0	0	0	0	0
11	0	0	0	0	0	0	0
12	2	2	0.010	0.011	0.010	0.011	0.02

*Tumor-bearing mice

The best way to express carcinogenicity is tumor rate, but the number of animals in this experiment was too small for rates to have any meaning. A reasonably good substitute is tumor expectancy, which is determined by dividing the number of osteogenic sarcomas still to appear by the number of animals still alive. This was done at 10-day intervals, and the average value from 200 days until the time when less than three mice remained alive is given in Table 29. According to this calculation, 2% of the control mice would be expected to die with osteogenic sarcomas, and the incidence would be three times greater if 0.16 μc Pu/kg were administered.

Seventy percent of the malignant bone tumors were located in the spine, 17% in the long bones, 9% in the girdles and ribs, and 4% in the head (Table 30). No association could be demonstrated between tumor location and dosage group or tumor location and time of death.

TABLE 30

Location of osteogenic sarcomas

Bone	Number of tumors
Cervical vertebra	3
Thoracic vertebra	29
Lumbar vertebra	39
Sacral vertebra	19
Caudal vertebra	5
"Spine"	2
Femur	11
Tibia	4
Humerus	4
Ulna	3
Metatarsal	1
Ilium	6
Scapula	1
Rib	5
Head	6

Miscellaneous tumors. A variety of other neoplasms was found, as listed in Table 31. Very few were in animals that died sooner than 400 days after injection. As a consequence, the proportion of mice with these various tumors was greater in the groups that lived longer. There was no indication that any of them had been induced by plutonium.

TABLE 31

Miscellaneous tumors

Tumor	Total number	Dosage group									
		3	4	5	6	7	8	9	10	11	12
Uterine polyp	13		1		1		1	2	2	2	4
Uterine fibromyoma	3								2	1	
Uterine hemangioma	4								1	3	
Uterine sarcoma	3							1	1	1	
Ovarian luteoma	6	1			1		1		2	1	
Ovarian granulosa cell tumor	34			1	1	1	5	5	8	5	8
Ovarian hemangioma	1										1
Osteoma	29	1				2	2	4	7	8	5
Bone fibroma	6				1			4		1	
Skeletal hemangio-endothelioma	2							1	1		
Synovioma	1							1			
Epidermoid carcinoma of skin	9							1	2	3	3
Papilloma of skin	5						2			1	2
Basal cell carcinoma of skin	2						2				
Hemangioma of liver	1										1
Subcutaneous fibrosarcoma	4							1		1	2
Rhabdomyosarcoma	1								1		
Sarcoma of stomach	1										1
Nasal epidermoid carcinoma	1									1	
Adenocarcinoma of hibernating gland	2							1			1
Number of tumors	128	2	1	1	4	3	13	21	27	28	28
Number of mice	885	26	44	45	59	73	90	88	104	119	208
Incidence, %	14.4	7.7	2.3	2.2	6.8	4.1	14.4	23.9	26.0	23.5	13.5

Discussion

It is possible to derive information from a mouse experiment as full of infectious disease as this one, but only if the presence of disease is recognized and if the data are properly handled. Without adequate examination, for example, these survival data could be interpreted as demonstrating that 0.34 μc Pu/kg did not reduce life span but that 0.69 μc/kg reduced it by 43%. A case could even be made for 0.08 μc/kg increasing average survival time. In fact, on more than one occasion these and similar data have been the basis for the statement that a small amount of radiation prolongs life.[8]

Because of the association between cage unit and infectious disease, it is often proposed that mice belonging to different dosage groups be caged together. The chief arguments against such a procedure are: 1) animals potentially debilitated by the experimental treatment are placed

in competition with less debilitated or normal mice, and 2) it introduces the possibility of error in identification. The ideal solution, of course, is individual caging.

Those characteristics that were influenced by the administration of plutonium are summarized in Table 32. The survival data for 1.7 and 0.69 μc/kg were equivocal, and for 0.34 μc/kg or less they were not different from the control data. This lack of evidence of life shortening, however, might be due to the limited number of animals and to the complications imposed by the extraneous diseases.

TABLE 32

Indicator of toxicity

Group	Dosage, μc/kg	Survival	Hemoglobin	WBC	Liver degeneration	Liver nuclear inclusions	Osteogenic sarcoma
1	40.6	+	+	+	+	+	-
2	26.5	+	+	+	+	0	-
3	15.6	+	+	+	+	+	+
4	6.1	+	0	+	+	0	+
5	3.1	+	0	+	+	+	+
6	1.7	?	0	+	+	0	+
7	0.69	?	0	0	+	0	+
8	0.34	0	0	0	0	0	+
9	0.16	0	0	0	0	0	+
10	0.08	0	0	0	0	0	0
11	0.04	0	0	0	0	0	0

Peripheral blood samples from moribund animals were examined as an aid in diagnosing the terminal illness, not as an indicator of plutonium toxicity per se. Serial sampling during the first few months of the experiment might have shown changes in hemoglobin values and number of leukocytes at lower dosages than those indicated in Table 32.

Since a large portion of the plutonium retained after intravenous injection is present in the liver, changes occur within the liver,[2,9,10] and it was most unfortunate that amyloid disease and the intestinal infections complicated the picture. Placing the dividing line for effective and noneffective dosages for fatty and parenchymatous degeneration between 0.69 and 0.34 μc/kg is quite arbitrary.

In previous experiments the presence of inclusion bodies within hepatic cell nuclei had been considered to be more diagnostic of plutonium poisoning than was hepatic degeneration, but in this experiment the condition was not frequent, and never severe. Perhaps a larger amount of

plutonium in longer-lived mice is required for maximum response. Nuclear inclusions cannot be a specific reaction to plutonium deposition because they have been found occasionally in old, untreated mice. However, the number of cells involved and the number of inclusions per cell never have been as great as in mice that received plutonium.

Also in previous experiments bile duct proliferation had been seen in response to plutonium deposition in the liver. This change occurred in only one animal in this experiment, one which had received 15.6 μc/kg. There was no other indication that plutonium localized in the liver might be carcinogenic.

One would not expect tumors of any other soft tissues to be influenced by the intravenous administration of plutonium, except, perhaps, tumors of the blood-forming organs. Even these seemed to be unaffected, however, leaving only osteogenic sarcomas to prove that plutonium is carcinogenic.

The largest number of malignant bone tumors was induced by 6.1 μc Pu/kg; the next higher dosage produced fewer tumors, perhaps because non-neoplastic damage was so extensive. No osteogenic sarcomas appeared among the mice that had received 0.08 and 0.04 μc/kg even though 195 mice were alive in these two groups 200 days after injection. On the basis of the control value of 0.02, four tumors would have been expected among these 195 mice. It is probable that the tumor expectancy of 0.06 after the administration of 0.16 μc/kg represents a real increase over the control value.

None of the tumor ratios nor the tumor expectancy values given in Table 29 falls along a straight line when they are plotted against injected amounts of plutonium. Consequently, they are not very useful for predicting minimum carcinogenic amounts. A semilog plot is no better, but a log-log straight line represents the tumor expectancy values quite well (Figure 39).

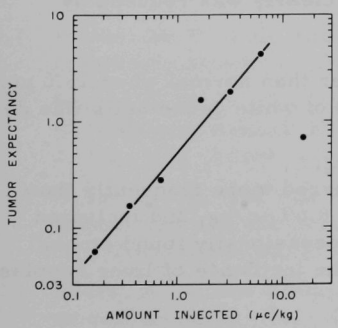

Figure 39

Logarithm of tumor expectancy plotted against logarithm of amount of plutonium injected.

The extensive histopathologic changes seen in the skeleton will be the subject of a separate report.

It would be appropriate at this point to state the magnitude and the duration of the dose responsible for the malignant bone tumors. We expect this to be possible some day. At present we can only say that dosimetry in relation to carcinogensis in

the mouse skeleton is a fascinating and difficult study, and we are not neglecting it. An important clue probably lies in the location of the tumors. The great preponderance of neoplasms in the spine shows that plutonium in trabecular bone is more likely to induce tumors than plutonium in cortical bone. The situation was somewhat the same when Ra^{226} was the carcinogenic agent, but reversed when it was Sr^{90}.[11] The critical factor may be the volume of responsive tissue that receives an adequate dose.

Correlations between the data and retained amounts of plutonium or absorbed dose have not been attempted for several reasons. In the first place, retention studies were not done on animals that were completely comparable to the long-term toxicity animals. In the second place, we would not know over what period of time to integrate an absorbed dose responsible for any given change. In the third place, only values for average absorbed dose could be estimated, and there is no reason to believe that the average has any meaning when the dose is distributed as non-uniformly in space and in time as is the dose from intravenously injected plutonium. The best evidence against the validity of averaging the dose is the fact that the expectancy of having an osteogenic sarcoma at death does not increase linearly with the amount injected but comes close to increasing as a power of the amount injected.

Summary

CF No. 1 mice were given a single intravenous injection of plutonium citrate in amounts ranging from 0.04 to 40.6 $\mu c/kg$, after which they were permitted to live until moribund. Several extraneous diseases complicated the survival data, but life expectancy clearly was reduced by 3.1 $\mu c/kg$ or more.

Terminal hemoglobin values were lower than normal when 15.6 $\mu c/kg$ or more had been given, and the concentration of white blood cells was decreased by 1.7 $\mu c/kg$ or more.

Degenerative changes in the liver occurred more frequently than normal among mice that had received at least 0.69 $\mu c/kg$, and inclusion bodies within the nuclei of hepatic cells were occasionally found among those that had received 3.1 $\mu c/kg$ or more. The incidence of liver neoplasms was not increased.

The number of osteogenic sarcomas surpassed the number among the control mice when the injected amount of plutonium was 0.16 $\mu c/kg$ or more. There were no tumors among the mice that had received 0.04 or 0.08 $\mu c/kg$. Seventy percent of the malignant bone tumors were located in the spine.

We are indebted to Gertrude Hirsch Schribner for her contributions during the course of the experiment, to a large number of technicians and animal caretakers whose efforts made the experiment possible, and to Merlin Dipert and Carol Vancina for their assistance with electronic data processing.

References

1. Brues, A. M., H. Lisco and M. P. Finkel. Carcinogenic action of some substances which may be a problem in certain future industries. Cancer Research 7, 48 (1947).

2. Lisco, H., M. P. Finkel and A. M. Brues. Carcinogenic properties of radioactive fission products and of plutonium. Radiology 49, 361-363 (1947).

3. Finkel, M. P. Relative biological effectiveness of radium and other alpha emitters in CF No. 1 female mice. Proc. Soc. Exptl. Biol. Med. 83, 494-498 (1953).

4. Finkel, M. P. Internal emitters and tumor induction. Proc. Intern. Conf. Peaceful Uses Atomic Energy, United Nations, New York, 1955 Vol. 11, pp. 160-164.

5. Finkel, M. P. The relative biological effectiveness of internal emitters. Radiology 67, 665-672 (1956).

6. Finkel, M. P. Induction of tumors with internally administered isotopes. Radiation Biology and Cancer. University of Texas Press, Austin, 1959, pp. 322-335.

7. Finkel, M. P. Late effects of internally deposited radioisotopes in laboratory animals. Radiation Research Suppl. 1, 265-279 (1959).

8. Henry, H. F. Is all nuclear radiation harmful? AEC Research and Development Report, K-1470. Condensation and revision by M. Brucer, J. Am. Med. Assoc. 176, 671-675 (1965).

9. Brues, A. M. The effects of plutonium on the liver. Liver Injury: Transactions of the Seventh Conference. Josiah Macy, Jr. Foundation, New York, 1948, pp. 59-63.

10. Brues, A. M. and Reitz, L. Effects of external and internal radiation on cell division. Ann. N. Y. Acad. Sci. 51, 1497-1507 (1951).

11. Finkel, M. P. The induction of malignant bone tumors in mice by radioisotopes. Acta Union Intern. contra Cancrum 15, 99-106 (1959).

PROGRESS REPORT: TOXICITY AND METABOLISM OF RADIONUCLIDES
III. SEMIANNUAL REPORT FOR PERIOD ENDING MAY 31, 1962

William P. Norris, Louise S. Lombard, Carl E. Rehfeld,
Thomas W. Speckman and Herman M. Slatis

This is the third semiannual report of studies on the metabolism and toxicity of fission products in purebred beagle dogs. The primary object is to study the effects of injected Ce^{144} and Cs^{137}. The first experiment to determine whether the acutely lethal dose ($LD_{50/30}$) of Cs^{137} is age-dependent has already been performed.

Personnel

In addition to 4 staff members there are 1 technical assistant, 4 technicians and 1 records secretary. There is also 1 part-time laboratory assistant. Two animal caretakers, including a caretaker group leader, have been added, bringing the total to 5. This is now an adequate crew to handle the present number of dogs.

Dr. Herman Slatis is participating in the genetic aspects of the breeding program. Drs. Henry M. Rosenberg and Thomas Emmering, University of Illinois, School of Dentistry, are studying tooth development and dental disease in the dog colony.

Physical Plant

Installation of laboratory furniture, sinks, piped utilities and electric outlets in the laboratory space associated with the kennels was completed in April, 1962.

The Dog Colony and the Genetic Program for Production of a Uniform Strain of Beagles

Animals for these studies have thus far been almost entirely outbred. However, a serious attempt is also being made to produce inbred strains. In this program dealing with the toxicity and metabolism of radionuclides, it could be argued that there is an intention of extrapolating the results to man, a nonuniform animal. However, the data of these experiments will often be observations of qualities such as changes in physiological parameters or tumor frequencies. It is obvious from statistical considerations that changes of these types will more easily be detectable

against a uniform background than against a variable one. The numbers of animals needed to show the various observable effects will be fewer if the strain used has a narrow range of responses. The goal of uniformity can be reached only through a process of selection for genetic homogeneity. An additional advantage is that once a uniform strain has been developed, there will not be much change with the passage of time.

In most organisms it is a rule that inbred animals are less hardy than outbred animals and that hybrids between two inbred strains are the best. Although this rule holds for mice, it has not been tested on large mammals. The inbreeding program began with several distinct strains so that it would be possible to switch to a hybrid of two inbred lines if this appears to be best.

The inbreeding program was begun with four lines of beagles that were already partially inbred. Of these lines, one was purchased because of its history of successful inbreeding and three lines were derived from separate instances of single generations of inbreeding that had taken place within the Argonne beagle colony. Two of these Argonne strains are not proving successful, but the third Argonne strain and the purchased strain have both produced two further inbred generations within two years. These last generations have inbreeding coefficients of about 0.55* in each of the strains. One of these lines now contains a large number of dogs all similar in appearance, so that by stopping further inbreeding and using closed-family, selective breeding it could shortly supply our needs.

There has been only one observation of a congential anomaly among the 59 inbred puppies born in this program, although all dead puppies were necropsied. In addition, there is no evidence of a reduced litter size or decreased fertility among the inbred animals in the two major lines.

The complete record shows that a total of 307 pups have been whelped in the entire breeding program. In the outbred group about 30% of the pups failed to survive to weaning, whereas about 40% of the pups from each of the two prospering inbred lines failed to survive the same period. Some of this difference may be associated with the fact that the inbred bitches have generally been bred at relatively younger (i.e. 16 months or less) ages. Mean litter size was nearly identical in inbred and outbred groups, about 4.5.

---

*This is on a scale that runs from zero for an outbred animal to 1.00 for an animal with an almost infinite number of highly inbred crosses in its ancestry. Among future crosses, further inbreeding of full sibs will increase the inbreeding coefficient each generation by about one-fifth of the difference between 1.00 and the value of the coefficient in that generation.

Among 118 necropsies performed on the stock, breeding and special nonradioactive experimental animals, the following subdivisions have been made: 36 stillborn deaths; 52 newborn deaths (deaths occurring within the first 7 days of life); 20 infectious diseases; and 10 noninfectious diseases (tumors, trauma).

Over one-third of the newborn deaths may be attributed to noninfectious causes, such as failure of the bitch to take care of her offspring, trauma inflicted by bitch and exposure to extreme variations in temperature. Most of the remaining (newborn deaths) were associated with infectious disease processes, such as pneumonia, bacteremia and enteritis; congential anomalies and intussusception were rare. The 20 adult dogs dying of infectious disease were almost entirely limited to the epidemic in the summer of 1960, when an outbreak of distemper and hepatitis occurred. The noninfectious deaths in adult dogs may be divided into the following categories: 4 tumors; 6 trauma.

The Epidemiology and Incidence of Periodontal Disease in Beagle Hounds*

It has been observed previously that beagle hounds maintained in a controlled environment exhibited diseases of the periodontium. From these observations it appeared that the periodontium is subject to abnormal changes at an early age (approximately 9 months) and that the progression of these changes in the periodontium is correlated with aging. Advanced changes in the periodontium result in severe inflammation with eventual loss of gingivae and supporting structures accompanied by loosening and occasional exfoliation of teeth.

Similar observations have been made in the beagle colony at Argonne National Laboratory.

Specific Aims

The proposed research project, which utilizes a colony of purebred beagle hounds in a controlled environment has the following aims: 1) to observe the growth and development of dento-alveolar tissues in beagle hounds (maintained in a controlled environment) in order to assess the morphologic characteristics of the periodontium, 2) to determine the incidence of gingival and periodontal disease based upon objective evidence, 3) to correlate presence or absence of calculus with alterations of the periodontium, and finally, 4) to establish a longitudinal assessment of the morphophysiology of the periodontium.

---

*Dr. Henry M. Rosenberg and Dr. Thomas Emmering, School of Dentistry, University of Illinois.

Methods

Six female and 6 male beagles which could be classified as representative animals of their age groups were selected. Of the 6 females (Group I) 2 were born September 30, 1960, 3 on October 1, 1960, and 1 on October 12, 1960. Of the 6 males (Groups II) 1 was born April 18, 1961, 3 on April 23, 1961, and 2 on April 24, 1961.

Observations include 1) clinical examination of oral cavity, charting specifically for evaluation of tooth cleanliness and calculus, and gingival tissue; (normal or inflamed) 2) evaluation of lateral cephalometric radiographs of each jaw to provide radiographs for serial study; and 3) special procedures including intra-oral photographs (Kodachrome) to record observations objectively, and surface texture buccal impressions and comparison photographs. In addition, representative tissue samples will be taken for histologic study.

General Observations

1. Initial Clinical Assessment of Oral Health Status

Tooth cleanliness. At 9 months of age, definite calculus was observed on upper 4th maxillary premolar at the level of the cemento-enamel junction; it had not progressed to mid-crown. The amount of calculus was less on maxillary 3rd and 2nd premolars. The deposition pattern was irregular on 3rd and 2nd premolars, primarily on the disto-buccal surfaces of the teeth. Light calculus was observed also on mesial surface of the maxillary 1st molar tooth. The canine tooth appeared fairly clean at this age.

Gingival inflammation. Assessment of gingivae was based on color, contour and consistency of the tissue. Inflammation was observed in areas of calculus deposition and ranged from moderate to mild, depending upon the amount of calculus deposition. It appeared to be limited to the free margin of the gingival tissue.

Heaviest calculus deposition was accompanied by swelling, glazing and redness of gingival tissue; this was classified as moderate inflammation. A slight change in the color and contour of the gingival tissue, classified as mild inflammation, was observed in areas of lesser calculus deposition.

2. Periodic Clinical Assessments of Oral Health Status

At 11 months of age, the amount of calculus deposition was increasing, i.e. spreading toward the incisal edge of the 4th premolar and 1st molar teeth approximately at mid-crown level.

At 14 months of age, calculus on the maxillary 4th premolar and the mesial surface of the maxillary 1st molar had definitely progressed to an area between mid-crown and the incisal edge of the teeth. The other maxillary premolars exhibited irregular calculus formation and an accumulation of soft debris. A definite calculus formation was not observed on maxillary canine teeth. Gingival inflammation appeared to be mild to moderate in the maxillary 4th premolar and 1st molar areas. At this time an accumulation of calculus was observed on the mandibular 4th premolar and 1st molar teeth. In addition, stain and soft debris were now observed on the lingual surfaces of maxillary and mandibular teeth accompanied by a very mild gingival inflammation.

It was observed that the rate of deposition and the amount of calculus varied even in animals of equivalent chronological ages. This may be an indication that some animals are more predisposed toward calculus formation and gingival inflammation.

A thorough scaling and prophylaxis were performed on four females of approximately 14-15 months of age. One side of the jaw was treated, the opposite side serving as the control. The animals, when observed 5-6 weeks after treatment, showed accumulation of calculus and soft debris in a pattern similar to the original condition. On the control side (i.e. no treatment), there was marked separation between the gingival edge of the margin of calculus and gingival tissue. Observations 19-26 weeks after treatment showed similar patterns of calculus deposition and gingival inflammation on the treated and control sides. No differentiation could be made between the treated and control sides of the jaws with respect to their oral health status.

At 19-20 months of age, calculus deposition on the maxillary 4th premolar and 1st molar had progressed to the incisal edge of the teeth. All maxillary teeth canine through the 3rd premolar showed definite calculus formation at the gingival margin of the teeth, not extending to mid-crown. The degree of gingival inflammation varied from moderate to severe, depending upon the amount of calculus deposition. Where the greatest change in color, contour and consistency of gingival tissue was observed, a periodontal lesion (pocket) was also noted. Moderate inflammation of lingual gingival tissue was observed around the 2nd and 3rd maxillary premolar teeth together with an accumulation of stain and soft debris.

Mandibular teeth. The canines and 1st and 2nd premolars showed signs of calculus accumulation about the gingival margin. The 4th premolar and 1st molar exhibited calculus formation which approached the mid-crown accompanied by mild to moderate gingival inflammation. Mandibular lingual gingival tissue showed mild to moderate inflammation about the 1st, 2nd and 3rd premolar teeth.

Synthetic diet animal (No. 174). This animal, which for about two years had been maintained solely on a diet compounded of casein, sucrose, cottonseed oil, minerals and vitamins, exhibited the same pattern of calculus accumulation as seen in animals on the Rockland diet, but in addition showed an accumulation of soft debris film or stain on all buccal and lingual surfaces of maxillary and mandibular teeth. Gingival inflammation was much more marked, with increased redness, glazing and edema.

Radiographic Observations

Observations of a limited number of lateral skull radiographs suggested a definite relationship between calculus deposition, tissue inflammation and alveolar bone disease. The earliest observed alveolar bone changes in this group of animals appeared radiographically in the maxillary 4th premolar and 1st molar areas at 19 months of age. The possibility exists that these changes occur at an earlier age, but lateral skull radiographs were not available. Additional radiographic observations were made on a limited number of beagle hounds varying in ages from 19-72 months. Animals were selected at random from the entire colony. The radiographs showed evidence of marked changes in the supporting structures of the dentition which ultimately may result in loosening and exfoliation of teeth.

Semisynthetic Dog Diet

The study of the feasibility of using a semisynthetic food for dogs is continuing with the two diet variations previously described.(1)

Hemoglobin regeneration studies have now been completed on fourteen dogs (7 received the semisynthetic diet and 7 the control diet). In each group the animals were of two ages - 13 months and 7 months at the time of initial bleeding. Approximately 20 percent of the blood was removed from the jugular vein once each week for 5 consecutive weeks. Thereafter, blood was sampled weekly for 6 weeks, biweekly for 6 weeks, and monthly for 5 months. Preliminary study of the data shows that the blood values returned to normal within 5 months after cessation of bleeding in both diet groups and both age groups (Tables 33 and 34). Growth continued normally and appetite was unaffected. The semisynthetic diet appears to be as effective as the control diet in supporting normal hematopoiesis even under the stress of severe phlebotomy.

TABLE 33

Effect of semisynthetic diet on hematopoiesis in 7-month-old beagles

	Semisynthetic diet				Rockland diet			
	Dog				Dog			
	0280	0281	0284	0285	0326	0344	0341	0324
Total blood removed, g	810	714	544	761	851	791	606	771
	Control values (before bleeding)							
Red blood cells, $10^6/mm^3$	6.89	6.92	7.53	6.25	7.15	7.56	6.80	6.70
Packed cell volume, %	48.0	48.0	37.5	41.0	39.5	45.0	40.5	41.5
Hemoglobin, grams/100 ml	12.0	12.0	9.2	10.0	10.6	10.9	10.4	10.6
Mean corpuscular volume, μ^3	68.2	68.0	50.3	68.7	55.3	59.8	59.5	62.6
Mean corpuscular homoglobin, μμg	1.8	1.8	1.2	1.7	1.5	1.4	1.6	1.6
Mean corpuscular hemoglobin concentration, %	26	26	25	24	27	26	26	24
	Values 1 day after final bleeding							
Red blood cells, $10^6/mm^3$	5.41	4.81	6.12	5.87	5.72	5.46	5.66	5.64
Packed cell volume, %	29.0	24.0	26.0	30.0	32.0	31.0	29.0	29.0
Hemoglobin, grams/100 ml	8.3	6.0	5.4	7.6	8.3	7.9	7.7	7.5
Mean corpuscular volume, μ^3	53.6	49.9	42.5	51.1	55.9	56.8	51.2	51.4
Mean corpuscular hemoglobin, μμg	1.5	1.2	1.1	1.3	1.5	1.4	1.4	1.3
Mean corpuscular hemoglobin concentration, %	29	25	21	25	26	25	27	26
	Values 5 months after final bleeding							
Red blood cells, $10^6/mm^3$	6.72	6.98	8.75	7.95	6.72	6.65	6.60	5.97
Packed cell volume, %	46.5	45.5	41.0	44.5	49.0	51.0	45.0	43.0
Hemoglobin, grams/100 ml	12.5	12.0	10.5	11.2	12.0	13.2	12.2	11.7
Mean corpuscular volume, μ^3	69.2	65.2	46.9	56.0	72.9	76.7	68.2	72.0
Mean corpuscular hemoglobin, μμg	2.2	2.2	1.4	1.7	1.8	2.0	1.8	2.0
Mean corpuscular hemoglobin concentration, %	32	33	30	31	24	26	26	27

TABLE 34

Effect of semisynthetic diet on hematopoiesis in 13-month-old beagles

	Semisynthetic diet			Rockland diet		
	Dog			Dog		
	0172	0173	0174	0215	0219	0221
Total blood removed, g	797	826	828	850	900	752
	Control values (before bleeding)					
Red blood cells, $10^6/mm^3$	7.38	7.13	7.74	7.54	6.90	7.08
Packed cell volume, %	47.0	47.0	47.0	47.0	45.0	45.0
Hemoglobin, grams/100 ml	13.5	12.5	13.2	12.6	11.8	12.2
Mean corpuscular volume, μ^3	63.7	65.9	60.7	62.6	65.0	63.5
Mean corpuscular hemoglobin, μμg	1.8	1.8	1.7	1.6	1.7	1.7
Mean corpuscular hemoglobin concentration, %	29	27	28	26	26	27
	Values 1 day after final bleeding					
Red blood cells, $10^6/mm^3$	5.75	4.11	4.94	6.34	4.43	4.97
Packed cell volume, %	35.0	29.0	30.0	40.0	36.0	35.0
Hemoglobin, grams/100 ml	7.8	7.5	8.0	10.0	9.6	9.6
Mean corpuscular volume, μ^3	60.9	70.6	60.7	63.1	81.3	70.4
Mean corpuscular hemoglobin, μμg	1.4	1.8	1.6	1.6	2.2	2.0
Mean corpuscular hemoglobin concentration, %	22	26	26	25	27	28
	Values 5 months after final bleeding					
Red blood cells, $10^6/mm^3$	8.61	8.84	7.55	7.00	6.94	7.07
Packed cell volume, %	52.0	54.5	47.5	47.0	47.0	47.0
Hemoglobin, grams/100 ml	12.6	12.5	12.6	12.2	12.3	12.2
Mean corpuscular volume, μ^3	60.4	61.7	63.0	67.2	67.8	66.5
Mean corpuscular hemoglobin, μμg	1.8	1.8	1.9	2.2	2.3	2.2
Mean corpuscular hemoglobin concentration, %	30	30	30	33	34	33

The Toxicity of Cs^{137}

Experiment 004

As reported previously,[1] dogs given intravenous doses of about 2500 μc of Cs^{137} per kg did not die. These animals had survived 255 days as of May 31, 1962. Four other 13-month-old beagles have now been given Cs^{137} intravenously in doses of about 3500 μc Cs^{137} per kg. Three of these died at about 30 days after injection, but the fourth still survives. The actual values are summarized in Table 35. From the limited sample it is apparent that 3500 $\mu c/kg$ is close to the $LD_{50/30}$ for dogs of this age.

TABLE 35

Survival of beagles following intravenous administration of 3500 μc of Cs^{137} per kg body weight

(Experiment 004)

Dog No.	Cs^{137} Injected, μc	Survival after injection, days
Aged 13 months at time of injection		
0237	28,210	28
0239	32,550	>134
0241	23,520	33
0243	37,835	35
Aged 5 months at time of injection		
0397	29,085	>44
0398	27,685	26
0399	28,175	>44
0401	24,605	27
0404	26,075	>44

In an initial attempt to determine the importance of age in radiosensitivity of the dog, five 5-month old dogs were given approximately the same dose of Cs^{137} intravenously. Two of these died at about 30 days after injection; the other 3 still survive in apparent good health (Table 35). It would appear that these younger animals are at least as radioresistant as the 13-month-old dogs mentioned above - and perhaps even more so.

Pathology

Methods. Tissues taken as soon as possible after the death of the animal are prepared as histologic sections in one of three ways: 1) fresh, unfixed cryostat-cut sections; 2) acetone-fixed, plastic-embedded, e.g., bone

and eye; 3) fixation in neutral formalin, Technicon fixative solution, Genders, Mossman's, and Baker's calcium-cadmium formol, paraffin-embedding. The neutral formalin-fixed tissues as well as the plastic-embedded undecalcified bone sections, are used for radioautographs. The histochemical tests, performed mostly on frozen tissue sectioned in a cryostat, include alkaline and acid phosphatase and lipid-staining technics,and tests for hemosiderin, bile pigments, glycogen, aldehyde groups, calcium salts, lipids, and nucleic acids.

Fifty-five tissues are taken for section. In animals receiving Ce^{144}, many additional lymph nodes from varied locations over the body are taken for section and for radioautographs. In animals injected with Cs^{137}, muscle from many different parts of the body is taken for section. With the latter, organ radioautographs are made from bone and muscle masses.

After death, animals are weighed intact,and their total radioactivity is determined. At necropsy, photographs of lesions are taken, each organ being weighed as it is removed and described. When sections for histologic study are removed, each organ is reweighed and stored at -10°C for radioactivity determination.

The sections are cut on the cryostat and stained, whenever possible, on the same day as the post mortem examination. Paraffin and plastic embedding is done later. Photomicrographs are taken of representative lesions from each group of experimental animals.

Gross pathology. In the two previous semiannual reports(1,2) the pathologic changes for the first groups of Ce^{144}, Cs^{137}, and γ-irradiated dogs were described. These dogs included 9 animals that died following the intravenous injection of Ce^{144} at 47 $\mu c/kg$ to 250 $\mu c/kg$; 4 that received Cs^{137} at approximately 2000 $\mu c/kg$; 2 pregnant animals that received Cs^{137} at 250 $\mu c/kg$, and their offspring; and 5 animals that received 325 r of γ-radiation from a Co^{60} source. Comparisons of lesions produced by lethal doses of Ce^{144}, Cs^{137}, and γ-radiation revealed some differences. Hemorrhages within muscle were more numerous and extensive in animals receiving Cs^{137}. Because the highest concentrations of Cs^{137} were found in muscle, the extent and severity of hemorrhages found in muscle is not unexpected; it was estimated that portions of muscle received as much as 2300 rads in 30 days. Spermatogenesis ceases in animals receiving 2000 $\mu c/kg$ of Cs^{137}, whereas after injection with Ce^{144} or irradiation with γ-rays, the process appears to be halted only temporarily.

The 5 animals that died following Cs^{137} 3500 $\mu c/kg$ were dehydrated at necropsy, with blood-tinged fluid about the nares and mouth. Tarry black feces about the anus were observed only in the 13-month-old animals (0237, 0241 and 0243). Large hemorrhagic areas were noted over the jugular veins

used for collecting blood samples; the only exception was dog No. 0398. All the dogs had hemorrhages of the paranasal mucosa, and one of the 5-month-old dogs (0398) had a unilateral necrotic paranasal sinusitis.

There were massive hemorrhagic effusions in the intercostal muscles, mediastinum, diaphragm, pericardium, heart and lungs (Figure 40) in all but one (0398), which had a few scattered petechial to ecchymotic hemorrhages in these organs. In the animals with extensive thoracic hemorrhages, adhesions appeared between the visceral and parietal pleura. Hemorrhages occurred in all major organs, muscles and subcutaneous tissue. Only those instances in which hemorrhages were particularly severe or significant will be considered in more detail. Hemorrhages in the heart involved the endocardium, myocardium and epicardium of the ventricles, auricles and atrioventricular septum. Hemorrhages within the renal cortex and medulla were extensive and resulted in one instance in filling of the renal pelvis with clotted blood and in macroscopically visible blood in the urine (Figure 41).

Hemorrhages in the mucosa of the tongue, esophagus, stomach small intestine and colon were petechial to ecchymotic in size. Hemorrhagic extravasations occurred in the rectum and adjoining colon, and were associated with ulceration (Figure 42).

The spleen was firm, contracted and homogeneously dark reddish-purple on the surface and cut section. Lymphoid follicles were not apparent on gross examination. The lymph nodes were enlarged, dark reddish-purple and oozed blood-tinged fluid on cut section. The bone marrow was reddish-purple and fatty throughout the shaft and head of the femur.

Histopathology. In the lungs, alveoli were filled with acidophilic finely granular material. In scattered areas the alveolar walls were disrupted or replaced by large areas of hemorrhage. Acidophilic granular material similar to that found in the alveoli infiltrated the pleura. Within the edematous fluid were abundant fibrin strands. Marked edematous swelling occurred within the walls of the veins. Bacteria were seen both inside and outside the cells. There were focal areas of necrosis as well as scattered pyknotic and karyolytic nuclei. Within the lumen and in the walls of bronchi and bronchioles large numbers of fat droplets appeared. Fat droplets lay within the cytoplasm of free and fixed histiocytes. Dense alkaline phosphatase activity occurred over the bronchial and bronchiolar epithelium near the free margin, over mucous cells and over alveolar walls. In the latter the deposition was less than in the bronchial epithelium.

Myocardial cells had vacuolated nuclei and cytoplasm. In scattered areas the myocardium had undergone hyaline change. The interstitial tissue was prominent, because of relative increase in cell numbers, swelling

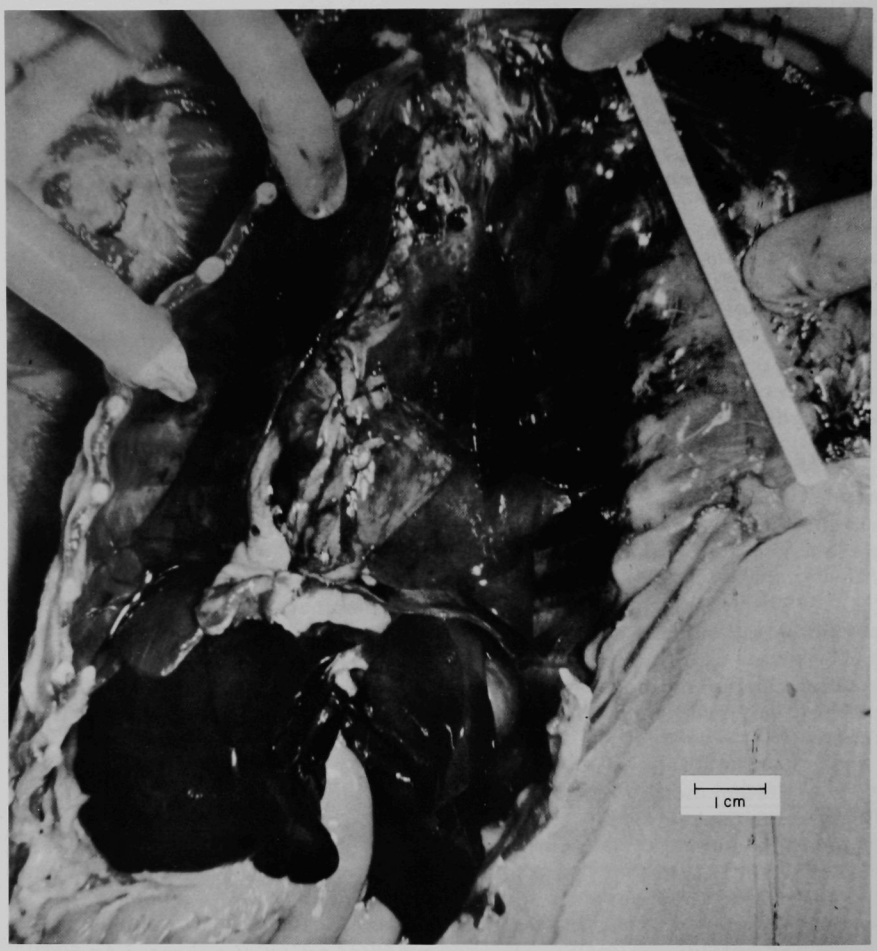

Figure 40. Thorax of dog 0401. Note extensive hemorrhages in visceral and parietal pleura, intercostal muscles, diaphragm, heart and lungs.

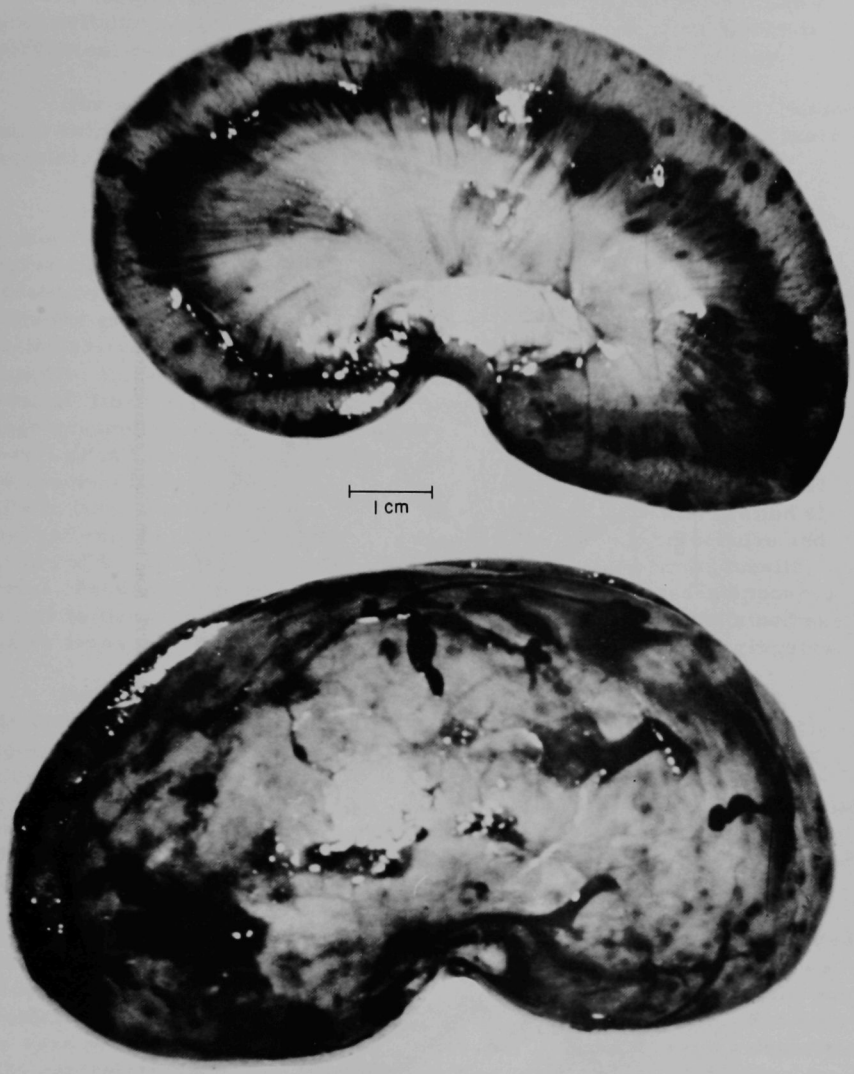

Figure 41. Kidney of dog 0243. Note hemorrhages in renal cortex and medulla, clotted blood in the pelvis.

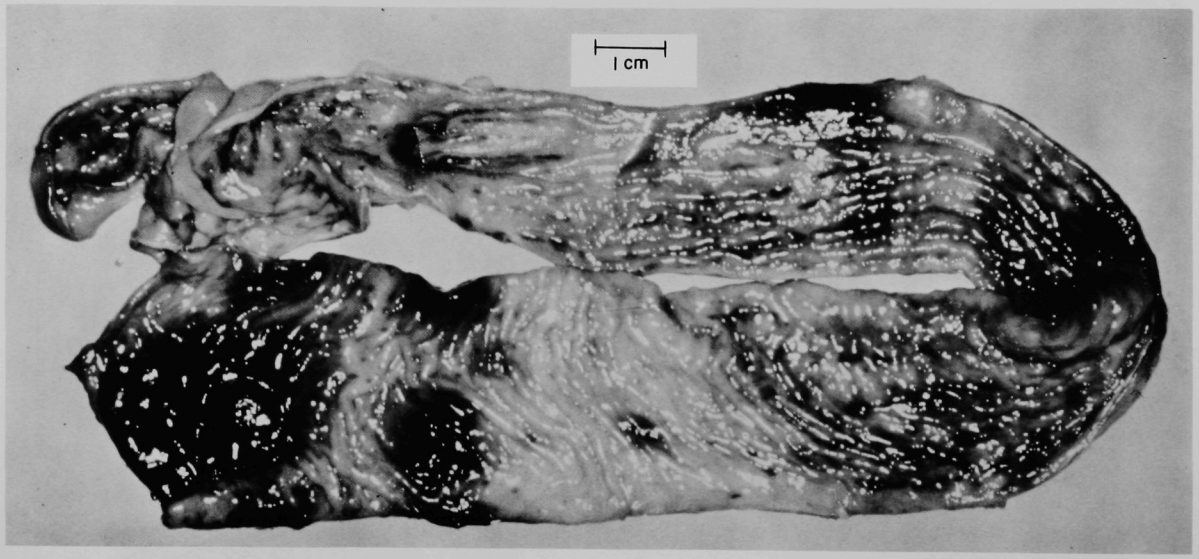

Figure 42. Colon and rectum of dog 0237. Note hemorrhagic extravasations in the mucosae.

of cytoplasm of fibrocytes, and fibrinoid change in areas surrounding coronary vessels. Myocytes were reduced in size, giving the sections a highly cellular appearance. Alkaline phosphatase activity was patchy in distribution, being limited mostly to the areas surrounding vacuoles.

The walls of the coronary veins were markedly edematous. Hemorrhagic extravasations were seen occasionally within their walls, but more frequently in the surrounding tissue.

Lymphoid tissue within the nodes and spleen was sparse, consisting of a few blast cells surrounded by a narrow rim of lymphocytes, plasma-like cells and hemosiderocytes. Many necrotic cells were interspersed within the malpighian bodies. Occasional foci of necrosis occurred within the germinal center. Nuclear vacuolation and intranuclear acidophilic inclusions were prominent within lymphocytes. The venous and lymphatic sinuses were distended with erythrocytes, acidophilic granular material, fibrin strands, hemosiderocytes, necrotic debris and bacteria. Large accumulations of fat droplets were seen within hemosiderocytes, as well as in free and fixed macrophages. Alkaline phosphatase activity was heaviest over the centers of the malpighian bodies and over arterial walls in both nodes and spleen. Acid phosphatase activity was limited almost entirely to phagocytic cells. Many myofibers in the trabeculae and capsule of the spleen were hyalinized. Lymphoid lesions in the tonsils, thymus, Peyers patches, and in solitary and aggregated masses appeared similar to those in the spleen and lymph nodes. The tonsils contained extensive areas of necrosis, multiple ulcers and large bacterial aggregates.

Bone marrow was aplastic in the 13-month-old animals (0237, 0241 and 0243), and hypoplastic in the 5-month-old ones (0398 and 0401). Megakaryocytes were not recognizable, either being absent or markedly distorted. The marrow cavity contained fat cells, erythrocytes, plasma-like cells, hemosiderocytes and aggregates of bacteria. In the 5-month-old animals, scattered small foci of erythropoiesis could be found. Organ radioautographs of bones from the 5-month-old animals showed concentration of activity in the cartilagenous parts.

Liver changes consisted of chronic passive congestion. The dilated central veins and sinusoids were filled by erythrocytes, hemosiderocytes and necrotic debris. The intima of the central vein was edematous and the endothelium either was absent or contained many pyknotic cells. Fat droplets were present in all hepatic cells, with only a slightly heavier deposition in the centrolobular zones. Fat droplets also appeared in blood vessel walls and lumina. Extensive fat deposition occurred in bile duct epithelium. Vacuolation of hepatic cell nuclei and acidophilic intranuclear crystalloids were observed frequently throughout the liver. Alkaline phosphatase activity was distributed evenly over hepatic cells in the mid and peripheral lobular zones but was missing over the centrolobular cells. Activity was heavy over the bile duct epithelium. Acid phosphatase activity was concentrated over bile canaliculi and bile duct epithelium.

Special staining of the gastrointestinal tract was not attempted because of the rapid autolytic changes associated with hemorrhage, ulceration and bacterial invasion. Because of the importance of the intestinal lesions in the acute irradiation syndrome, these studies must be considered in the future, but they necessitate the use of sacrificed animals. (It has been noted that material taken from live irradiated mice shortly before death is unsatisfactory for cell counts because of advanced autolysis.)

In the pancreas a few acinar cells contained acidophilic intranuclear inclusions. Alkaline phosphatase activity occurred over all acini and islets, the intensity being greatest over the islets of Langerhans.

In the adrenal gland individual necrotic cells were scattered throughout the medulla. The thyroid gland was highly cellular, many acini being compressed closely together. Few acini contained colloid, and when present it was fibrillar and weakly acidophilic. The acini varied considerably in size, many having little or no lumen. Alkaline phosphatase activity over the acinar walls occurred in glands with and without colloid.

The testes of two animals (0243 and 0398) showed severe damage with no spermatogenesis. Pathobiotic Sertoli cells and type A spermatogonial cells were the only ones seen in one (0398), and in the other (0243) spermatozoa and spermatids were seen, though rarely. Nuclear vacuolation occurred frequently within the remaining cells of the seminiferous tubules.

The ovaries of the two 13-month-old animals (0237 and 0241) contained several corpora lutea and a few degenerating Graafian follicles with no apparent ova or cumulus oopherus. In one (0241) there were five recently ruptured Graafian follicles, as evidenced by the hypertrophy and infolding of the granulosa, invasion of the theca interna and accumulation of blood within the central cavities. In the 5-month-old female (0401), there were only a few degenerating Graafian follicles.

Sections from the following muscles were studied: biceps femoris, temporalis, longus capitis, diaphragm, and tongue. In the animals injected with Cs^{137}, there was an apparent reduction in width of muscle fibers and an increased cellularity, in comparison with controls of similar age. The thickness of the epimysium was increased through swelling. Fat droplets were frequently seen lying along the endomysium. Hyaline degeneration of muscle fibers appeared in scattered individual bundles and more frequently in association with areas of hemorrhage. While the blood vessel walls were positive for alkaline phosphatase, the muscle bundles were negative.

In summary, the lesions in the animals receiving Cs^{137} were similar to those described previously:(1) widespread hemorrhage, bacteremia, pulmonary edema, chronic passive congestion of the liver, lymphoid hypoplasia, bone marrow aplasia and cessation of spermatogenesis or as in the case of the female, degenerative changes in Graafian follicles.

The bone marrow aplasia may be explained in part by prolonged circulation of Cs^{137} in the blood stream. The lesions were relatively less severe in dog 0398, a 5-month-old male; there was considerably less hemorrhage, and foci of hematopoiesis persisted in the marrow. The distribution of hematopoietic tissue in long bones of dogs has been reported to vary with age and breed; active tissue is found throughout the shaft up to and occasionally including 6 months, and in rare instances up to 12 months. Such widespread distribution might account for survival of hematopoietic centers in young animals.

Hematology

Of the four 13-month-old dogs given 3500 μc of Cs^{137} per kg, 3 died from the effects of this dosage, with survival times of 28, 33 and 35 days. In each of the decedents the circulating leukocytes had diminished to about 150/mm^3 within 25 to 28 days. The erythrocytes had decreased to one-half to one-third the pre-injection numbers in this same period and the sedimentation rate had reached the maximum possible. A decrease in hemoglobin reflected the decrease in cells; however, cell volume and other factors did not appear to change in these 3 dogs.

One dog (0239) survives this dosage of Cs^{137} although its blood-forming capacity was affected nearly to the same degree as that of those which died. This dog exhibited one major difference in that its ability to produce leukocytes was showing recovery at the time when the sedimentation rate was greatest. At 124 days after injection the leukocyte number was only half of the pre-injection value.

Erythrocyte numbers in this same dog (0239) were reduced at least 50% after 39 days, but recovery has been slow and persistent since that time. Hemoglobin does not appear to have reduced in proportion to the decrease in number of erythrocytes; this is primarily due to an increased concentration of hemoglobin per cell, although the cells are generally larger also. As a result of this compensatory action this dog did not suffer an anemia comparable to that seen or predictable for the dogs that died.

In the five 5-month-old dogs injected with 3500 μc/kg Cs^{137}, the leukocytes in the peripheral blood decreased by factors of 2 to 4 within 9 days. No more than 750 leukocytes/mm^3 were recorded from any of the animals on the 23rd day, and there was no correction of this extreme leukopenia. In the 3 dogs surviving on the 28th day the numbers remained at the same level. Erythrocyte numbers had decreased markedly by the 23rd day with a corresponding decrease in packed cell volume. Eosinophilia

occurred on the ninth day in dogs 397, 399 and 401 but counts had returned to normal or below by the sixteenth day. Since dogs 398 and 401 died between the 23rd and 28th days, eosinophilia could not be correlated with death or survival.

There was no evidence of parasitism in these dogs just prior to injection of the Cs^{137}.

Urinalysis

The successive 16-hr urine samples from dogs 0239 and 0243 (ca. 3500 μc Cs^{137} per kg) were tested for protein (Albustix,* 3% acetic acid and heat, and sulfosalicylic acid); reducing substances (Benedict's qualitative reagent); glucose (Clinistix*); ketone bodies (Ketostix*); pentose; and glucuronic acid. Dog 0243 died on the 35th day after injection, while 0239 survives to this date (134 days). All determinations were negative except those for protein and glucuronic acid.

Neither animal excreted protein prior to injection; on the sixth day after injection, both animals began excreting trace quantities (30-100 mg/100 ml). Dog 0239 is still excreting this small amount.

Glucuronic acid excretion increased appreciably in both dogs after injection of Cs^{137}. Dog 0243 normally excreted 100 ml of urine in a 16-hr period. After injection the volume was maintained at approximately 125 ml/16 hr for 25 days. An abrupt drop to 50 ml preceded death. Control values for glucuronic acid were 200 μg/ml or 20 mg per 16 hr. Ten to 12 days after injection this value had risen to 300 μg/ml ($\cong$ 30 mg/16 hr). There was then a drop in concentration for about ten days to control values; this was followed by a rapid rise to 550 μg/ml on the 26th to the 31st day. During this period, the total excretion averaged 25 mg, reached a peak of 48 mg on the 24th day and then fell again to 25 mg.

Dog 0239 showed a slightly different pattern of excretion in that his urinary volume remained unchanged from a control average of 125 ml/16 hr for about 20 days after injection. At this time the volume dropped 40% and remained low for about 30 days when it begin to increase slowly to control values. Glucuronic acid, prior to injection, had been excreted at a rate of 150 μg/ml or 18 mg in 16 hr. After injection, the excretion followed a wave-like pattern; the first peak of 300 μg/ml (or 50 mg/16 hr) occurred on the 19th day; the second of 500 μg/ml (45 mg/16 hr) on the 31st day and the third of 900 μg/ml (80 mg/16 hr) on the 43rd day. After each peak, the values dropped to near control levels. By the 60th day the concentration had risen to 300 μg/ml (38 mg/16 hr); this plateau has held for 70 days.

---

*Ames Diagnostic Tests.

The Toxicity of Ce^{144}

Experiment 003

The survivors in this experiment include two groups of dogs, one injected at 50 $\mu c/kg$, the other at 25 $\mu c/kg$.(1,2)

Since the last reporting one of the dogs (0016) died 376 days after an intravenous dose of 28 $\mu c/kg$.

Pathology

Gross pathology. Yellow discoloration was noted in the skin of the ventral abdomen, foot pads, buccal mucosa and conjunctiva. The pelt adhered tightly to the ribs. Little subcutaneous adipose tissue was apparent, and the connective tissue of the abdominal wall had a yellow tinge. A large hematoma (3.5 x 2.0 x 1.9 cm) lay over the right jugular vein and the surronding fascia and muscle were hemorrhagic. Petechial and ecchymotic hemorrhages occurred in the subcutis over all major parts of the body.

The thoracic cavity contained 35 ml of blood-tinged fluid; the lungs were collapsed and pale pink. The pericardium was diffusely edematous and its sac contained 14 ml of clear fluid. The three coats of the heart were studded with hemorrhages of varying sizes.

The spleen was small and medium-reddish-purple and, on cut section, was homogeneously reddish-purple. The right cervical lymph nodes were edematous, enlarged and dark reddish-purple. Most of the superficial and deep lymph nodes were similar in appearance to those of the cervical nodes, but they varied in size from normal to slightly enrlarged.

The liver was firm and yellow-brown with distinct red lobular markings. The papilla of Vater was enlarged, edematous and hemorrhagic. The common bile ducts were patent. Upon cut section, the liver was fatty and had the same distinct lobular markings seen on the surface.

The stomach contained blood clots and dark reddish-brown fluid. The mucosae were reddened and contained several nematodes. The lumen of the duodenum and jejunum was filled with a reddish-purple pulpy material, dark reddish-purple near the stomach and bright red in the ileum. The mucosae of the jejunum and lower duodenum were the sites of hemorrhagic extravasation and ulceration. The large intestines contained black, formed fecal matter.

The medulla of the kidney was pale yellow, while the cortex was tan, streaked with brown linear markings. A hemorrhagic infarct measuring 1.6 cm at its base appeared in the left kidney.

The marrow of the femur was reddish-purple and fatty throughout.

The adrenal cortex was cream-colored. The ratio of cortex to medulla was 1:1. The thymus gland was markedly edematous and contained numerous petechial to ecchymotic hemorrhages.

Histopathology. Examination of the liver disclosed extensive centrolobular hyaline degeneration and necrosis as well as midlobular fatty change (Figure 43). Both alkaline and acid phosphatase activity were absent in the centrolobular zone; heaviest phosphatase activity occurred in the peripheral lobular zones. Alkaline phosphatase activity occurred relatively evenly over the hepatic cells, whereas acid phosphatase activity was concentrated over the bile canaliculi. There was a relatively even distribution of radioactivity over the hepatic cells and concentrated radioactivity over free and fixed phagocytic cells, as determined by autoradiographic studies.

The lungs were emphysematous and atelectatic. Thickening of intraalveolar septa was prominent.

Within the lymph nodes, the lymphoid follicles appeared normal in size and number. Large numbers of hemosiderocytes appeared throughout the medulla and subcapsular spaces and occasionally in lymphoid follicles. Fat stains demonstrated that macrophages throughout the lymph nodes contained large quantities of fat droplets within their cytoplasm. Acid phosphatase activity was heaviest over these phagocytic cells and, as a rule, absent over lymphocytes. Within the spleen, lymphoid tissue was sparce. The sinusoids contained large numbers of hemosiderocytes. Phagocytic cells containing large amounts of lipid droplets were also seen throughout the organ.

The glomerular tufts of the kidney were enlarged by increased cellular content and by pink amorphous material. Bowman's space was obliterated; necrotic epithelial cells were seen within the glomerular tuft, as well as within the convoluted tubules. Acidophilic intranuclear crystalloids were numerous within the convoluted tubules.

The bone marrow was hypoplastic. No megakaryocytes were found in the marrow of the head or shaft of the femur. Foci of granulocytes and erythrocytes were found in which both blast and maturing stages were present. Mast cells were especially numerous throughout the marrow. Autoradiographs of the femur revealed activity localized in the endosteum of the shaft and in trabeculae as well as within the inner layers of both.

Figure 43. Liver of dog 0016, which received Ce^{144} approximately one year before death. Note centrolobular lipid deposition. Oil red O stain.

Several foci of necrosis and degeneration occurred within the zona glomerulosa of the adrenal gland; the foci of necrosis were also sites of radioactivity (Figure 44). Many acini within the thyroid gland were devoid of colloid and lined by two or more layers of epithelial cells. The acini varied in size, many having little or no lumen. The colloid stained faintly acidophilic.

Hematology. This animal (0016), which died one year after receiving 25 μc of Ce^{144} per kg, represents the only death among the 10 injected at this dose level. There are also 5 animals out of 7 still living who received approximately 50 μc/kg; the 2 deaths at this higher level occurred at 78 and at 90 days after injection. The dogs remaining from the two dose groups have survived over 16 months, and their blood values, although they have not reached pre-injection levels, are either increasing or remaining constant.

In the dead animals, lymphoid regeneration was seen both in the two (0022 and 0030) that received 50 μc/kg Ce^{144} and in the one (0016) that received 25 μc/kg. In all three a reversal of the granulocyte/lymphocyte ratio developed; this was noted as early as 59 days after injection. Similar reversals occurred in those surviving the two dose levels, with, however, variations in the time first observed and in the degree of reversal. In the 3 succumbing to Ce^{144} the erythrocyte count decreased to a million or less coincidentally with the drop in segmented leucocytes.

Electron Microscopy

Little attention has been given to alterations in the ultrastructure of lymphoid and renal tissue following irradiation. Because of this deficiency, a program was established to study such changes in the kidney, spleen and lymph node of the dog and rat as a result of external and internal irradiation. Observations are also made of normal tissue from animals of known age, source, and history.

Materials and Methods

The animals used were 5 beagle dogs, 10 to 16 months old, male and female, and two 2-month-old Sprague-Dawley rats, male and female, averaging 300g (Table 36). Tissues were taken from kidney, spleen and lymph nodes. All of the dogs may be considered as controls except for one (0150), which received 325 r of Co^{60} γ-radiation unilaterally 76 days before sacrifice. The two Ce^{144}-tracer animals were considered to have received such small amounts of the radionuclide that toxic effects were minimal or absent.

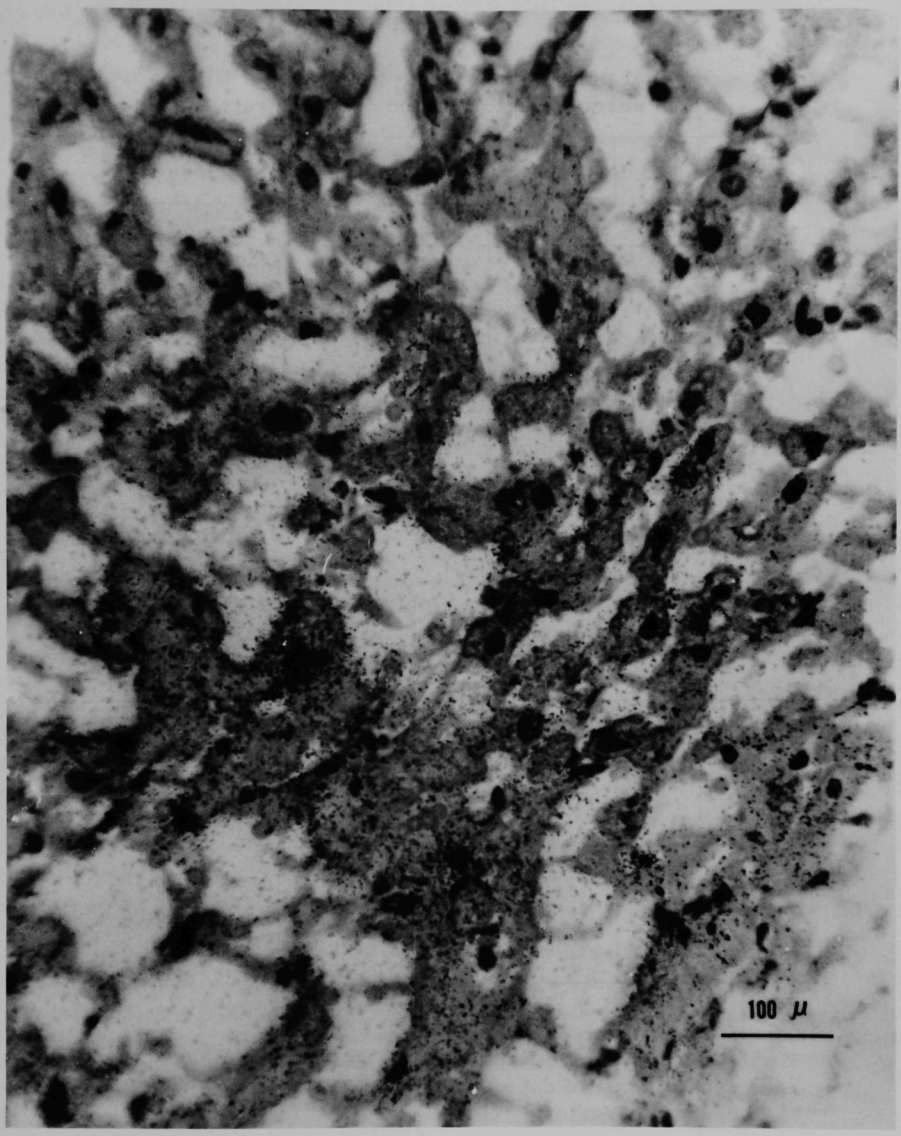

Figure 44. Adrenal gland from animal 0016. Autoradiograph overlies a section stained with hematoxylin and eosin. Note relationship between focus of necrosis and deposition of silver grains.

TABLE 36

Experimental plan for electron microscopy of tissues from normal and irradiated dogs and rats

Animal number	Sex	Age, months	Treatment	Tissue**
			Dogs	
0150	F	16	Co^{60}, 325 r	Kidney
0265	M	$9\frac{1}{2}$	Control	Kidney
0214	M	14	Control	Kidney Cervical lymph node
0248	M	14	Ce^{144}, 10 μc*	Kidney Cervical lymph node
0253	F	13	Ce^{144}, 7.5 μc*	Kidney Cervical lymph node Liver
0307	F	14	Control	Kidney Cervical lymph node Liver Spleen
			Rats	
1	M	2	Control	Kidney Cervical lymph node Liver Spleen
2	F	2	Control	Kidney Cervical lymph node Liver Spleen

*Total dose.

**All tissues were fixed in OsO_4. All were embedded in Epon except those of dogs 0265 and 0253, and rat 1, which were embedded in Vestopal W.

Tissues were taken either immediately upon death or while the animal was under nembutal anesthesia. The tissue was immediately fixed in buffered 2% osmium tetroxide, pH 7.4, for $\frac{1}{2}$ to 2 hr, dehydrated through

graded alcohols, embedded in either Epon or Vestopal W, sectioned at 900 to 1100 A, stained with 2% uranyl acetate, and viewed with either an RCA 2A or an RCA 3E electron microscope.

Observations

In sections taken from the interior region of cortical nodules of lymph nodes, both in the dog and in rat, the cells are predominately small lymphocytes, large lymphocytes, primitive reticular cells, occasional macrophages, plasma cells and reticuloendothelial cells containing fibers. The cells are very closely packed with little or no intercellular space. In tissue sectioned at the periphery of the lymph node, near or including a sinus, the cells are farther apart, with considerable intercellular space or matrix between them. The predominant cells in such areas are reticuloendothelial cells with fibers, fixed and free macrophages, plasma cells, and cells of the lymphocytic series in various stages of development. The sinuses contain many large and small lymphocytes and an occasional eosinophil or neutrophil.

The cell types observed in the cervical lymph nodes and the spleens of the dog and rat are quite similar. Where species differences exist, they will be pointed out. The lymph node of the rat contains a greater percentage of plasma cells in the lymphoid follicles and sinuses than does that of the dog. The ultrastructure of the plasma cell is very similar in the two species, however. The nucleus is spherical and contains large, electron-dense clumps of chromatin distributed both at random and concentrated at intervals along the nuclear envelope. Occasionally a single large nucleolus is seen. The cytoplasm has a complex and extensive endoplasmic reticulum. The cisternae are usually dilated, though empty. In a small number of cells, electron-dense material is seen within the cisternae. Large, round to elongate mitochondria are found infrequently between the membranes of the ergastoplasm. Electron-dense ribosomes are usually associated linearly along the endoplasmic reticular membranes. Frequently a complex Golgi zone is found near the nuclear envelope (Figures 45 and 46).

Primitive reticular cells in the dog and in the rat are also very similar. The round to oval nucleus has a rather homogeneous, granular appearance. A single nucleolus is sometimes seen. The cytoplasm is relatively abundant, bounded by a very irregular plasma membrane. Infrequent spherical to elongate, poorly-formed mitochondria, a sparse endoplasmic reticulum with associated ribosomes, and numerous vacuoles can be found. A Golgi complex, however, could not be detected (Figure 47).

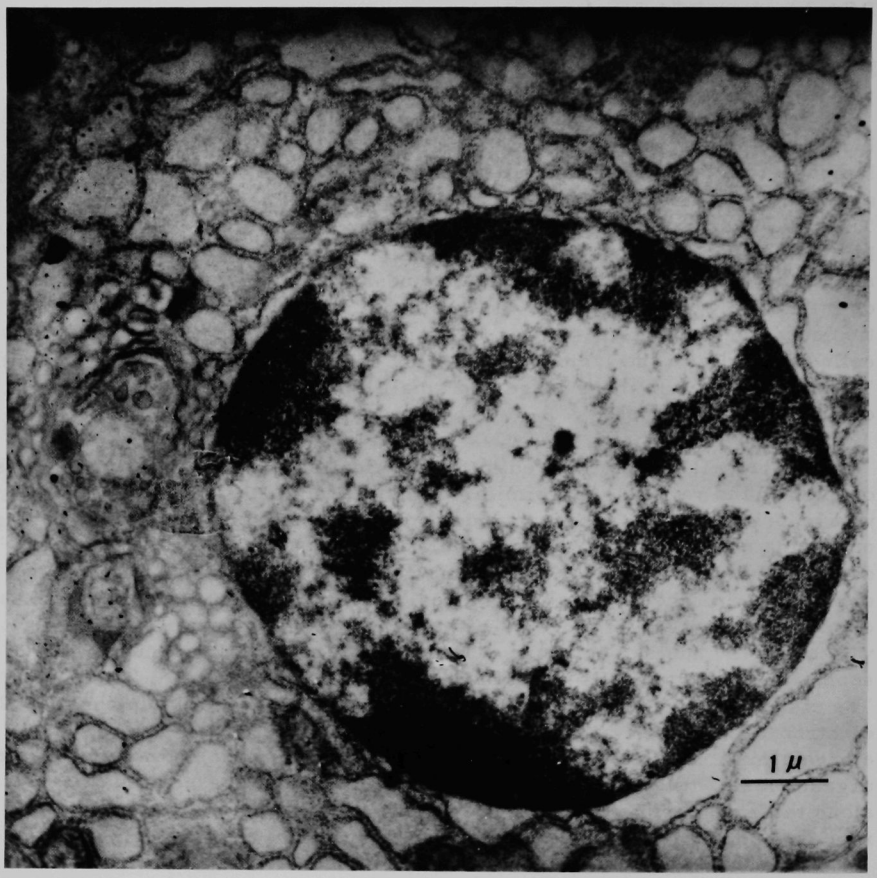

Figure 45. Plasma cell in the cervical lymph node of dog 0248. Note clumped chromatin in the nucleus and extensive endoplasmic reticulum. A Golgi complex is visible to the left of the nuclear envelope.

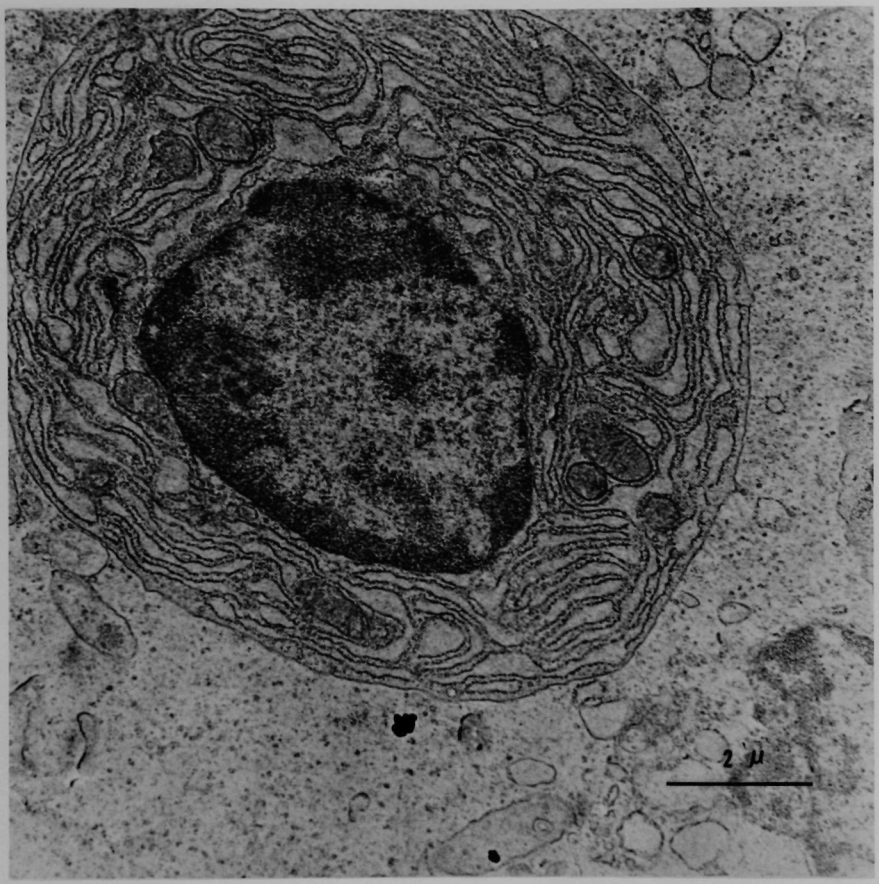

Figure 46. Plasma cell from the cervical lymph node of rat 1. Note the complex endoplasmic reticulum, with randomly distributed mitochondria.

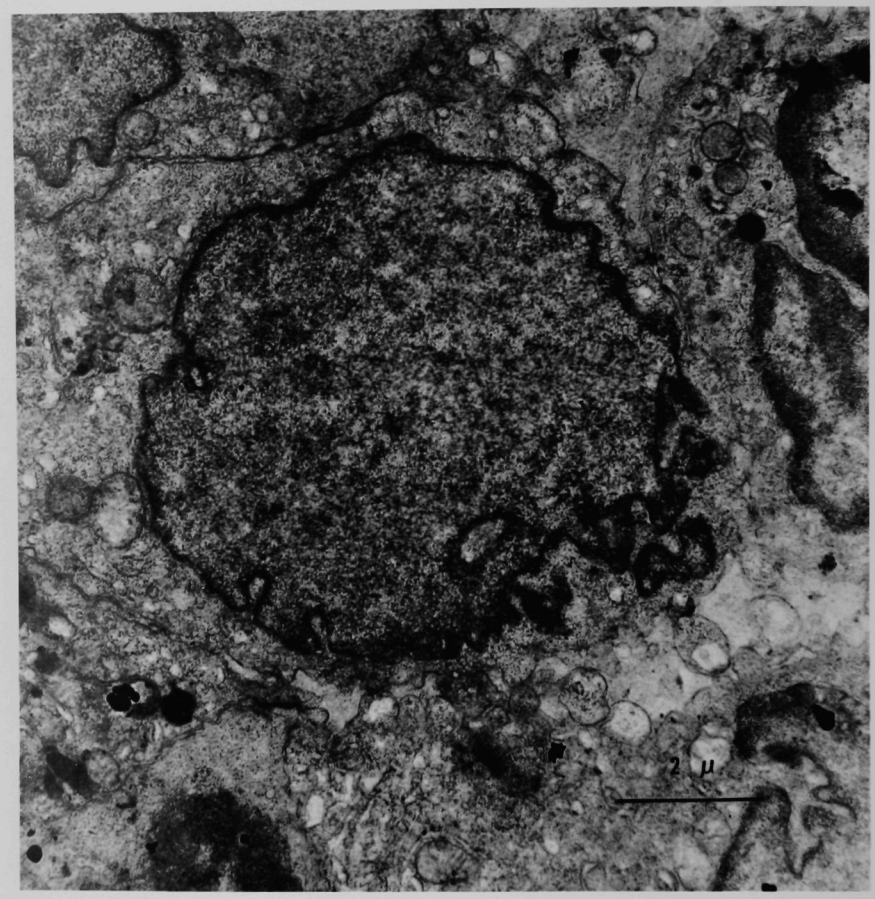

Figure 47. Primitive reticular cell from the cervical lymph node of rat 1. Note the irregularly outlined, homogeneous nucleus and the lack of cytoplasmic organelles.

The cells of the lymphocytic series are very similar in the dog and the rat. The following descriptions apply to both species.

The lymphoblast, intermediate in development between the primitive reticular cell and the large lymphocyte, differs from the former in the shape of its nucleus which is more rounded and regular in outline, also in having a more extensive endoplasmic reticulum and more numerous poorly formed oval to elongate mitochondria (Figure 48).

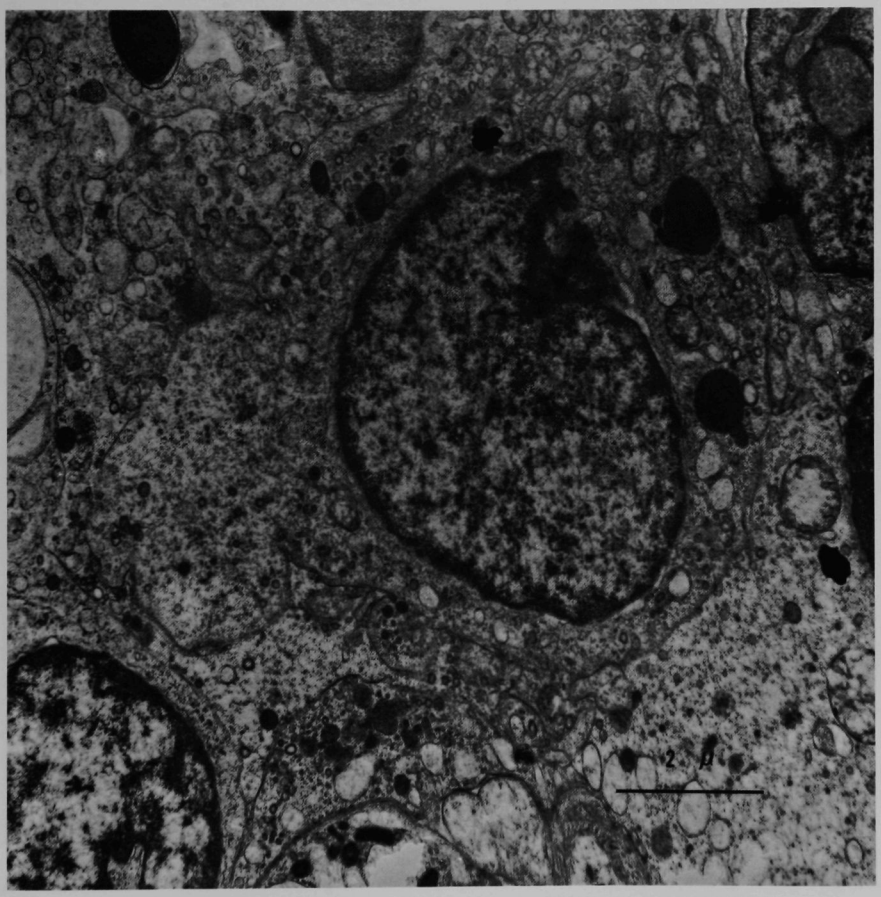

Figure 48. Lymphoblast from the cervical lymph node of dog 0307. Note the poorly formed mitochondria in the cytoplasm.

The large lymphocyte has localizations of dense material within the nucleus, a pattern which is not found in the more primitive cells of this series. The shape of the nucleus is sometimes irregular, with slight indentations along the border. The cytoplasm is abundant, with well-formed mitochondria and vacuoles distributed at random. A Golgi complex is usually visible (Figures 49 and 50).

Figure 49. Large lymphocyte from the cervical lymph node of dog 0307. Note cristae in the mitochondria. A Golgi complex can be seen to the left of the nuclear envelope. The nucleus exhibits a light and dark pattern.

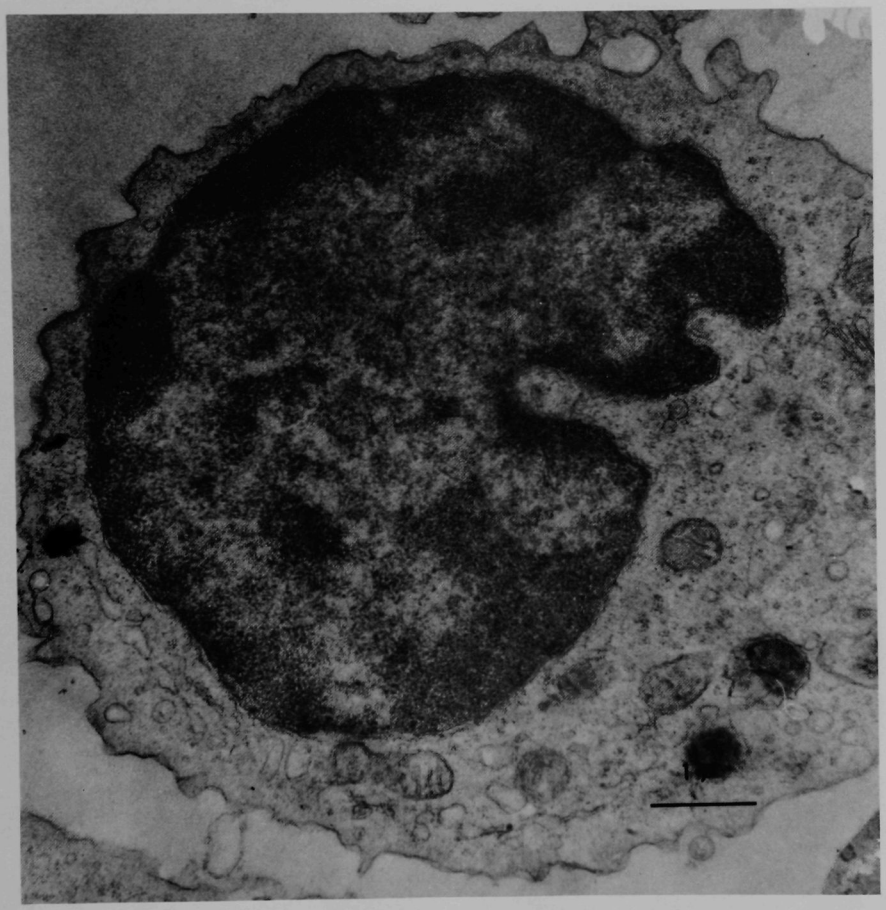

Figure 50. A large lymphocyte from the spleen of rat 1. Two nuclear indentations can be seen. A Golgi complex is found to the far right of the nucleus. The endoplasmic reticulum is scattered sparsely throughout the cytoplasm.

The small lymphocyte (Figures 51 and 52) has distinct patterns of dense and light material in the nucleus, with definite chromatic clumps dispersed throughout, as well as concentrated at the nuclear envelope. The nucleus of this cell is sometimes spherical, but often exhibits very deep invaginations, usually associated with mitochondria in the cytoplasm, near the nuclear membrane. A single nucleolus is often present. In the cytoplasm, one finds a scant endoplasmic reticulum, a few round or rod-shaped mitochondria; the Golgi zone is simple or absent.

Figure 51. Small lymphocyte in the cervical lymph node of rat 1. An indistinct nucleolus is seen in the center of the nucleus. Note the frequent invatinations at the nuclear margin.

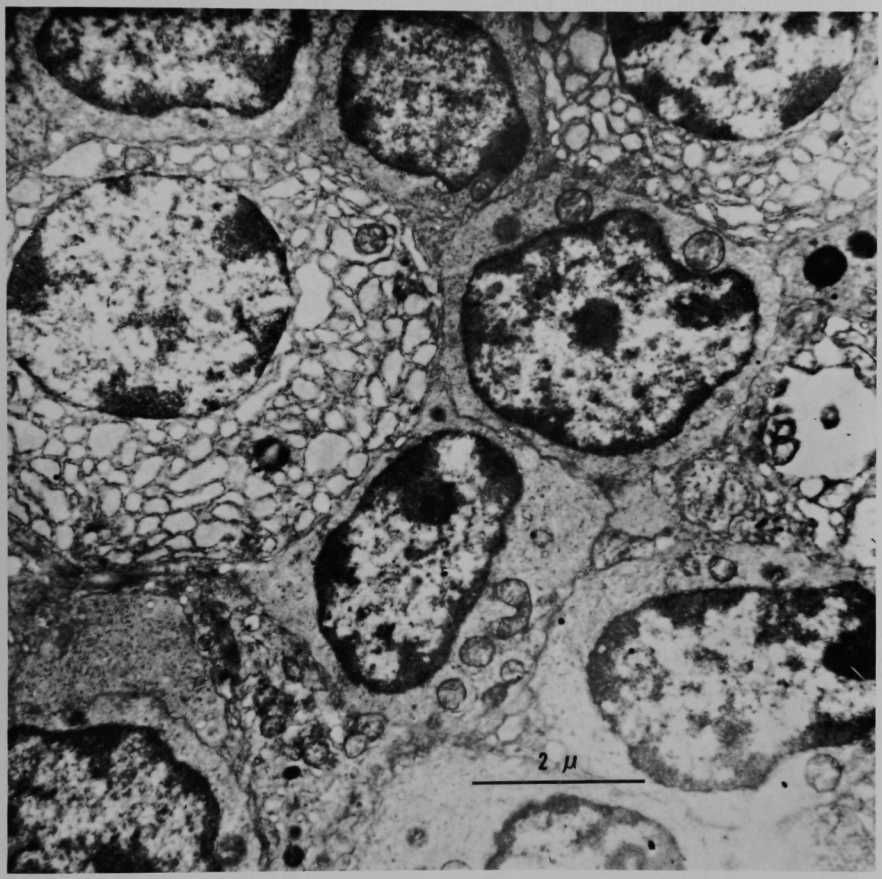

Figure 52. Small lymphocytes and plasma cells in the cervical lymph node of dog 0248. The small lymphocytes are found toward the center of the field. A single nucleolus is visible in both. The upper right lymphocyte exhibits a slight invagination with an associated mitochondrion at the nuclear envelope.

The macrophages of the dog and the rat differ only in the appearance of the nucleoplasm. That of the rat is homogeneous in density, containing fine, electron-dense structures distributed fairly evenly throughout the nucleus, being concentrated only about the nucleolus (Figure 53). In comparison, that of the dog contains large electron-dense clumps of granules concentrated at the nuclear envelope (Figure 54). In both the dog and rat

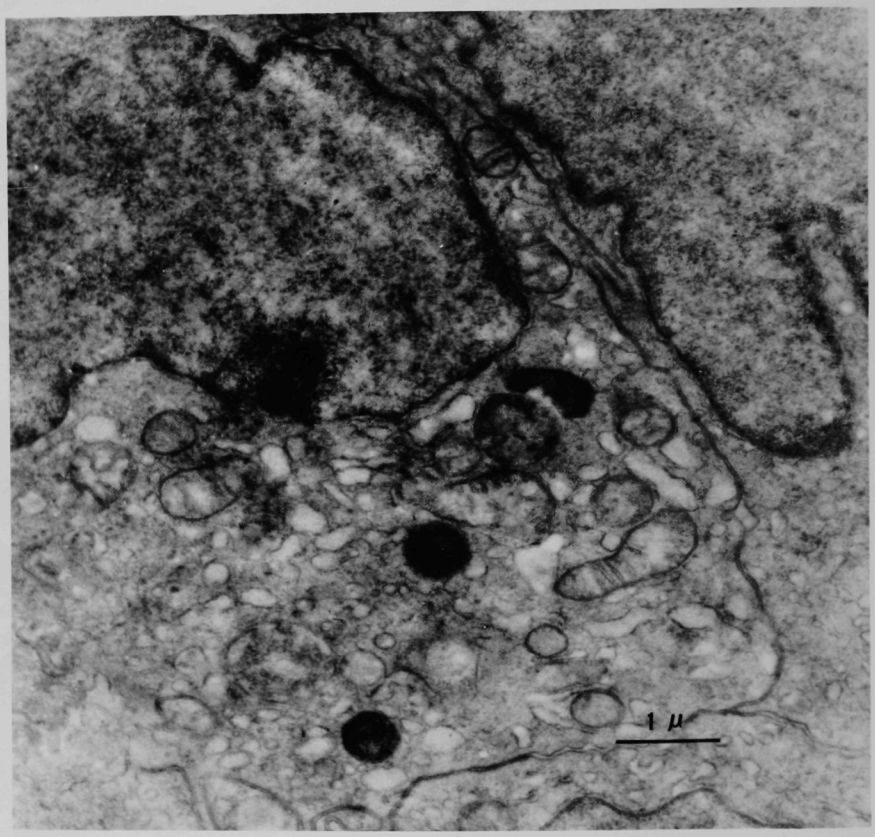

Figure 53. Macrophage in the cervical lymph node of rat 1. The nucleus is homogeneous. The nucleolus is located at the lower right. Numerous vacuoles, electron-dense droplets and complex vesicles are evident in the cytoplasm. Note the projections at the cytoplasmic membrane.

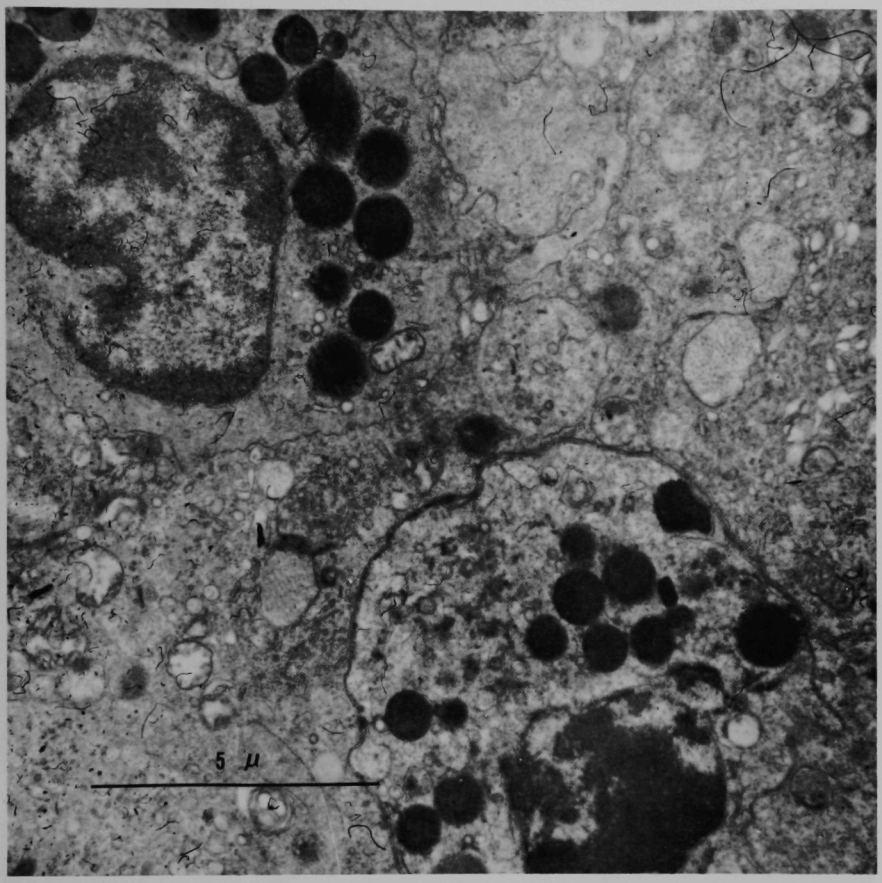

Figure 54. Macrophage in the cervical lymph node of dog 0248. Portions of two macrophages can be seen. The nuclei exhibit large clumps of chromatin. Many electron-dense droplets are visible in the cytoplasm.

the abundant cytoplasm is irregular in outline, and contains numerous and varying types of vesicles and inclusions (both simple and complex), dense endoplasmic reticulum with associated ribosomes, groups of free ribosome particles, large oval to elongate mitochondria, and a well-formed Golgi apparatus. In both species, evidence of pinocytosis can be found at the cell membrane (Figure 55).

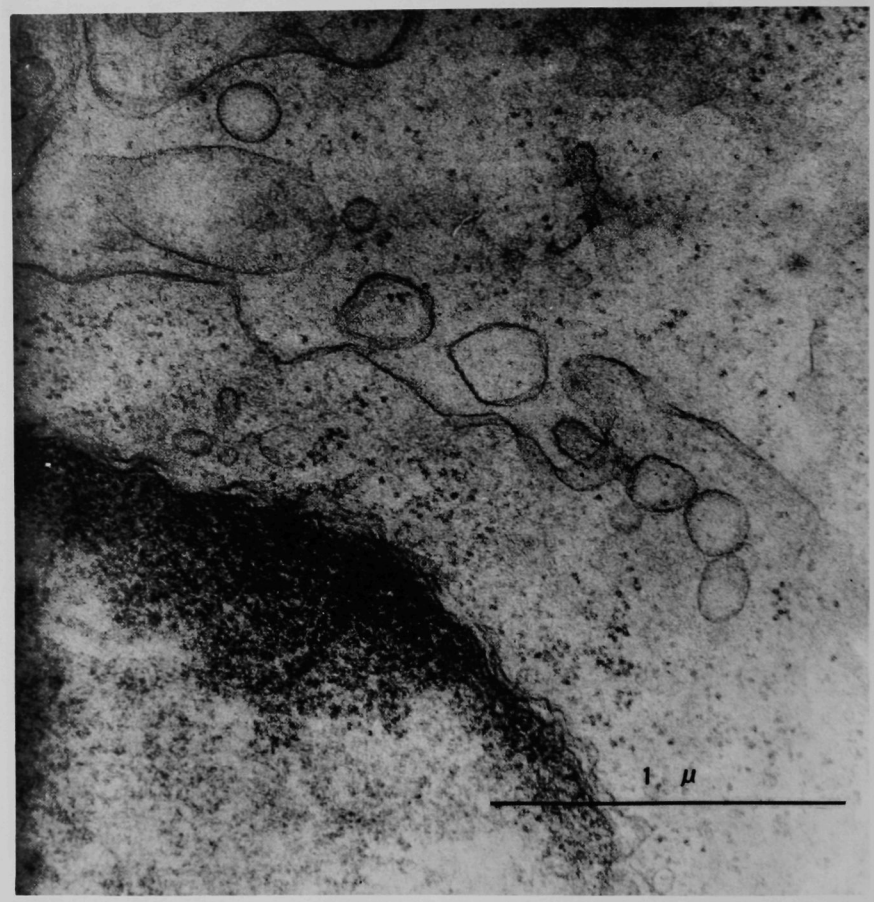

Figure 55. Macrophage in the spleen of rat 2. Pinocytosis is evident at the cytoplasmic membrane.

The reticular cells associated with fibers vary in size and shape in both species. The nucleus is usually irregular in shape and has dense chromatin clumps scattered throughout the nucleoplasm. The cytoplasm is very abundant and is bounded by an extremely irregular cytoplasmic membrane. The cytoplasm is usually extended into long processes enclosing the fiber bundles. The fibers are surrounded by a membrane, probably

the plasma membrane, which can be seen to infold around the fiber near the cytoplasmic border. Very large, elongate to ovoid mitochondria, a distinct Golgi complex, and abundant endoplasmic reticulum can be seen. Electron-dense droplets are often found scattered throughout the cytoplasm (Figure 56).

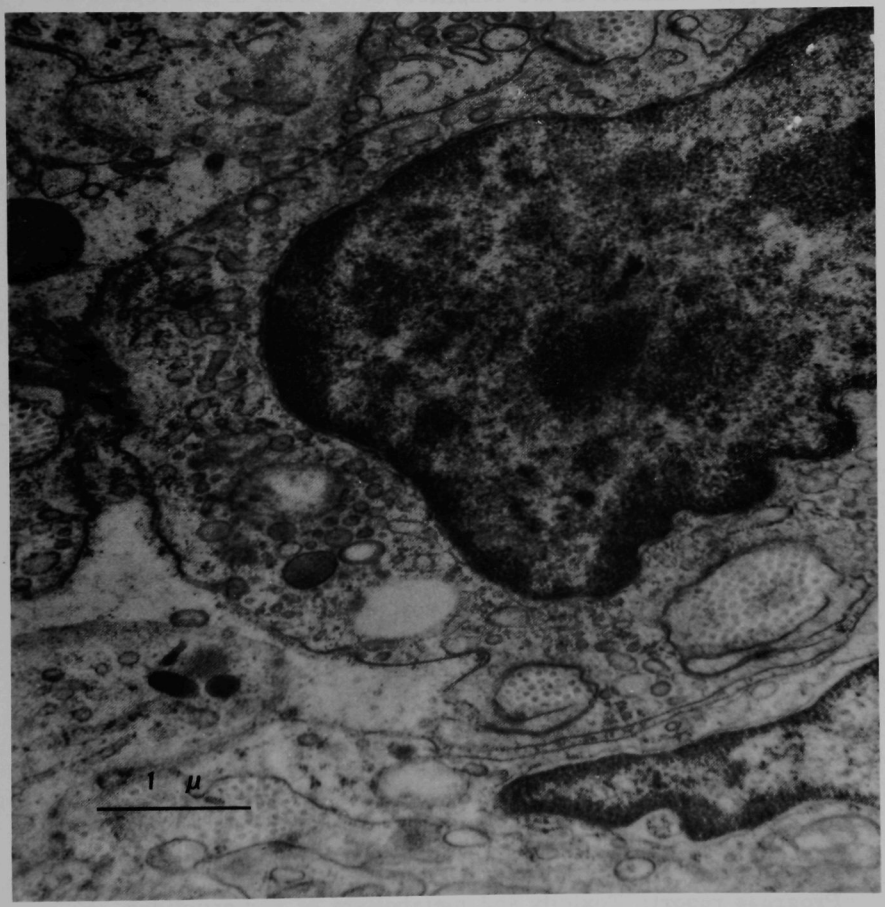

Figure 56. Reticular cell with associated fibers from the cervical lymph node of dog 0307. Note the infolding of the plasma membrane about the fibers at the lower margins of the cytoplasm. Numerous cytoplasmic vesicles and free ribosomes are evident.

Discussion

Low and Freeman,[3] while studying the ultrastructure of free lymphocytes in the peripheral blood of man noted as a distinguishing characteristic of the mature small lymphocyte a nucleoplasm exhibiting "no clear patternization of two densities, as is found in neutrophils and eosinophils." The findings of Bessis were similar.[4] The lack of a pattern in the distribution of densities is not a fixation artifact since many other cells in the same sample show distinct localization. The small lymphocyte of the dog and rat as observed here has a distinct pattern, concentrated at the nuclear envelope.

Han[5] noted in a study of the mesenteric lymph node of the rat that the nucleoplasm of the macrophage had a homogeneous density, containing fine, electron-dense structures, distributed evenly throughout the nucleus except at the nucleolus, where it was concentrated. Sorenson, in a study of macrophages within the popliteal lymph nodes of the rabbit, described a nucleoplasm that varies in density from cell to cell;[6] in some it is rather electron-lucent, with fine granules evenly distributed throughout the nucleus, as in the rat. In other cells, the nucleoplasm, though homogeneous, was much denser. The appearance of lymphoid cells in Sorenson's article may be dissimilar to those described by others by reason of differences in methods used. Sorenson employed Dalton's osmium dichromate fixative, whereas we and the others mentioned here have used 2% buffered osmium tetroxide. This difference may also account for the variance in appearance of the nucleoplasm of the plasma cells in rabbits described by Sorenson; as in almost all cells described in his report, it is homogeneous and without pattern.

References

1. Norris, W. P., L. S. Lombard, C. E. Rehfeld, and T. W. Speckman. Progress report: Toxicity and metabolism of radionuclides in dogs. II. Biological and Medical Research Division Semiannual Report, July through December 1961, Argonne National Laboratory. ANL-6535. pp. 36-52.

2. Norris, W. P., L. S. Lombard, C. E. Rehfeld, and T. W. Speckman. Progress report: Toxicity and metabolism of radionuclides. I. Biological and Medical Research Division Semiannual Report, January through June 1961, Argonne National Laboratory. ANL-6464. pp. 50-71.

3. Low, F. N., and J. A. Freeman. Electron Microscopic Atlas of Normal and Leukemic Human Blood. McGraw-Hill Book Company, Inc., New York, 1958. pp. 22-24, 30-32, 64-76.

4. Bessis, M. Structures cellulaires decouvertes par le microscope electronique dans les leucocytes. Rev. hematol. 11, 295-320 (1956).

5. Han, S. S. The Ultrastructure of the mesenteric lymph node of the rat. Am. J. Anat. 109, 183-225 (1961).

6. Sorenson, G. D. An electron microscopic study of popliteal lymph nodes from rabbits. Am. J. Anat. 107, 73-95 (1960).

ABSENCE OF REPAIR OF MUTATIONAL DAMAGE IN CONTINUOUS CULTURES

Herbert E. Kubitschek and Harold E. Bendigkeit

In continuous cultures the manner of accumulation of mutants resistant to bacteriophage T5 in Escherichia coli B/r/1, try$^-$ depends not only upon the mutagen, but also upon the factor used to regulate growth. With caffeine as mutagen, mutants accumulate at a constant rate in cultures regulated with tryptophan, but when growth is regulated with glucose, accumulation is proportional to growth rate.[1] If these qualitatively different responses reflect rates of induction, then they might be indicative of the presence of quite different mutational processes.

We can show that these different responses are, indeed, the result of different rates of induction of mutation, and are not due to repair of latent mutational damage in these cultures. In the absence of selection the rate of induction, μ, in a culture must equal the rate of expression of mutation, μ_0. Then the number, L, of latent mutants in the culture can be calculated from the rate of expression and the average residence time, D, for latent mutants:

$$L = \mu_0 N_0 D \quad , \tag{1}$$

where N_0 is the total cell concentration in the culture.

For generation times between 4 and 10 hr, we find[1,2] that the average time required for the expression of the phenotype for resistance to T5 is 3.4 cell divisions. Thus, in units of time, D = 3.4 T, where T is the generation time of the culture. From Equation (1), the latent mutant concentration is

$$L/N_0 = 3.4\ \mu_0\ T \quad . \tag{2}$$

Table 37 gives measured values of latent mutant concentrations, as well as values calculated from Equation (2). The good agreement between corresponding values shows that selection against latent mutants is negligible with either growth factor. That is, there is no evidence for repair of mutational damage in these cultures. Furthermore, the rates of accumulation of mutants must, therefore, represent the rates of induction of mutation in these cultures.

We draw the same conclusions when ultraviolet light induces mutation in these and derivative strains. With this mutagen, however, the mutational response is constant for each of the growth regulating factors.

TABLE 37

Absence of selection for latent mutants*

Mutagen	Growth regulating factor	Mutant accumulation rate, μ_0	L, calculated	L, observed
Caffeine	glucose	44 per gen.	150	170
	tryptophan	330 per day	(460)	(440)
Ultraviolet light	glucose	120 per day	(170)	(170)
	tryptophan	130 per day	(185)	(190)

*All values are for population N_0 of 10^8 cells. Values in parentheses are those calculated or observed for generation time of 10 hr.

References

1. Kubitschek, H. E. and H. E. Bendigkeit. Latent mutants in chemostats. Genetics 46, 105-122 (1961).

2. Kubitschek, H. E. and H. E. Bendigkeit. Delay in the appearance of caffeine-induced T5-resistance in Escherichia coli. Genetics 43, 647-661 (1958).

THE STUDY OF NORMAL VARIATION II. OBSERVATIONS ON THE INHERITANCE OF HAIR ON THE PINNA OF THE EAR

Herman M. Slatis

Studies of the genetic effects of radiation on man have stressed the sex ratio of the offspring of irradiated persons as the most sensitive indicator of genetic damage.(1) A large part of the effect on sex ratio is ascribed to a lowering of the proportion of sons among the children of irradiated men, and this is related to dominant lethal effects associated with the Y chromosome. Therefore, it is of direct interest to our interpretation of these sex ratio data that we have information on the role of the Y chromosome. As information is collected which shows that this chromosome has a very different action in mice and in men, investigations of its role in man must be expanded.

Recently, it was suggested that the previously held belief that some traits in man are determined by genes located on the Y chromosome is invalid.(2) This had led to a renewed interest in the most easily studied of these characters: coarse hair on the pinna of the ear.

This condition is limited to men and varies in the frequency of its occurrence in various races. A study has been completed of the frequency of hairy pinna among about 900 men in Israel, where it was found that this type of hair occurs in about one percent of men in their early twenties and in increasing frequency in older men, up to a frequency of about 25 percent in men over the age of sixty. The condition is highly variable in its expression and it appears that the country of origin is related to the mode of expression.

Family studies resulted in the observation of 67 male relatives of affected individuals. Of the men over the age of 40, 28 were affected and 9 were not. On the theory that this condition is caused by a gene on the Y chromosome, all of these men should have been affected. On the theory that this condition is caused by an autosomal dominant gene, 20.8 should have been affected, while an autosomal recessive gene would have given an expectation of 18.0 affected men. Actually, although there are nine exceptions to the theory of Y-chromosome linkage, they are most frequent in the younger men. Only one of the 15 oldest men in this series did not have hair on the pinna of the ear, though autosomal inheritance theories would have expected about seven to unaffected. These results are confirmatory of the original suggestion that hairy pinna is determined by a Y-linked gene.

These observations also included studies of other characters and the interrelationships between them. There appears to be a relationship between hair on the pinna and hair around the external auditory meatus of the ear. However, this relationship is complicated by the fact that both of

these conditions increase in frequency with increasing age. Correction for age does not completely remove the correlation between these two forms of ear hair. Hair on the chest and baldness (which are themselves correlated) are not significantly correlated with hair on the pinna. Color blindness is no more common in men with hair on the pinna than in other men.

This study provides evidence in favor of the theory that the gene for hair on the pinna of the ear is transmitted on the Y chromosome. It suggests that genes of the standard type exist on the Y chromosome, which is contrary to a widely held opinion. The interpretation of data on the sex ratio of the offspring of irradiated persons is affected by this finding. We can now suggest that irradiation might cause some Y-linked deaths through dominant lethal gene mutations. Previously, many geneticists had assumed that Y-linked deaths could only be caused through a pair of chromosome breaks, one of which was on the Y chromosome and the other on some other chromosome.

References

1. Schull, W. J., and J. V. Neel. Radiation and the sex ratio in man. Science 128, 343-348 (1958).

2. Stern, C. The Problem of complete Y-linkage in man. Am. J. Human Genetics 9, 147-166 (1957).

STROPHANTHIN AND ISONICOTINIC ACID HYDRAZIDE AS POSSIBLE RADIATION PROTECTORS

Robert N. Feinstein and Marilyn Coulon

Rationale for the testing of these two agents was extremely tenuous, yet it seemed worth brief preliminary tests:

Isonicotinic acid hydrazide (IAH) was found by Yoshikawa et al.[1] to decrease the urinary excretion of taurine by rats. Whole body irradiation, on the other hand, has been found to increase the excretion of taurine.[2,3] Because of these opposing effects, it was considered worth while briefly to test IAH as a possible radioprotector.

According to Máchová and Selecký,[4] strophanthin actively inhibits the transport of potassium across the membrane of the human erythrocyte. Since radiation usually increases potassium transport, strophanthin was also considered worth a brief test as radioprotector.

At radiation doses of 850 r, no significant radioprotective action was found for either agent administered intraperitoneally into mice. The data are given in Table 38.

TABLE 38

Effect of strophanthin and isonicotinic acid hydrazide (IAH) on radiation lethality in mice

Expt.	Treatment	No. of mice	No. of mice dead at 30 days	Lethality, %	Survival time, days
1	Saline, then X-ray	5	2	40	13.0
	IAH, then X-ray	10	5	50	8.2
	IAH, no X-ray	5	1	20	9.0
2	Saline, then X-ray	5	5	100	10.3
	Strophanthin, then X-ray	5	5	100	10.6
	Strophanthin, no X-ray	5	0	0	-

Dose of IAH: 100 mg/kg
Dose of strophanthin: 2 mg/kg
Dose of X-rays: 850 r, at 38 r/min
Mice were CF No. 1/ANL females, 2 months of age

References

1. Yoshikawa, K., T. Aoki, K. Matoba, and I. Matsumoto. Change of taurine excretion in urine by the administration of isonicotinic acid hydrazide to rats. Nara Igaku Zasshi 11, 71-74 (1960). [Chem. Abstr. 54, 12390f (1960)].

2. Aebi, H., L. Bernays, H. Flueckiger, B. Schmidli, and A. Zuppinger. Die Taurinausscheidung roentgen- und betatronbestrahlter Ratten. Helv. Physiol. Acta 13, C49 - C51 (1955).

3. Kay, R. E., J. Early, and C. Entenman. Increased urinary excretion of taurine and urea by rats after X-irradiation. Radiation Research 6, 98-109 (1957).

4. Máchová, J., and F. V. Selecký. Inhibiting action of the glycoside isolated from Asclepia syriaca on the potassium transportation through the erythrocyte membrane. Arch. Exptl. Path. Pharmakol. 236 245-247 (1959). [Chem. Abstr. 53, 13409b (1959)].

PROGRESS REPORT: PLUTONIUM REMOVAL, TUMOR INCIDENCE STUDIES. III

Marcia W. Rosenthal, Joan Fried Markley, and Arthur Lindenbaum

Bone tumor incidence has been correlated with the skeletal content of plutonium following administration of a colloidal form of plutonium to mice, with and without delayed therapy with diethylenetriaminepentaacetic acid (DTPA). Experimental methods have been described.(1, 2) A single intravenous injection of 2.6 $\mu c/kg$ of Pu^{239} was followed in 3 days by single daily intraperitoneal injections of saline or 500 mg/kg of DTPA. The present report summarizes the effects of 2 and of 12 days of DTPA therapy, which have been described in more detail elsewhere.(3)

The index of radiation effect used in this study is the proportion of mice that had at least one malignant bone tumor at death. Tumors included are those positive on the roentgenogram (i.e., outside the normal limits of the bone) and those histologically identified in mice that had either roentgenographic or clinical evidence (paralysis) of a bone tumor.

DTPA treatment given for 12 days removed 43.2% of the plutonium deposited in the bone and reduced the fraction of mice with bone tumors by 42.5% at the time the last untreated mouse died (515 days), as shown in Figure 57. Treatment for only 2 days had less effect on removal and tumor incidence, and the two indices of effect were not as closely correlated. Additional mice in the treated groups that lived longer than the untreated animals did not raise the final tumor incidence values significantly above those computed at 515 days.

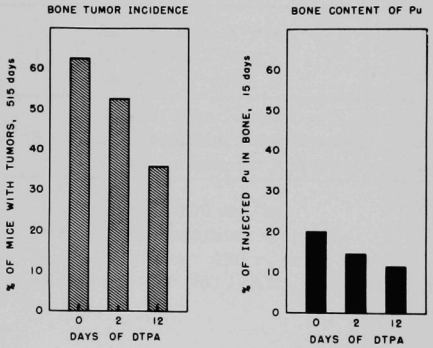

Figure 57

Effect of DTPA therapy on bone tumor incidence and bone content of plutonium. Tumor incidence data are based on mice dying from 250 to 515 days after plutonium, i.e., from the end of the latent period to the death of the last untreated control mouse. Numbers of mice included are 99 in the control group, 38 and 75 in the groups treated 2 and 12 days, respectively.

The relationship between the probability of having a bone tumor at death and time was approximately linear (Figure 58). Tumor rate increased with time in all groups and was reduced by DTPA therapy.

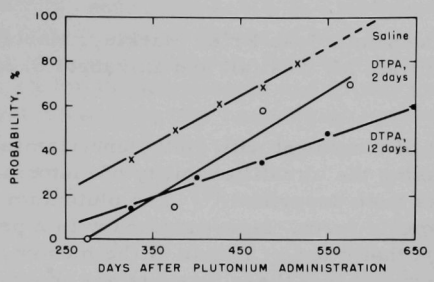

Figure 58. Effect of DTPA on bone tumor rate in plutonium-injected mice. The points represent the proportion of the group dying with a bone tumor in the given time interval. The lines are calculated by the method of weighted least-squares, using as weights the number of animals represented by each point. The constants of the least-squares lines for the saline control group, the group treated with DTPA for 2 days, and that treated for 12 days are as follows: intercept (at 250 days) = 0.2196 ± 0.0274, -0.0484 ± 0.1632, and 0.0569 ± 0.0247, respectively; slope = 0.002187 ± 0.000142, 0.002411 ± 0.000628, and 0.001377 ± 0.000095, respectively. Numbers of mice represented in the three groups are 99, 46, and 100 respectively.

References

1. Rosenthal, M. W., J. F. Fried, A. Lindenbaum, and J. Schubert. Progress report: Relationship of plutonium removal to tumor incidence. I. Experimental design and preliminary results. Biological and Medical Research Division Semiannual Report, July through December 1959, Argonne National Laboratory. ANL-6264, pp. 172-176.

2. Rosenthal, M. W., J. F. Fried, A. Lindenbaum, and J. Schubert. Progress report: Plutonium removal, tumor incidence studies. II. Biological and Medical Research Division Semiannual Report, January through June 1961, Argonne National Laboratory, ANL-6464, pp. 82-84.

3. Rosenthal, M. W., J. F. Markley, A. Lindenbaum, and J. Schubert. Influence of DTPA therapy on long-term effects of retained plutonium. Health Physics 8, 741-745 (1962).

PROGRESS REPORT: PLUTONIUM REMOVAL. V. ULTRAFILTERABILITY AND DISAPPEARANCE OF PLUTONIUM FROM PLASMA AS A FUNCTION OF DTPA TREATMENT AND OF THE PHYSICAL STATE OF THE PLUTONIUM

Arthur Lindenbaum, Joan Fried Markley, Marcia W. Rosenthal, William M. Westfall and Elizabeth S. Moretti

The effect of treatment with diethylenetriaminepentaacetic acid (DTPA) on increasing the ultrafilterability of plutonium in the plasma and tissues of rats has been described.(1) The plutonium used was injected in essentially monomeric form. Investigations with a polymeric form of plutonium have shown that more of it than of the monomeric form deposits in the liver and spleen and that these deposits are more refractory to removal by DPTA.(2) In view of these differences, it was of interest to compare the early behavior of these two types of plutonium solutions with respect to their ultrafilterability and rate of disappearance in the blood, both in the absence and presence of DTPA.

Methods

Two plutonium injection solutions were prepared from stock solutions of $Pu(NO_3)_4$ in concentrated HNO_3 and solutions of sodium citrate. The one designated as monomeric contained 9.7 μc Pu per ml; citrate:Pu ratio = 60; pH = 6.0. The polymeric solution contained 7.8 μc Pu per ml; citrate:Pu ratio = 2; pH = 7.1. The degree of polymerization of these solutions was measured by determining the fraction which was ultrafilterable through a cellophane membrane by a centrifugation technique;(1) the monomeric solution was 92% ultrafilterable and the polymeric 50%.

Ninety Sprague-Dawley female rats, weighing about 250 g, were injected intravenously with the plutonium solutions in either form at 7.2 or 10.6 μc/kg. The treated rats received CaDTPA at 500 mg/kg intraperitoneally $\frac{1}{2}$ hr after plutonium administration; the controls received no injection at this time. Blood was removed at various time intervals by cardiac puncture in duplicate samples which contained blood from at least two rats per sample. Plutonium analyses were performed on whole blood, plasma and plasma ultrafiltrates by α-counting of 25-50μl aliquots directly plated onto planchets.

Results

The plutonium content of the total plasma was about equal to that of the total blood, indicating that there is no significant fraction of the plutonium contained in the cellular components of the blood. This was expected from the results of Foreman.(3)

Figure 59 (upper graph) shows that, although the plasma levels of the two forms of plutonium in the untreated rats were about the same at the beginning (40% at $\frac{1}{2}$ hr) and at the end (8-10% at 24 hr) of the period examined, the rate of disappearance was faster for the polymeric form than for the monomeric (at 2 hr, polymeric = 21% and monomeric = 32%). DTPA therapy increased the rate of disappearance of both forms markedly; for example, at 2 hr after plutonium injection, the Pu levels in the plasma of the treated rats were 4% for the monomeric and 9% for the polymeric. This increase was somewhat greater for the monomeric form than for the polymeric.

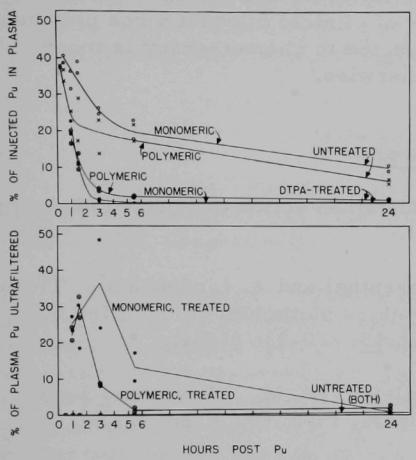

Figure 59

Upper graph, the effect of DTPA treatment on the disappearance of monomeric and polymeric plutonium from the plasma of rats. Lower graph, the effect of DTPA treatment on the ultrafilterability of monomeric and polymeric plutonium from the plasma of rats.

- O controls, monomeric plutonium, intravenous.
- × controls, polymeric plutonium, intravenous.
- ● treated, 500 mg/kg CaDTPA, intraperitoneal 1/2 hr after intravenous monomeric plutonium.
- ⊗ treated, 500 mg/kg CaDTPA, intraperitoneal 1/2 hr after intravenous polymeric plutonium.

Each point represents a sample of heparinized blood drawn from at least two rats by cardiac puncture and mixed before centrifugation.

The percentage of the plasma plutonium that was ultrafilterable was very low for both forms ($<0.01\%$) in the absence of DTPA therapy (Figure 59, lower graph). Treatment increased this considerably, and exerted a more pronounced and sustained effect on the monomeric form. For example, at 3 hr, the monomeric plasma Pu was about 37% ultrafilterable as compared with about 9% for the polymeric plasma Pu; corresponding values at 12 hr were about 10% and 1%.

Discussion

In untreated rats, the accelerated rate of disappearance of the polymeric form of plutonium as compared with the monomeric is a reflection of the activity of the reticuloendothelial system in removing colloidal particles. In the present experiment, the difference between the two solutions was not as great as had been expected. It is probable that the solution designated as monomeric contained a mixture of both monomeric and polymeric forms since 8% was not ultrafilterable. This is borne out by the

initially steep slope of the monomeric curve for the untreated animals in Figure 59 (upper graph), and by the fact that in other studies using monomeric plutonium[4, 5] the drop in plutonium content with time was shown to be more nearly a straight-line function.

The effects of DTPA therapy on increasing the rate and amount of plutonium removed from plasma as well as on increasing the ultrafilterability of Pu from the blood are in accord with the demonstrated therapeutic effectiveness of this compound for plutonium removal.[2, 6, 7] The fact that these effects are more pronounced on plutonium injected in monomeric form than in polymeric is in agreement with observations on tissues other than blood.[2] These considerations are of clinical interest since plutonium in the blood and tissues of a patient subjected to chemotherapy is more likely to be in a polymeric state than otherwise.

References

1. Lindenbaum, A. and J. Schubert. Sustained action of injected chelating agents. Nature 187, 575-576 (1960).

2. Schubert, J., J. F. Fried, M. W. Rosenthal and A. Lindenbaum. Tissue distribution of monomeric and polymeric plutonium as modified by a chelating agent. Radiation Research 15, 220-226 (1961).

3. H. Foreman. Metal-Binding in Medicine, ed. M. J. Seven and L. A. Johnson. J. B. Lippincott, Philadelphia, 1960. Ch. 9, pp. 82-94.

4. Schubert, J., M. P. Finkel, M. R. White and G. M. Hirsch. Plutonium and yttrium content of the blood, liver and skeleton of the rat at different times after intravenous administration. J. Biol. Chem. 182, 635-642 (1950).

5. Rosenthal, M. W. and J. Schubert. Kinetics of body distribution of plutonium as influenced by zirconium. Radiation Research 6, 349-354 (1957).

6. Fried, J. F., E. H. Graul, J. Schubert and W. Westfall. Superior chelating agents for the treatment of plutonium poisoning. Atompraxis 5, 1-5 (1959).

7. Smith, V. H. Removal of internally deposited plutonium. Nature 181, 1792-1793 (1958).

METABOLISM OF METHIONINE AND S-ADENOSYLMETHIONINE IN NEUROSPORA

Lila Abrahamson

The metabolism of methionine and S-adenosylmethionine (S-AM) was studied in Neurospora crassa, strains 5256a and 38706, by determining the amount of S-AM accumulated in the presence of varying concentrations of L-methionine and other compounds in the growth medium. Strain 5256a is a prototroph that can grow in medium lacking methionine, while strain 38706 is a methionineless auxotroph that cannot convert homocysteine to methionine and requires methionine for growth.(1)

Materials and Methods

Organisms. Neurospora crassa strains 5256a and 38706 were obtained from the American Type Culture Collection and are ATCC 10815 and ATCC 10780, respectively.

Culture methods. The cultures were transferred monthly to stock agar slants as suggested by Horowitz,(1) using potassium sodium tartrate instead of potassium tartrate. The basal medium of Horowitz and Beadle(2) was used for the experimental cultures. This medium was dispensed either as 150 ml in 500-ml erlenmeyer flasks or as 40 ml in 240-ml flasks. Sterilized media were inoculated with 1 ml of a water suspension of Neurospora hyphae and conidia and placed on a reciprocal shaker at 25 C for 72 hr. The cultures were harvested by filtration, washed with distilled water and weighed.

Determination of S-AM concentration in mycelia. The harvested and washed mycelial mat was extracted overnight in 10 ml/g wet weight of 1.5 N perchloric acid, and the S-AM was separated from other components on a Dowex 50 H^+ column by a modification(3) of the method of Schlenk and De Palma.(4) The presence of S-AM in the 6 N H_2SO_4 eluate was verified by an ultraviolet absorption spectrum.

Resting cell suspensions in the presence of S-AM in the substrate. During some experiments it was noted that the amount of added material absorbing at 260 mμ decreased in the medium after 72 hr growth. This effect was checked by incubating a sterile, washed, resting suspension of hyphae with S-AM at pH 5.

Strain 5256a was inoculated into basal medium without methionine and grown as described above. After 72 hr the mycelium in each flask was individually and sterilely harvested, washed, weighed, and placed in 40 ml

of substrate. The substrates used were the following: (a) 1.07 μmoles/ml S-AM in distilled water; (b) 1.07 μmoles/ml S-AM in 2% KH_2PO_4; (c) distilled water; (d) 2% KH_2PO_4. Control flasks containing 1.07 μmoles/ml S-AM in distilled water and in 2% KH_2PO_4 were not inoculated.

The flasks were placed on the shaker after 0.1 ml samples of substrate were removed for analysis at 260 mμ. At intervals, 0.1 ml samples of substrate were removed and analyzed. After 21 hr the mycelia were harvested, washed, weighed, extracted with 1.5 N perchloric acid, and chromatographed as described above.

Results

Prototroph 5256a. Mycelia grown in basal medium without methionine and in basal medium plus 5 μmoles/ml adenosine and 20 mg/ml KH_2PO_4 showed no accumulation of S-AM. That grown in basal medium plus 5 μmoles/ml L-methionine or basal medium plus 5 μmoles/ml adenosine, 5 μmoles/ml L-methionine and 20 mg/ml KH_2PO_4 showed a small accumulation of ultraviolet-absorbing material that had a peak at 240 to 248 mμ. S-AM shows a peak at 256 mμ.[5] The accumulated material was not characterized further.

The results of the resting cell suspension are shown in Table 39. There was a 9.4% decrease of ultraviolet-absorbing material in the substrate containing S-AM, without added phosphate, after 3 hr and a 54%

TABLE 39

Loss of substrate S-AM in the presence of a resting cell suspension *Neurospora crassa*, strain 5256a

Flask contents	Time after initial inoculation, hr	Material absorbing at 260 mμ,* moles/0.1 ml
S-AM plus mycelium	0	0.118
	3	0.107
	8	0.096
	21	0.054
S-AM plus KH_2PO_4 and mycelium	0	0.118
	3	0.121
	8	0.135
	21	0.122
Distilled water plus mycelium	0	0.000
	21	0.016
KH_2PO_4 plus mycelium	0	0.000
	21	0.037
S-AM	0	0.114
	21	0.117
S-AM plus KH_2PO_4	0	0.109
	21	0.114

*The substrate was diluted 1:50 for the readings.

decrease after 21 hr. The 54% decrease represents an approximate decrease of 10% every 3 hr. The total substrate loss of S-AM per flask was 25.6 μmoles, while the total increase of S-AM in the mycelium was only 0.56 μmoles. The remainder of the substrate S-AM appeared in the total ultraviolet-absorbing material extracted by perchloric acid from the mycelium and was not characterized.

Methionineless auxotroph 38706. Mycelia grown in basal medium plus 0.1 μmoles or 5 μmoles/ml L-methionine showed a very slight accumulation of S-AM, 0.83 μmoles and 0.66 μmoles S-AM/g of tissue, respectively. In the presence of 2.68 μmoles/ml S-AM the auxotroph produced 3 g wet weight of mycelium which is approximately that produced in the presence of 0.25 μmoles/ml L-methionine. No growth was noted in basal medium plus 0.57 μmoles/ml adenosylhomocysteine.

Discussion

Unlike yeast,[5] *Neurospora* did not accumulate appreciable quantities of S-AM when grown in the presence of excess L-methionine. This was in accord with early work of Smith *et al.*[6] in which it was found that *Neurospora crassa* accumulated methylthioadenosine (MTA) to the extent of 0.6 μmoles/g, while *Saccharomyces cerevisiae* accumulated 5.7 μmoles/g and *Aspergillus niger* 2.5 μmoles/g.

Under the culture conditions used in these experiments S-AM is chemically stable.[7] However, the disappearance of S-AM from the media may be accounted for by enzymatic activity of the fungus. Shapiro and Mather[8] described the enzymatic decomposition of S-AM by extracts of *Aerobacter aerogenes*, *Escherichia coli* and *Saccharomyces cerevisiae*, and noted that 10% of the S-AM was decomposed after 3 hr incubation by the latter two and 25% in 3 hr by the first. The rate of loss of S-AM from the medium in which resting cells of *Neurospora* were placed is in agreement with the results for *E. coli* and *S. cerevisiae* extracts in the presence of S-AM. However, the presence of MTA, one of the decomposition products, was not verified in the perchloric acid extract of the mycelia.

The slight growth of the auxotroph in medium containing 2.68 μmoles/ml S-AM may be the result of the presence of a small quantity of MTA as a contaminant in the S-AM solution used. It would be of interest to see if the auxotroph could grow with MTA in the medium instead of L-methionine, and an experiment to test this point is planned.

References

1. Horowitz, N. H. Methionine synthesis in Neurospora. The isolation of cystathionine. J. Biol. Chem. 171, 255-264 (1947).

2. Horowitz, N. H. and G. W. Beadle. A microbiological method for the determination of choline by use of a mutant of Neurospora. J. Biol. Chem. 150, 325-333 (1943).

3. Schlenk, F., J. L. Dainko and S. M. Stanford. Improved procedure for the isolation of S-adenosylmethionine and S-adenosylethionine. Arch. Biochem. Biophys. 83, 28-34 (1959).

4. Schlenk, F. and R. E. De Palma. The preparation of S-adenosylmethionine. J. Biol. Chem. 229, 1051-1057 (1957).

5. Schlenk, F. and R. E. De Palma. The formation of S-adenosylmethionine in yeast. J. Biol. Chem. 229, 1037-1050 (1957).

6. Smith, R. L., E. E. Anderson, Jr., R. N. Overland and F. Schlenk. The occurrence, formation and isolation of thiomethyladenosine. Arch. Biochem. Biophys. 42, 72-82 (1953).

7. Parks, L. and F. Schlenk. The stability and hydrolysis of S-adenosylmethionine: isolation of S-ribosylmethionine. J. Biol. Chem. 230, 295-305 (1958).

8. Shapiro, S. K. and A. N. Mather. The enzymatic decomposition of S-adenosyl-L-methionine. J. Biol. Chem. 233, 631-633 (1958).

BETA-SCINTILLATION COUNTING OF RADIOACTIVE TRACERS ON FILTER PAPER

Walter E. Kisieleski and Donald Logsdon

Scintillation counting of weak β-emitters on filter paper has frequently been attempted and in most cases utilized with some degree of success. Radioactive samples are frequently collected on filter paper, lens tissue, or millipore filters during the processes of separation or purification of labeled material. By direct scintillation counting of these samples the difficulties arising from insolubility of the sample in the typical aromatic liquid scintillation solvents are circumvented. Direct counting should also help to overcome the marked decrease in the fluorescence efficiency noted when biological samples, in particular, are dissolved in scintillating solutions.

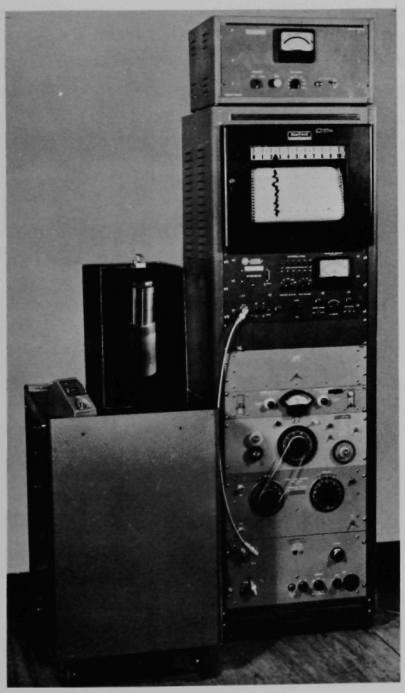

Figure 60. Scintillation counter: complete assembly with photomultiplier contained in shielded box, linear amplifier, super stable high-voltage supply, scaler, strip-chart recorder and a count-rate meter.

We have investigated the technique of Roucayrol,(1) which consists of wetting a piece of filter paper that contains a deposit of activity with a liquid scintillator solution and counting the paper directly on the surface of a photomultiplier tube. The organic solvent renders the paper relatively transparent, and good light collection is possible.

The method was tested by pipetting 0.1-ml aliquots of aqueous solutions of C^{14}, Ca^{45}, and P^{32} onto Whatman No. 1 filter paper $1\frac{3}{8}$ inches in diameter. The active filter papers were dried and then wetted with a liquid scintillator solution containing p-terphenyl (4.0 g/liter) and 1, 4-di-(2,5-phenyloxazolyl)-benzene (POPOP) (0.1 g/liter) in a low volatility solvent, monoisopropylbiphenyl. The impregnated filter paper was placed in a transparent plastic container, in order to avoid tube contamination, and then placed directly on the surface of a Dumont 6292 photomultiplier tube. The scintillation counting assembly without phototube refrigeration or anticoincidence circuitry is shown in Figure 60.

Counting efficiency for the various isotopes under these conditions of measurement could then be determined, absolute activity having been measured previously by internal scintillation counting. The counting efficiencies determined were as follows: C^{14}, 30%; Ca^{45}, 70%; and P^{32}, 75%. The background counting rates were in the order of 1 count per second. Much the same results were found when this procedure was followed using lens tissue or millipore filters rather than ordinary filter paper.

The results indicate that direct filter paper counting can be employed with good detection efficiency and a minimum of sample preparation. The success with millipore filters also affords the possibility of counting labeled cells or organisms that are usually collected on millipore filters for scoring purposes.

Reference

1. Roucayrol, J. C., E. Oberhausen, and R. Schuler. Radioisotopes in scientific research. Proceedings of First UNESCO International Conference, Pergamon Press, New York, 1958. Vol. I, p. 648.

DIFFERENTIAL MIGRATION OF STEROL ACETATES ON SILICA GELS AND ITS APPLICATION TO THE FRACTIONATION OF STEROL MIXTURES

Peter D. Klein and Patricia A. Szczepanik

The fractionation of sterols by chromatographic means has been the subject of considerable interest. To date the most prominent of such means has been gas-liquid chromatography.[1-3] In parallel development to the analytical determination of the composition of sterol mixtures, several groups have reported the fractionation of free sterol mixtures by adsorption chromatography on silicic acid.[4-6] While gas-liquid chromatography offers the considerable advantage of speed, adsorption chromatography offers the possibility of preparative scale isolations which facilitate metabolic studies by permitting the recovery of intermediates for chemical and radiochemical examination. Our experiences with the ability of silica gel columns to fractionate esters of cholesterol according to the constituent fatty acid[7] suggested that different sterols as the same ester (acetate) might be resolved under similar conditions. The fractionation of sterol acetates offers one further advantage over the chromatography of free sterols: a means of quantitating sterol composition by radiochemical techniques employing C^{14}-acetic anhydride as the acetylating agent.[8] Such a technique could reduce the problems of colorimetry standards for the Lieberman-Burchard reaction as well as those evolving from two types of spectra and two types of reaction rates in this reaction.

Early experiences with the fractionation of sterol acetates led to the realization that both the column efficiency and the separation factors in such a fractionation were strongly dependent on the structure of the silica gel employed. Several features contributing to column efficiency (pore diameter and surface energy) have been investigated;[9, 10] we wish to report here the mapping of retention volumes for thirteen sterols on four silica gels whose average pore diameters range from 20 to 170 A. These values permit the selection of a silica gel appropriate for a given separation.

Experimental

Materials. Dihydrocholesterol, cholesterol, 7-dehydrocholesterol and ergosterol were purchased from Nutritional Biochemicals Corporation and were recrystallized before use. The following sterols were obtained as gifts: a 1:1 mixture of 24, 25-dihydrolanosterol-lanosterol from Dr. Paul O'Connell (Upjohn Company); zymosterol from Dr. O. N. Breivik (Fleischman Laboratories); 25-ketonorcholesterol from Dr. William Gebert (Schering Corporation); sitosterol and stigmasterol from Dr. E. R. Diller (Eli Lilly); agnosterol from Dr. C. H. Duncan (University of Louisville);

methostenol from Dr. W. W. Wells (University of Pittsburgh). The hypocholesteremic drug Triparanol® was a gift of Dr. T. R. Blohm (William S. Merrill Company). Δ^7-Cholestenol was prepared by hydrogenation of 7-dehydrocholesterol over Raney nickel by the method of Fieser and Herz;[11] 24-dehydrocholesterol was prepared from 25-ketonorcholesterol by the method of Ryer, et al.[12]

Sterol acetates were prepared by the micro method of Johnston, et al.[13] and were purified by column chromatography[7] before use.

Silica gels were products of the Davison Company, Baltimore, Md.: they will be designated by their Davison code numbers as #12, #950, MS and #62. The lots used in these studies were characterized by the independent measurements of surface area and pore volume listed in Table 40; these properties have been found to adhere closely to the specifications listed for them by Davison.[9] All gels were screened to obtain the fraction between 200 and 325 mesh.* The final fraction was rescreened twice to remove all particles smaller than 325 mesh.

TABLE 40

Properties of silica gels used in sterol fractionations

	Davison code number			
	#12	#950	MS	#62
Surface area, m^2/g	805	672	547	274
Pore volume, ml/g	0.41	0.45	0.71	1.16
Av. pore diameter, A	20	27	67	170
Bulk density, g/ml	0.61	0.60	0.40	0.29
Equilibration, % humidity	7.05	7.05	7.05	11.02
Retention volume of cholesterol acetate per ml column volume, ml 16% benzene in hexane	62	85	72	27

*Coarser particles can be reduced to the proper mesh size by subjecting the dry gel to high-speed shearing forces in a Waring blender for short periods of time (30 sec to 2 min). The blender treatment is interspersed with screening to remove finer particles. It is advisable to use a dozen or so $\frac{1}{2}$-inch porcelain balls on each screen to reduce clogging.

It is advisable to equilibrate the gels at the relative humidity that provides the lowest retention volume consistent with maxium efficiency.[10] This humidity must be determined for each type of silica gel structure; for #12, #950 and MS a relative humidity of 7% appears optimal, for #62, 11%.*

Operation of the column. The column consisted of 110 cm of 0.45-cm I.D. glass tubing. At the lower end, a Luer tip was fused to the tubing; at the upper end, a 24/40 standard tapered female joint provided a reservoir above the column bed. A small pad of glass wool was tamped into the bottom of the column, and the Luer tip was plugged by slipping a sealed needle shank over the tip. The column was filled with 16% benzene in hexane (pure grade solvents) and the appropriate gel was introduced into the reservoir through a funnel. The introduction of the gel was followed by stirring and tapping to permit the gel to settle evenly. The column was filled to about 110 cm and then allowed to settle while draining (assisted, if necessary, by slight positive pressure from a well-controlled air-pressure source). When settling was complete, the column was shut off and the level of the bed was brought to exactly 100 cm by removal of the excess gel: at no time was the bed permitted to become dry. When the bed was prepared, the supernatant solution was removed and the sample (2 to 10 mg total sterol acetates in 16% benzene in hexane) was pipetted onto the top of the column. The sample was passed onto the bed and rinsed in with a few ml of 16% benzene in hexane. A reservoir (500; 1000-or 2000-ml capacity) made of a round-bottomed flask with an outlet of a 24/40 standard tapered male joint at the bottom, having an inner drip tip, was placed on top of the column and filled with 16% benzene in hexane. The column reservoir was filled from the upper reservoir, and elution was begun.

The eluate was led through a needle and a length of small-diameter polyethylene tubing to the fraction collector. It was found advisable to collect the fractions directly in the tubes without the intervention of the usual funnel. The flow rate was set between 15 and 20 ml/hr, or fractions of 5 to 7 ml per 20-min period. The fractions, or an aliquot of each, were evaporated to dryness, and the sterol content was determined by the Lieberman-Burchard reaction. It was found convenient to use two colorimeters, each set at the appropriate wave length, to measure the blue-green reactions at 660 mμ and the yellow reaction at 440 mμ.

Determination of Relative Elution Volumes. The relative elution volume of a sterol acetate was defined to be the ratio of the volume of solvent required to elute 50% of that sterol to the volume of solvent required

---

*These are provided by desiccators containing saturated solutions of sodium hydroxide and of lithium chloride, respectively. The equilibration is hastened by daily stirring of the gel, followed by re-evacuation of the desiccator to the vapor pressure of the solution, and is essentially complete after 2 weeks' storage.

to elute 50% of the cholesterol acetate. The graphic method of determining the 50% point, described earlier, was used in all instances.[9] In all runs, 2 mg of cholesterol acetate were used for reference purposes; samples of 0.2 to 2.0 mg of the other sterols (depending upon the color yield of the sterol) were added and the mixture was chromatographed. In those instances in which the relative elution volumes were within 10 to 15% of the standard volume, final calculations were made on separate elutions of each sterol from two columns run in parallel.

Results

The relative retention volumes of thirteen sterols on the four Davison gels are listed in Table 41. The column designated "Mallinckrodt" lists values obtained in the early stages of this work with a silica gel product of unknown structure; on the basis of retention values it appears to have been between 20 and 25 A average pore diameter. Subsequent products have had different properties.

TABLE 41

Relative elution volumes* of sterol acetates on various silica gels

Gel	12	Mallinckrodt	950	MS	#62
Av. pore diameter, A	20	Unknown (24?)	27	60	170
Dihydrolanosterol	0.74	0.72	0.72	0.72	0.89
Dihydrocholesterol	0.86	0.90	0.98	0.93	0.97
Cholesterol	1.00	1.00	1.00	1.00	1.00
Sitosterol	1.04		0.93	0.94	1.07
Stigmasterol	1.09		0.96	0.99	1.08
Lanosterol	1.34	1.28	1.21	0.91	1.10
Methostenol	1.22	1.38	1.17	1.15	1.18
Δ^7 Cholestenol	1.40	1.40	1.39	1.41	1.45
Agnosterol	1.64	1.48	1.43	1.09	1.20
24-Dehydrocholesterol	1.98	1.58	1.67	1.32	1.32
7-Dehydrocholesterol	1.77	1.68	1.40	1.34	1.43
Ergosterol	2.04	1.91	1.66	1.62	1.52
Zymosterol	2.42	2.20			1.69

*All values are reproducible to within 3%.

The largest range of relative elution volumes appears to be achieved on a small-pore gel (#12); in part this is due to the selective retardation of sterols with unsaturated bonds in the tail structure. Figure 61 illustrates this feature of gel structure applied to sterols with 24, 25 double bonds.

The three sterols shown all exhibit an increased retention volume relative to cholesterol as the pore diameter of the gel is decreased. A further distinction can be noted in the retardation as a function of the hydrocarbon tail structure (Figure 62). The retardation of ergosterol begins at a lower pore diameter and does not increase to the same extent as does that of the 24-dehydrosterols: furthermore substitution of an ethyl group in the side chain almost completely abolishes the selective retardation. We interpret this as being caused by a "shielding" of the adsorptive group by the ethyl addition.

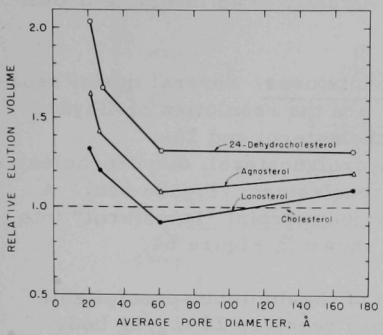

Figure 61. Relative elution volumes of 24-dehydrocholesterol, agnosterol and lanosterol acetates as a function of average pore diameter.

Several other effects of gel structure are discernible in Table 41; for example, the elution position of a sterol may be changed by a change in pore diameter. Thus in the region between 40 and 100 A, lanosterol will migrate ahead of cholesterol; below and above this range it will migrate behind cholesterol. Similar effects are noted in the behavior of sitosterol and stigmasterol, while agnosterol and Δ^7-cholestenol, as well as 24-dehydrocholesterol and 7-dehydrocholesterol, exhibit "crossover" behavior with respect to the other. Indeed the only sterol which maintains the same elution volume relative to cholesterol throughout the whole pore diameter range is Δ^7-cholestenol.

Recoveries of each sterol acetate were calculated during these studies; all but three of the thirteen showed consistent recoveries of 80% to 100%. Zymosterol, 7-dehydrocholesterol and ergosterol recoveries ranged downward from 75% to 15%. Of these three, it is likely that the zymosterol sample had already undergone decomposition during prolonged storage in solution, but ergosterol and, in particular, 7-dehydrocholesterol were found to be extremely prone to decomposition upon adsorption on the silica surface. This decomposition was accompanied by the formation of dark blue-green bands at

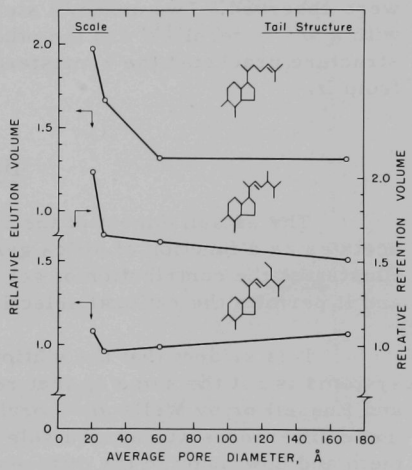

Figure 62. Effect of tail structure on the relative retention volume changes produced by small-pore gels. Top curve, 24-dehydrocholesterol acetate; middle curve, ergosterol acetate; lower curve, stigmasterol acetate.

the top of the column reminiscent of the Lieberman-Burchard reaction. The reaction involved the formation of a more polar molecule which could be eluted with ethyl ether but proceeded eventually to an insoluble brown resin.

Application to model and biological mixtures. Several model separations are illustrated in Figure 63. These are the resolution of dihydrocholesterol and cholesterol (Figure 63a); cholesterol and 24-dehydrocholesterol (Figure 63b); 24, 25-dihydrolanosterol, dihydrocholesterol, cholesterol, Δ^7-cholestenol and 24-dehydrocholesterol (Figure 63c). A preparative scale fractionation of 40 mg of commercial "lanosterol" into 24, 25-dihydrolanosterol and lanosterol is shown in Figure 64.

Figure 65 shows the chromatogram of the digitonin-precipitable sterols from the liver of an animal which had received 20 mg/kg body weight of Triparanol for 7 days and 20 μc of mevalonic acid-C^{14} 30 min before sacrifice. Only two peaks are detectable colorimetrically, cholesterol and 24-dehydrocholesterol, although traces were found in the interval between these two peaks (indicated by dots) which were below the level of quantitative determinability. The radioactivity in these fractions, measured by liquid scintillation counting,(14) showed a number of other features which were of interest. In addition to Δ^5 and $\Delta^{5,24}$ sterols, peaks migrating with the elution volumes of lanosterol, 7-dehydrocholesterol and zymosterol were observed. Two unknown sterols, one with a migration rate consistent with a $\Delta^{7,24}$ sterol(15) and the other with a rate consistent with a $\Delta^{5,7,24}$ structure bracketed the zymosterol peak but were clearly distinguishable from it.

Discussion

The establishment of the relative elution volumes of these sterol acetates as a function of silica gel structure serves two purposes: it illustrates the contribution of gel structure to the chromatographic process and it permits the rational selection of a silica gel for a desired separation.

It is evident that the elution order of the sterol acetates in these systems is not the same as that reported for the free sterols by Kandutsch and Russell or by Wells and Lorah in they systems.(5, 6) How many of these differences are attributable to the structure of the silica gels used by them and how many to the difference between free and acetylated sterol usage cannot be established at this time. In all three systems (including ours) the addition of angular methyl groups to the sterol nucleus reduces its retention volume (e.g., methostenol vs. Δ^7-cholestenol, lanosterol vs. zymosterol). The pivotal difference appears to be in the effect of the Δ^8 bond which, in the system of Kandutsch and Russell reduces the retention volume compared to that of the Δ^5 bond, while in our system it increases the retention volume (zymosterol vs. 24-dehydrocholesterol).

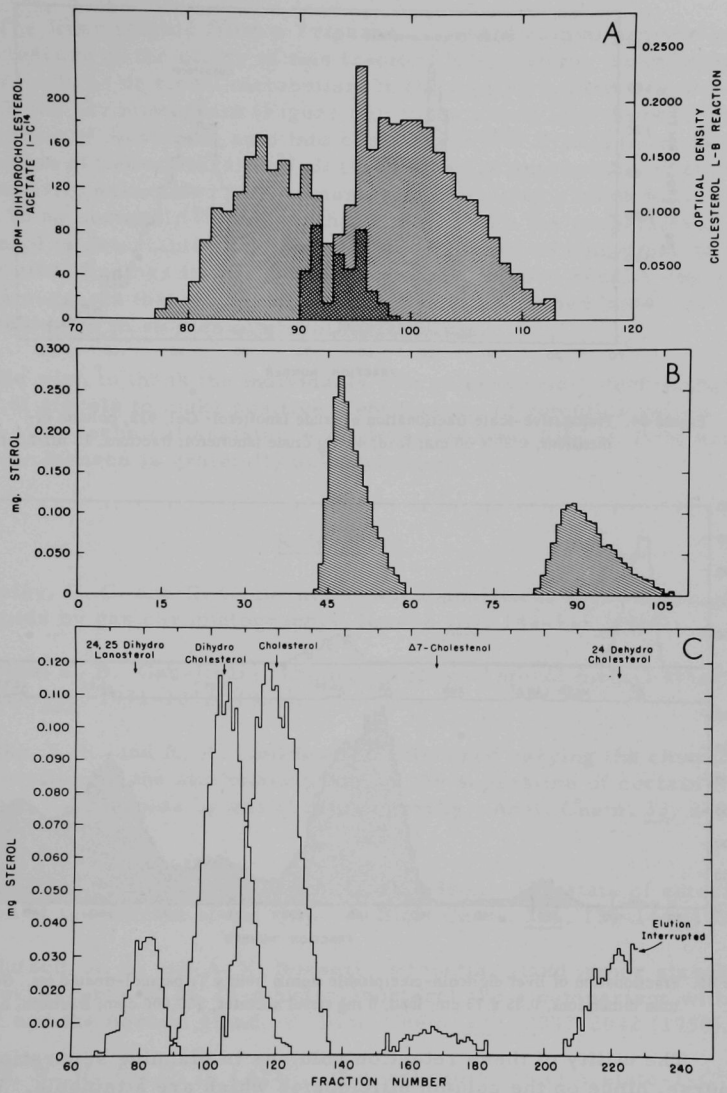

Figure 63. Fractionation of model mixtures. All compounds are listed in order of emergence.

A - gel #12; column dimensions, 0.45 x 100 cm; load, 0.6 mg dihydrocholesterol acetate-C^{14}, 1.2 mg cholesterol acetate; fractions, 2.9 ml/10 min.

B - gel #12; column dimensions, 0.25 x 40 cm; load, 2.0 mg cholesterol acetate, 2.0 mg 24-dehydrocholesterol acetate; fractions, 1.5 ml/15 min.

C - gel #12; column dimensions, 0.45 x 103 cm; load, 0.4 mg 24, 25 dihydrolanosterol acetate, 2.0 mg dihydrocholesterol acetate, 2.0 mg cholesterol acetate, 0.2 mg Δ^7-cholestenol acetate, 2.0 mg 24-dehydrocholesterol acetate; fractions, 6.0 ml/15 min.

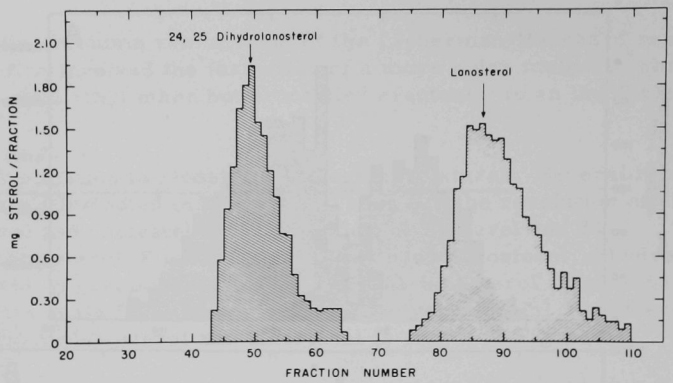

Figure 64. Preparative-scale fractionation of crude lanosterol. Gel, #12, column dimensions, 0.90 x 50 cm; load, 40 mg crude lanosterol; fractions, 15 ml/20 min.

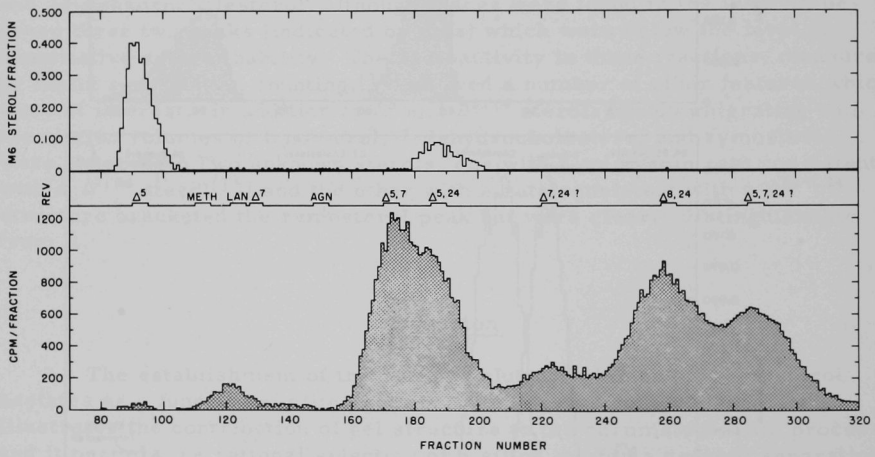

Figure 65. Fractionation of liver digitonin-precipitable sterols from a Triparanol-treated rat. Gel, #12, column dimensions, 0.45 x 75 cm; load, 6 mg sterol acetates, 130,000 cpm; fractions, 5.5 ml/22 min.

The utility of these retention volumes in planning separations will, of course, hinge on the column efficiencies which are attainable. Within the load ranges described in these studies, a 1-meter column can resolve two components whose retention volumes differ by a factor of 1.15-1.20, the nominal equivalent of 500 to 750 plates. A more detailed prediction of column efficiency cannot be given at this time because it appears to be intimately related to the orientation assumed by the sterol acetate molecules in the adsorbed state. These considerations, however, do not affect the retention volumes reported here.

The liver sterols from a Triparanol-treated animal provide an excellent measure of the utility of this fractionation system. Four previously reported features of sterol metabolism in the treated animal are demonstrable in the chromatogram (Figure 65); these are 1) that there is negligible incorporation of mevalonic acid into cholesterol;(16) 2) that there is an accumulation of desmosterol;(17) 3) that there are appreciable quantities of radioactivity associated with zymosterol, indicating a block in its hydrogenation to zymostenol;(18) and 4) that a sterol with the properties of a $\Delta^{7,24}$-sterol is detectable.(15) The close correlation of colorimetric and radiochemical findings in this chromatogram with those results reported by others suggests that the fractionation system described here may be of considerable use in studies of sterol metabolism.

We wish to thank the individuals who so generously contributed samples of sterols to make positive identification of retention values possible. The technical assistance rendered by Mrs. Rita M. Dahl and Barbara A. Johnson is gratefully acknowledged.

References

1. Sweeley, C. C. and E. C. Horning. Microanalytical separations of steroids by gas chromatography. Nature 187, 144-145 (1960).

2. Clayton, R. B. Gas-liquid chromatography of sterol methyl ethers. Nature 190, 1071-1072 (1961).

3. Lipsky, S. R. and R. A. Lansdowne. Effects of varying the chemical composition of the stationary phase on the separation of certain C_{19}, C_{20} and C_{27} steroids by gas chromatography. Anal. Chem. 33, 818-828 (1961).

4. Frantz, I. D. Jr., E. Dulit and A. G. Davidson. The state of esterification of the sterols of rat skin. J. Biol. Chem. 226, 139-144 (1957).

5. Kandutsch, A. A. and A. E. Russell. Preputial gland tumor sterols I. The occurrence of 24, 25-dihydrolanosterol and a comparison with liver and the normal gland. J. Biol. Chem. 234, 2037-2042 (1959).

6. Wells, W. W. and C. L. Lorah. The incorporation of acetate-1-C^{14} into methostenol of rat tissues and the conversion of synthetic methostenol-4-C^{14} to cholesterol in vivo. J. Biol. Chem. 235, 978-982 (1960).

7. Klein, P. D. and E. T. Janssen. The fractionation of cholesterol esters by silicic acid chromatography. J. Biol. Chem. 234, 1417-1420 (1959).

8. Clark, A. J. and K. Bloch. The absence of sterol synthesis in insects. J. Biol. Chem. 234, 2578-2582 (1959).

9. Klein, P. D. Silica gel structure and the chromatographic process. Effect of pore diameter on the adsorption and differential migration of sterol acetates. Anal. Chem. 33, 1737-1741 (1961).

10. Klein, P. D. Silica gel structure and the chromatographic process. Surface energy and activation procedures. Anal. Chem. 34, 733-736 (1962).

11. Fieser, L. H. and J. E. Herz. Synthesis of 11-ketosteroids II. 11-ketocholestanol. J. Am. Chem. Soc. 75, 121-124 (1953).

12. Ryer, A. I., W. H. Gebert and N. W. Murrill. The preparation of cholesterol from 25-ketonorcholesterol. J. Am. Chem. Soc. 72, 4247-4248 (1950).

13. Johnston, J. D., F. Gautschi and K. Bloch. Isolation of lanosterol from "isocholesterol." J. Biol. Chem. 224, 185-190 (1957).

14. Klein, P. D. and R. A. Martin. Heterogeneity in the turnover rates of liver cholesterol esters. J. Biol. Chem. 234, 1685-1687 (1959).

15. Frantz, I. D., Jr. and M. L. Mobberly. $\Delta^{7,24}$-cholestadien-3 β-ol, a probable intermediate in cholesterol synthesis. Federation Proc. 20, 285 (1961).

16. Blohm, T. R. and R. D. MacKenzie. Specific inhibition of cholesterol biosynthesis by a synthetic compound (MER-29). Arch. Biochem. Biophys. 85, 245-249 (1959).

17. Avigan, J, D. Steinberg, M. J. Thompson and E. Mosettig. Mechanism of action of MER-29, an inhibitor of cholesterol biosynthesis. Biochem. Biophys. Res. Commun 2, 63-65 (1960).

18. Schroepfer, G. J. The conversion of zymosterol-C^{14} and zymostenol-C^{14} to cholesterol by rat liver homogenates and intact rats. J. Biol. Chem. 236, 1668-1673 (1961).

PROGRESS REPORT: BIOSYNTHESIS OF METHIONINE FROM HOMOCYSTEINE AND SULFONIUM DERIVATIVES IN ESCHERICHIA COLI

Morris Pfeffer and Stanley K. Shapiro

Methyltransferases catalyzing the transfer of a methyl group from a suitable methyl donor to the sulfur atom of methionine have been described in animals,[1-9] plants[10] and microorganisms.[5,11-13] S-Methylmethionine-homocysteine methyltransferase and S-adenosylmethionine-homocysteine methyltransferase have been described in various yeasts,[14-18] Aerobacter aerogenes, Lactobacillus arabinosus and Escherichia coli K12.[11,13] E. coli K12 appeared to be unusual in this respect because no other strains of this organism were found to contain this methyltransferase.[11,13] Dubnoff had reported that E. coli 113-3 (a vitamin B12-methionineless auxotroph of E. coli W (ATCC 9637) gave a growth response to dimethyl-β-propiothetin plus homocysteine,[19] and McRorie et al.[20] found that S-methylmethionine reversed sulfonamide toxicity to E. coli (Texas) and E. coli (Texas) M, a methionineless mutant thereof.

Cell-free extracts of E. coli (Texas) and E. coli (Texas) M, prepared in a 10 KC Raytheon sonic oscillator, were assayed for S-methylmethionine- and S-adenosylmethionine-homocysteine methyltransferase activity by the method of Shapiro and Yphantis,[5] using C^{14}-labeled sulfonium compounds, and found to possess the enzyme (Table 42). Paper chromatograms of reaction mixtures were scanned with a recording scanner to confirm the fact that methionine was the labeled reaction product being assayed. These determinations led to the observation that

TABLE 42

Comparison of the homocysteine methyltransferase activities of E. coli (Texas) and E. coli (Texas) M

Source of enzyme	Substrate		
	S-Methyl-L-(Me-C^{14})-methionine	S-Methyl-DL-methionine-$2C^{14}$	S-Adenosyl-L-(Me-C^{14})-methionine
	Methionine-C^{14} formed, mμ moles/ml/hr		
E. coli (Texas)	93.6	71.2	22.7
E. coli (Texas) M	109.2	80.4	22.9

The reaction mixtures contained, per ml; 8 μ moles L-homocysteine, 0.2 μ moles substrate, 0.2 ml cell-free extract, and 0.1 M phosphate buffer (pH 6.8). Incubations were carried out at 37°C for 1 hr. Specific activities of substrates in cpm/μ mole: S-methyl-L-(Me-C^{14}-methionine, 343,000; S-methyl-DL-methionine-$2C^{14}$, 86,000; S-adenosyl-L-(Me-C^{14})-methionine, 1,040,000. Methionine formed from labeled S-methylmethionine was determined by assuming that the reaction:

S-methylmethionine + homocysteine → 2 methionine

had occurred and that the specific activity of the methionine was half that of the S-methylmethionine. Methionine formed from S-adenosylmethionine was assumed to have the same specific activity. All results were calculated after subtraction of control values obtained when L-homocysteine was omitted from the reaction mixture.

S-methylmethionine is a more active methyl donor than S-adenosylmethionine. Since its isolation by Cantoni,[21] S-adenosylmethionine has been thought to be the true "active methionine" and implicated as the actual methyl donor. S-methylmethionine has been found to occur naturally only in a few plant tissue extracts.[22,23] The lower activity of S-adenosylmethionine as a methyl donor is paralleled by its lower growth-promoting activity for intact E. coli (Texas) M, as compared with S-methylmethionine (Figures 66 and 67). This phenomenon deserves extensive study.

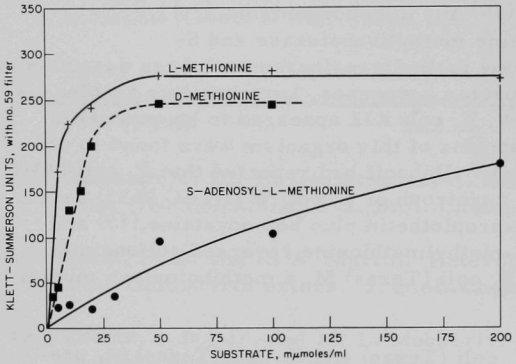

Figure 66

Growth response of E. coli (Texas) M to L- and D-methionine and S-adenosylmethionine. Cultures were grown in cotton plugged culture tubes containing 10 ml minimal medium plus the specified amounts of substrate. Incubated 18 hr at 37°C.

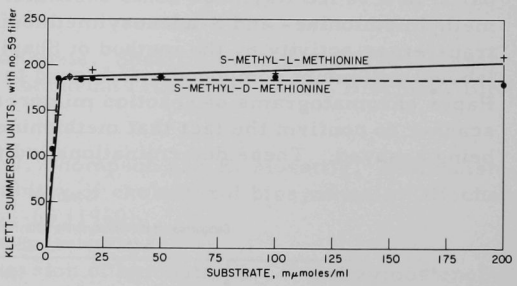

Figure 67

Growth response of E. coli (Texas) M to S-methyl-L- and S-methyl-D-methionine. Experimental conditions identical to those described in Figure 66.

E. coli (Texas) M was tested on a series of possible substrates to determine growth response curves (Figures 66, 67, and 68). Again, these results raised several questions. McRorie et al.,[20] who have also noted the ability of ethionine to support partial growth of E. coli (Texas) M, suggested that this was due to incorporation of ethionine into protein, a phenomenon which had previously been noted in rats.[24] However, Shapiro and Schlenk[25] have pointed out the existence of ethionine sulfonium derivatives and their physiological activity. Ethionine, in this instance, might be operating by either, or both, of these modes. The same possibilities might explain the partial growth-promoting effects of S-methylcysteine. Wiebers and Garner[26] have found that labeled S-methylcysteine methyl groups are incorporated into methionine by Neurospora. This is suggestive of a transmethylation function for an "active S-methylcysteine" analogous to "active methionine."

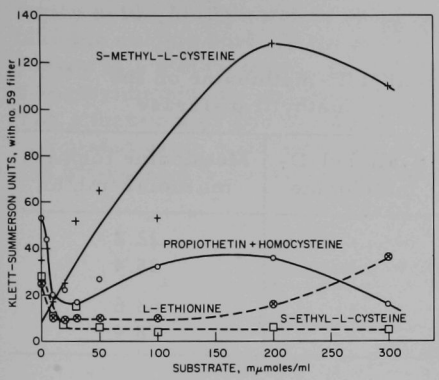

Figure 68

Growth response of E. coli (Texas) M to S-methyl-L-cysteine, dimethyl-β-propiothetin plus homocysteine, L-ethionine, and S-ethyl-L-cysteine. Experimental conditions identical to those described in Figure 66.

The results described in Table 43 and Figure 66 reveal that E. coli (Texas) M may possess a racemase that can convert D-methionine to L-methionine. Also, S-methyl-D-methionine is almost as active a growth-promoting agent as S-methyl-L-methionine. The same racemase, or another, may be acting on S-methyl-D-methionine; or the methyltransferase may not be stereospecific. In any case, S-methyl-D-methionine does not appear to inhibit the activity of the methyltransferase toward the L-isomer (Table 44).

TABLE 43

Growth responses of E. coli (Texas) M to various supplements

Supplement (200 mμmoles/ml minimal medium)	Turbidity (Klett-Summerson units with No. 59 filter)
None	0
L-Methionine	254
D-Methionine	229
S-Adenosyl-L-methionine	185
S-Methyl-L-methionine	243
S-Methyl-D-methionine	220
L-Ethionine	45
Dimethyl-β-acetothetin	0
Dimethyl-β-propiothetin	10
Betaine	0
L-Serine	0
5'-Methylthioadenosine	0
L-Homocysteine	0
DL-Cystathionine*	0
S-Methyl-L-cysteine	84
S-Adenosyl-L-methionine and L-homocysteine	185
S-Adenosyl-L-methionine and DL-cystathionine	185
S-Methyl-L-methionine and L-homocysteine	240
S-Methyl-L-methionine and DL-cystathionine	245
L-Homocysteine and DL-cystathionine	0
Dimethyl-β-acetothetin and L-homocysteine	0
Dimethyl-β-propiothetin and L-homocysteine	60

*DL-Cystathionine was used at a concentration of 400 μmoles/ml. Growth responses were measured in a Klett-Summerson colorimeter after 18-hr incubation on a reciprocal shaker at 37°C in cotton-plugged culture tubes containing 10 ml of supplemented minimal medium.[13]

TABLE 44

Effect of the presence of S-methyl-D-methionine on the activity of E. coli homocysteine methyltransferase

Source of enzyme	S-Methyl-L-(Me-C^{14})-methionine	S-Methyl-D-methionine	Methionine formed, mμ moles/ml/hr
E. coli	+	-	22.2
(Texas)	+	+	25.4
E. coli	+	-	63.6
(Texas) M	+	+	78.4

+ present, - absent.

The basic reaction mixture and experimental conditions are the same as those described in Table 42. In the reaction mixtures which contain S-methyl-D-methionine, its concentration was 0.2 μmole/ml.

It can be seen, in Table 43, that homocysteine and its immediate precursor, cystathionine, have no effect on the growth enhancing activity of any of the active substrates. This might indicate accumulation of homocysteine by E. coli (Texas) M and, therefore, that the block in methionine synthesis occurred at the stage of homocysteine methylation. This biosynthetic system is unusual in that methionine is a precursor of one of its own precursors. In the absence of methionine the methylsulfonium derivative of methionine, necessary for methionine synthesis (or vice-versa) cannot be formed. However, the observation that the growth-promoting effect of dimethyl-β-propiothetin toward intact cells is enhanced by homocysteine raises some doubt that homocysteine really accumulates; this suggests the presence of a dimethyl-β-propiothetin-homocysteine methyltransferase that might be, but probably is not, identical with S-methylmethionine- and S-adenosylmethionine-homocysteine methyltransferase. As mentioned previously, Dubnoff[19] found that E. coli 113-3 was similarly enhanced by dimethyl-β-propiothetin plus homocysteine.

A series of experiments is now being carried out to determine the amount of incorporation of label from various compounds into the protein methionine of E. coli (Texas) and E. coli (Texas) M (Table 45). The results so far have been rather surprising since, if protein methionine were derived solely from the methionine moiety of the added S-methylmethionine, the specific activity would have been very much higher than it was. The most likely explanation is that E. coli (Texas) M is not a methionine auxotroph and that S-methylmethionine is serving as a source of carbon and methyl groups for other purposes. This can be seen in Table 46. Most of the C^{14} taken up by the cells is found in the protein fraction, but only a small amount of this label is found in methionine, the only methylated

amino acid. Methylation is occurring in the synthesis of lipids, phospholipids, and nucleic acid. If the primary role of methionine is that of a precursor to a methyl donor, its greater growth-promoting effect relative to S-methylmethionine and S-adenosylmethionine appears rather anamalous. The situation may become clear when this series of experiments has been completed using methionine-Me-C^{14}, S-adenosyl-L-(Me-C^{14}) methionine and S^{35}-labeled S-methyl- and S-adenosylmethionine.

TABLE 45

Incorporation of label into protein methionine

Source of protein	Substrate	
	S-Methyl-L-(Me-C^{14})-methionine	S-Methyl-DL-methionine-$2C^{14}$
	Specific activity of protein methionine, cpm/μmole	
E. coli (Texas)	4400	-
E. coli (Texas) M	2400	2100

Microorganisms were grown in 1-liter flasks, containing 250 ml minimal medium plus 30 μmoles/ml substrate for 18 hr at 37°C on a rotary shaker. Specific activities of substrates are given in Table 42. Protein was isolated by the method of Roberts et al.[27] and hydrolyzed in 6 N HCl for 3.5 hr at 108°C. Methionine was determined by the quantitative ninhydrin method of Yemm and Cocking.[28]

TABLE 46

Distribution of label taken up in vivo from S-methylmethionine by E. coli

Fraction	Substrate		
	S-Methyl-L-(Me-C^{14})-methionine		S-Methyl-DL-methionine-$2C^{14}$
	E. coli (Texas)	E. coli (Texas) M	E. coli (Texas) M
	Percentage of label in fractions extracted from microorganisms		
Metabolic intermediates	1.4	1.5	1.2
Lipids and phospholipids	15.3	12.4	2.2
Alcohol-soluble protein	9.1	9.1	6.9
Nucleic acid	9.0	7.0	3.2
Protein	71.5	67.8	33.8
Recovery, %	106.3	97.8	46.9

Experimental conditions and methods identical to those described in Table 45.

The biosynthetic pathway leading to methionine has been generally accepted to be:

homoserine + cysteine → cystathionine → serine + homocysteine

homocysteine + C_1 → methionine

(C_1 = active one-carbon fragment)

However, Schlenk[29] suggests the possibility of the following reaction:

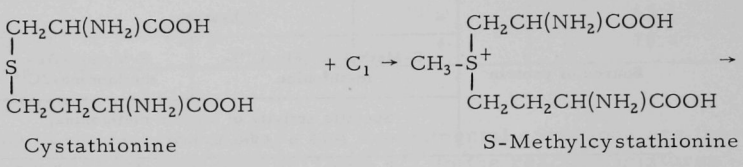

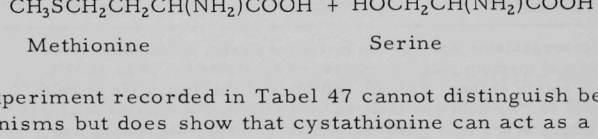

The experiment recorded in Tabel 47 cannot distinguish between these two mechanisms but does show that cystathionine can act as a precursor for methionine in these two microorganisms. Indeed, cystathionine seems to be just as effective as homocysteine over the one-hour period of the assay.

TABLE 47

Methionine synthesis from DL-cystathionine

Source of enzyme	Methyl acceptor	
	L-Homocysteine	DL-Cystathionine
	Methionine formed mμmoles/ml/hr	
E. coli (Texas)	146.8	173.2
E. coli (Texas) M	137.2	126.0

The basic reaction mixture and the experimental conditions are the same as those described in Table 42. S-Methyl-L-(Me-C^{14})-methionine was the only methyl donor used. DL-Cystathionine or L-homocysteine concentration, 8 μmoles/ml.

References

1. Dubnoff, J. W., and H. Borsook. Dimethylthetin and dimethyl-β-propiothetin in methionine biosynthesis. J. Biol. Chem. 176, 789-796 (1948).

2. Ericson, L. E., J. N. Williams and C. A. Elvehjem. Studies on partially purified betaine-homocysteine transmethylase of liver. J. Biol. Chem. 212, 537-544 (1955).

3. Maw, G. A. Thetin-homocysteine transmethylase. Biochem. J. 70, 168-173 (1958).

4. Maw, G. A. Thetin-homocysteine transmethylase. Biochem. J. 63, 116-124 (1956).

5. Shapiro, S. K., and D. A. Yphantis. Assay of S-methylmethionine and S-adenosylmethionine homocysteine transmethylases. Biochim. Biophys. Acta 36, 241-244 (1959).

6. Maw, G. A. Thetin-homocysteine transmethylase. Biochem. J. 72, 602-608 (1959).

7. Durrell, J., D. G. Anderson and G. L. Cantoni. The synthesis of methionine by enzymatic transmethylation. Biochim. Biophys. Acta 26, 270-282 (1957).

8. Ericson, L. E. Transmethylation in Anodonta cygnea. Nature 185, 465-466 (1960).

9. Klee, W. A., H. H. Richards and G. L. Cantoni. The synthesis of methionine by enzymatic transmethylation. VII. Existence of two separate homocysteine methylpherases in mammalian liver. Biochim. Biophys. Acta 54, 157-164 (1961).

10. Turner, J. E., and S. K. Shapiro. S-methylmethionine- and S-adenosylmethionine-homocysteine transmethylase in higher plant seeds. Biochim. Biophys. Acta 51, 581-584 (1961).

11. Shapiro, S. K. Biosynthesis of methionine from homocysteine and S-adenosylmethionine in bacteria. J. Bacteriol. 72, 730-735 (1956).

12. Shapiro, S. K. Adenosylmethionine-homocysteine transmethylase. Biochim. Biophys. Acta 29, 405-409 (1958).

13. Shapiro, S. K. The utilization of S-adenosylmethionine by micro-organisms. J. Bacteriol 83, 169-174 (1962).

14. Schlenk, F., and R. E. DePalma. The formation of S-adenosylmethionine in yeast. J. Biol. Chem. 229, 1051-1057 (1957).

15. Schlenk, F., and R. E. DePalma. The preparation of S-adenosylmethionine. J. Biol. Chem. 229, 1051-1057 (1957).

16. Spence, K. D., and L. W. Parks. Repression of methionine biosynthesis in wild-type and analog insensitive mutants of Saccharomyces cerevisiae. Bacteriol. Proc. 1962, 114.

17. Pigg, C. J., and L. W. Parks. Terminal reactions in the biosynthesis of methionine in yeast. Bacteriol. Proc. 1962, 120 (1962).

18. Duerre, J. A., and F. Schlenk. Formation and metabolism of S-adenosyl-L-homocysteine in yeast. Arch. Biochem. Biophys. 96, 575-579 (1962).

19. Dubnoff, J. W. The role of B12 in methionine synthesis in E. coli. Arch. Biochem. Biophys. 37, 37-45 (1952).

20. McRorie, R. A., M. R. Glazener, C. G. Skinner and W. Shive. Microbiological activity of the methylsulfonium derivative of methionine. J. Biol. Chem. 211, 489-497 (1954).

21. Cantoni, G. L. Activation of methionine for transmethylation. J. Biol. Chem. 189, 745-754 (1951).

22. McRorie, R. A., G. L Sutherland, M. S. Lewis, A. D. Barton, M. R. Glazener and W. Shive. Isolation and identification of a naturally occurring analog of methionine. J. Am. Chem. Soc. 76, 115-118 (1954).

23. Greene, R. C., and N. B. Davis. Biosynthesis of S-methylmethionine in the jack bean. Biochim. Biophys. Acta 43, 360-362 (1960).

24. Levine, M., and H. Tarver. Studies on ethionine. III. Incorporation of ethionine into rat proteins. J. Biol. Chem. 192, 835-850 (1951).

25. Shapiro, S. K., and F. Schlenk. The biochemistry of sulfonium compounds. Advances Enzymol, 22, 237-280 (1960).

26. Wiebers, J. L., and H. R. Garner. Utilization of S-methylcysteine and cystathionine by methionineless Neurospora mutants. Bacteriol. Proc. 1962, 120.

27. Roberts, R. B., P. H. Abelson, D. B. Cowie, E. T. Bolton and R. J. Britten. Studies of biosynthesis in Escherichia coli. Carnegie Inst. Pub. 607, Washington, D.C., 1955, pp. 13-30.

28. Yemm, E. W., and E. C Cocking. Determination of amino acids with ninhydrin. Analyst 80, 209-213 (1955).

29. Schlenk, F. Personal communication.

PHOSPHATE METABOLISM AND EFFECT OF THIOPHOSPHATE IN CHLORELLA

Takuya R. Sato

Since phosphorus metabolism is of such importance in bioenergetics, this research was designed to study the effects on plant and animal tissue preparations of various phosphates, in particular those containing P-O-P, P-P, and P-S bonds. Early experiments indicated that the effects of thiophosphate were of especial interest. The work reported here includes primarily the effects of phosphate compounds on growth and respiration in algae, and secondarily the effects of thiophosphate on a mammalian enzyme system i.e., the ATP-inorganic phosphate exchange reaction. Little is known about the effects of replacing orthophosphate by other inorganic phosphates. By the use of algae, which store large amounts of phosphate as polyphosphate, it should be possible to determine whether compounds such as diphosphite, hypophosphate, thiophosphate, etc., (a) inhibit competitively the utilization of orthophosphate, (b) alter cellular function by some other mechanism, or (c) can be utilized, converted to orthophosphate, and stored in the cell.

Summary of Results

Phosphate Metabolism of Normal Chlorella. Cells of *Chlorella pyrenoidosa*, strain 7-11-05, grown in phosphorus-rich media, contain large phosphate stores, sufficient to support growth for 25 days and 5-fold multiplication in the absence of external phosphate. Behavior of such cells is relatively insensitive to the phosphorus concentration of the external medium. The minimum requirement of phosphorus by Chlorella is very small; an initial concentration of 0.5-1 μg P/ml would supply the normal growth needs.

On prolonged cultivation in P-free media, the intracellular phosphorus level decreases to a minimum of about 2 to 3 x 10^{-8} μg P/cell, after which division ceases. When phosphate is again supplied, it is rapidly accumulated within the cell, restoring the phosphate reserves. This accumulation is accompanied by a marked increase of oxygen consumption; approximately one extra oxygen atom is consumed for every two molecules of phosphate accumulated (P/O ratio $\approx$2).

Maximal phosphate assimilation and stimulation of oxidative metabolism by phosphate were obtained in the range of pH 6.0-6.5. In this range, $H_2PO_4^-$ is the predominant ionic species of phosphate, making up about 95 percent of the total phosphate at pH 6.0, and about 80 percent at pH 6.5.

If $H_2PO_4^-$ were the active form of phosphate, the decreasing effects in alkaline media could be explained since the $H_2PO_4^-$ concentration decreases rapidly with increasing pH above pH 6.5. The decreased stimulation below pH 6.0 cannot be explained on this basis, however. Possibly low pH alters the "phosphate receptors" on the Chlorella cell, decreasing their affinity for phosphate in media more acid than pH 6.0.

Chlorella cultures synchronized by cycles of alternating light and darkness show a distinct correlation between phosphate metabolism and the stages of the division cycle. Phosphate accumulation is rapid during the early, "growth" phase of the cycle. The rate of phosphate consumption falls off during the "ripening" and "maturation" stages, and remains low during division. These results and those of other investigators[1-3] on Chlorella and other cells suggest that a reservoir of intracellular phosphate compounds, such as the "insoluble polyphosphate" that is accumulated during the growth phase, is used during the succeeding division.

In keeping with this hypothesis, inhibition of phosphate accumulation during the growth stages blocks later division far more effectively than does inhibition after accumulation is complete (but still some hours before division).

Effects of Phosphate Analogs. Among 6 phosphorus compounds tested for their effects on respiration and cell multiplication, thiophosphate (a known uncoupler of oxidative phosphorylation) was the only one that caused an increase in oxygen consumption while inhibiting cell multiplication. In all other cases, decreases in respiration were accompanied by decreases in cell multiplication. Diphosphite and hypophosphate support slight growth and hence are probably converted to phosphate for utilization. Thiophosphate, which does not support growth, presumably stimulates respiration by its uncoupling action.

Among various uncouplers of oxidative phosphorylation, thiophosphate and dinitrophenol (DNP) appear to be about equally efficient in stimulating respiration. Azide produces stimulation at concentrations some ten times lower. The concentration of arsenate required for maximum stimulation is similar to those of DNP and thiophosphate, but the extent of stimulation is considerably less. The cause of these differences is unknown.

With DNP, azide, and arsenate, very little stimulation of respiration occurs unless phosphate is also present. With thiophosphate, marked stimulation occurs in the absence of phosphate, and the stimulation is actually reduced in the presence of phosphate. It is tentatively suggested that this difference results from the great structural similarity between thiophosphate and phosphate.

When the intracellular phosphorus level falls below about 0.7 $\mu g/ml^3$ Chlorella, thiophosphate inhibits, rather than stimulates, respiration.

Thiophosphate exerts its greatest stimulatory action at about pH 6.0, near the pK_2 of 5.8. At this pH, slightly more than half (~60%) of the thiophosphate present should be in the form of the ionic species $H_2PO_3S^-$, and slightly less than half (~40%) in the form of $HPO_3S^=$. The presence of the maximum effect near a pK_2, where no single species is predominant, suggests that pH affects both the ionization state of thiophosphate and the "sensitive sites" of the cell.

The extent of reversal of thiophosphate stimulation by phosphate is relatively constant from pH 4.5 to pH 6.0, then decreases rapidly as the pH is raised from 6.0 to 6.5. From the dissociation constants for phosphate, it may be calculated that, over the pH range where phosphate is most effective, 93-99% of the phosphate present is in the form of $H_2PO_4^-$. The sharp decrease in the ability of phosphate to reverse thiophosphate inhibition occurs in the pH range in which the proportion of $H_2PO_4^-$ ions decreases rapidly with increasing pH.

The curves of respiration vs. pH for phosphate and thiophosphate are very similar, the major difference being that the curve for thiophosphate is shifted toward the lower end of the pH scale. This shift is in keeping with the lower pK_2 (5.8) of thiophosphate as compared with that of phosphate (7.1).

Phosphate uptake by Chlorella is much greater in the light than in the dark. Thiophosphate inhibits phosphate uptake in both the light and the dark, but the inhibition is stronger in the light. Other uncoupling agents decreased phosphate uptake in the light; they were not tested in the dark.

With the highest concentration of thiophosphate tested, multiplication was reduced from the usual ~4-fold to ~2-fold. Twofold multiplication was also noted as a result of phosphate deficiency. It was found to be accompanied by division of each mother cell into two daughters, instead of the usual four.

Effects of the ATP-P_i exchange in mitochondria from rat liver. In isolated mitochondria, thiophosphate did not replace phosphate in the formation of ATP, nor was there evidence for formation of any other complex derivative of thiophosphate in this system, though the electrochromatographic analytical technique which was employed would be expected to detect any such derivative.

It is suggested that most of the effects of thiophosphate on the phosphate metabolism of Chlorella can be explained in terms of the known ability of thiophosphate to uncouple phosphorylation from oxidative metabolism, and an (assumed) similar uncoupling effect on photosynthetic phosphorylation.

Intracellular accumulation of thiophosphate and the competitive effects of phosphate and thiophosphate on intact cells cannot readily be explained on this basis. These effects may indicate an additional competitive interaction of phosphate and thiophosphate for penetration into the cell.

References

1. Juni, E., M. D. Kamen, S. Spiegelman, and J. M. Wiame. Physiological heterogeneity of metaphosphate in yeast. Nature 160, 717-718 (1947).

2. Schmidt, R. R. and K. W. King. Synchronous growth of Chlorella pyrenoidosa. Exptl.Cell Research 23, 209-217 (1961).

3. Wiame, J. M. The occurrence and physiological behavior of two metaphosphate fractions in yeast. J. Biol. Chem. 178, 919-929 (1949).

ALKALINE HYDROLYSIS OF S-ADENOSYLMETHIONINE IN TRITIATED WATER

F. Schlenk and Julia L. Dainko

Alkaline hydrolysis of S-adenosylmethionine under mild conditions yields adenine and a pentose-containing sulfonium compound which tentatively has been termed S-ribosylmethionine.[1] It was demonstrated that the unusual lability of the glycosidic bond is caused by the presence of the sulfonium group in the molecule, but details of the mechanism of hydrolysis remained obscure.

In a recent note, Frank et al.[2] have suggested an ethylenic intermediate with the double bond at carbon atoms 4 and 5 of the ribose. After loss of the adenine, furanoid ring closure at carbon 4 can occur in either direction, yielding derivatives of D-ribose and L-lyxose:

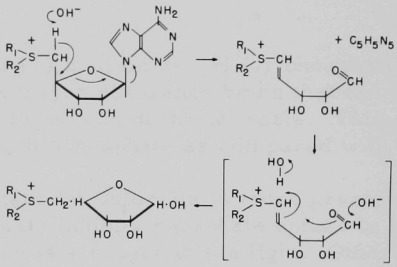

Experiments with nonbiological model compounds support this reaction sequence. Extensive racemization at carbon atom 4 in the carbohydrate part was ascertained by degradation and polarimetry.[2]

It appeared desirable to test the proposed mechanism using the biological methyl donor S-adenosylmethionine. In particular, the transitory formation of an ethylenic intermediate appeared amenable to verification by carrying out the alkaline hydrolysis in tritiated water. The isotope should be incorporated at carbon atom 5, whether the intermediate forms a D-ribose or L-lyxose sulfonium compound.

S-Adenosylmethionine, prepared from yeast as the sulfate,[3] was dissolved in tritiated water, neutralized, and adjusted with $Ba(OH)_2$ solution to 0.1 N. All operations were carried out at ice-bath temperature. The concentration of the sulfonium compound was 36.5 μM/ml, the radioactivity of the tritiated water was 2.93×10^9 cpm/ml. After 4 hours the

solution was neutralized with 1 N H_2SO_4 and the precipitate of $BaSO_4$ removed. Samples of the solution (0.1 to 0.3 μM) were analyzed by paper chromatography.[1] Scanning of the papers for radioactive spots showed considerable activity in the orcinol- and ninhydrin-positive material ("S-ribosylmethionine") formed by splitting of the glycosidic bond of S-adenosylmethionine. The radioactivity persisted after repeated chromatography. No activity was found in the adenine, nor in the methionine obtained by further alkaline hydrolysis at 100°C for 5 min. It is obvious, therefore, that the activity is located in the pentose. To eliminate the possibility of a nonspecific tritiation of the carbohydrate part, adenosine, 5'-methylthioadenosine, ribose, and lyxose were exposed under identical conditions to tritiated water and 0.1 N $Ba(OH)_2$. No radioactivity was found in these compounds after chromatographing spots containing 0.3 μM and scanning the papers.

For quantitative measurement of the radioactivity in the pentose sulfonium compound, 2.0 ml of the hydrolyzate were analyzed by chromatography with Dowex 50 (H^+) resin, 100 to 200 mesh, in a column 8.5 x 0.5 cm, using 1.0 N HCl for elution (Expt. A). In a second experiment (B) the material was first purified by large-scale paper chromatography of 1.0 ml of hydrolyzate and elution of the bands containing the sulfonium compound; the combined eluates were applied to the column. On elution with 1.0 N HCl, the pentose sulfonium compound appeared ahead of adenine. Orcinol tests[4] were carried out to determine its concentration, and liquid scintillation counting was used for assay of the radioactivity. Table 48 shows the data obtained with the appropriate 50-ml fractions of the eluate.

TABLE 48

Radioactivity in eluate fractions of S-pentosylmethionine

Experiment and fraction	Pentose, μM/ml	Radioactivity, cpm/ml	Specific activity, cpm/μM
A 6	0.183	5476	29,900
7	0.276	7760	28,100
8	0.141	4440	31,500
B 7	0.043	1156	26,900
8	0.11	3005	27,400
9	0.131	3474	26,600

In the orcinol tests the time of heating was extended to 40 min, and the acidity of the reference standards was adjusted to match that of the acid eluates. Lyxose and ribose gave virtually identical results. In the

determination of the radioactivity, the inhibition caused by the acidity of the eluates was less than 10%; a correction was made by using acidified reference standards. As expected, the specific activity of the compound was about 50% of that of the water in the incubation mixture (53,000 cpm/μM); only one hydrogen or tritium atom is bound per molecule of pentose.

The present data on the alkaline hydrolysis of S-adenosylmethionine are in agreement with the mechanism suggested by Frank et al.[2] Transitory desaturation of the ribose and rehydration after, or concomitant with, the splitting of the glycosidic bond is indicated by the uptake of tritium into the carbohydrate part. Because of the racemization resulting from this process the product should be termed S-pentosylmethionine rather than S-ribosylmethionine.

References

1. Parks, L. W., and F. Schlenk. The stability and hydrolysis of S-adenosylmethionine; isolation of S-ribosylmethionine. J. Biol. Chem. 230, 295-305 (1958).

2. Frank, W., J. Wieczorkowski, N. A. Hughes, and J. Baddiley. Alkali hydrolysis of sulphonium nucleosides. Proc. Chem. Soc. (London) 1961, 449.

3. Schlenk, F., J. L. Dainko, and S. M. Stanford. Improved procedure for the isolation of S-adenosylmethionine and S-adenosylethionine. Arch. Biochem. Biophys. 83, 28-34 (1959).

4. Mejbaum, W. Ueber die Bestimmung kleiner Pentosemengen, insbesondere in Derivaten der Adenylsaeure. Z. physiol. Chem. 258, 117-120 (1939).

USE OF MIXTURES OF DPND ISOMERS IN ESTABLISHING REACTION MECHANISMS OF DEHYDROGENASES

John F. Thomson and Jacqueline J. Darling

Baker and Mahler[1] have recently reviewed the methods available for characterization of mechanisms for two-substrate (or coenzyme-substrate) systems that obey the rate equation:

$$\frac{E_0}{v_0} = \phi_0 + \frac{\phi_1}{C} + \frac{\phi_2}{S} + \frac{\phi_{12}}{SC} \qquad (1)$$

where E_0 is the concentration of the enzyme, v_0 the initial reaction velocity, C and S the concentrations of coenzyme and substrate, respectively, and the ϕ's are constants, the significance of which depends on the mechanism involved.

In practice, these constants can be evaluated by measuring the initial rate for a number of coenzyme concentrations at a series of different substrate concentrations. A plot of $1/v$ against $1/C$ will then yield a series of straight lines with intercepts of $(\phi_0 + \phi_2/S)/E_0$ and slopes of $(\phi_1 + \phi_{12}/S)/E_0$. Secondary plots of these intercepts and slopes against $1/S$ will yield lines, from the slopes and intercepts of which the individual constants can be obtained directly, provided the molar concentration of the enzyme is known.

Most of the tests for mechanisms depend on measuring each of the constants (in some cases for both the forward and back reactions) under a variety of conditions; and Baker and Mahler point out that because of the large errors involved in these measurements, some of the criteria have only limited value.

This report is concerned with another procedure that can be used to help discriminate between mechanisms of reactions involving DPNH by the use of the stereoisomeric mixture of DPND prepared by nonenzymatic reduction of DPN in D_2O (designated hereafter as α, β-DPND).

In the "rapid equilibrium" mechanism, it is assumed that equilibrium is rapidly established among the enzyme, substrate, and coenzyme, so that the rate equation (Equation 1) can be written:

$$\frac{1}{v_0} = \frac{1}{V}\left[1 + \frac{K_4}{C} + \frac{K_3}{S} + \frac{K_1K_3}{CS}\right] \qquad (2)$$

where V is the maximum velocity, and the K's are dissociation constants:

$$K_1 = \frac{(E)(C)}{(EC)}, \quad K_2 = \frac{(E)(S)}{(ES)}, \quad K_3 = \frac{(EC)(S)}{(ESC)}, \quad K_4 = \frac{(ES)(C)}{(ESC)}.$$

It may be noted that $K_1K_3 = K_2K_4$.

When a mixture of coenzymes (C_α and C_β) is used, under conditions where $C_\alpha = C_\beta = 0.5\ C_t$, the total concentration, additional equilibria must be considered, and the over-all reaction velocity then becomes:

$$\frac{1}{v} = \frac{K_{4\alpha} + K_{4\beta}}{V_\alpha K_{4\beta} + V_\beta K_{4\alpha}} \left[1 + \frac{2K_{4\alpha}K_{4\beta}}{K_{4\alpha}+K_{4\beta}} \cdot \frac{1}{C_t} + \frac{K_{3\alpha}K_{4\beta} + K_{3\beta}K_{4\alpha}}{K_{4\alpha} + K_{4\beta}} \cdot \frac{1}{S} + \frac{2K_2K_{4\alpha}K_{4\beta}}{K_{4\alpha}+K_{4\beta}} \cdot \frac{1}{SC_t} \right] \quad (3)$$

By comparison with Equation 2, it can be seen that the apparent values of the constants calculated by the method described above are as follows:

$$V_{M_{app}} = \frac{V_\beta K_{4\alpha} + V_\alpha K_{4\beta}}{K_{4\alpha} + K_{4\beta}}$$

$$K_{1_{app}} = \frac{2K_{1\alpha}K_{1\beta}}{K_{1\alpha} + K_{1\beta}}$$

$$K_{2_{app}} = K_2$$

$$K_{3_{app}} = \frac{K_{3\alpha}K_{4\beta} + K_{3\beta}K_{4\alpha}}{K_{4\alpha} + K_{4\beta}}$$

$$K_{4_{app}} = \frac{2K_{4\alpha}K_{4\beta}}{K_{4\alpha} + K_{4\beta}}$$

The other basic type is a steady-state mechanism, with ordered binding of coenzyme and substrate:

$$E + C \underset{k_2}{\overset{k_1}{\rightleftharpoons}} EC$$

$$EC + S \underset{k_4}{\overset{k_3}{\rightleftharpoons}} ESC \underset{k_6}{\overset{k_5}{\rightleftharpoons}} EC_0S_r \underset{k_8}{\overset{k_7}{\rightleftharpoons}} EC_0 + S_r$$

$$EC_0 \underset{k_{10}}{\overset{k_9}{\rightleftharpoons}} E + C_0$$

where C_0 is the oxidized coenzyme and S_r is the reduced substrate.

When the α, β-DPND mixture is employed, and $C_\alpha = C_\beta = 0.5\ C_t$, the following expression is obtained:

$$\frac{E_t}{v} = \frac{(\phi_{12} + \phi_1 S)(\psi_{12} + \psi_1 S)}{S[\phi_{12} + \psi_{12} + (\phi_1 + \psi_1)S]} \left[\frac{2}{C_t} + \frac{\phi_2 + \phi_0 S}{\phi_{12} + \phi_1 S} + \frac{\psi_2 + \psi_0 S}{\psi_{12} + \psi_1 S} \right] \qquad (4)$$

The ϕ constants represent various combinations of kinetic constants for one species of coenzyme:

$$\phi_0 = \frac{k_5k_7 + k_5k_9 + k_5k_9 + k_7k_9}{k_5k_7k_9}$$

$$\phi_1 = \frac{1}{k_1}$$

$$\phi_2 = \frac{k_4k_6 + k_4k_7 + k_5k_7}{k_3k_5k_7}$$

$$\phi_{12} = \frac{k_2}{k_1} \cdot \phi_2$$

whereas the ψ constants are the corresponding combinations of constants for the other stereoisomer.

This equation is linear with respect to C, but not with respect to S. Hence the initial plot of $1/v$ against $1/C$ would yield straight lines, but the secondary plots would not give linear relationships.

Equation 4 is also given by mechanisms involving none, one, or three ternary complexes, so that the use of the isotopic mixtures will not differentiate among these variations of the steady-state mechanism.

Applications of this test are shown in Figures 69 and 70, which are secondary plots of data obtained with yeast alcohol dehydrogenase and rabbit muscle lactic dehydrogenase. These data confirm the observation that the former obeys an equilibrium mechanism[2] and the latter a steady-state mechanism.[3]

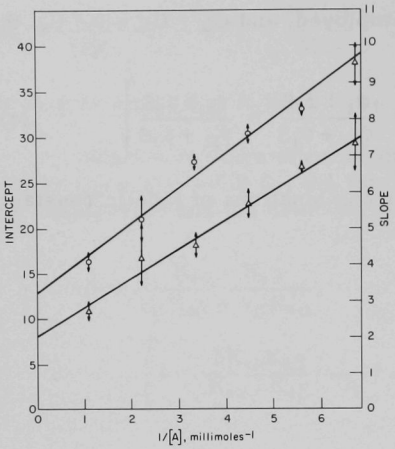

Figure 69. Kinetic data for alcohol dehydrogenase. Circles, intercepts from 1/v vs. 1/DPND plots (left-hand ordinate); triangles, slopes from 1/v vs. 1/DPND plots (right-hand ordinate). Both plotted against reciprocal of acetaldehyde concentration. Vertical arrows indicate standard errors.

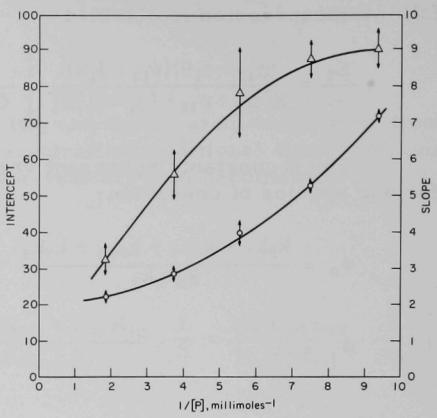

Figure 70. Kinetic data for lactic dehydrogenase. Symbols same as in Figure 69. Slopes and intercepts plotted against reciprocal of pyruvate concentration.

References

1. Baker, R. H., Jr., and H. R. Mahler. Studies on the mechanism of enzyme-catalyzed oxidation reduction reactions. II. Methods for characterization of the mechanism for two-substrate systems. Biochemistry 1, 35-40 (1962).

2. Shiner, V. R., Jr., H. R. Mahler, R. H. Baker, Jr., and R. R. Hiatt. Secondary deuterium isotope effects in chemical and biochemical reactions. Ann. N. Y. Acad. Sci. 84, 583-595 (1960).

3. Takenaka, Y. and G. W. Schwert. Lactic dehydrogenase. III. Mechanism of the reaction. J. Biol. Chem. 223, 157-170 (1956).

ELECTRON MICROSCOPY OF CENTRIFUGED *AMOEBA PROTEUS*

Edward W. Daniels

The subcellular components within living interphase amoebae were stratified by centrifugation (5000 *g* to 10,000 *g*/10 min) and fixed immediately thereafter in OsO_4, dehydrated in graded alcohols, embedded in Epon resin, sectioned, and examined with an RCA electron microscope.

For convenience in presentation, the strata are classified into 4 major zones, A through D, the A zone being at the centripetal pole and containing the least dense of the components. These are the lipid globules, contractile vacuoles and the large irregular vacuoles averaging several microns in diameter. Stratifying below (centrifugally) these in the A zone are smaller vesicles, about 0.5-2 μ in diameter, and relatively clear cytoplasm.

The B zone contains most of the cytoplasm which is essentially clear of vesicles. However, many of the smaller (ca. 0.5 μ to 1.0 μ) vesicles are also present in this zone, suspended by the cytoplasm. The upper (centripetal) portion of this zone contains some larger vesicles (1-5 μ), whereas the lower portion of the B zone, at the border of the C zone, contains Golgi bodies in high concentration.

The C zone, by definition, contains the nucleus and all other components found within its stratum. The nucleus in *Amoeba proteus* is large, approximately 40-45 μ in diameter, but no intranuclear stratification was observed. The upper and middle portions of the C zone contain an abundance of Golgi bodies with a few mitochondria intermingled. The mitochondria are densely packed below the nucleus at the lower border of the C zone. The nucleus is frequently found lying between the mitochondrial and Golgi strata, essentially on top of the densely packed mitochondria with many Golgi bodies covering and surrounding the nucleus.

The upper third of the D zone contains a high concentration of mitochondria. Food vacuoles are found throughout the entire zone, but particularly in the central area, and crystals in vacuoles are found at the extreme lower portion at the centrifugal pole of the cell. After centrifugation at 10,000 *g*, electron-dense 40 mμ-particles that resemble ribosomes are concentrated in the lower portion of the D zone.

DEVELOPMENT AS THE MEANS OF MULTIPLICATION OF ORGANELLES AND ORGANELLE SYSTEMS IN PARAMECIUM*

Charles F. Ehret and Gérard de Haller

The cell surface of Paramecium not only contains, but is composed of, thousands of ciliated and nonciliated organelles.[2] These are so regularly arranged in organelle complexes and systems that structural diagrams and formulations can be written for the entire cell surface in terms of unit organelles.[3] From one cell division to the next, thousands of new cilia and trichocysts arise in the new cell surfaces, but little is known about their mechanism of multiplication. The prevailing hypothesis (from studies on other ciliates) has been that these arise by division of the ciliary basal body.[4] Some evidence from light microscopy[2] suggests that this is not the case, and we have brought forward the alternative hypothesis that as organelles they arise de novo: that is, through synthesis and development from suborganellar level pools, with specificity determined at the molecular level by interactions of gene products and the microenvironment of the cell.[3]

Our general aim was to introduce strict spatial control into a study of the ultrastructural changes associated with the multiplication of organelles and organelle systems at precisely selected phases of the division cycle.[5] More specifically, we have asked what evidence can the electron microscope bring to bear on the mechanisms whereby new cilia, new trichocysts and new systems of organelles such as the gullet are produced in the cell surface.

In our studies of about 100 single cells, most of which were fixed in the 45-min period preceding fission and at the height of production of thousands of new organelles, we could see no evidence of organelle division, although we observed well over 10^5 presumably (according to the old hypothesis) fissionable organelles. On the other hand we clearly established an orderly developmental sequence for each of these cell structures: 1) the new gullet with its 1,000 cilia in 3 ribbons, 2) the new trichocysts, and 3) the new body ciliature.

Figure 71 shows the new gullet anlage developing on the pellicle wall at the right side of the old gullet at an early stage in its invagination; invagination begins at the anterior end and proceeds posteriorly.

---

*Work done at the Institut de Biophysique and the Laboratoire de Protozoologie, University of Geneva on a USPHS Special fellowship. The authors express their gratitude to Professor Edouard Kellenberger for his hospitality. An abstract of some of the work has appeared elsewhere.[1]

Figure 71. Development of the new gullet on the right wall of the vestibular region of the pellicle.

Figure 72 represents the succession of changes in the development of mature trichocysts from pretrichocysts during the 40-minute interval just preceding cell division. The pretrichocysts are distributed through the cytoplasm, and are characterized by a centrally located crystalloid with 70-A spacings.

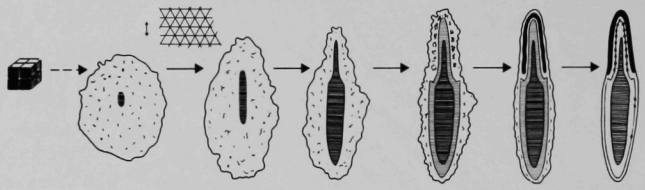

Figure 72. Development of the trichocyst from the pretrichocyst. From left to right: 1) unknown pro- or pre-trichocyst; 2) pretrichocyst is sub-spherical with crystalloid center having 70-A spacings; 3) elongation of fine-tubuled matrix and crystalloid; 4) crystalloid acquires shape of central core of mature trichocyst; 5) outer portions of tip and body crystallize around central core, cap develops on tip, fine-tubuled matrix diminishes; 6) traces of fine-tubuled matrix present only at body periphery; 7) dense granules having 220-A spacings appear packed about the tip and dispersed about the body.

Figure 73 represents the succession of changes in mitochondrion-like bodies, the vacuolated mitochondria, at and near the cell surface just before cell division. The vacuolated mitochondria are characterized by cytoplasmic invaginations and/or vacuoles containing RNP granules and small vesicles, and swollen, distended tubules. The new cilia and ciliary corpuscles develop in intimate association with these bodies, and

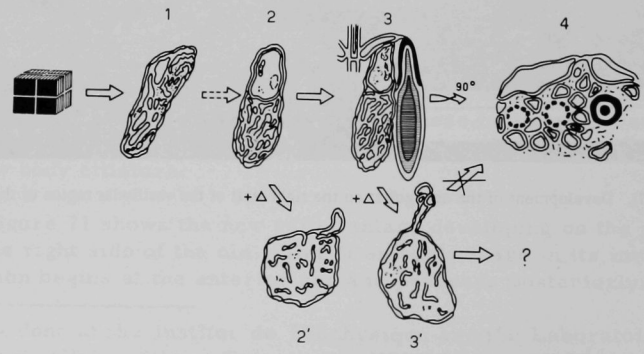

Figure 73. Development of the ciliary corpuscle of the cell surface from the vacuolated mitochondrion-cytoplasm complex. The effect of thermal blockade upon these pre-organelles is represented in the lower half of the figure.

apparently out of them. When the prefission cell is heated (4 min, 40.5°C), then cell division is entirely prevented for many hours, despite the presence of thousands of pre-organelles in the cytoplasm at the time of heating. The fate of these bodies is represented in the lower half of Figure 73: in this case, following heat treatment the cells were returned to 25°C for half an hour, then fixed. A primary effect of heat blockade is, thus, alteration of normal pre-organelles into the incompetent anomalous bodies shown in the figure.

Our complete report will include an analysis of cytoplasmic diversity and stage-correlated changes in the macronuclear nucleoli.

The most significant aspect of this work is not merely the proof of the developmental origin of at least some, and probably all, of the cytoplasmic organelles, but the implication of the possibility of experimental control over the processes governing structural differentiation and the synthesis of structural proteins. By illustration, we have represented the black-box precursor of the pretrichocyst as itself composed of black boxes. We must now learn whether these represent uniform heterotypic sets of determinants, of say messenger RNA's on ribosomes, that under one group of physical conditions become trichocysts and under another group of conditions become cilia. Or are pre-organelles determined from the start by the particular assortment of heterotypes in the large box? Are the large boxes constructed by fortuitous collisions, or do quasi-templates, maps and blueprints exist for them? How much of the genomic message-potential of the cell is impressed upon a given one of its organelles? With our present system, each of these questions is not only theoretically valid, but experimentally approachable.

References

1. Ehret, C. F. and G. de Haller. Formation des organelles et des systèmes d'organelles cytoplasmiques en cours de la division chez Paramecium. Proc. First Intern. Conf. Protozoologists (1961) pp. 125-126.

2. Ehret, C. F. and E. L. Powers. The cell surface of Paramecium. Intern. Rev. Cytol. 8, 97-133 (1959).

3. Ehret, C. F. Organelle systems and biological organization. Science 132, 115-123 (1960).

4. Lwoff, A. Problems of morphogenesis in ciliates. Wiley, New York, 1950.

5. de Haller, G., C. F. Ehret and R. Naef. Technique d'inclusion et d'ultramicrotomie, destinée à l'étude du développment des organelles dans une cellule isolée. Experientia 17, 524-526 (1961).

AN ELECTRON MICROSCOPE STUDY OF THE SPORE OF THE MICROSPORIDIAN THELOHANIA CALIFORNICA

R. R. Kudo* and Edward W. Daniels

This report presents electron microscope observations of the spores of a microsporidian protozoan, Thelohania californica, parasitic in the larvae of Culex tarsalis mosquitoes. Typical spores are pyriform in shape and about 5 μ to 10 μ long. When the spores are subjected to mechanical pressure, the polar filament, a long, tubular, thread-like structure, is extended; it is approximately 10 times as long as the spore case. In other microsporidian spores the sporoplasm is known to be ejected through the polar filament. In nature, this is presumably the manner in which the sporoplasm is injected into the host tissue with resultant infection.

Since Thelohan[1] first published his observations in 1894 on the structure of the microsporidian spore, diverse views have been held about its internal morphology. As seen in life, microsporidian spores are extremely refractile bodies and reveal no internal structure except a clear space or "vacuole" which may be present near one or both ends of a spore. Fixed and stained, the spores show structures variously interpreted as sporoplasm, nuclei, polar filament, and polar capsule. Conflicting observations and interpretations have been reported not only for different species but even for a single species.[2-5] Recent electron microscope studies have revealed the finer detail of the content of the spore.

Materials and Methods

The microsporidian studied, Thelohania californica Kellen and Lipa,[6]** was subjected to a thorough light and phase microscopic study prior to our electron microscopic investigation. For permanent light-microscope preparations, smears or sections were fixed in Schaudinn or Carnoy fluid and stained with Giemsa or subjected to Feulgen's nuclear reaction. For electron microscopy the spores were fixed in buffered (pH 7.4) 1% osmium tetroxide for 1 to 2 hr, dehydrated in a graded ethanol series, and embedded in methacrylate. Sections were cut with a Porter-Blum microtome at 25 to 100 mμ and examined with an RCA EMU-3E electron microscope. Some other details of the procedure have been published.[7]

---

*Department of Zoology, Southern Illinois University, Carbondale, Illinois. This investigation was supported in part by a grant (E-3741) from the National Institutes of Health, United States Public Health Service.

**We are indebted to Dr. William R. Kellen, California State Department of Public Health, Fresno, California, for placing the material at our disposal.

Light Microscope Observations

The spore is broadly pyriform with a narrowed anterior end from which the filament is extruded. At the opposite end is a large conspicuous "vacuole" and, except in this area, the spore is highly refractile. Mechanical pressure on the spore results in extrusion of the polar filament and loss of refractility; hence, this property appears to result from the presence of the coiled filament.

The spore membrane is uniform in thickness and in close contact with the spore contents. Under the phase microscope, the coiled filament is visible in part within spores under slight pressure. Within the open posterior coils of the filament, a rounded mass is often seen projecting into the vacuole. When the pressure on the spore is increased, the polar filament is extruded. In the spores of microsporidia parasitic in nonaquatic hosts, filament extrusion can be precipitated by rinsing the spores in distilled water and drying them on a glass microscope slide;[8,9] this is not true of T. californica.

Feulgen's nuclear reaction reveals a single nucleus in the sporoplasm, which usually lies lengthwise within the spore. The nucleus in sporoblasts and immature spores is a more or less compact spherical structure, but in mature spores it is irregularly elongated at a slight angle to the spore axis.

Electron Microscope Observations

The internal structure of the mature spore is shown in Figures 74 to 77. The outer surface of the spore is usually smooth. The complex, thick outer membrane (Figures 75 and 76, OM) is approximately 200 mμ thick and has on its external surface a thin (ca. 100 A) electron-dense border (Figures 75 and 76, EDB). Immediately surrounding the spore is a relatively thick inner surface membrane (Figures 74 and 75, ISM), which appears to be considerably thicker in the anterior half of the spore than in the posterior half (Figures 74 and 75, ISM). In nearly all spores, the outer and the inner membranes are separate to some degree, leaving a space of approximately 500 mμ (as in Figure 74, SPA), but this appears to be an expansion artifact due to fixation and methacrylate polymerization. The space is usually divided into outer and inner compartments by a diffuse line (Figure 75, DL).

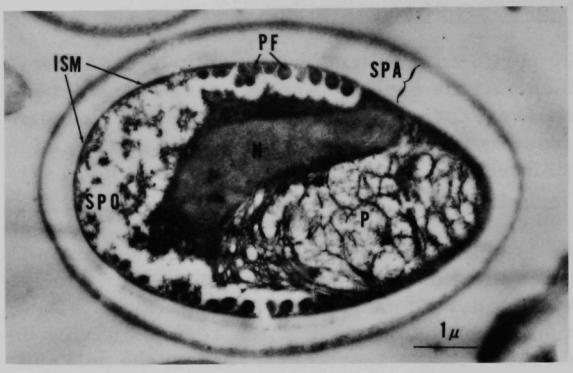

Figure 74

Electron micrograph of a longitudinal section of a spore of T. californica.

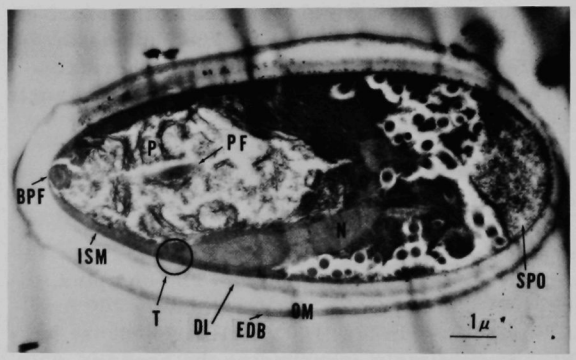

Figure 75

Electron micrograph of a longitudinal section of a spore showing the anterior portion of the polar filament passing through the polaroplast.

Figure Legend Symbols

APF = Anterior polar filament(s).

BPF = Basal portion of the polar filament. This is anterior relative to the non-extruded filament, but posterior relative to the extruded filament.

DL = Diffuse line.

EN = Endosomes.

EDB = Electron dense border.

ISM = Inner surface membrane.

N = Nucleus.

OM = Outer membrane.

P = Polaroplast.

PF = Polar filament.

PM = Polar mass and polaroplast membrane.

PPF = Posterior polar filament(s).

SPA = Space between OM and ISM.

SPO = Sporoplasm.

T = Tubules.

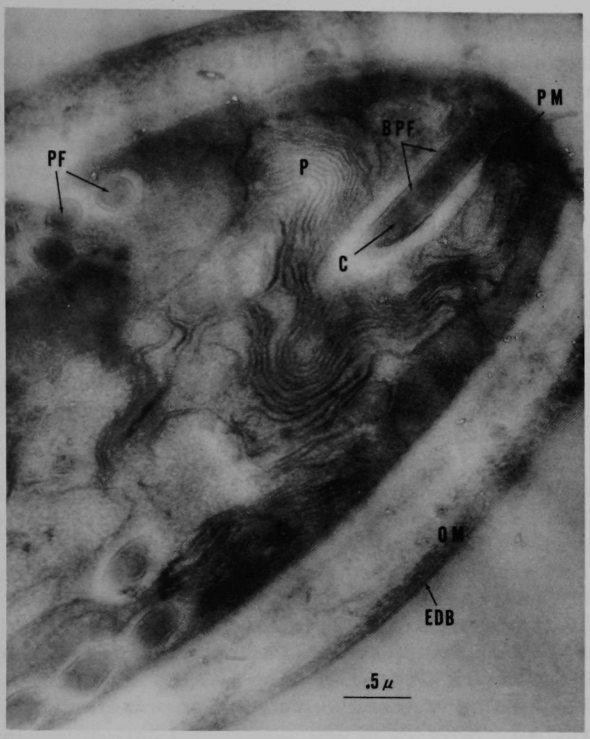

Figure 76

Electron micrograph of the anterior half of a longitudinally sectioned spore showing the attached base of the polar filament.

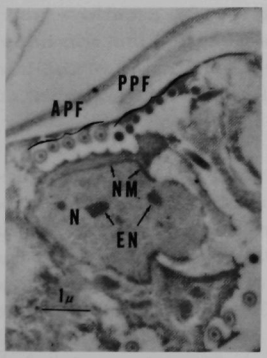

Figure 77

Micrograph of a sectioned spore showing 5 anterior polar filament coils of larger diameter and 7 of the smaller posterior coils. A nucleus, nucleoli or endosomes (EN), and the nuclear membrane (NM) are also shown.

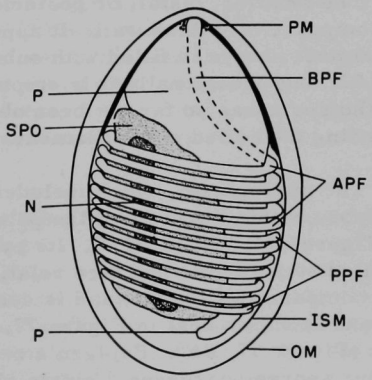

Figure 78

Schematic drawing showing the structure of the spore of T. californica as revealed by electron microscopy.

Surrounding the anterior (basal) portions of the polar filament and extending beyond the first spiral coil of the filament is a system of laminated structures within a ground substance (Figures 74-76, 78, P), which resembles the "polaroplast" observed by Huger[10] in the spore of Nosema locustae. In T. californica this often extends into the posterior region of the spore, and in some areas appears as minute (25-mμ) tubules (Figure 75 T).

The base of the polar filament (Figures 75 and 76, BPF) is closely adjacent to the anterior tip of the spore and is surrounded by an irregular mass of high electron density (Figure 76, PM) which may be similar to the structure(s) in N. locustae called by Huger[10] polar granules. The polar filament runs inward lengthwise, soon curves obliquely down to come in contact with the inner surface membrane and there begins to coil spirally toward the posterior region of the spore (Figures 74-76, PF). Spirals most commonly consist of 12-14 coils and the axis is frequently at an angle with the longitudinal axis of the spore.

In almost all cases, the polar filament is distinctly and uniformly larger in diameter (200 mμ) in the first five coils than in the remainder of the coils (150 mμ) (Figures 74-78, PF, PPF and APF). In the anterior coils the filament wall appears to be made up of 2 to 3 layers of electron-dense material and is 40 to 50 mμ thick (Figures 74 and 76, PF). The filament is tubular in structure; in the five anterior coils the space within the lumen often contains a cylindrical body of high electron density which is about 65 mμ in diameter (Figure 77). In other spores the anterior portion of the filament is filled with a uniformly electron-dense material (Figures 74-76).

The smaller, distal, or posterior portion of the filament (7 to 9 coils) has a comparatively thick wall. It appears also to be a hollow tube; the lumen almost always is filled with substances of high electron density (as in Figure 77), but occasionally it is empty. The termination of the filament within the spore has so far not been observed. There is no polar capsule surrounding the coiled polar filament.

The sporoplasm, which includes the nucleus, is located posteriorly in the spore within the coils of the polar filament and close to the polaroplast (Figures 74, 75, 78, SPO). Its cytoplasm contains both granulated and reticulated structures which are relatively electron-dense. The nucleus is single, comparatively large, and is seen in various shapes. The nuclear membrane is shown best in Figure 77, NM. The endosomes are shown in the nucleus (Figure 77, EN). Feulgen's reaction confirms that the sporoplasm of mature spores possesses a single elongate nucleus lying obliquely in the area of the coiled filament.

Discussion

The great majority of the microsporidian spores fall into one of the two following structural plans[3] on the basis of observations on permanent light microscope preparations. Type 1 consists of pyriform spores in which the anterior two-thirds is occupied by a coiled polar filament, which may or may not be encased in a polar capsule, and in which the sporoplasm is located in the posterior and middle parts of the spore. Plistophora macrospora[5] is an example. Type 2 includes ovoidal or ellipsoidal spores; the sporoplasm, in a girdle-like ring, is located near the middle and surrounds the coiled polar filament which may or may not be enclosed in a polar capsule. An example is Thelohania giardi[11]. Examination of the literature suggests that microsporidian spore structure differs much among the different species.

Krieg,[12] apparently was the first to employ electron microscopy for a study of microsporidian spores. He reported the external surface of the spore membrane of Plistophora melolonthae to be corrugated, and the polar filament to be a solid cord. He suggested, without electron-microscopic evidence, that the filament is coiled spirally in the polar capsule. Weiser[13] reported that the surface of the spore of Nosema laphygmae was generally warty, although sometimes smooth. He considered the degree of shrinkage to be influenced by the fixation and drying of the spore, and we agree with this view. Weiser reported that the sporoplasm lies directly under the spore membrane and in the anterior-median portion of the spore, an ill-defined vacuole in which the solid polar filament (0.06-0.12 μ in diameter) is "coiled irregularly and in unspiral windings."

Observations of Huger,[10] Lom and Vavra,[14] and Ludvik[15] are in agreement with what we have seen in the spore of T. californica. The inner and outer portions of the spore membrane and the smooth outer surface are similar. Huger's[10] "outer spore coat" appears to be equivalent to our "thick outer membrane," his "inner spore coat" to our "space" which is approximately 500 mμ, and his "surrounding membrane" like our "inner surface membrane."

We have observed in T. californica a structure which appears similar to the polarplast described by Huger.[10] The fibrous elements of the polaroplast are distinctly laminated (Figure 76, P) and often reticulated (Figures 74 and 75, P). As to its function, Huger suggested that perhaps it serves "as swelling substance for increasing the turgor within the spore, thus causing extrusion of polar filament and sporoplasm." The polaroplast of T. californica extends toward the middle of the spore and, in some cases, possibly into the posterior part. The thick anterior half of the inner surface membrane may further assist in extrusion of the polar filament and the sporoplasm.

Huger[10] noted that the spirally coiled polar filament is embedded in the peripheral region of the sporoplasm. The filament is circular in cross section and its diameter successively decreases from 230 mμ at the bast to 70 mμ at the tip. He considers the polar filament of the spore of Nosema locustae to be not a hollow tube but a solid organelle. However, the polar filament of T. californica appears to be tubular although the nature of the contents within the tube is not known.

Morgenthaler[8] first suggested that the polar filament of microsporidian spores was tubular after a fluid mass was seen to emerge from the tip of the extruded polar filament of Nosema apis. More recent reports, culminating in Lom and Vavra's[14] demonstration of the process of filament extrusion and emergence of the sporoplasm in the spore of Plistophora hyphessobryoconis, leave no doubt as to the tubular nature of the polar filament. When the filament appears solid in electron micrographs, it is because the lumen of the coiled filament is completely or partially occupied by certain materials.

The partial double coiling observed by Huger[10] in Nosema locustae occurs occasionally in one to a few coils in the distal portion of the filament in T. californica (Figures 74 and 76, PF). In this connection, it is interesting to note that Kudo[16] predicted such double coiling in Nosema apis, on the basis of dark-field observations of extruded filaments containing undulations of two different wave lengths. This prediction has since been confirmed in an electron microscope study of this microsporidian non-extruded polar filaments in sectioned spores.[15]

Feulgen's nuclear reaction reveals that the microsporidian sporoplasm possesses one or two nuclei;[4,17] the multinucleation reported by Mercier[11] and others, apparently does not occur. Seemingly, a uni- or bi-nucleated sporoblast develops without any nuclear division into a mature spore, unlike the process known to take place in the sporoblast and young spore of myxosporidia.

Aside from the so-called polar capsule, the spores of Plistophora macrospora[5] and Stempellia magna[2] are structurally similar to that of Thelohania californica as seen in electron micrographs. Our present concept of the spore of T. californica is presented in Figure 78.

References

1. Thelohan, P. Sur la présence d'une capsule à filament dans les spores des microsporidies. Compt. rend. 118, 1425-1427 (1894).

2. Kudo, R. R. On the structure of some microsporidian spores. J. Parasitol. 6, 178-182 (1920).

3. Kudo, R. R. A biologic and taxonomic study of the Microsporidia. Illinois Biol. Monogr. 9, 83-344 (1924).

4. Kudo, R. R. Morphology and development of Nosema notabilis Kudo parasitic in Sphaerospora polymorpha Davis, a parasite of Opsanus tau and O. beta. Illinois Biol. Monogr. 20, 1-83 (1944).

5. Leger, L. and Hesse, E. Sur la structure de la spore des microsporidies. Compt. rend. Soc. Biol. 79, 1049-1053 (1916).

6. Kellen, W. R. and Lipa, J. J. Thelohania californica n. sp., a microsporidian parasite of Culex tarsalis Coquillett. J. Insect Pathol. 2, 1-12 (1960).

7. Roth, L. E. and E. W. Daniels. Electron microscopic studies of mitosis in amoeba. II. The giant amoeba, Pelomyxa carolinensis. J. Cell Biol. 12, 57-78 (1962).

8. Morganthaler, O. Der Polfaden von Nosema apis Zander. Arch. Bienenkunde 4, 53-60 (1922).

9. Kramer, J. P. Observations on the emergence of the microsporidian sporoplasm. J. Insect Pathol. 2, 433-439 (1960).

10. Huger, A. Electron microscope study on the cytology of a microsporidian spore by means of ultrathin sectioning. J. Insect Pathol. 2, 84-105 (1960).

11. Mercier, L. Contribution à l'étude de la sexualité chez les Myxosporidies et chez les Microsporidies. Mem. Class. Sci. Acad. Royal Belg. 2, (2) 50 (1909).

12. Krieg, A. Ueber Infektionskrankheiten bei Engerlingen von Melolontha spec. unter besonderer Beruecksichtung einer Microsporidien-Erkrankung. Zentralbl. Bakt., Abt. II 108, 535-538 (1955).

13. Weiser, J. Nosema laphygmae n. sp. and the internal structure of the microsporidian spore. J. Insect Pathol. 1, 52-59 (1959).

14. Lom, J. and Vavra, J. Contribution to the knowledge of microsporidian spore. I. Electron Microscopy. II. The sporoplasm extrusion. Abstracts of papers presented at the International Conference of Protozoologists, Prague (1961) pp. 259-260.

15. Ludvik, J. Neue elektronenmikroskopische Befunde an parasitischen Protozoen. Abstracts of papers presented at the International Conference of Protozoologists, Prague (1961) p. 270.

16. Kudo, R. R. Notes on Nosema apis Zander. J. Parasitol. 7, 85-90 (1921).

17. Jírovec, O. Studien ueber Mikrosporidien. Mém. Soc. Zool. Tchécoslovaque (Prague) 4, 1-75 (1936).

AN AUTORADIOGRAPHIC TECHNIQUE FOR LIGHT AND ELECTRON MICROSCOPY

O. T. Minick

When making autoradiographic studies with the electron microscope, it is often convenient to use the light microscope for orientation. Since preparation techniques for electron microscopy are quite different from those used in light microscopy it is helpful to have a method that can be used for making autoradiographs for either or both light and electron microscopy.

Method

Tetrahymena pyriformis (W strain) was grown in 50 ml of culture fluid. Three days after inoculation tritiated thymidine (H^3T), with a specific activity of 3 c/millimole, was added to the flasks. The concentration of H^3T was 8 μc/ml, making a total of 400 μc per flask. Twenty-four hours after H^3T was added, organisms were fixed for electron microscopy in 1% buffered OsO_4, pH 7.5 and were dehydrated in 50, 75, 95, and 100% ethanol, 10-min changes in each. They were then embedded in a mixture of 60% n-butyl and 40% ethyl methacrylate, using 1% Luperco CDB as catalyst, and polymerized overnight in an oven at 60°C.

Sections were cut at 2 μ thickness, placed on glass slides, covered with stripping film in the conventional manner, and exposed for 3 weeks. Sections were also cut at 0.1 μ, placed on grids, and prepared for electron microscopy as follows: A grid support made from glass was used to hold the grids for the film-coating process, as well as the photographic development procedures (Figure 79). Each grid support was coated with "subbing solution" (0.5% gelatin and 0.05% chrome alum in distilled water), after which one grid, containing sections, was placed on each grid support and allowed to dry in position for at least half an hour. A light-tight box containing about 100 ml water in a 250-ml beaker was set up in the darkroom and a small vial of nuclear track emulsion, type NTB-3, was placed in the water. The box and its contents were placed in a Technicon constant-temperature water bath at 44°C. When the emulsion became liquid, a 1:10 dilution

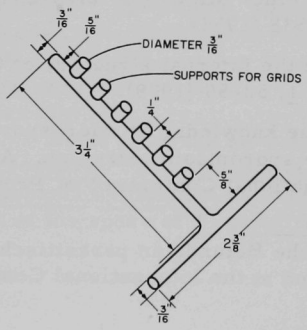

Figure 79. Grid support used for coating grids with nuclear emulsion for electron microscope autoradiography.

was made with distilled water. A platinum loop slightly larger than the grid support was coated with a very thin layer of emulsion and gently stripped down over the grid, depositing a thin layer of emulsion on the grid. The grid support with the grids in place was then put into a light-tight plastic box containing a small amount of anhydrous $CaSO_4$ desiccant (Drierite). Exposures were made for 3 weeks in a refrigerator at 4°C, at the end of which time the grid support with grids was removed, placed in Kodak D-19 developer for 5 min, fixed in Kodak acid fixer for 10 min, washed thoroughly in running tap water, rinsed in distilled water and allowed to dry. The grids were then removed from the grid support and examined in the electron microscope.

Results and Discussion

Autoradiographs prepared in this manner and examined under the light microscope offer an improvement over those obtained by conventional methods; this may be due in part to the thinner sections (Figure 80).

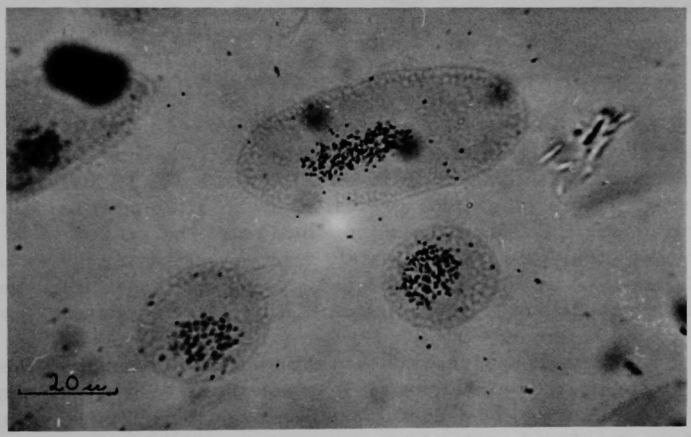

Figure 80. Incorporation of H^3-thymidine in nucleus of Tetrahymena pyriformis. Light microscope autoradiograph obtained by using electron microscope embedding method and conventional stripping film technique.

For the electron microscope good autoradiographs are obtained by this method (Figure 81); however, the technique yields a limited amount of information, because the fine detail is somewhat obscured by partially or wholly developed photographic grains.

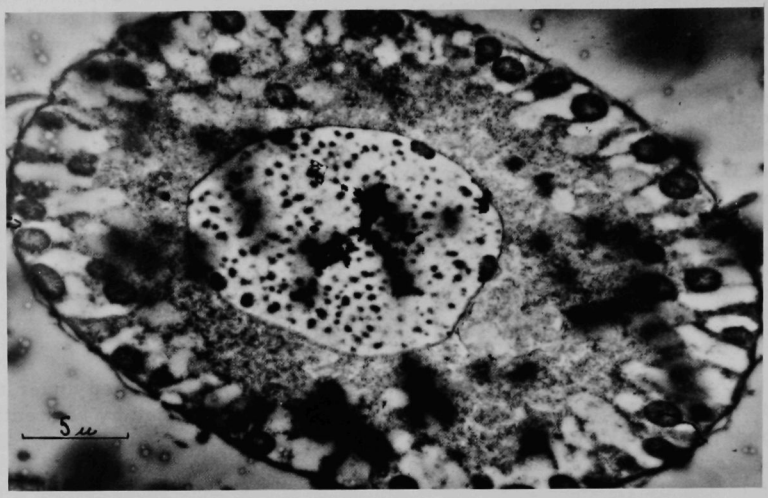

Figure 81. Incorporation of H^3-thymidine in nucleus of Tetrahymena pyriformis. Electron microscope autoradiograph using the same preparation technique as that in Figure 80.

In most cases the detail that can be observed in an autoradiograph is limited by (a) the spread of the image, because the ionizing particles are emitted in all directions, (b) the energy and range of the particles, and (c) the size of the photographic grains. Pelc,(1) after consideration of the first two factors mentioned above, concluded that the grain size of the photographic emulsions will ultimately limit the resolving power of the autoradiographs. On this basis one can only hope to make improvements in autoradiographic methods when finer grained emulsions are produced.

In electron micrographs it would be useful to have less obscuring of detail, especially if higher magnifications are to be used and smaller sites of labeling are to be traced. One approach toward eliminating the mass of the developed grains is the use of "physical" methods of development. Techniques for this are available and, in general, consist of bathing exposed photographic material in a solution that can deposit gold.(2) The gold will then become attached to the latent image centers and increase their size enough to be detectable with the electron microscope. Therefore, instead of the entire grain being developed, only the latent image centers, about 60-120 mμ in size, would be visible in the autoradiograph. If this technique can be adapted to electron microscope autoradiography, much more information should be gained. Preliminary results in developing the latent image centers look promising and will be reported in detail shortly.

I wish to thank Walter E. Kisieleski for help with the light microscope autoradiography and for encouragement in this work and Dr. Bernard R. Nebel for help in working out some of the procedures.

References

1. Pelc, S. R., J. R. Coombes and G. C. Budd. On the adaptation of autoradiographic techniques for use with the electron microscope. Exptl. Cell Research 24, 192-195 (1961).

2. James, T. H. The site of reaction in direct photographic development. II. Kinetics of development initiated by gold nuclei. J. Colloid Science 3, 447-455 (1948).

EXAMINATION OF STIMULATORY EFFECTS OF IONIZING RADIATIONS IN PLANTS

John Skok* and William Chorney

Claims for radiation-induced growth stimulation in plants have been made from almost the time of the discovery of X-rays. Since much of the reported work is conflicting and considerable disagreement has resulted, studies on the subject were initiated here.

Plants or leaf disks of sunflower, buckwheat, tobacco and bean were X-irradiated. About 1600 plants and over 400 leaf disks were employed, and over 28,000 individual measurements were made.

Small, but significant, growth increases were produced in certain instances, but such results were not always reproducible from one experiment to another. Also, when increases did occur, they were not always produced by the same dose levels. On the basis of these results i.e., the amount of variability associated with the appearance of positive stimulatory effects and the relatively small increases that are produced, it is doubtful that ionizing radiations are likely to become useful in increasing agricultural crop yields on a commercial scale, as has been the hope of some investigators. (This does not include, of course, the successful applications in genetics and plant breeding.)

The work also points out that plant tissues respond differentially to ionizing radiations, depending upon the type of growth occurring at the time. Radiation of growing buds, expanding internodes, and expanding leaf disks permitted study of the effects on dividing cells and on expanding cells. It appears that low doses of radiation delivered to dividing cells result in growth depression, but delivered to expanding cells, may result in growth stimulation.

*Present address: Northern Illinois University, De Kalb, Illinois.

AUTORADIOGRAPHIC INVESTIGATION OF THE MITOTIC CYCLE OF EHRLICH ASCITES TUMOR CELLS IN VIVO

Renato Baserga* and Walter E. Kisieleski

Preliminary experiments in this Laboratory have confirmed the findings of Hornsey and Howard(1) on the mitotic cycle of Ehrlich Ascites Tumor (EAT) cells growing in the peritoneal cavity of mice. During the exponential phase of tumor growth, these cells have a mean generation time of about 18 hr, partitioned as follows: S phase (DNA synthesis phase) = 11 hr; G_2 = 2 hr; prophase = 4 hr; and meta- to telophase = 1 hr. During the exponential phase of growth, practically all tumor cells synthesize DNA and divide, and there is no G_1 period in the mitotic cycle of these cells. Therefore, when EAT cells are labeled with tritiated thymidine, they can be divided into 4 groups, recognizable by autoradiography and microscopic observation, i.e.: 1) cells in DNA synthesis; 2) cells in the G_2 plus early prophase period, not labeled with tritiated thymidine and not in mitosis; 3) cells in late prophase; 4) cells in the period extending from meta- to telophase.

To investigate other metabolic activities in the various phases of the mitotic cycle of EAT cells, a two-emulsion autoradiographic technique was designed.(2) This technique takes advantage of the fact that, in nuclear emulsions, β-particles from tritium have an average range of less than 1 μ, while the β-particles from C^{14} have an average range of 10 μ. If cells are labeled with both radioisotopes and autoradiographed, the emulsion, which is about 4 to 6 μ thick, will register β-particles from both H^3 and C^{14}. If now a second emulsion is laid over the first one, the two being separated by an inert layer of celloidin, this second emulsion, about 5 to 6 μ away from the labeled locus, will register only the β-particles from C^{14}. It is then possible to determine if a given cell is labeled only with H^3 (no developed silver grains in the second emulsion), with C^{14} only (about the same number of silver grains in both emulsions), with both (many more grains in the first than in the second emulsion), or neither. Actually, about half of the C^{14} beta-particles are arrested by the first emulsion plus celloidin coating, but the decrease in the number of grains in the second emulsion is still higher by at least a factor of 10.

The technique has been used to study the relative rates of RNA and protein synthesis in the various phases of the mitotic cycle of EAT cells. To determine the rates of RNA synthesis, tumor-bearing mice were injected with tritiated thymidine and C^{14}-uridine. The animals were killed after 30 min, and two-emulsion autoradiographs were made of smears of EAT cells. The emulsion used was NTB bulk emulsion (Eastman Kodak Co.),

---

*Department of Pathology, Northwestern Medical School, Chicago, Illinois.

and the exposure time was 20 days. Comparative grain counts in the second emulsion layer showed that EAT cells in the exponential phase of tumor growth synthesize RNA at the same rate for the entire length of the mitotic cycle, with the exception of a very brief period between late prophase and completion of telophase, during which time no RNA is synthesized.(3)

To determine the rates of protein synthesis, tumor-bearing mice were injected with tritiated thymidine and C^{14}-leucine, and two-emulsion atuoradiographs made of the tumor cells, as described above. Grain counts in the second emulsion showed that these cells synthesize proteins at a higher rate during the period of DNA synthesis. At the end of the S phase, protein synthesis decreases progressively until it reaches a minimum during the period from meta- to telophase.

References

1. Hornsey, S., and Howard A. Autoradiographic studies with mouse Ehrlich ascites tumor. Ann. N. Y. Acad. Sci. 63, 915-927 (1956).

2. Baserga, R. Two-emulsion autoradiography for the simultaneous demonstration of precursors of deoxyribonucleic acids. J. Histochem. Cytochem. 9, 586 (1961). Abstract.

3. Baserga, R. A study of nucleic acid synthesis in ascites tumor cells by two-emulsion autoradiography. J. Cell Biol, in press.

BIOCHEMISTRY OF GLUCOSE OXIDASE I. METHEMOGLOBIN FORMATION AFTER GLUCOSE OXIDASE INJECTION IN MICE

Robert N. Feinstein and Marilyn Coulon

The reaction carried out by the enzyme glucose oxidase is:

$$\text{glucose} + \text{oxygen} \xrightarrow{\text{glucose oxidase}} \text{gluconic acid} + H_2O_2 \quad .$$

For reasons that will be discussed in later sections of this study, glucose oxidase was injected into mice in the hope of raising blood and tissue H_2O_2 concentration. It was shown by Takahara(1) and by Aebi et al.,(2) with acatalatic (catalase-free) human blood, that the addition of H_2O_2 will cause methemoglobin formation. This report will describe the production of methemoglobinemia in mice in vivo after the injection of potent glucose oxidase preparations.

Materials and Methods

Animals used were normal adult female CF#1/Anl mice. Glucose oxidase was a commercial preparation ("Type IV") purchased from Sigma Chemical Corporation, originally obtained from a mold, and so heavily contaminated with catalase that, in the absence of a catalase inhibitor (e.g., azide), little or no H_2O_2 will accumulate in in vitro incubation.

Total blood pigment and per cent methemoglobin were determined by the technique of Hunter.(3) The figures presented in this report must be considered semi-quantitative only since our spectrophotometer was only secondarily calibrated from another instrument commercially calibrated to read hemoglobin directly; we did not calibrate from oxygen saturation curves, as is necessary for maximum accuracy.

Results and Discussion

The results of a series of experiments on the effect of injected glucose oxidase on methemoglobin formation are shown in Table 49. Each figure is the average of three animals. It is clear from this table that (a) the effect on total pigment and on per cent methemoglobin is dependent on the concentration of the injected glucose oxidase; and (b) after higher doses of glucose oxidase, not only does methemoglobin appear in the circulation, but the total blood pigment sharply decreases.

Not shown in the table is the concomitant fact that with a decreased total pigment there also appears a considerable decrease in hematocrit. The hematocrit, however, is extremely difficult to read because much

pigment has also appeared in the plasma. Animals reaching this stage will not live long; the appearance of visible "bluing" of the tail, eyes, etc., is, of course, a very bad prognostic sign. An animal at this stage will excrete highly pigmented urine, and if the mouse is sacrificed, all organs will be found to be dark, the spleen appearing congested with pigment.

TABLE 49

Effect of injected glucose oxidase (G. O.) on methemoglobin formation

Dose of G. O., mg/kg	Time after G. O., min	Total pigment, g/100 ml of blood	Methemoglobin, %
50	(no G. O.)	15.0	0
	10	13.7	0
	20	14.4	0
	30	14.2	0
	45	14.8	0
	60	15.2	1
100	(no G. O.)	13.3	0
	10	12.9	0
	20	14.3	0
	45	8.4	7
	60	9.3	7
150	(no G. O.)	14.6	0
	10	14.8	0
	20	14.9	0
	30	12.1	0
	45	6.0	15
	60	7.1	19

Each datum represents the average for 3 mice. Injections were made intraperitoneally.

It thus appears quite probable that there is indeed enough H_2O_2 production to overwhelm the catalase defenses of the erythrocyte and produce methemoglobin. It is also possible that catalatic activity generates sufficient oxygen to disrupt any erythrocytes into which formed H_2O_2 has diffused, thus accounting for the decreased hematocrit and the plasma pigment.

An interesting point to note is that in vitro, this glucose oxidase preparation contains so much catalase contaminant that no H_2O_2 accumulates. Yet upon intraperitoneal injection, we find apparently excessive H_2O_2 formation in the blood stream. The most probable explanation would be that the glucose oxidase, a flavoprotein enzyme, readily penetrates membranes, whereas the catalase, a very high molecular weight heme protein, cannot do so. The H_2O_2-former, and the H_2O_2-destroyer, are thus perhaps biologically separated.

Summary

The injection of sufficient glucose oxidase into mice causes methemoglobin formation, decrease of total blood pigment, appearance of pigment in plasma and urine, and death of the animal.

References

1. Takahara, S. Progressive oral gangrene probably due to lack of catalase in the blood (acatalasemia). Lancet 263, 1101-1104 (1952).

2. Aebi, H., J. P. Heiniger, R. Buetler and A. Hässig. Two cases of acatalasia in Switzerland. Experientia 17, 466 (1961).

3. Hunter, F. T. The Quantitation of Mixtures of Hemoglobin Derivatives by Photoelectric Spectrophotometry. Charles C. Thomas, Springfield, (1951).

CATALASE ACTIVITY IN VARIOUS INBRED MOUSE STRAINS

Robert N. Feinstein and Marilyn Coulon

In the past, the enzyme catalase has been considered an ubiquitous constituent of all living organisms with the single exception of obligate anaerobic microorganisms. Partly because of this distribution, and partly because of the known toxicity of its substrate, hydrogen peroxide,(1) catalase has been considered an essential part of all aerobic existence. It was therefore a most unexpected finding by Takahara(2) that certain Japanese individuals exhibit a total lack of this enzyme in their blood and in those tissues which have been measured. It might be noted that Aebi et al.(3) have also recently, in an intensive screening test, discovered two acatalatic individuals in Switzerland.

No animal strain has yet been reported to be comparably low in catalase. Radev(4) has developed a hypocatalatic strain of guinea pigs, but these animals, though subnormal in catalase, still have appreciable tissue and blood catalase activity. Because of the considerable advantages to be derived from catalase-free experimental animals in radiation biology and oncology research, some effort is being made here to derive such strains. As a starting point, we have investigated the catalase activity of nineteen different inbred strains of mice.

Experimental and Results

Approximately five specimens of each of 19 inbred mouse strains were obtained by the courtesy of Dr. John Storer, Jackson Memorial Laboratory, Bar Harbor, Maine. All were males, all were caged at Argonne for at least two weeks prior to sacrifice, and all were used at 20 to 24 weeks of age. Catalase assays were performed by the perborate method.(5) Either two or three mice of each strain were blended in the Waring blender for the determination of whole-body catalase, and the rest were sacrificed for blood and liver catalase activities.

The results are given in Table 50, where both individual values and averages are listed in order to provide an estimate of intrastrain variability. It will be noted that average whole body catalase ranges from 58 units/g (LP/J) to 114 units/g (ST/J); liver catalase, from 780 units/g (C58/J) to 1270 units/g (CBA/J); and blood catalase, from 74 units/ml (MA/J) to 145 units/ml (SJL/J and C57BR/cd). Generally liver and whole-body catalase levels correlate well, as is to be expected from the fact that, in the mouse, liver catalase represents about 67% of the total body catalase.(6) Blood catalase correlates less well with either of the two other parameters.

TABLE 50

Whole body, liver, and blood catalase of inbred strains of mice*

Strain	Whole body		Liver		Whole blood	
	Individuals	Average	Individuals	Average	Individuals	Average
ST/J	114	114	988 866 777	877	104 106 112	107
SJL/J	95 75 89	92	1230 1190	1210	138 149	145
129/J	87 86 91	89	1210 1030	1120	126 131	129
DBA/2J	88 85	87	1070 1030 1080	1060	90 94 99	94
BALB/CJ	96 114 77	96	914 1260	1090	112 111	112
C_3HeB/FeJ	91 82	87	1220 1210 1240	1220	88 96 96	93
CBA/J	83 89 87	85	1240 1300	1270	120 108	114
A/J	78 85	82	1340 1140 1310	1260	123 124 121	123
SM/J	76 81	79	1030 1080 1000	1040	104 99 98	100
C57BR/cd	71 52 78	75	870 871	871	(lost) 145	145
RF/J	74	74	874 924	900	117 101	109
MA/J	73 75	74	849 925 917	897	74 74 74	74
BDP/J	74 70	72	778 1010 1070	955	93 95 93	94
BDF_1/J (C57BL6 x DBA2)	71 88 73	77	854 872	860	110 106	108
SWR/J	67 72	70	876 822 1060	919	95 96 96	96
DBA/1J	64 67	66	1050 1090 1030	1060	79 79 81	80
C57BL/6J	55 69 71	63	748 884	820	128 114	121
C58/J	60 59	60	638 872 830	780	(lost) 122 116	119
LP/J	51 64	58	1040 1140 1130	1100	113 116 121	117

*Figures are perborate units per g whole body, per g liver, or per ml whole blood.

An experiment is now in progress to exploit these differences further by selective breeding.

References

1. Feinstein, R. N., G. J. Cotter and M. M. Hampton. Effect on radiation lethality of various agents relevant to the H_2O_2-catalase hypothesis. Am. J. Physiol. 177, 156-160 (1954).

2. Takahara, S. Progressive oral gangrene probably due to lack of catalase in the blood (acatalasemia). Lancet 263, 1101-1104 (1952).

3. Aebi, H., J. P. Heiniger, R. Buetler and A. Hässig. Two cases of acatalasia in Switzerland. Experientia 17, 466 (1961).

4. Radev, T. Inheritance of hypocatalasaemia in guinea-pigs. J. Genetics 57, 169-172 (1960).

5. Feinstein, R. N. Perborate as substrate in a new assay of catalase. J. Biol. Chem. 180, 1197-1202 (1949).

6. Feinstein, R. N., M. Hampton and G. J. Cotter. Species specificity of catalase. Enzymologia 16, 219-225 (1953).

ATTEMPTS AT REDUCTION OF ERYTHROCYTE CATALASE LEVEL

Robert N. Feinstein, Marilyn Coulon, and Elizabeth Thompson*

The desirability of reducing the erythrocyte catalase level in cancer therapy by radiation or hydrogen peroxide administration has been discussed in detail.(1) 3-Amino-1,2,4-triazole (AT) has been shown to be effective in reducing the catalase of all tissues except the erythrocytes.(2) The present report describes other attempts to lower the red cell catalase activity. All catalase assays described were made by the perborate method.(3)

Allylisopropylacetamide. According to Talman et al.,(4) allylisopropylacetamide (AIA)** blocks the synthesis of new catalase in the liver. Price et al.(5) demonstrated a decrease of liver catalase to about 20% of normal after three days of AIA administration. Since the best drug known at present for the prolonged reduction of liver catalase activity, 3-amino-1,2,4,-triazole (AT), is without effect on erythrocyte catalase,(2) it was hoped that perhaps AIA, working through a different mechanism, might also block the synthesis of erythrocyte catalase.

Table 51 shows the results of these studies. Maximum reduction of erythrocyte catalase achieved was approximately 30%, and even this figure could be neither improved nor regularly duplicated.

3-Amino-1,2,4-triazole (AT) and methylene blue. It is known that, although AT will reduce the catalase activity of lysed erythrocytes, it has no effect on intact red blood cells.(1) Tephly et al.(6) indicate that if methylene blue is added to an in vitro incubation mixture of AT and intact erythrocytes, the catalase activity will be reduced. We attempted the same experiment in vivo. A barely sublethal dose of methylene blue (50 mg/kg) was injected intraperitoneally into 3 normal female mice. This was followed in 15 min by 750 mg of AT per kg body weight. After a further 45 min, the mice were sacrificed, as were 3 mice treated identically except for the injection of saline instead of methylene blue. The average blood catalase levels were: saline, 164 perborate units/ml; methylene blue, 171 perborate units/ml. We have made no effort to verify the in vitro effect of AT and methylene blue described by Tephly et al.(6)

---

*Argonne Semester Student from Knox College.

**We are indebted to Dr. W. E. Scott of Hoffman-LaRoche, Inc., for a generous gift of allylisopropylacetamide.

TABLE 51

Effect of allylisopropylacetamide (AIA) on catalase of liver and blood

Expt.	Mode of AIA administration	Time assayed	Liver			Blood		
			Saline	AIA	% Inhib.	Saline	AIA	% Inhib.
1	200 mg/kg, i.p., twice daily for 5 days. Sampling began after 1st days' injection.	day 1	1108	1099	1	224	221	1
		2	1174	750	36	214	236	-9
		3	1160	662	43	198	202	-2
		4	961	663	31	206	211	-2
		5	978	568	42	211	217	-4
		8	1204	1118	8	178	151	15
		9	-	1057	-	-	159	-
2	200 mg/kg, i.p., 4 times in single day; sample timing begins from first injection.	$\frac{1}{4}$ hr		835			174	
		1 hr		691			161	
		6 hrs		672			173	
		24 hrs		580			201	
		28 hrs		666			182	
3	200 mg/kg, i.p., twice daily for 9 days, beginning day 0.	day 0*		1045			225	
		3		690	34		224	0
		6		531	49		152	32
		9		722	31		171	24
		10		389	63		175	22
4	1% AIA mixed with standard powdered food.	day 0*		737			166	
		2		298	60		163	2
		4		320	57		165	0
		7		384	48		164	1

Each datum represents the average of three mice. Figures are given as perborate units per g liver or per ml whole blood.

*Control.

1,2,4-Triazole. This compound, which may be regarded as the deaminated "parent compound" of AT, was tested for effect on red blood cell catalase, on the rationale that perhaps the modification of electrical charge caused by loss of the amino group would permit the molecule to penetrate the erythrocyte. In the first experiment, with two triazole-treated and two saline-treated mice, erythrocyte catalase was decreased 48% by the triazole, liver catalase being essentially unaffected. However, in a continuing series of four further experiments, with triazole administered singly or repeatedly, in doses reaching the lower limit of lethality, it was not again possible to achieve significant catalase inhibition in either tissue. The efficacy of triazole as a catalase inhibitor in vitro has not been tested; it is, however, unlikely that it would be effective since no effect on liver catalase was seen, and the liver cell is generally fairly permeable to low molecular weight agents.

Monosaccharide derivatives of AT. Gentile and Fredrick[7] prepared a glucose "adduct" of AT which showed properties distinctly different from those of either parent compound. We have prepared adducts of AT with glucose, galactose, mannose, xylose, arabinose, and ribose. In all these cases, the product showed a negative Fehling's test for reducing sugars, and a decreased test for free AT.[8] Since the latter test involves heating in acid, it is probable that the residual AT test was due to hydrolysis of the sugar-AT compound.

These 6 sugar-AT compounds have been tested for effect on the catalase of normal mice. In no case has any effect been observed on either blood or liver catalase. Thus it appears that either these "adducts" cannot penetrate even the hepatic cell, or else the compound does not dissociate within the cell to liberate the free, active AT.

Sublethal whole-body irradiation. Because it is often suggested, on the basis of a variety of experimental data, that irradiation increases tissue permeability, the possibility was considered that sublethal whole body irradiation might sufficiently increase the permeability of the erythrocyte to permit the entrance of subsequently administered AT. This has been tried, with completely negative results.

The over-all conclusion drawn from the above experiments is that no agent or technique has yet been found which will effectively and reproducibly reduce the catalase level of the red blood cell.

References

1. Feinstein, R. N., and J. L. Dainko. Use of 3-amino-1, 2, 4-triazole to reduce body catalase activity in cancer studies. Cancer Research 19, 612-617 (1959).

2. Feinstein, R. N., S. Berliner and F. O. Green. Mechanism of inhibition of catalase by 3-amino-1, 2, 4-triazole. Arch. Biochem. Biophys. 76, 32-44 (1958).

3. Feinstein, R. N. Perborate as substrate in a new assay of catalase. J. Biol. Chem. 180, 1197-1202 (1949).

4. Talman, E. L., R. F. Labbe and R. A. Aldrich. Porphyrin metabolism. IV. Molecular structure of acetamide derivatives affecting porphyrin metabolism. Arch. Biochem. Biophys. 66, 289-300 (1957).

5. Price, V. E., M. Rechcigl, Jr. and R. W. Hartley, Jr. Methods for determining the rates of catalase synthesis and destruction in vivo. Nature 189, 62-63 (1961).

6. Tephly, T. R., G. J. Mannering and R. E. Parks, Jr. Studies on the mechanism of inhibition of liver and erythrocyte catalase by 3-amino-1, 2, 4-triazole (AT). J. Pharmacol. Exptl. Therap. 134, 77-82 (1961).

7. Gentile, A. C., and J. F. Fredrick. Chemical activity of the glucose adduct of 3-amino-1, 2, 4-triazole. Physiol. Plantarum 12, 862-867 (1959).

8. Green, F. O., and R. N. Feinstein. Quantitative estimation of 3-amino-1, 2, 4-triazole. Anal. Chem. 29, 1658-1660 (1957).

EFFECT OF NICOTINAMIDE ON GROWTH OF MOUSE EHRLICH ASCITES TUMOR

Robert N. Feinstein, Marilyn Coulon,
and Elizabeth Thompson*

The rationale for testing the effect of nicotinamide (NA) on the growth of the ascites tumor is rather tenuous. It is based on the work of Pantlitschko,[1] who found that dilute H_2O_2 inhibits the glycolysis of ascites tumor cells, and that this inhibition of glycolysis is completely reversed, even after a period of time, by nicotinamide. On this basis one would expect, if there were any effect, that NA would accelerate the growth of tumors.

The first experiment, in which NA was injected intraperitoneally at 1 g/kg on the day of implantation of the ascites, and on each of the next 4 days, indicated a prolonged survival time in the NA-treated mice. The group of 6 saline-injected mice survived an average of 7.5 days after the implantation of the tumor; the 6 NA-injected mice survived an average of 11.0 days. The latter figure would have been a trifle higher, but the last 2 survivors, moribund, were sacrificed on the 12th day for humanitarian reasons.

In the second experiment, NA was not injected, but rather was incorporated into the diet of groups of 5 mice. Preliminary tests indicated that mice consumed, at the normal rate, a diet containing 10 mg NA per gram of powdered standard laboratory chow. Ascites-bearing mice eating plain food survived an average of 10.8 days. Ascites-bearing mice eating food containing NA from the time of tumor implantation survived an average of 10.6 days. Ascites-bearing mice eating food containing NA beginning on the 4th day after tumor implantation survived an average of 12.0 days.

The difference in survival time observed in the injection experiment thus appears due primarily to an unusually rapid death rate among saline-injected mice, rather than to any life prolongation from NA. Experiments with nicotinamide have, therefore, been discontinued.

Reference

1. Pantlitschko, M., and F. Seelich. Ueber die Beeinflussung des Stoffwechsels von Tumorasciteszellen durch Wasserstoffperoxyd. Biochem. Z. 333, 78-83 (1960).

---

*Argonne Semester Student from Knox College

DYNAMICS OF TUMOR GROWTH

Anna Kane Laird

In an extension of our previous studies of the dynamics of cell proliferation in precancerous liver,[1-3] we have initiated a study of the dynamics of tumor growth. Reviewing the appropriate measurements of tumors reported in the literature,[4-13] we have found that the anticipated exponential, or semilog growth of tumors has been observed only rarely, and then only for relatively brief periods of tumor growth. Nearly all reported tumors grow in such a way that the diameter (if a solid tumor) or the cube root of total cell number (if an ascites tumor) when plotted against time gives a close approximation to a straight line. Although this empirical fact has been clearly established, it is difficult to relate such growth either to exponential cell proliferation or to the coordinated growth of the normal whole organism.

Figures 82 and 83 show, respectively, a semilog and a cube-root plot of the growth of the Ehrlich ascites tumor, from the data of Klein and Revesz.[10] If the ascites cells had multiplied exponentially, the experimental points should fall on a straight line in Figure 82; instead they describe a smooth asymptotic curve. The fact that the cube root of cell number plotted against time does give a straight line, as shown in Figure 83, indicates that the specific growth rate of such tumors decreases with time (i.e., the second derivative of the growth curve is negative), in contrast to semilog growth in which the specific growth rate remains constant.

In a study of the dynamics of normal growth of the human fetus and child, Osgood[14] showed that when the log of body weight or organ weight is plotted against the log of time, a series of straight lines is obtained, connected to one another at "inflection points" which occurred at times known to be associated with physiological changes in the growth rate of the developing organism. Since both cube-root and log-log growth share the property of deceleration of the specific growth rate, it seemed appropriate to plot the reported tumor measurements against time on a log-log plot.

Except for tumors that are known to arouse an effective immune response in the host, growth of all the tumors for which adequate growth data are available has been fitted successfully to a log-log plot. One example of such a plot is given in Figure 84, which shows the growth of the Ehrlich tumor, using the same data presented in Figures 82 and 83. It is clear from inspection of the figure that log tumor size plotted against log time gives a very close approximation to a straight line. The adequacy of the fit to a straight line was tested mathematically in two ways: 1) the ratios of the observed to the calculated tumor sizes were determined for each time interval, and were found for all the tumors, with the exceptions

noted above, to vary randomly about a value of 1.00 throughout the period of log-log growth of the tumors; and 2) when the fit of a quadratic was compared with the fit of a linear equation to the data, the quadratic term was found in all cases to be not significantly different from zero, and the quadratic formulation did not reduce the variance significantly. Hence, one can conclude that a straight line gives a satisfactory representation of the data.

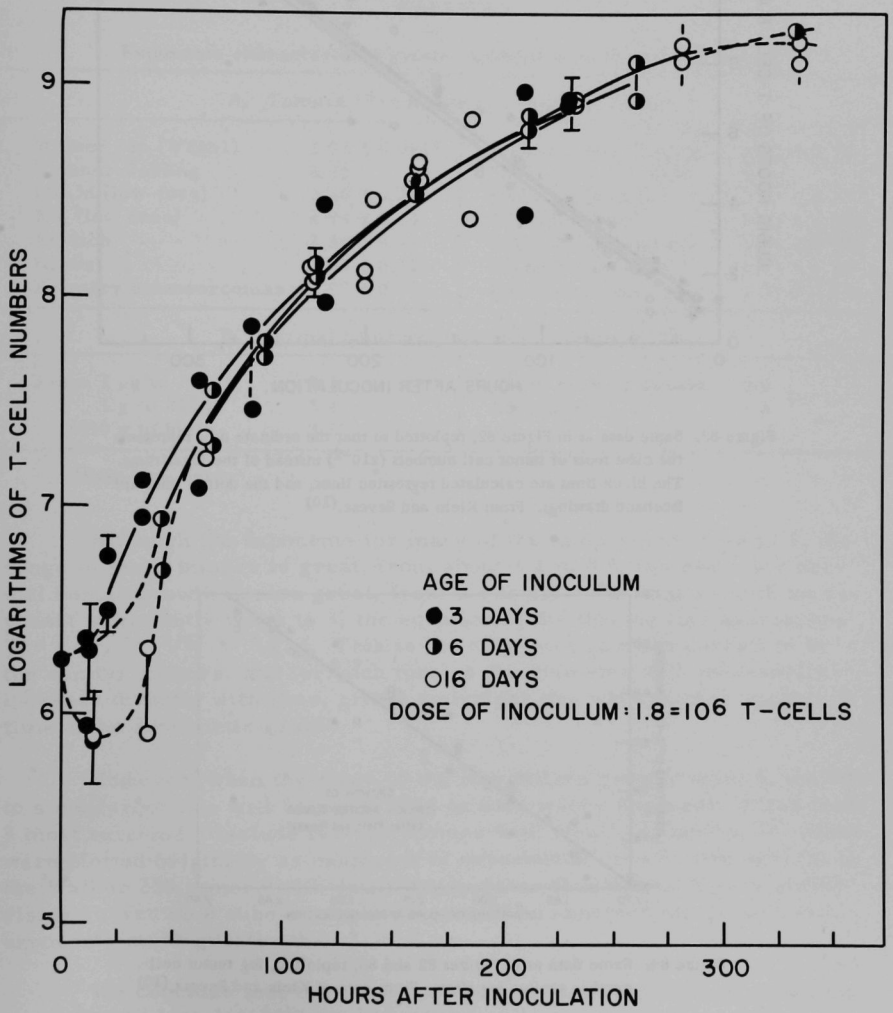

Figure 82. Growth of the Ehrlich ascites tumor. Log number of tumor cells plotted against time. Dose of inoculum kept constant while physiological age of inoculum varied. Dotted lines are freehand drawings; black curves represent authors' equation fitted to the data. From Klein and Revesz.(10)

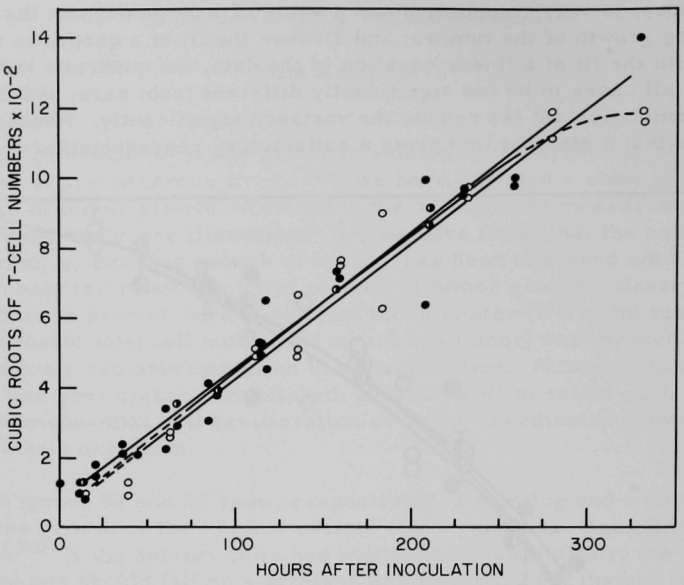

Figure 83. Same data as in Figure 82, replotted so that the ordinate now represents the cube roots of tumor cell numbers ($x10^{-2}$) instead of the logarithms. The black lines are calculated regression lines, and the dotted lines are freehand drawings. From Klein and Revesz.(10)

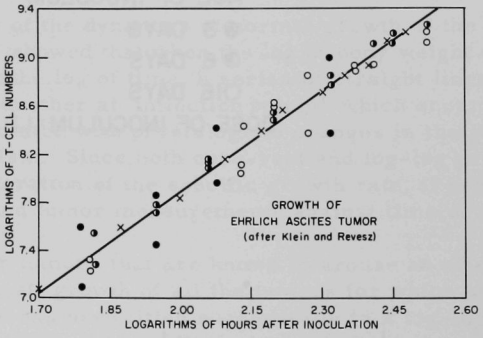

Figure 84. Same data as in Figures 82 and 83, replotted, log tumor cell number against log time. From data of Klein and Revesz.(10)

The log-log line describes a power function of the form $W = a \cdot t^k$, where W = tumor size (weight or total cell number), t = time, and a and k are constants. The exponent k gives the slope of the log-log line. The slopes calculated for a number of tumors reported in the literature are given in Table 52A; for comparison the values calculated by Osgood for normal growth of the human fetus and child are given in Table 52B.

TABLE 52

Exponents characterizing growth according to equation $W = a \cdot t^k$

A. Tumors (From data of various authors)

Walker 256 (W26b1)	3.02 ± 0.062*	Walker 256 (W23b34)	6.07 ± 0.38
Flexner-Jobling	2.95	Walker 256 (W10b4)	8.50
MC_1M (low dose)	2.40 ± 0.21	MC_1M (high dose)	1.17 ± 0.12
El_4 (low dose)	2.79 ± 0.14	El_4 (high dose)	1.60 ± 0.085
Ehrlich	2.82 ± 0.11	$6C_3HED$ (high dose)	1.07 ± 0.055
Krebs	3.53 ± 0.11	$6C_3HED$ (low dose)	1.53 ± 0.16
Primary osteosarcomas	2.93 ± 0.075	DBA lymphoma	1.93 ± 0.21

B. Normal human growth [From Osgood(14)]

Fetus 1 μg to 1 g	9.1	Child, birth to puberty	0.4
1 g to 250 g	5.4	Adolescence	1.3
250 g to birth	3.2		

*Standard error

Although the exponents for many of the tumors are close to 3, the range in these tumors is great, from about 1.1 to 8.5; the range for normal human growth is also great, from 0.4 to 9.1. For tumors with an exponent sufficiently close to 3, the equation of the log-log line approaches $W = a \cdot t^3$, or $\sqrt[3]{W} = \sqrt[3]{a} \cdot t$. This is the cube root function described by the earlier authors, and for such tumors the diameter will necessarily increase directly with time, giving a straight line when plotted against time on an arithmetic graph.

However, when the slope of the line differs greatly from 3, the fit to a cube-root line will be poor. The tumors whose exponents differ from 3 most extremely include two lymphomas with small exponents,(11) which were plotted originally as examples of exponential growth, and several of the Walker 256 tumors with exponents greater than 6, which gave slowly rising curves on a cube-root plot, as would be expected for growth with exponents much greater than 3.

We conclude that the cube-root growth observed for many tumors is log-log growth in which the slope of the log-log line is approximately 3, but that an exponent of 3 is not a necessary condition for either tumor

or normal growth. Hence the log-log line is the more general description of the dynamics of tumor growth, of which cube-root growth is a special case.

We can conclude further from the nature of the log-log function that tumors generally grow in such a way that the time required for doubling the tumor mass increases in a regular way as the tumor grows, and it is for this reason that the anticipated semilog growth has been observed only rarely, and for only relatively brief periods of tumor growth.

Tumor growth, therefore, does not appear to be analogous to the growth of bacteria and other free-living cells in culture. However, it might be more appropriate to look for a resemblance between the dynamics of growth of tumors, which are tissues growing within a metazoan organism, and the dynamics of growth of such an organism and its parts. When we do this we see that indeed both types of growth are well approximated by a straight line on a log-log plot, which indicates that the time required for doubling the total mass increases progressively during growth according to the same mathematical function in both cases.

Since the growth of both the whole organism and its parts shows a log-log relation to time, then for simple mathematical reasons, if the log of the size of one part is plotted against the log of the size of another part or of the whole organism, the points will approximate a straight line very closely. This log-log relation between the growing parts of an organism has already been established for a wide range of growth phenomena in many species of plants and animals, including man.[15-17] Growth that follows this principle is called allometric growth.

In this paper we have shown that tumor growth bears a log-log relation to time, as does the normal growth of its animal host, in whole and in its parts. These relationships suggest very strongly that tumor growth constitutes one more example of the familiar allometric growth. If this is true, then for many tumors, if not all, the tumor plus host together comprise a new closed system of growth, analogous to the closed system that defines the normal metazoan organism in its growth and development.

When first observed, the log-log relation of tumor growth to time suggests a restriction of tumor growth by an immune response of the host, or by a limitation in the availability of nutritional factors. However, when we note the similarities between log-log growth of the tumors and allometric growth of normal body parts, it becomes evident that the situation is much more complex than these simple concepts would suggest. Knowledge of the nature of allometric growth and the factors controlling it would offer us a new and important frame of reference for the study of the dynamics of tumor growth.

References

1. Laird, A. K., and A. D. Barton. Cell growth and the development of tumors. Nature 183, 1655-1657 (1959).

2. Laird, A. K., and A. D. Barton. Cell proliferation in precancerous liver: linear growth curve. Nature 188, 417-418 (1960).

3. Laird, A. K., and A. D. Barton. Cell proliferation in precancerous liver: Relation to presence and dose of carcinogen. J. Natl. Cancer Inst. 27, 827-839 (1961).

4. Mayneord, W. V. On a law of growth of Jensen's rat sarcoma. Am. J. Cancer 16, 841-846 (1932).

5. Schrek, R. A quantitative study of the growth of the Walker rat tumor and the Flexner-Jobling rat carcinoma. Am. J. Cancer 24, 807-822 (1935).

6. Schrek, R. Further quantitative methods for the study of transplantable tumors. The growth of the R_{39} sarcoma and Browne-Pearce carcinoma. Am. J. Cancer 28, 345-363 (1936).

7. Schrek, R. The effect of the size of the inoculum on the growth of transplantable rat tumors. Am. J. Cancer 28, 364-371 (1936).

8. Schrek, R. Permanent and transient (fortuitous) variations of the growth components of transplantable rat tumors. Am. J. Cancer 28, 372-388 (1936).

9. Schrek, R. A comparison of the growth curves of malignant and normal (embryonic and postembryonic) tissues of the rat. Am. J. Pathol. 12, 525-530 (1936).

10. Klein, G., and L. Revesz. Quantitative studies on the multiplication of neoplastic cells in vivo. I. Growth curves of the Ehrlich and MC_1M ascites tumors. J. Natl. Cancer Inst. 14, 229-272 (1953).

11. Revesz, L., and G. Klein. Quantitative studies on the multiplication of neoplastic cells in vivo. II. Growth curves of three ascites lymphomas. J. Natl. Cancer Inst. 15, 253-271 (1954).

12. Patt, H. M., and M. E Blackford. Quantitative studies of the growth response of the Krebs ascites tumor. Cancer Research 14, 391-396 (1954).

13. Finkel, M. P., P. J. Bergstrand, and B. O. Biskis. The latent period, incidence, and growth of Sr^{90}-induced osteosarcomas in CF_1 and CBA mice. Radiology 77, 269-281 (1961).

14. Osgood, E. E. Development and growth of the hematopoietic tissues, with a clinically practical method of growth analysis. Pediatrics 15, 733-751 (1955).

15. Huxley, J. S. Problems of Relative Growth. The Dial Press, New York, 1932.

16. Reeve, E C R., and J. S. Huxley. Some problems in the study of relative growth. Essays on Growth and Form, ed. W. E. L. Clark and P. B. Medawar, Clarendon Press, Oxford, 1945.

17. von Bertalanffy, L. Principles and theory of growth. Fundamental Aspects of Normal and Malignant Growth, ed. W. W. Nowinski. Elsevier Publ. Co., Amsterdam, 1960.

RADIATION-INDUCED CHROMOSOMAL ABERRATIONS AND VARIANT CLONES IN MAMMALIAN CELLS CULTIVATED IN VITRO

Agnes N. Stroud, Austin M. Brues, and Beverly R. Svoboda

Much experimental work has been carried out on the induction of chromosome changes by irradiation of Drosophila sperm[1-4] and salivary gland,[5-7] various plant materials,[8-12] grasshopper neuroblasts[13] and various other organisms, but only recently have detailed data been reported on radiation-induced chromosomal aberrations of mammalian cells in vitro.[14-25] The present paper is concerned with the persistence of chromosome aberrations and radiosensitivity of long-term survivors of pig kidney cells isolated from irradiated populations. Various modern techniques used in conjunction with tissue culture methods have enabled us to study several features of the postirradiation responses of these cells: (a) multiplication rates of whole cell populations and of clones isolated from them by quantitative cell counting; (b) chromosome injuries of specific types (chromatid and isochromatid breaks and exchanges) by spreading techniques; and (c) the course of DNA synthesis as indicated by uptake of tritiated thymidine. In addition, we have examined the radiosensitivities of cells derived from previously irradiated cultures.

Briefly, our results show that during the 30 hr following irradiation the frequency of chromosome aberrations increases with time as well as with dose, approaching a theoretical dose-effect relation only at times somewhat beyond 24 hr, and that surviving cells derived from cultures that received 500 r have 1) growth rates inversely related to the frequency of aberrations, 2) different patterns of DNA synthesis, and 3) certain chromosome aberrations that persist indefinitely.

Materials and Methods

The diploid pig kidney cell line used in these experiments, obtained originally from Dr. Morgan Harris,[14] has been maintained in our laboratory for 3 years. It is grown on 95 percent Morgan's 199 medium with 5% calf serum. The karyotype has remained constant with a stemline number of 37. For subculture, cells were removed by treatment with Versene-trypsin, counted, and the inoculum adjusted to 1 to 2 x 10^5 cells/ml. The cells were grown in Leighton tubes and, when tritiated thymidine was used, coverslips were used in these tubes. Cultures were irradiated with 250 kvp X-rays, at 100 r/min. Chromosome studies were made by the smear or air-dry method of Hsu. A more detailed description of the methods has been published previously.[14]

Forty or more metaphase smears were scored for chromosome aberrations. A chromatid break was scored when it occurred in one of the two chromatids of a chromosome. An isochromatid break was recognized as a break appearing on both chromatids of a chromosome, and usually at the same site. Both the former and latter intrachanges were scored as 1-hit phenomena.[25] Chromatid exchanges (interchanges) occur between both chromatids of one chromosome and both chromatids of another chromosome, between both chromatids of one chromosome and one chromatid of one other chromosome, or between chromatids of two different chromosomes. Exchanges were scored as 2-hit phenomena.[25] When the results are calculated as total breaks, exchanges are considered as resulting from 2 breaks.

Cell population studies were made on replicate cultures with a Coulter counter after cells were treated with Versene-trypsin (0.25% solution) for 10-15 min to produce single cells. In Figures 89 and 90, which were derived from Table 56, the initial cell numbers differed somewhat but were adjusted to one value for the purpose of drawing the graphs. For clarification, B-2, the control, is the original stemline from which a fraction of the population was irradiated with 500 r 9 months earlier; from this surviving fraction, single cells were isolated and 500-r clones (designated in the text as Clones 3, 8, 10, and 14) were taken.

Results

Initial Population Studies

The pig kidney cell line was irradiated with doses of 200 r, 500 r, or 1000 r 18 hr after subculture, which was just prior to the time when most of the cells were entering their first division. We have previously found, using tritiated thymidine, that at this time 70% of the cells are in DNA synthesis,[14] indicating that they are approaching synchrony.

Typical growth curves of unirradiated and irradiated cultures are shown in Figure 85. The mean cell number of replicate cultures for each dose given is plotted against time after irradiation. The data give an estimate of the fraction of cells surviving these doses of irradiation. The unirradiated cell population exhibited a nearly exponential increase in growth over a period of 6 days, with a mean doubling time of 1.35 days (30 hr). Cells exposed to 200 r show a slight delay in cell growth for 48 hr, but after this time the growth rate parallels that of the controls. After 500 r there was a temporary decrease in growth rate beginning 2 days after irradiation, which was followed by an increase between the 4th and 6th day; during the lag period, inhibition of mitosis as well as cell death appeared to play a significant role. A marked decrease in the growth curve was evident after 1000 r 2 days after irradiation. For this particular

cell line, recovery of cells after 1000 r has occurred in only one or two experiments to date, and the small fraction of cells surviving this dose eventually died. The mean D_0 for this cell line has been estimated to be 180 r, based on the assumption that the cell number 6 days after irradiation is an index of the proportion of cells surviving following treatment. On this index it is estimated that 25% of the initial population survives after 500 r.

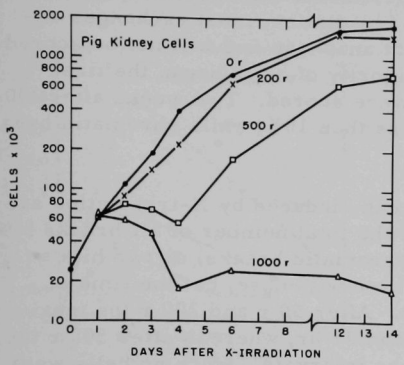

Figure 85. Growth curves of unirradiated and irradiated pig kidney cells. Mean cell number of 3 cultures is plotted against days after irradiation.

Early Chromosome Aberrations

Visible chromatid breaks appear soon after irradiation and are detected after doses as low as 50 r.[15,19] The numbers of chromosome aberrations in cells scored at 24, 27 and 30 hr, and 2 weeks following 50 r, 200 r and 500 r are presented in Table 53 as percentages of chromatid breaks, isochromatid breaks and exchanges for each dose and time interval. The proportion of single chromatid breaks (one-hit) scored is higher than that for isochromatid breaks (one-hit, but involving 2 chromatids) or exchanges (2 hits). The data also indicate that for any dose used in this experiment, breaks and exchanges predominate throughout a 30-hr period, while isochromatid breaks are fewer. This may be explained on the basis that the majority restitute, or unite with other broken ends to form exchanges which may appear as variants that persist and duplicate.

TABLE 53

The percent of aberrations occurring as chromatid breaks, isochromatid breaks and exchanges after X-irradiation

Hours after X-ray	X-ray dose, r	Metaphase cells scored	Number aberrations	Percent aberrations		
				Chromatid	Isochromatid	Exchanges
	0*	280	4	100	0	0
24	50	50	26	73	8	19
27	50	50	31	52	3	45
40	50	50	13	85	0	15
24	200	52	48	56	13	31
27	200	40	41	59	12	29
30	200	42	47	72	13	15
2 weeks	200	100	22	91	0	9
24	500	50	51	53	10	37
27	500	40	72	61	15	24
30	500	41	88	52	18	30
2 weeks	500	101	63	92	3	5

*The average of all controls for each individual experiment.

The percentage of exchanges is unusually high among the 50-r group. Other investigators working with mammalian cells[15,19] have not reported results paralleling these after 50 r. The discrepancy could find its basis in the time elements of the different experiments. If cells are permitted to go through one or two divisions after irradiation, most exchanges resulting in two centromeres will be lost at anaphase and will not be scored. Since this study was made before the majority of cells began the first division, these aberrant chromosomes were scored. Two weeks after 200 r and 500 r the exchanges decreased to less than 10%, while chromatid breaks increased accordingly.

The frequencies of chromatid breaks induced by X-irradiation are presented in Table 54 and Figure 86, as the total number of all breaks resulting from one hit (chromatid and isochromatid breaks) or two hits (exchanges). The breaks per cell increased with dose, but the time of maximum increase changed with dosage. After 50 r and 200 r the maximum increase was reached between 24 and 27 hr, whereas after 500 r the breaks continued to increase beyond these intervals. Since no cells were scored after 30 hr it is not known whether the maximum was reached at this time. The apparent delay in reaching a maximum value at 24 or 27 hr after 500 r probably reflects the mitotic delay, which is very pronounced after this dose.[14] Two weeks after irradiation with 200 r or 500 r the number of breaks per cell diminished to a minimum.

TABLE 54

The frequency of chromosome and chromatid breaks of pig kidney cells induced by X-irradiation

Time after X-ray	X-ray dose, r	Metaphase cells scored	Number breaks**	Breaks per cell	Breaks per r per cell x 10^{-2}
24 hr to 2 weeks	0*	280	8	0.03	-
24 hr	50	50	31	0.62	1.24
27 hr	50	50	45	0.90	1.80
40 hr	50	50	17	0.34	0.68
70 hr	50	45	16	0.36	0.72
24 hr	200	52	67	1.29	0.65
27 hr	200	40	53	1.32	0.66
30 hr	200	42	54	1.29	0.64
2 weeks	200	100	21	0.21	0.11
24 hr	500	50	66	1.32	0.26
27 hr	500	40	94	2.35	0.47
30 hr	500	41	114	2.78	0.56
2 weeks	500	101	65	0.64	0.13

*The average of all controls for each individual experiment.

**1-Hit breaks scored as one (chromatid and isochromatid breaks); 2-hit breaks scored as two (exchanges).

The relative efficiencies of the three doses used in producing chromosome aberrations are shown in Table 54 (expressed as breaks/r/cell). With each dose used there is a different effective time interval and maximum efficiency. Following a dose of 50 r the most effective time after irradiation appeared to be 27 hr, when there were 1.8 breaks/r/cell. With

200 r the relative efficiency was the same at 24, 27 and 30 hr. After 500 r, breaks/r/cell continued to increase up to 30 hr after irradiation. Since no samples were taken after this time the relative efficiency of this dose could not be determined.

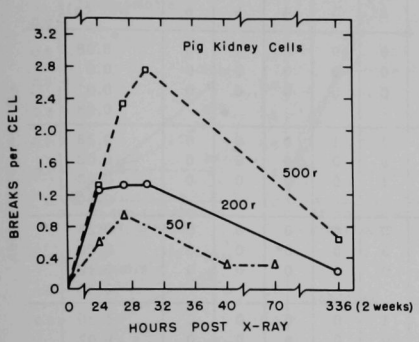

Figure 86. Mean number of chromosome breaks per cell for each dose as a function of time after irradiation.

The number of breaks per cell as a function of dose and time after irradiation is plotted in Figure 87. Breaks per cell at 24 hr were non-linear with dose; the departure from linearity is partially explained by a delay in mitosis after 500 r. At 27 and 30 hours breaks per cell increased linearly with increasing dose. The data indicate that breaks occurred as a function of time after irradiation as well as dose. At 30 hr and 2 weeks after irradiation, the number of breaks was directly proportional to the dose, whereas this was not true at 24 and 27 hr after irradiation.

Number of Aberrations Per Cell

The numbers of cells containing one or more aberrations following 50 r, 200 r, or 500 r are presented in Table 55. The type of break, chromatid or isochromatid, exchanges and total aberrations are likewise found in Table 55 and are plotted against dose in Figure 88. Among the cells having aberrations, one aberration per cell occurs in 61% of the cells for any dose or time period, while 24% of the cells contain 2 aberrations per cell and 8% contain 3 aberrations per cell and 7% have between 4 and 6 aberrations per cell. Isochromatid breaks 27 hr and 30 hr after irradiation increased linearly with dose (Figure 88). Exchanges increased as the square of the dose at 30 hr, whereas chromatid breaks failed to exhibit linearity at any time period studied. When all types of aberrations were grouped together, mean aberrations per cell increased linearly with dose and time except at 24 hr; in addition all aberrations were consistent with the Poisson distribution at 27 and 30 hr after

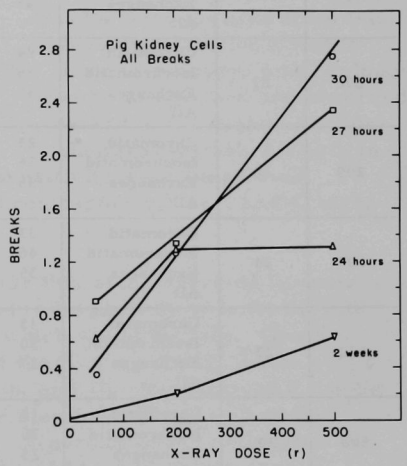

Figure 87. The frequency of chromosome breaks as counted at various times after irradiation. The data represent all breaks resulting from one and 2 hits.

TABLE 55

The number of cells containing one or more aberrations 24, 27, 30 hr, and 2 weeks after X-irradiation

Dose, r	Hours after X-ray	Aberrations	Number of aberrations per cell							Mean aberrations per cell
			0	1	2	3	4	5	6	
0	24-30	Chromatid	46	4	0	0	0	0	0	0.08
		Isochromatid	0	0	0	0	0	0	0	0.0
		Exchanges	0	0	0	0	0	0	0	0.0
		All								0.08
50	24	Chromatid	42	10	2	1	0	0	0	0.28
		Isochromatid	49	1	0	0	0	0	0	0.02
		Exchanges	41	8	1	0	0	0	0	0.20
		All								0.50
50	27	Chromatid	31	9	0	0	0	0	0	0.23
		Isochromatid	40	0	0	0	0	0	0	0.00
		Exchanges	35	5	0	0	0	0	0	0.12
		All								0.35
50	40	Chromatid	49	10	1	0	0	0	0	0.20
		Isochromatid	59	1	0	0	0	0	0	0.02
		Exchanges	56	4	0	0	0	0	0	0.07
		All								0.29
200	24	Chromatid	28	21	3	0	0	0	0	0.52
		Isochromatid	47	4	1	0	0	0	0	0.12
		Exchanges	43	4	4	1	0	0	0	0.29
		All								0.93
200	27	Chromatid	24	10	5	1	0	0	0	0.58
		Isochromatid	35	5	0	0	0	0	0	0.13
		Exchanges	30	8	2	0	0	0	0	0.30
		All								1.00
200	30	Chromatid	23	11	3	3	2	0	0	0.81
		Isochromatid	36	6	0	0	0	0	0	0.14
		Exchanges	35	7	0	0	0	0	0	0.17
		All								1.12
500	24	Chromatid	33	11	3	2	1	0	0	0.54
		Isochromatid	46	3	1	0	0	0	0	0.10
		Exchanges	35	10	2	0	0	0	0	0.28
		All								0.92
500	27	Chromatid	13	14	9	4	0	1	0	1.10
		Isochromatid	30	9	1	0	0	0	0	0.27
		Exchanges	27	10	4	0	0	0	0	0.45
		All								1.82
500	30	Chromatid	15	14	6	4	2	0	0	1.12
		Isochromatid	30	7	3	1	0	0	0	0.39
		Exchanges	23	12	4	2	0	0	0	0.63
		All								2.14
200	336	Chromatid	80	20	0	0	0	0	0	0.20
		Isochromatid	100	0	0	0	0	0	0	0.0
		Exchanges	98	2	0	0	0	0	0	0.02
		All								0.22
500	336	Chromatid	64	25	8	1	2	0	1	0.57
		Isochromatid	100	0	1	0	0	0	0	0.02
		Exchanges	98	3	0	0	0	0	0	0.03
		All								0.62

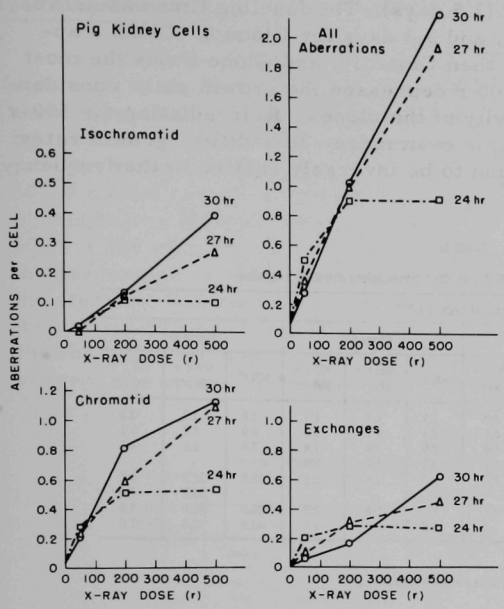

Figure 88. Mean number of aberrations per cell (chromatid and isochromatid breaks, exchanges, and total aberrations) as a function of dose and time after irradiation.

irradiation but not at 24 hr. We may assume that the departure from linearity at 24 hr after irradiation is due to a metaphase block which occurs a few hours after irradiation, and that after 500 r recovery from the block is incomplete, with the less severely damaged cells having a higher probability of going into mitosis at this early time. At this time cells of the 200 r and 500 r groups are out of phase with respect to their mitotic and intermitotic times.

Long-term Survivors

It was noted from the growth curves that 25% of the cells survived 500 r. Single cells were isolated from the surviving fraction a month after irradiation, and 14 clones were established and observed later for cytological and biochemical lesions due to irradiation. Four parameters of radiation sensitivity were measured: 1) growth rates, 2) DNA synthesis, 3) chromosome number, and 4) structural chromosome aberrations.

Only 5 of the 14 clones isolated for this study survived beyond the first month, although all clones appeared to be growing well during this time, and it was not possible to predict which would survive. Growth rates are shown in Table 56 for three of the five surviving clones. The 500-r clones, designated as numbers 3, 8, and 10, were derived 8 months earlier from a fraction of the control or stemline, designated as B-2, which had been given 500 r at that time. A portion of the cells from the 500-r clones were reirradiated with 200 r, 500 r and, in the case of Clone 3, 1000 r. These appear in the table as 500 r + 200 r, 500 r + 500 r, and 500 r + 1000 r. The data for the 500-r clones before the second irradiation (or 9 months earlier) appear in the column labeled "500 r." The mean cell number over a 7-day period for all groups appears in Table 56, and the 500-r data before the first irradiation, and after a second dose of 500 r, are plotted in Figures 89 and 90. The data indicate that the mean doubling time is longer for the clones 9 months after the first irradiation

than for the control stemline B-2 (1.5 days). The doubling time was 1.75 days for Clone 3, 2 days for Clone 10, and 3.3 days for Clone 8. Clone 3 appeared to be less radiosensitive than Clone 10, and Clone 8 was the most sensitive. The second dose of 500 r depressed the growth rates considerably, and in the order of sensitivity of the clones. Reirradiating the 500-r clones lengthened the doubling time even more. In addition, growth rates of the individual clones were found to be inversely related to the frequency of chromosome aberrations.

TABLE 56

Cell number of stemline control (B-2) and 500-r clones before and after irradiation

Time, days	Number of cells, 1 x 10^4										
	B-2	Clone 3				Clone 8			Clone 10		
	Control	500 r*	500 r + 200 r**	500 r + 500 r**	500 r + 1 Kr**	500 r*	500 r + 200 r**	500 r + 500 r**	500 r*	500 r + 200 r**	500 r + 500 r**
0	1.5	4.0	4.0	4.0	4.0	1.9	1.9	1.9	3.8	3.8	3.8
1	2.4	6.1	4.7	4.6	4.5	2.7	1.9	1.6	4.9	4.8	5.1
2	3.1	9.1	6.8	5.8	4.9	2.9	2.6	1.8	7.9	6.6	6.4
3	-	13.0	8.4	6.1	5.1	3.5	3.0	1.9	-	-	-
4	9.3	19.4	10.1	13.0	3.4	5.0	3.6	2.1	16.0	11.2	6.7
5	13.9	-	-	-	-	-	-	-	-	16.2	7.1
6	26.4	25.0	8.3	7.3	2.2	8.0	5.8	2.5	28.0	22.0	9.0
7	-	-	-	-	-	16.0	5.6	1.7	42.0	31.0	17.0

* Initial irradiation of 500 r only.

** Initial irradiation of 500 r, followed 8 months later by a second irradiation.

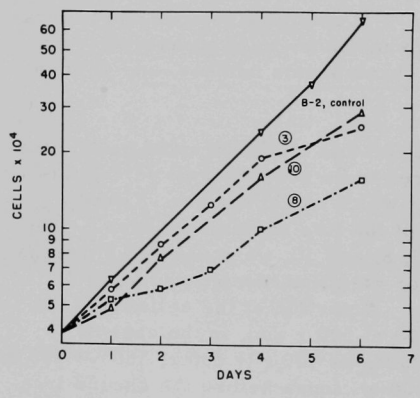

Figure 89. Growth curves of the stemline (B-2) and Clones 3, 10 and 8 eight months after 500 r.

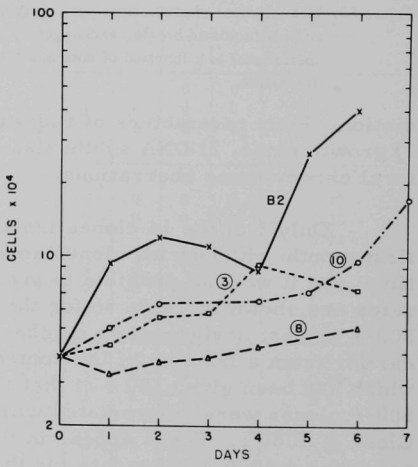

Figure 90. Growth curves of the stemline (B-2) and Clones 3, 10 and 8. Points were taken immediately after irradiation with 500 r, given eight months after a first dose of 500 r.

DNA Synthesis

While the growth rates were being investigated, the rates of DNA synthesis of the 500-r clones were studied by flash labeling with tritiated thymidine. Table 57 shows the extent of incorporation of tritiated thymidine by the control stemline B-2 cells and by the 500-r clone cells. A comparison of the stemline B-2 control and B-2 500-r (given at the time the 500-r clones received a second 500 r), as well as the data for the 500-r clones before (designated 500 r) and after the second 500 r (designated as 500 r + 500 r) are shown in Table 57 and Figure 91. The data indicate that the percentage of cells incorporating tritiated thymidine is depressed below the stemline B-2 control values for Clones 14 and 8 both before and after the second 500 r. Clone 14 showed the greatest depression. Clone 8 showed a marked depression in thymidine uptake after the second 500 r, whereas the uptake was lower in the B-2 cells after the first 500 r than in

TABLE 57

The mean percentage of pig kidney cells labeled before and after the second dose of 500 r

Hours after irradiation	Percentage of cells labeled							
	B-2		Clone 8		Clone 10		Clone 14	
	Control	500 r	500 r	500 r + 500 r	500 r	500 r + 500 r	500 r	500 r + 500 r
0	35.2	35.2	36.5	36.5	40.3	40.3	20.8	20.8
6	50.4	40.5	40.2	50.9	60.2	54.8	22.4	35.0
24	48.5	38.1	57.8	34.8	76.8	59.6	32.4	29.1
48	65.9	46.5	-	33.0	77.7	66.2	39.7	33.7
72	80.6	48.0	64.9	29.5	-	-	-	-
120	45.5	43.1	40.0	23.6	25.8	33.9	-	-
144	39.5	27.7	-	14.1	31.0	32.7	32.0	1.26
216	-	-	-	-	-	-	11.4	1.56

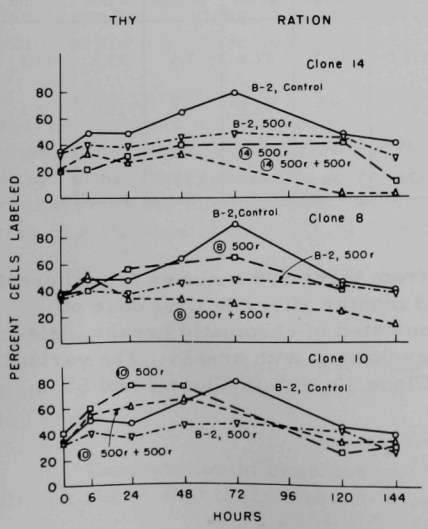

Figure 91

Thymidine incorporation of 3 clones isolated from irradiated stemline B-2 and cultivated for 8 months, compared with unirradiated and irradiated stemline. Percent of labeled cells is plotted against hours after time of second irradiation. B-2 control: unirradiated stemline. B-2, 500 r: stemline irradiated at 0 hr. 500 r: clone from previously irradiated culture. 500 r + 500 r: same, irradiated at 0 hr.

the 500-r clone. The percentage of cells incorporating tritiated thymidine was higher in Clone 10 than in the stemline groups and other clones, whether before or after the second dose of 500 r. The reason for the increase in the proportion of labeled cells in Clone 10 during a 2-day period is not clear, but it could mean either that the synthetic phase is occupying a greater proportion of the intermitotic time, or that a greater proportion of cells is in the synthetic phase at the time of observation due to a synchrony induced by the experimental conditions. In either instance the situation could be caused by a biochemical lesion.

Late Chromosome Aberrations

The chromosomes of four of the 500 r clones were examined for aberrations 8 and 13 months after the initial irradiation (Table 58). In all cases except Clone 3 the percent of cells with aberrant chromosomes and permanent chromosome aberrations (translocations) was lower at 13 months than at 8 months. Clone 10, which exhibited an increase in the percent of cells utilizing tritiated thymidne, also had the highest percentage of cells with permanent chromosome aberrations. Clone 14 was the only clone which showed a shift of the modal chromosome number, which decreased from 37 to 35 at 13 months.

TABLE 58

Chromosome aberrations persisting in Clones 3, 10, 8, and 14 eight and thirteen months after 500 r of X-rays

Clones	#3		#10		#8		#14	
	8 mo	13 mo	8 mo	13 mo	8 mo	13 mo	8 mo	13 mo
Percent cells with aberrant chromosomes*	5.3	18.2	52.0	36.0	27.2	7.5	17.5	13.3
Percent cells with permanent chromosome aberrations*	5.3	13.6	47.7	2.3	15.2	7.5	15.0	3.3
Chromosomes, modal number	37	37	37	37	37	37	37	35
Percent at modal number	68	53	70	70	64	72	60	69

*In excess of stemline.

Early examination of the cells from these 500 r clones for different types of aberrations were made 1 and 3 months after the first dose of X-ray. At this time the aberrations consisted of chromatid breaks, deletions, exchanges (translocations), and exchanges with breaks. The variant chromosomes were as high as 50% in Clone 10, 36% in Clone 8 and 5% in Clone 3.

Discussion

It will be noted that while all of the several clones derived from the stemline a month after it was irradiated were cytologically abnormal and showed depression in their growth rates, the stemline after eight or more months had recovered its original growth rate and other visible characteristics, including response to irradiation. Since all of the aberrant clones taken at one month either died out or showed persistently retarded growth rates, it may be assumed that a majority of aberrant cells was present after a month, but that during the ensuing several months they were almost entirely overgrown by the competing uninjured survivors.

This is in contrast to the situation prevailing in in vivo blood-cell formation,[26] where the long-term persistence of a rather stable percentage of aberrant cells has been indicated. This would appear to find an explanation along the following lines: in vitro, all cells are in competition, and the more slowly growing ones are gradually eliminated, while in vivo, the cells under observation are derived from stem cells which are not in the same sort of competition and which, if injured, may continue indefinitely to yield descendants showing evidence of this injury.

It is of particular interest that the dose-effect relation for the various types of chromosome anomaly varies with time after irradiation, and comes much closer to the theoretical relationships at 30 hr than at 24 hr. We have indicated that this may be due to differences in effects of irradiation on mitotic and intermitotic times and on the relative probabilities of appearance of abnormalities at given times after irradiation. This finding makes it clear that in examining dose-effect relationships, the factor of time after irradiation must be carefully evaluated and controlled.

The persisting breaks in clones after long-term cultivation are of interest because of the high frequency of apparently identical single-chromatid breaks, the predominant form of lesion seen under these conditions. It seems reasonable to assume that these are due to an inherent weakness in the chromosome, which frequently but not invariably gives rise to a chromatid having a visible break.

Summary

A culture of diploid pig kidney cells (37 chromosomes) was irradiated with various X-ray dosages. The estimated D_0 of this line is 180 rads.

Examination of chromosome aberrations 24, 27 and 30 hr after irradiation shows that their frequency increases not only with dose but with

time after irradiation; this is most marked after the higher doses, so that a theoretical dose-effect relation is approached only after 30 hr. At this time, 200 r produces an average of more than one break per cell, and 500 r two or more breaks per cell.

Clones started one month after irradiation and kept under cultivation for 8 or 9 months have variously reduced growth rates, persisting chromosome aberrations, and various alterations in the pattern of thymidine uptake. The growth rates of these clones were inversely related to the frequency of aberrations.

When the stemline was reirradiated after 9 months' cultivation it showed the same temporary retardation of growth as it did originally; reirradiation of 4 of the 5 surviving clones showed a reduction in growth rate that was of longer duration, and more marked in the slower growing ones.

The aberrations in the clones, which persisted after several months, were predominantly chromatid breaks or gaps, and in many cases the same break (gap) was seen repeatedly at a particular site on the chromatid.

References

1. Catcheside, D. G. Frequency of induced structural changes in the chromosomes of Drosophila. J. Genet. 36, 307-320 (1938).

2. Mickey, G. H. Effect of temperature on frequency of translocations produced by X-rays in Drosophila. Genetics 23, 160-162 (1938).

3. Muller, H. J. Analysis of process of structural change in chromosomes of Drosophila. J. Genet. 40, 1-66 (1940).

4. Koller, P. C. and I. A. R. S. Ahmed. X-ray induced structural changes in chromosomes of Drosophila pseudoobscura. J. Genet, 44, 53-55 (1942).

5. Kaufmann, B. P. Distribution of induced breaks along the X chromosomes of Drosophila. Proc. Natl. Acad. Sci. U. S. 25, 571-577 (1939).

6. Kaufmann, B. P. and M. Demerec. Frequency of induced breaks in chromosomes of Drosophila. Proc. Natl. Acad. Sci. U. S. 23, 484-486 (1937).

7. Bauer, H., M. Demerec, and B. P. Kaufmann. X-ray induced chromosomal alterations in Drosophila melanogaster. Genetics 23, 610-630 (1938).

8. Marshak, A. Alteration of chromosomal sensitivity to X-rays with NH_4OH. Proc. Soc. Exp. Biol. Med. 38, 705-713 (1938).

9. Sax, K. and E. V. Enzmann. Effect of temperature on X-ray induced chromosome aberrations. Proc. Natl. Acad. Sci. U. S. 25, 397-399 (1939).

10. Revell, S. H. The accurate estimation of chromatid aberrations and its relevance to a new interpretation of chromatid aberrations induced by ionizing radiations. Proc. Roy. Soc. (London) B 150, 563-589 (1959).

11. Newcombe, H. B. Effects of X-rays on chromosomes. J. Genet. 43, 145-147 (1942).

12. Sax, K. Behaviour of X-ray-induced chromosomal aberrations in onion root-tips. Genetics 26, 418-421 (1941).

13. Carlson, J. G. Mitotic behavior of induced chromosomal fragments lacking spindle attachments in the neuroblast of the grasshopper. Proc. Natl. Acad. Sci. U. S. 24, 500-507 (1938).

14. Stroud, A. N., A. M. Brues, and B. R. Svoboda. DNA synthesis in mammalian kidney cells in tissue culture after single and periodic doses of irradiation. Ann. N. Y. Acad. Sci. 97, 942-959 (1961).

15. Bender, M. A. X-ray-induced chromosome aberrations in normal diploid human tissue cultures. Science 126, 974-975 (1957).

16. Bender, M. A. X-ray-induced chromosome aberrations in mammalian cells in vivo and in vitro. Low Level Effects of Ionizing Radiations, ed. A. A. Buzzati-Traverso. Intern. J. Radiation Biol. (Suppl.) 103-118 (1960).

17. Bender, M. A. and S. Wolff. X-ray-induced chromosome aberrations and reproductive death in mammalian cells. Am. Naturalist, 95, 39-52 (1961).

18. Wakonig, R. and D. K. Ford. Chromosome aberrations in irradiated cells of Chinese hamster grown in tissue culture. Can. J. Zool. 38, 203-207 (1960).

19. Puck, T. T. Action of radiation on mammalian cells. III. Relationship between reproductive death and induction of chromosome anomalies by X-irradiation of euploid and human cells in vitro. Proc. Natl. Acad. Sci. U. S. 44, 772-780 (1958).

20. Puck, T. T. Growth and genetics of somatic mammalian cells in vitro. J. Cell. Comp. Physiol. 52, 287-292 (1958).

21. Chu, E. H. Y. and N. H. Giles. Comparative chromosomal studies on mammalian cells in culture. I. The HeLa Strain and its mutant clonal derivatives. J. Natl. Cancer Inst. 20, 383-401 (1958).

22. Fogh, J., J. L. Biedler, and A. R. T. Denues. X-ray effects on cultured human amnion cells. Ann. N. Y. Acad. Sci. 95, 758-773 (1961).

23. Ohnuki, Y., A. Awa, and C. M. Pomerat. Chromosomal studies on irradiated leukocytes. Ann. N. Y. Acad. Sci. 95, 882-900 (1961).

24. Munro, T. R. Irradiation of selected parts of single cells. Ann. N. Y. Acad. Sci. 95, 920-931 (1961).

25. Lea, D. E. Actions of Radiations on Living Cells. 1st ed. Cambridge University Press, Cambridge, 1947.

26. Bender, M. A. and P. C. Gooch. Persistent chromosome aberrations in irradiated human subjects. Radiation Research 16, 44-53 (1962).

UTILIZATION OF DNA AND RNA PRECURSORS AS INDICATORS OF DRUG EFFECT ON CANCER CELLS

Agnes N. Stroud, Gerald O. McDonald,* Beverly R. Svoboda, and Austin M. Brues

Experiments have been carried out to study the effects of anticancer drugs on DNA and RNA synthesis in several mouse tumor systems, using tritium-labeled thymidine and uridine. Using these labeled precursors we have measured the biochemical damage to cells resulting from four drugs: 5-fluorouracil (5-FU), actinomycin D (ACTD), nitrogen mustard (HN-2), and triethylenethiophosphoramide (TSPA). These measurements were made at two different time intervals, using a single concentration or amount of each drug. Further experiments are in progress using different concentrations of the agents and other time intervals.

In vivo and in vitro experiments were performed using two mouse tumors; the Ehrlich ascites carcinoma, and the Andervont breast carcinoma. The in vitro preparations included cell cultures, cell suspensions, and tissue slices.

Our results show a lack of correlation between in vitro and in vivo labeling of ascites tumor cells with thymidine, possibly because of different metabolic conditions depending on the techniques and media used. Labeling of cells in vitro continues throughout the period of exposure to the radioactive nucleosides, in contrast to the "flash labeling" by an in vivo injection. Synthesis of DNA was effectively inhibited by all drugs as shown by alterations in the uptake of tritiated thymidine and uridine.

Methods

Preliminary studies were made using human tumors in primary short-term culture. It became obvious that extensive background information had to be obtained from animal tumor systems in which replicate experiments could be made. Two transplanted mammary tumors were used: the Andervont tumor carried in the C3H mouse as a solid tumor, and the Ehrlich carcinoma in solid or ascites form. For in vitro studies tissue slices and tissue culture preparations of the Andervont tumor were exposed to the drug in stoppered tubes or flasks at 37°C for 24 hr, followed by incubation with the tritiated nucleoside for 1 hr. In the in vivo experiments tumor-bearing mice were injected with the agents, followed 24 hr later by

*Department of Surgery, College of Medicine, University of Illinois, Chicago, Illinois.

an injection with tritiated thymidine or uridine. In the case of the Andervont tumor the animals were injected subcutaneously, whereas with the Ehrlich ascites tumor the drugs and labeled precursors were injected intraperitoneally.

The concentrations of the drugs used in the in vivo and in vitro experiments are found in Table 59.

TABLE 59

Drugs used in the in vivo and in vitro experiments
(Dilution in Tyrode's solution)

5-FU	HN-2	TSPA	ACTD
In vivo, mg/kg body weight			
50	1.0	2.0	0.04
In vitro, mg/liter of nutrient			
263	2.8	7.0	0.35

In the in vivo experiments, the tumors were removed for study 1 hr and 24 hr after drug injections, and 24 hr after the first of 2 drug injections, 5 hr apart. For the in vitro tissue culture experiments the cells were exposed to the drugs for 24 hr.

The labeled compounds used for determining DNA and RNA synthesis were obtained from Schwartz BioResearch Inc. Specific activity of tritiated thymidine was 0.36 curies/millimole and of tritiated uridine was 0.38 curies/millimole. In either case 1 μc/g of animal was injected. For in vitro studies of ascites tumor cells, samples of about 10^8 cells (1 ml of ascitic fluid) were suspended in an equal volume of Eagle's nutrient[1] plus glutamine, containing the drugs; after removal of the drugs, 12.5 to 25 μc of tritiated thymidine or uridine in 2 ml of Eagle's nutrient plus glutamine were added.

For autoradiography, tumor cells exposed to tritiated thymidine or uridine were plated out on glass slides (in the case of ascites tumor), or were sectioned at 6 μ and mounted on glass slides (in the case of solid tumors), or were grown directly on glass coverslips (in the case of tissue cultures). The slides were dipped briefly in warm Kodak Nuclear Track emulsion NTB 3 and placed in a refrigerator in black plastic boxes containing a drying agent until the time of development 7 to 14 days later (ordinarily not over 10 days). For microscopic observations the cells were stained through the emulsion with hematoxylin-eosin; estimates were made

of the percent of cells labeled and of the number of grains per cell. The number of cells counted in each experimental group was 500 or more; for estimation of the number of grains per cell, 25 to 50 cells were studied.

Results

In the Andervont tumor, the extent and rate of incorporation of both tritiated thymidine and uridine by the tissue slices appeared to be correlated with that observed in the solid tumors in vivo. However, with the dosages and the amount of radioactivity used, incorporation was low compared with tissue cultures, and occurred only at the edge of the slice, at the point of greatest exposure to both the drugs and the tritiated compounds. This made quantitative evaluation quite difficult. The cell culture method appeared to be much more sensitive, undoubtedly because of the direct exposure of the cells to the drugs and tritiated compounds, with no competitive action from other body tissues.

Data on the action of the four drugs on thymidine and uridine incorporation in the in vivo system, using the Ehrlich ascites tumor cells, are presented in Table 60 and Figure 92, which show the percent of cells labeled and the average number of grains per cell. In the case of 5-FU, the percent of cells labeled with thymidine or uridine was increased over the control after drug treatment for 24 hr, but not after treatment for 1 hr. The percent of cells labeled after 1-hr and 24-hr treatment with HN-2, TSPA, and ACTD was depressed below the controls. The greatest depression was seen 24 hr after a single injection of HN-2. After 2 injections of any of these 3 drugs, however, the values were comparable with the controls.

TABLE 60

Ehrlich ascites tumor cells in vivo

Duration of drug, hr	Number of drug injections	Cells labeled, mean %					Av number grains				
		Control	5-FU	HN-2	TSPA	ACTD	Control	5-FU	HN-2	TSPA	ACTD
		Thymidine									
1	1	54.2	51.8	15.4	49.3	28.4	76	83	21	46	12
24	1	54.1	85.6	27.0	46.0	37.1	58	101	13	22	43
24	2*	58.7	89.1	59.6	53.8	45.2	66	77	34	28	47
		Uridine									
1	1	45.4	54.9	23.3	-	26.1	28	12	9	-	18
24	1	61.7	84.6	54.9	50.4	71.2	25	60	22	19	18
24	2*	58.0	69.8	62.1	61.4	55.7	25	26	36	14	13

*5 hours apart.

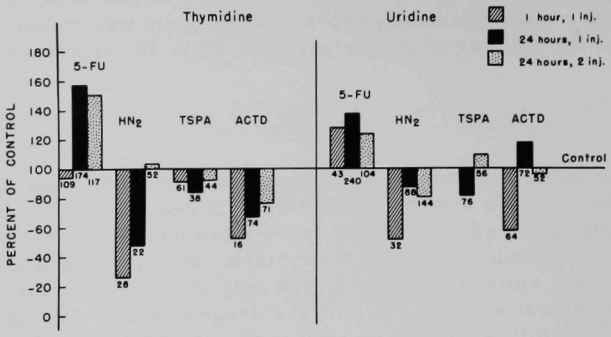

Figure 92. Percent of Ehrlich ascites tumor cells labeled and the average number of grains per cell in vivo. Times indicated are durations of exposure to drugs. Heights of columns indicate the number of cells labeled as percent of controls; figures indicate average grain count per cell.

The rate of DNA synthesis is related to the grain count. After 5-FU and thymidine the average number of grains per cell was above control values at each time interval, but grain counts were very much depressed as compared with the controls, after the other 3 drugs. However, after 2 injections of these 3 drugs variable increases in grain counts were seen.

With 5-FU and uridine the percent of cells labeled was unchanged after 1 hr but increased over control values at 24 hr. With HN-2 and ACTD there was a decrease in the percent of labeled cells with 1-hr treatment and a return to control values at 24 hr (with 2 injections). Cells treated with TSPA followed a similar course.

The average number of grains per cell after uridine decreased to 43% of control value with 5-FU given for 1 hr, whereas there was a significant increase above the control value with 24-hr treatment. There was no change from the control value 24 hr after 2 injections of the drug. A depression in grain counts was seen with the other drugs for any time interval or duration of drug, with the exception of HN-2 at 24 hr (2 injections), where there was a 14% increase over controls.

A comparison of Ehrlich ascites tumor cells in vivo and in vitro following 1-hr exposure to the drugs and thymidine or uridine is shown in Table 61 and Figure 93. The percent of cells labeled with thymidine after 5-FU was the same in vivo as in vitro; however, a greater percentage of cells was labeled after 5-FU in vitro than in the controls. After HN-2 a greater percentage of cells was labeled in vitro than in vivo. The number of HN-2 treated cells labeled in vitro was 120% of the control value; but only 28% of the control value in vivo. The pattern for ACTD was similar to HN-2 in both cases.

TABLE 61

Ehrlich ascites tumor cells in vivo and in vitro

Duration of drug, hr	Number of drug injections	Cells labeled, mean %					Av number grains				
		Control	5-FU	HN-2	TSPA	ACTD	Control	5-FU	HN-2	TSPA	ACTD
		Thymidine									
1[a]	1	54.2	51.8	15.4	-	28.4	76	83	21	46	12
1[b]	1	38.9	50.2	47.0	-	50.6	60	37	31	47	43
		Uridine									
1[a]	1	45.5	54.9	23.3	-	26.1	28	12	9	-	18
1[b]	1	95.4	78.7	89.4	-	81.9	175	175	175	-	112

[a]in vivo
[b]in vitro

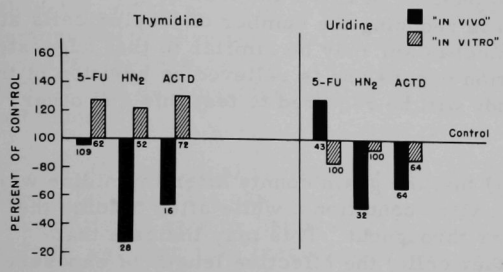

Figure 93

Percent of Ehrlich ascites tumor cells labeled and the average number of grains per cell in vivo and in vitro. Cells were exposed to the drugs for 1 hr. Heights of columns indicate the number of cells labeled as percent of controls; figures indicate average grain count per cell.

The percent of cells labeled by uridine in the in vivo and in vitro controls was quite different. In the in vitro system 95% were labeled, as compared with 45% in vivo. With 5-FU there was an increase of 20% over the control value in vivo, and a decrease to 83% of the control value in vitro. There was a 50% decrease in percent labeled cells after treatment with either HN-2 or ACTD in vivo, and a less significant decrease in vitro. In the controls after uridine the average grain count was 175 in vitro, but only 28 in vivo. The grain counts after uridine and 5-FU were less than half of the control in vivo, but unchanged in vitro. A similar decrease in grain counts was observed in vivo for HN-2 and ACTD, without much difference from the control value in vitro.

Discussion

In evaluating these results it must be kept in mind that the percentage of cells that are labeled is a measure of the number in the synthetic phase during the one-hr period of labeling (probably somewhat less in the observation in vivo) and that the grain count indicates the rate at which the labeled precursors are incorporated into the DNA that is being synthesized in these cells.

Both of these indicators were sharply reduced in vivo where thymidine was the precursor and HN-2 and ACTD were the drugs. Where uridine was the precursor, the picture was similar except that the reduction in number of synthesizing cells was more transitory.

With 5-FU, there were increases in the rate of incorporation and in the number of cells in the synthetic period. The former may be associated with depletion of endogenous thymidine and uridine due to interference by the drug with de novo synthesis. The increase in the number of labeled cells indicates that a synchrony exists; this might be due to an accumulation of cells in G_1 phase (before DNA synthesis) which pass into synthesis when the tracer thymidine and its carrier are given, or to an accumulation in S phase (during DNA synthesis). We have also noticed some accumulation of cells in mitosis, as indicated by a higher proportion of metaphases.

It is not clear why two injections of HN-2 and ACTD were less effective than a single injection in reducing the number of labeled cells at 24 hr. It is possible that the mechanism may be similar to that suggested for 5-FU, namely, that a depletion occurs and is relieved by addition of the labeled compound. Further study will be required to test this and other possible explanations.

We have noted (Table 61) that the grain counts after thymidine were comparable under in vivo and in vitro conditions, while after uridine the in vitro counts were much higher throughout. This may indicate that (because of competition from other cells) the effective length of exposure of cells to uridine after a single injection is much shorter than is the case with thymidine. This might also account for the lower percentages of labeled cells in ascitic fluid.

Reference

1. Eagle, H. The specific amino acid requirements of mammalian cells (strain L) in tissue culture. J. Biol. Chem. 214, 839-841, 1955.

CHROMOSOME STUDIES OF VARIOUS STRAINS OF HUMAN TUMORS H.Ad.1 AND H.Ep.3 MAINTAINED IN RODENTS

Agnes N. Stroud, Beverly R. Svoboda, and Harold B. Haley*

Conditioning of rats and hamsters with cortisone and total-body irradiation has made it possible to maintain a small number of human tumors in laboratory animals.(1) Toolan first isolated human tumor H.Ep.3 in 1953(2) and H.Ad.1 in 1955.(3) Since that time, these tumors have been maintained in her laboratory and in the laboratories of other workers in heterologous hosts, with, however, varying growth characteristics.(4) This communication reports chromosome studies of these two tumors with two objects in mind: 1) to see whether the differing behavior of these tumors in different laboratories can be accounted for on the basis of chromosomal changes, and 2) to examine the chromosome karyotypes of these human tumors which have been maintained in laboratory animals for more than 5 years. In 1956 Levan(5) reported a chromosome structure of tumor H.Ep.3; the chromosome number of H.Ad.1 has not been previously published.

The principal variation in growth patterns of the same tumor in different laboratories has been in the ability of the tumor to grow in normal unconditioned rats or hamsters. In the original laboratory H.Ad.1 will grow only in weanling rats treated with total-body irradiation and cortisone or in weanling hamsters treated with cortisone. In the laboratory of Dr. David Yohn, at the University of Pittsburgh,(4) this tumor has been maintained for more than 45 transplant generations in the cheek pouches of normal untreated hamsters.

One of us (H.B.H.) is maintaining the tumor in conditioned animals at Loyola University. When taken from a conditioned weanling rat and transplanted subcutaneously as a cell suspension into either 60-g or 200-g untreated rats, the tumor will grow for 2 or 3 weeks as well as it grows in the conditioned rat. After this time, regression takes place, and in most animals the tumor has completely regressed 4 weeks after implantation. In the conditioned rat, no further growth occurs after the 2- to 3-week period, but the tumor mass usually remains constant in size for many months. In the normal rat, if the tumor is taken after 2 weeks of growth and transplanted to a second generation of normal rat, tumor growth will occur, although it is usually significantly smaller than in the first generation. When this process is repeated to a third generation, insufficient growth occurs to allow subsequent passage.

---

*Department of Surgery, Stritch School of Medicine of Loyola University, Chicago, Illinois.

We have found H.Ep.3 to behave similarly in our laboratory (H.B.H.), and it has not grown in normal animals in Toolan's laboratory. Such differences in transplantation behavior could be due to changes in the tumor or to variations in defense mechanisms in different strains or substrains of host animals.

Methods

The basic structure of the H.Ad.1 tumor consists of small clusters of tumor cells enclosed in connective-tissue capsules. The connective-tissue capsule is so firm that individual cells cannot be easily separated to provide satisfactory "squash" preparations for chromosome analysis. Various combinations of trypsin, Versene, and hyaluronidase have been used unsuccessfully. This tumor does not grow well intraperitoneally; however, for purposes of these experiments, intraperitoneal preparations have been made as follows. H.Ad.1 stock in our laboratory (H.B.H.) has been maintained since 1958 in Wistar rats obtained from the Abrams Small Stock Breeders. A tumor is taken at 10-14 days of growth from a stock animal; a suspension of tumor cells is made and injected intraperitoneally into an Abrams weanling rat. At 3 or 4 days after injection, the abdomen is opened and the peritoneal fluid containing tumor cells is aspirated and used for chromosome preparations. H.Ad.1 was received by us again from Dr. Toolan's laboratory in 1961 in the strain of Wistar rats that she usually used. When the tumor was of proper size, a similar cell suspension was made. Part of the suspension was injected intraperitoneally into Abrams Wistar rats and the peritoneal fluid was withdrawn 3 or 4 days later for chromosome studies. The other part of the cell suspension was injected subcutaneously into conditioned Carworth Farms Wistar rats to maintain the tumor line in our laboratory (H.B.H.) but not in the animals received from our usual supplier. H.Ad.1 was also received by us from Dr. David Yohn as carried in hamster cheek pouches. The same procedure was carried out to obtain peritoneal fluid containing free tumor cells.

H.Ep.3 was studied in our laboratory (H.B.H.) two years after receiving it from Toolan, and also immediately after receiving a second supply of animals. H.Ep.3 contains less connective tissue, and, hence, adequate chromosome preparations can be made from subcutaneous solid tumors.

The chromosome smear technique used in this study is a modification of that of Moorhead,[6] and Hsu and Klatt.[7] Rats bearing the tumor as a solid or an ascites were injected with 2 μg of Colcemide (Ciba) per g body weight prepared in Hank's balanced salt solution. At the end of 4 hr, the tumors were removed, and in the case of the ascites the ascitic fluid was centrifuged and decanted. The cells were washed twice in Tyrode's salt solution (minus magnesium and calcium), placed in a centrifuge tube containing 10 ml of 0.25% trypsin-Versene solution, and incubated at 37°C for 15 to 30 min. After this time the suspension was mixed by pipetting

vigorously. Following this the cells and supernatant were poured through a fine nylon mesh to remove fragments of tissue not broken up by this procedure. The cells and supernatant were then centrifuged, decanted, and washed in 5 ml of warm Hank's solution, leaving 0.5 ml after the last wash, and adding 1.5 ml of warm distilled water to form a hypotonic solution. After 3 min in the hypotonic solution the cells were centrifuged for 5 min; the supernatant solution was then decanted, after which 5 ml of fresh fixative solution (absolute ethanol, 3 parts, glacial acetic acid, 1 part) was added to the pellet and left undisturbed for 20 min. Following this, the cells were centrifuged, the fixative was decanted, and the cells were resuspended in fixative and centrifuged for 5 min. To the pellet of cells was added 0.5-1.0 ml fixative; they were then plated out on precleaned glass slides which had been dipped in cold ice water. The cells were allowed to air-dry on the slides and for immediate observations were stained with a 2% solution of Gurr's synthetic Orcein. We found about 10-15% of the chromosomes spread at metaphase to be uncountable. For this study 30 or more cells were scored in each line.

Results

H.Ep.3 Tumor

Levan reported in 1956 that the chromosome number of H.Ep.3 was 69 with a range of 64-74.[5] The chromosomes were characteristic of the human. He consistently found 3 or 4 chromosomes carrying satellites, which he considered sufficiently distinctive to be used as markers for this tumor.

We examined the metaphase chromosome spreads for H.Ep.3 both as carried currently in Toolan's laboratory (Figure 94) and as carried by us 45 successive passages away from Toolan's laboratory (Figure 95). H.Ep.3 appeared to have essentially the same chromosome distribution as reported by Dr. Levan five years ago (Figures 94 and 95); the marker satellites were as he described. In the same tumor suspensions were found cells with 69 chromosomes that appeared typically human, plus satellites, and, also in the same tissue, other cells with 42 chromosomes of typical rat morphology. The tissue of origin of these rat cells was not obvious on morphological grounds although it might be assumed that they arose from stroma. A few cells were seen with the tetraploid number (138) of chromosomes.

Although the chromosome number of the typically human chromosomes is still 69 as in Toolan's laboratory, the range is much wider, from 53 to 75 (Figures 94 and 95). A few cells were seen carrying 35 chromosomes.

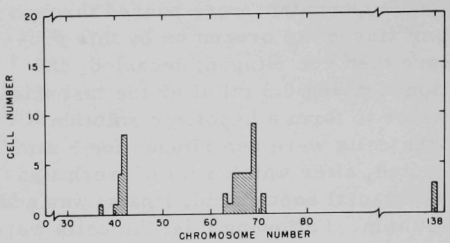

Figure 94

Chromosome modal number distribution in cells of human tumor H.Ep.3 as maintained in Toolan's laboratory in 1961.

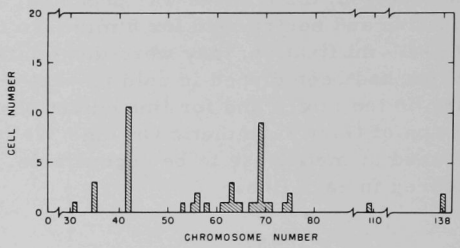

Figure 95

Chromosome modal number distribution of human tumor H.Ep.3 as maintained in Haley's laboratory, 45 transplant generations after it was received from Dr. Toolan in 1960.

The satellites noted by Levan,[5] which are evident in both of these lines of H.Ep.3, appear to be present on the larger acrocentric chromosomes, primarily of autsome pair 13.[8,9] Satellites are now recognized as being normally present on the human acrocentric chromosome pairs 13, 14, 15, 21, and 22.[10,11] H.Ep.3, with the triploid chromosome number of 69, has remained relatively constant since Levan's study, which incidentally was apparently one of the earlier demonstrations of satellites of human chromosomes.

Figure 96. Distribution of H.Ad.1 cells with various chromosome numbers. Open bars, tumors maintained in Toolan's laboratory in 1961; shaded bars, tumor maintained in Haley's laboratory for 40+ transplant generations after it was received from Dr. Toolan in 1958.

H.Ad.1 Tumor

This tumor was obtained from Dr. Toolan in 1958, and has been maintained in our laboratory (H.B.H.) as H.Ad.1 (Haley);[8] its chromosomes were studied in 1960. The tumor was again received from Toolan in 1961 and is being maintained as H.Ad.1 (Toolan) in our laboratory (H.B.H.). Idiograms of these two lines of H.Ad.1 are shown in Figure 96. Of 48 metaphase cells counted in H.Ad.1 (Haley), 37 had 46 chromosomes, 1 had 43, 5 had 44, 2 had 45, and 1 had 47 chromosomes. Two cells were seen with the tetraploid

number of 92. Thus H.Ad.1 (Haley) has a primary chromosome number of 46 with a small spread around that number. H.Ad.1 (Toolan), on the other hand, has a primary chromosome number of 45 with a few at 43, 44, 46, 47, and 92; 107 metaphase cells were scored. Figure 97 is a karyotype typical of these cells with 45 chromosomes. The missing chromosome is a small acrocentric, presumably from pair 21. One of the X chromosomes is seen to be elongated, suggesting that this is a translocation of a 21 onto an X chromosome. Figure 98 is an idiogram typical of cells with 44 chromosomes. The missing ones are 21 and an X chromosome.

H.Ad.1 (Toolan) seems to have transplantation characteristics differing somewhat from those of H.Ad.1 (Haley). The percentage of tumor "takes" is lower and growth is not as good. It must be emphasized again that we are carrying the two strains of H.Ad.1 in Wistar rats from different sources. The two strains of Wistar rats behave differently in cages and when handled, indicating that these two Wistar strains are no longer identical. Presumably, differences in host defense mechanisms could also be present.

Discussion

The chromosome karyotypes of two strains of tumor H.Ep.3 which have been maintained separately for more than 45 transplant generations are compared with those reported for the same tumor by Levan in 1956,[5] and the chromosome patterns of all three are remarkably similar. The stability of chromosome pattern in this tumor for over five years would appear to be established and to be significant. The stability of the satellites on the chromosomes has also been demonstrated. While Levan felt that these were distinctive,[5] more recent studies suggest that they are found normally on specific human chromosomes.[10,11]

Interpretation of our findings with tumor H.Ad.1 is less simple. Chromosome differences have been demonstrated, but direct correlation of these with transplantation behavior is not yet possible. The general consistency of chromosome karyotype through many animal passages, as shown with H.Ep.3, was also shown in 1961 in the H.Ad.1 strain received by us in 1958 (H.Ad.1 Haley) and carried by Dr. Toolan prior to and since that time. The changes found in the more recently received strain are definite. The primary chromosome number of 45 in this strain (H.Ad.1 Toolan) appears established. It has been recently shown [10-12] that the nucleolus-organizing, acrocentric chromosomes of man (pairs number 13, 14, 15, 21, and 22) are particularly susceptible to development of abnormalities. Translocation mongolism and the Ph' chromosome of chronic myeloid leukemia represent types of translocations within the acrocentric chromosomes, particularly chromosome 21.[10] Our strain H.Ad. 1 (Toolan) shows the absence of a small acrocentric chromosome (chromosome 21 or 22); one of the

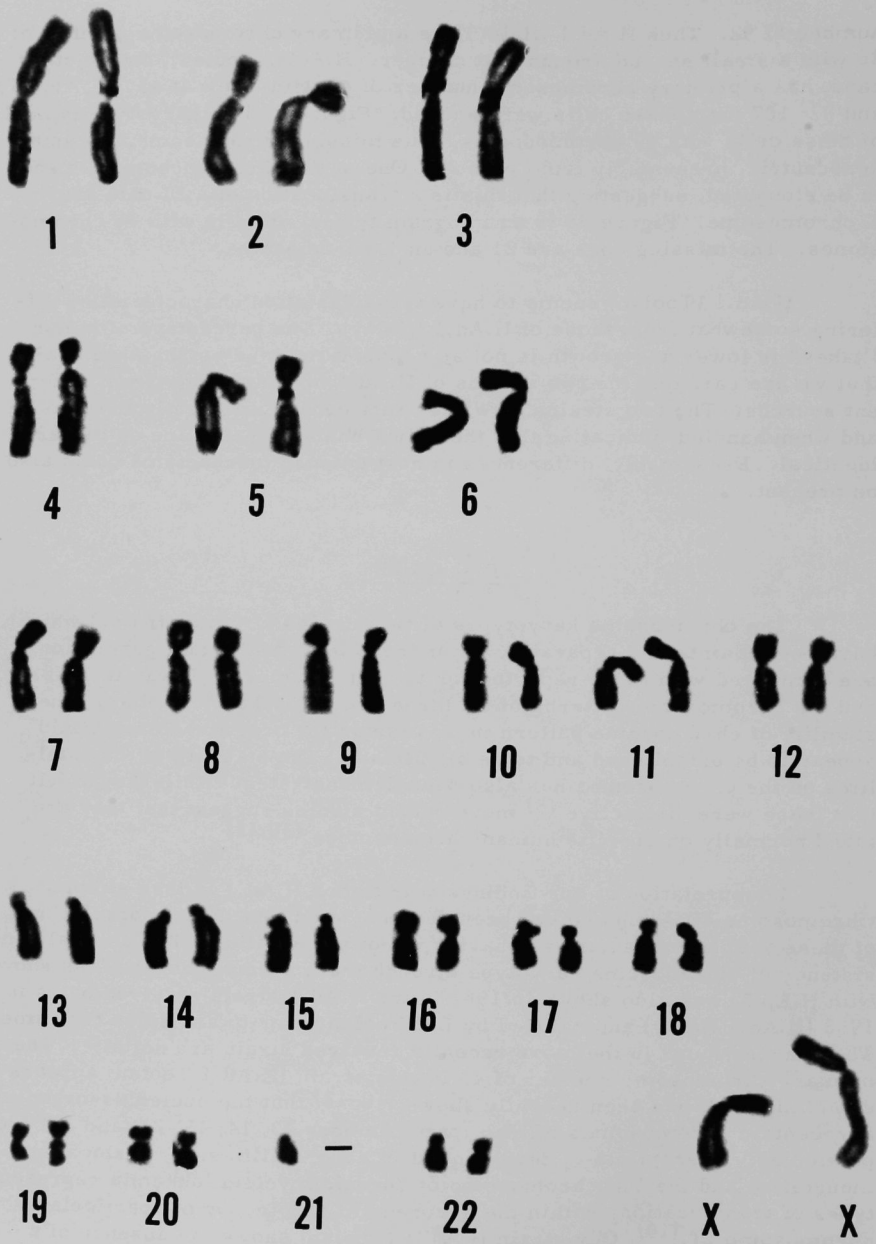

Figure 97. Karyotype of an H.Ad.1 cell with 45 chromosomes. Note the absent 21 and the elongated X chromosome (Denver classification).

Figure 98. Karyotype of an H.Ad.1 cell with 44 chromosomes. The absent chromosomes are seen to be a 21 and an X (Denver classification).

X chromosomes however has an apparent increase in the length of its long arms, possibly attributable to translocation of the missing small acrocentric chromosome to the X chromosome.

All tumors examined showed a small number of cells with tetraploid chromosomes. Several preparations contained not only cells with human chromosomes but others with 42 typical rat chromosomes. A few human cells also had 42 chromosomes. Differentiation between the two was made by karyotype identification. Cells with 35 chromosomes were frequently found in metaphase spreads from various tumors; idiograms did not define their type, so these remain as unexplained phenomena.

References

1. Toolan, H. W. Growth of human tumors in cortisone-treated laboratory animals. Cancer Research 13, 389-394 (1953).

2. Toolan, H. W. Transplantable human neoplasms maintained in cortisone-treated laboratory animals: H.S. #1, H.Ep.#1, H.Ep.#2, H.Ep.#3, and H.Emb.Rh.#1. Cancer Research 14, 660-666 (1954).

3. Toolan, H. W. Permanently transplantable human tumors maintained in conditioned heterologous hosts: H.Chon.#1, H.Ep.#4, and H.Ad.#1. Cancer Research 17, 418-420 (1957).

4. Yohn, D.S., W. McD. Hammon, R. W. Atchison, and B. C. Casto. Serial heterotransplantation of human adenocarcinoma #1 in the cheek pouch of unconditioned adult Syrian hamsters. Cancer Research 22, 443-448 (1962).

5. Levan, A. Chromosome studies on some human tumors and tissues of normal origin grown in vivo and vitro at the Sloan-Kettering Institute. Cancer 9, 648-663 (1956).

6. Moorhead, P. S., P. C. Nowell, W. J. Mellman, D. M. Battyrs, and D. A. Hungerford. Chromosome preparations of leukocytes cultured from human peripheral blood. Exptl. Cell Research 20, 613-616 (1960).

7. Hsu, T. G., and O. Klatt. Mammalian chromosomes in vitro. IX. On genetic polymorphism in cell populations. J. Natl. Cancer Inst. 21, 437-473 (1957).

8. Haley, H. B., and A. N. Stroud. 1961. Studies of human tumor karyotype during heterologous growth. Proc. Am. Assoc. Cancer Research 3, 153 (1961).

9. A proposed standard system of nomenclature of human mitotic chromosomes. Lancet 1, 1063-1065 (1960).

10. Ohno, S., J. M. Trujillo, W. D. Kaplan, and R. Kinosita. Nucleolus-organisers in the causation of chromosome anomalies in man. Lancet 2, 123-126 (1961).

11. Cooper, H. L. II. The use of human chromosome markers in linkage studies. Trans. N. Y. Acad. Sci. 24, 383-394 (1962).

12. Miller, O. J., B. B. Mukherjee, and W. R. Berg. Normal variations in the human karyotype. Trans. N. Y. Acad. Sci. 24, 372-382 (1962).

PUBLICATIONS

January 1, 1962 through June 30, 1962

Amarose, A. P. and D. M. Czajka. Cytopathic effects of deuterium oxide on the male gonads of the mouse and dog. Exptl. Cell Research 26, 43-61 (1962).

Baserga, Renato and W. E. Kisieleski. Comparative study of the kinetics of cellular proliferation of normal and tumorous tissues with the use of tritiated thymidine. I. Dilution of the label and migration of labeled cells. J. Natl. Cancer Inst. 28, 331-339 (1962).

Baserga, Renato, G. C. Henegar, W. E. Kisieleski and Herman Lisco. Uptake of tritiated thymidine by human tumors *in vivo*. Lab. Invest. 11, 360-364 (1962).

Bendigkeit, H. E., H. E. Kubitschek and L. R. Hedrick. Mutants of *Escherichia coli* showing intermediate resistance to bacteriophage T5. Bacteriol. Proc. 1962, p. 143. Abstract.

Bernstein, E. K. Changes in plasma amino acids during development of x-irradiated chick embryos. Intern. J. Radiation Biol. 3, 449-457 (1961).

Black, C. C., J. F. Turner, M. Gibbs, D. W. Krogmann and S. A. Gordon. Studies on photosynthetic process. II. Action spectra and quantum requirement for triphosphopyridine nucleotide reduction and the formation of adenosine triphosphate by spinach chloroplasts. J. Biol. Chem. 237, 580-583 (1962).

Brar, S. S., P. F. Gustafson, M. A. Kerrigan, B. C. Breidenstein, U. S. Garrigus and W. R. Usborne. Radioactivity in wool. Nature 192, 1094-1095 (1961).

Brar, S. S., A. Jacobson, T. Fields, I. G. Fels, E. Kaplan, P. F. Gustafson and Y. T. Oester. Practical application of neutron activation analysis for the determination of protein bound metals in blood serum. J. Nuclear Med. 2, 289-296 (1961).

Cater, D. B., Renato Baserga and Herman Lisco. Radiographic appearances of bone lesions in rats exposed to local external irradiation from gamma rays. The Year Book of Radiology, eds. J. F. Holt, W. M. Whitehouse, H. W. Jacox and M. M. Ligerman. Year Book Medical Publrs., Chicago, 1962. pp. 81-82.

PUBLICATIONS (Contd.)

Daniels, E. W. Limits of transplantation tolerance in large amoebae. I. Microfusion studies using Amoeba proteus, Pelomyxa illinoisensis, and three strains of Pelomyxa carolinensis. J. Protozool. 9, 183-187 (1962).

Driml, Marilyn. Electron and light microscope studies of Endamoeba terrapina. Proc. Iowa Acad. Sci. 68, 581-585 (1962).

Duerre, J. A. and F. Schlenk. Formation and metabolism of S-adenosyl-L-homocysteine in yeast. Arch. Biochem. Biophys. 96, 575-579 (1962).

Duerre, J. A. Preparation and properties of S-adenosyl-L-homocysteine, S-adenosyl-L-homocysteine sulfoxide and S-ribosyl-L-homocysteine. Arch. Biochem. Biophys. 96, 70-76 (1962).

Ehret, C. F. Radiobiology. The American Peoples Encyclopedia Yearbook. Spencer Press, Chicago, 1961. pp. 775-778.

Ehret, C. F., G. De Haller and R. Naef. Method of embedding and ultramicrotomy designed for study of development of organelles in an isolated cell. Experientia 17, 524 (1961).

Ehret, C. F. Photoreactivation of ultraviolet-induced conjugation delay in paramecium. Progress in photobiology. Proc. 3rd Intern. Congr. on Photobiology, Copenhagen, July 31 - August 5, 1960, eds. B. Christensen and B. Buchmann. Elsevier Publ. Co, Amsterdam, 1961. pp. 287-288.

Feinstein, R. N. and Ulrith Hagen. Stabilization and augmentation of the neutral deoxyribonuclease in mammalian tissues. Biochem. Biophys. Acta 55, 56-62 (1962).

Frigerio, N. A. Neutron penetration during neutron capture therapy. Phys. in Med. and Biol. 6, 541-549 (1962).

Frigerio, N. A. Prevention of spattering during high temperature ignitions. Chemist-Analyst 51, 30 (1962).

Frigerio, N. A. Fabricating thin neutron foils. Nucleonics 20 (3), 78 (1962). Note.

Frigerio, N. A. Vapor pressure measurements. J. Chem. Educ. 39, 35-36 (1962).

PUBLICATIONS (Contd.)

Frigerio, N. A. and T. P. Hettinger. Protein solubility in solvent mixtures of low dielectric constant. Biochim. Biophys. Acta 59, 228-230 (1962). Letter.

Fry, R. J. M., Samuel Lesher and H. I. Kohn. Influence of age on the transit time of cells of the mouse intestinal epithelium. III. Ileum. Lab. Invest. 11, 289-293 (1962).

Garber, E. D., W. F. Redding and William Chorney. Separation of anthocyanins by cellulose column chromatography. Nature 193, 801-802 (1962). Letter.

Ginski, J. M., J. F. Thomson and Akira Omachi. Phosphate release from dog erythrocytes. Am. J. Physiol. 202, 981-983 (1962).

Gordon, S. A. and Kenneth Surrey. Phosphorylation and red-spectrum photomorphogenesis effects of ionizing radiations on seeds. Proc. Symp. on the Effects of Ionizing Radiations on Seeds and Their Significance in Crop Improvement, Karlsruhe, Germany, Aug. 8-12, 1960. Intern. Atomic Energy Agency, Vienna, 1961. pp. 189-196.

Gordon, S. A., M. H. L. Ng and K. V. Thimann. The action spectrum for anthocyanin formation in Spirodela oligorrhiza. Plant Physiol. 36 (Suppl.) 46 (1961). Abstract.

Gordon, S. A. and L. G. Paleg. The formation of auxin from tryptophan through the action of polyphenols. Plant Physiol. 36, 838-845 (1961).

Gustafson, P. F. Measurement of air-borne radioactivity by gamma-ray scintillation spectrometry. Proc. of the Upper Atmosphere Sampling Symp., Sandia Laboratory, Albuquerque, April 11-13, 1961, Part I, ed. J. D. Shreve, Jr. SCR-420 (1961). pp. 113-130.

Gustafson, P. F., J. R. Banister, M. Markels, Jr. and H. R. Vaughn. Discussion of sampling principles and rockets. Proc. of the Upper Atmosphere Sampling Symp., Sandia Laboratory, Albuquerque, April 11-13, 1961, Part I, ed. J. D. Shreve, Jr. SCR-420 (1961). pp. 159-164.

Gustafson, P. F. and S. S. Brar. Gamma-ray dose from short-lived fission products. Radioactive Fallout from Nuclear Weapons Tests. Proc. Conf. Germantown, Md., November 15-17, 1961. TID-7632, Book 1. pp. 60-72.

PUBLICATIONS (Contd.)

Guttman, P. H., Samuel Lesher and H. I. Kohn. A study of the kidney in the LAF_1 mouse after continued daily gamma irradiation, with particular reference to progressive intercapillary glomerulosclerosis. Intern. J. Radiation Biol. 4, 49-59 (1961).

Jaroslow, B. N. and D. E. Smith. Antigen disappearance in hibernating ground squirrels. Science 134, 734-735 (1961).

Jaroslow, B. N. and W. H. Taliaferro. Restoration of hemolysin-forming capacity in irradiated rabbits. Intern. J. Appl. Radiation and Isotopes 13, 159 (1962). Abstract.

Kisieleski, W. E., Renato Baserga and John Vaupotic. The effect of autoradiographic stripping film applied to tissue sections containing tritiated thymidine. Atom Light 18, 1-6 (1961).

Klein, P. D. Silica gel structure and the chromatographic process. Surface energy and activation procedures. Anal Chem. 34, 733-736 (1962).

Kubitschek, H. E. Optical calibration of some monodisperse polystyrene latexes in arrays. Nature 192, 1148-1150 (1961).

Kubitschek, H. E. Normal distribution of cell generation rate. Exptl. Cell Research 26, 439-450 (1962).

Kubitschek, H. E. Loss of resolution in coulter counters. Rev. Sci. Instr. 33, 576-577 (1962).

Kubitschek, H. E. The cell generation rate distribution. Biophys. Soc. Abstracts WB-6 (1962). Abstract.

Laird, A. K. and A. D. Barton. Cell proliferation in precancerous liver. Relation to presence and dose of carcinogen. J. Natl. Cancer Inst. 27, 827-840 (1961).

Lesher, S., R. J. M. Fry and G. A. Sacher. Effects of chronic gamma irradiation on the generation cycle of the mouse duodenum. Exptl. Cell Research 25, 398-404 (1961).

Maloney, M. A., Alberto Monti, C. L. Weber and H. M. Patt. Comparison of cell renewal in normal and leukemic states. Blood 18, 793 (1961). Abstract.

PUBLICATIONS (Contd.)

Maloney, M. A., H. M. Patt and C. L. Weber. Estimation of deoxyribonucleic acid synthetic period for myelocytes in dog bone marrow. Nature 193, 134-135 (1962).

Nebel, B. R. Effect of chronic gamma irradiation on type A spermatogonia in the mouse. Proc. 10th Intern. Congr. for Cell Biology, Paris, September, 1960. p. 144 (1961). Abstract.

Powers, E. L., Bernard Smaller, C. A. Tobias, J. Lyman and T. Brustad. Free radicals in cells induced by heavy ions. Abstracts of Contributed Papers, Intern. Biophysics Congr., Stockholm, July 31 - August 4, 1961. Tryckeri Aktiebolaget Thule, Stockholm, 1961. p. 96. Abstract.

Powers, E. L., Bernard Smaller, C. A. Tobias and J. Lyman. Factors controlling radiation-induced free radicals in a biological system. Preprints of Papers Read at the 5th Intern. Symp. on Free Radicals, Univ. Uppsala, July 6-7, 1961. Almqvist and Wiksell, Stockholm, 1961. No. 54. Abstract.

Powers, E. L. Reversibility of x-irradiation-induced effects in dry biological systems. J. Cell Comp. Physiol. 58, 13-25 (1961).

Powers, E. L. Chemical species induced by x-rays in cells and their role in radiation injury. Proc. Intern. Symp. on Initial Effects of Ionizing Radiation on Living Cells, Moscow, Oct. 18-22, 1959. Academic Press, London, 1961. pp. 91-106.

Rahman, Y. E. Acid phosphatase and beta glucuronidase activities of thymus and spleen of rats after whole-body x-irradiation. Proc. Soc. Exptl. Biol. Med. 109, 378-381 (1962).

Rahman, Y. E. Electron microscopy of lysosome-rich fractions from rat thymus isolated by density gradient centrifugation before and after whole-body x-irradiation. J. Cell Biol. 13, 253-260 (1962).

Roth, L. E. and E. W. Daniels. Electron microscopic studies of mitosis in amoeba. II. The giant amoeba Pelomyxa carolinensis. J. Cell Biol. 12, 57-78 (1962).

Sacher, G. A. and Ernesto Trucco. The stochastic theory of mortality. Ann. N. Y. Acad. Sci. 96, 985-1007 (1962).

PUBLICATIONS (Contd.)

Sato, T. R. and H. H. Strain. Chemical effects produced by the neutron-irradiation of phosphorus compounds. Proc. IAEA Symp. on Chemical Effects of Nuclear Transformations, Prague, Oct. 23-28, 1960. Intern. Atomic Energy Agency, Vienna, 1961. pp. 503-519.

Schlenk, Fritz and George Svihla. Effects of ultraviolet irradiation on yeast cells. Abstracts of Contributed Papers, Intern. Biophysics Congr., Stockholm, July 31 - August 4, 1961. Tryckeri Aktiebolaget Thule, Stockholm, 1961. p. 181. Abstract.

Schlenk, Fritz. Effects of ionizing radiation on the metabolism of yeast cells. Abstracts, 5th Intern. Congr. Biochemistry, Moscow, Aug. 10-16, 1961. p. 495 (1961). Abstract.

Schlenk, Fritz and J. L. Dainko. Some effects of ionizing radiation on methionine sulfonium compounds. Radiation Res. 16, 327-335 (1962).

Schubert, Jack. Radioelement removal by chelating agents. Application of mass action laws and other factors. Federation Proc. 20, 219-221 (1961).

Shapiro, S. K. Utilization of S-adenosylmethionine by microorganisms. J. Bacteriol. 83, 169-174 (1962).

Skok, John. Effect of giberellic acid and light on the utilization of boron and the development of boron deficiency symptoms. Plant Physiol. 36, 15. Abstract.

Slatis, H. M. and A. J. Finkel. Interrelations of adiposity, ancestry and blood type. Proc. 2nd Intern. Conf. on Human Genetics, Rome, 1961. p. E-28 (1961). Abstract.

Straube, R. L. and H. M. Patt. Effect of local x-irradiation on growth capacity of mouse kidney. Proc. Soc. Exptl. Biol. Med. 108, 808-810 (1961).

Stroud, A. N., A. M. Brues and B. R. Svoboda. DNA synthesis of mammalian kidney cells in tissue culture after single and periodic doses of irradiation. Ann. N. Y. Acad. Sci. 95, 942-959 (1961).

PUBLICATIONS (Contd.)

Stroud, A. N. and A. M. Brues. DNA synthesis of Krebs-2 mouse ascites tumor under heterologous and irradiation conditions. Proc. 10th Intern. Congr. for Cell Biology, Paris, Sept. 4-9, 1960. p. 11 (1961). Abstract.

Suchy, J. T., Valeska Evertsbusch and E. D. Aebischer. The atomic search "peaceful uses of atomic energy." The Compton Yearbook. F. E. Compton and Co., Chicago, 1962. pp. 10-19.

Surrey, Kenneth. Spectral response of phosphate metabolism in germinating lettuce seeds. Plant Physiol. 36, 47 (1961). Abstract.

Surrey, Kenneth and S. A. Gordon. Influence of light on phosphate metabolism in lettuce seed. Spectral response red, far-red interaction. Plant Physiol. 37, 327-332 (1962).

Svihla, George, Fritz Schlenk and J. L. Dainko. Speroplasts of the yeast Candida utilis. J. Bacteriol. 82, 808-814 (1961).

Swick, R. W. Propionic acid metabolism. Mechanism of the methyl malonyl isomerase reaction and the reduction of acrylyl coenzyme A to propionyl coenzyme A by propionibacteria. Proc. Natl. Acad. Sci. 48, 233-293 (1962).

Tahmisian, T. N. Cytological effects. Mechanisms in Radiobiology, eds. Maurice Errera and Arne Forssberg. New York: Academic Press, Inc., 1961. Vol. 1, pp. 333-352.

Taliaferro, W. H. and J. H. Humphrey, eds. Advances in Immunology. New York: Academic Press, 1961, Vol. 1.

Taliaferro, W. H. Whither bound - how and why. Cancer Research 21, 1323-1324 (1961).

Taliaferro, W. H. and L. G. Taliaferro. Immunologic unresponsiveness during the initial and anamnestic Forssman hemolysin response. J. Infectious Diseases 110, 165-200 (1962).

Taliaferro, W. H. Biochemical aspects of antibody formation. Sci. Repts. Inst. Super. Sanita 2, 20-36 (1962).

Thomson, J. F. Radiation Protection in Mammals. New York: Reinhold Publ. Co., 1962.

PUBLICATIONS (Contd.)

Tyler, S. A. and S. P. Stearner. Discrimination among injury processes reflected in acute radiation mortality. Intern. J. Radiation Biol. 4, 495-510 (1962).

Walker, F. A., Hsia, D. Y., H. M. Slatis and A. G. Steinberg. Galactosemia. A study of twenty-seven kindreds in North America. Ann. Human Genet. 25, 287-311 (1962).

Webb, R. B. Evidence for an adsorption mechanism for protection against damage from x-rays. Biophys. Soc. Abstracts FF-6 (1962). Abstract.

ARGONNE NATIONAL LAB WEST
3 4444 00023073 0